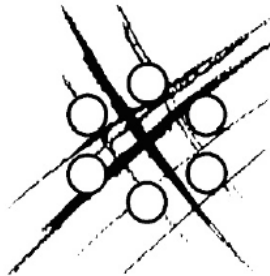


USER DOCUMENTATION : Validation Report TrioCFD v1.8.2



Code Version	Date	Code manager	Authors
v1.8.2	January 12, 2021	J. DARONA 	J.DARONA P.E. ANGELI A. CARTALADE
DES/ISAS/DM2S CEA SACLAY 91191 GIF-SUR-YVETTE CEDEX		<i>Input file : validation_report_TrioCFD.tex</i> <i>Software : TrioCFD</i>	
		DES/ISAS/DM2S/STMF/UD	

Contents

Contents	2
List of Figures	8
List of Tables	12
I Introduction	13
II Methodology for building the validation report	15
1 Introduction	16
1.1 Inventory and sort	16
1.2 Development of a new PRM template	17
1.3 Running with v1.8.2 and L ^A T _E X files	17
2 Overview of new PRM template	17
2.1 Old PRM syntax	18
2.2 New PRM syntax	19
General improvements	19
Modification of Python script	20
3 L^AT_EX files and report generation	23
3.1 L ^A T _E X files	23
3.2 New shell script for gathering all .tex files	24
3.3 Enhancement	24
III Laminar Flow	24
1 Poiseuille flow 2D with VDF and VEF meshes	26
1.1 Purpose	26
1.2 Problem Description	26
Geometry	26
Initial Conditions and Boundary Conditions	27
Fluid Properties	27
Flow Physics	27
1.3 Case Setup	27
Grid	27
Model Options	28
Other Options (calculation)	28
1.4 Results	28
Validation Specific Informations	28

Plot Data	29
1.5 Conclusion	30
1.6 Data Files	30
test	30
2 2D Lid driven cavity test	32
2.1 Purpose	32
2.2 Problem Description	32
Geometry	32
Initial Conditions and Boundary Conditions	32
Fluid Properties	32
Flow Physics	32
2.3 Case Setup	32
Grid	32
Other Options (calculation)	33
2.4 Results	34
Validation Specific Informations	34
Plot Data	34
2.5 Conclusion	36
2.6 References	36
2.7 Data Files	36
defilante	36
3 Cylinder in Laminar Cross Flow	39
3.1 Purpose	39
3.2 Problem Description	39
Geometry	39
Initial Conditions and Boundary Conditions	39
Fluid Properties	40
Flow Physics	40
3.3 Case Setup	40
Grid	40
Model Options	41
Other Options (calculation)	41
3.4 Results	41
Validation Specific Informations	41
Plot Data	42
3.5 Conclusion	46
3.6 References	46
3.7 Data Files	47
test	47
IV Thermal Laminar Flow	48
1 Convection Vahl Davis	50
1.1 Purpose	50
1.2 Problem Description	50
Geometry	50
Initial Conditions and Boundary Conditions	50
Fluid Properties	50
Flow Physics	51
1.3 Case Setup	51
Grid	51
Model Options	52
Other Options (calculation)	53

1.4	Results	53
	Validation Specific Informations	53
	Plot Data	54
1.5	Conclusion	59
1.6	References	59
1.7	Data Files	60
	test	60
2	Oscillatory convection flow	63
2.1	Purpose	63
2.2	Problem Description	63
	Geometry	63
	Initial Conditions and Boundary Conditions	63
	Fluid Properties	64
	Flow Physics	64
2.3	Case Setup	64
	Grid	64
	Model Options	65
	Other Options (calculation)	65
2.4	Results	65
	Validation Specific Informations	65
	Plot Data	66
2.5	Conclusion	69
2.6	References	69
2.7	Data Files	69
	test	69
V	Turbulent Flow	71
1	Turbulent flow in a 2D diffuser with the $k - \epsilon$ model	73
1.1	Purpose	73
1.2	Problem Description	73
	Geometry	73
	Initial Conditions and Boundary Conditions	74
	Fluid Properties	74
	Flow Physics	74
1.3	Case Setup	74
	Grid	74
	Model Options	75
	Other Options (calculation)	75
1.4	Results	75
	Validation Specific Informations	75
	Plot Data	76
1.5	Conclusion	82
1.6	References	82
1.7	Data Files	83
	Calcul	83
2	Mixing length in 2D and 3D VEF-plane channel	86
2.1	Purpose	86
2.2	Problem Description	86
	Geometry	86
	Initial Conditions and Boundary Conditions	86
	Fluid Properties	86
2.3	Case Setup	86

Grid	86
Model Options	89
Other Options (calculation)	89
2.4 Results	89
Validation Specific Informations	89
Plot Data	91
2.5 Conclusion	98
2.6 References	98
2.7 Data Files	98
2D	98
3D	100
3D_keps	102
 VI Thermal Turbulent Flow	 104
 1 Thermal stratification flow in a plenum	 106
1.1 Purpose	106
1.2 Problem Description	106
Geometry	106
Initial Conditions and Boundary Conditions	107
Fluid Properties	107
Flow Physics	107
1.3 Case Setup	107
Grid	107
Model Options	109
Other Options (calculation)	110
1.4 Results	110
Validation Specific Informations	110
Plot Data	110
1.5 Conclusion	120
1.6 References	121
1.7 Data Files	121
Plenum	121
 2 Turbulent flow inside a double-periodic plane channel with heated walls	 124
2.1 Purpose	124
2.2 Problem Description	124
Geometry	124
Initial Conditions and Boundary Conditions	124
Fluid Properties	125
Flow Physics	125
2.3 Case Setup	125
Grid	125
Model Options	126
Other Options (calculation)	126
2.4 Results	126
Validation Specific Informations	126
Plot Data	127
2.5 Conclusion	131
2.6 References	131
2.7 Data Files	131
Canal_plan_bi_periodique_M1	131

VII Two-phase Flows with Front-Tracking	134
1 Oscillation of a bubble	136
1.1 Purpose	136
1.2 Problem Description	136
Geometry	137
Initial Conditions and Boundary Conditions	137
Fluid Properties	137
1.3 Case Setup	137
Grid	137
Model Options	139
Other Options (calculation)	139
1.4 Results	139
Validation Specific Informations	139
Plot Data	139
1.5 Conclusion	151
1.6 References	151
1.7 Data Files	151
FTD_Oscillation_Bulle_3D_VDF	151
2 Drop hanged at the ceiling	155
2.1 Purpose	155
2.2 Problem Description	155
Geometry	158
Initial Conditions and Boundary Conditions	158
Fluid Properties	158
2.3 Case Setup	158
Grid	158
Model Options	159
2.4 Results	159
Validation Specific Informations	159
Plot Data	159
2.5 Conclusion	175
2.6 Data Files	176
goutte	176
goutte	178
VIII Fluid-structure interactions with ALE	181
1 Single-phase flow around a vibrating cylindrical tube	183
1.1 Purpose	183
1.2 Problem Description	183
Geometry	183
Initial Conditions and Boundary Conditions	184
Fluid Properties	184
1.3 Case Setup	184
Grid	184
Model Options	185
1.4 Results	185
Validation Specific Informations	185
Plot Data	185
1.5 Conclusion	189
1.6 References	189
1.7 Data Files	189
TwoCylinders	189

CONTENTS

2 Hydrodynamic interaction of two cylinders subjected to small oscillations	192
2.1 Purpose	192
2.2 Problem Description	192
Geometry	192
Initial Conditions and Boundary Conditions	193
Fluid Properties	193
2.3 Case Setup	193
Grid	193
Model Options	193
2.4 Results	193
Validation Specific Informations	193
Plot Data	194
2.5 Conclusion	197
2.6 References	197
2.7 Data Files	198
TwoOscillatingCylinders	198
3 Vibrations of a cylinder in a square tube bundle immersed in a viscous fluid	200
3.1 Purpose	200
3.2 Problem Description	200
Geometry	201
Initial Conditions and Boundary Conditions	201
Fluid Properties	201
3.3 Case Setup	201
Grid	202
Model Options	204
3.4 Results	204
Validation Specific Informations	204
Plot Data	205
3.5 Conclusion	211
3.6 References	211
3.7 Data Files	211
DIVA	211
IX Conclusion	213

List of Figures

II.2.1	Original PRM syntax version - Parameters part	18
II.2.2	Original PRM syntax version - Generated introduction	18
II.2.3	Original PRM syntax version - Chapter part	19
II.2.4	Original PRM syntax version - Generated chapter	19
III.1.1	Geometry: Dimensions and domain overview	26
III.1.2	VDF Mesh	27
III.1.3	VEF Mesh	28
III.1.4	Transverse velocity profile	29
III.2.1	MESH	33
III.2.2	VITESSE_X SOM	33
III.2.3	Evolution of residue	34
III.2.4	Velocity along line $x=0.5$	35
III.2.5	Velocity along line $y=0.5$	35
III.3.1	Geometry	39
III.3.2	Mesh overview	40
III.3.3	Zoom of the vicinity of the cylinder	41
III.3.4	Pressure fields at $t = 90s$	42
III.3.5	Velocity vectors at $t = 90s$	43
III.3.6	Pressure course at the cylinder surface at $y = \pm 0.5d$ with a Muscl convection scheme	43
III.3.7	Pressure course at the cylinder surface at $y = \pm 0.5d$ with an EF_stab ($\alpha = 0.2$) convection scheme	44
III.3.8	Zoom of the pressure evolution at the cylinder surface (Muscl)	44
III.3.9	Zoom of the pressure evolution at the cylinder surface (EF_stab with alpha = 0.2)	45
III.3.10	Comparison of the mean pressure distribution along the cylinder surface with different convection and time schemes	46
IV.1.1	2D VDF Mesh	51
IV.1.2	2D coarse VEF Mesh	52
IV.1.3	2D fine VEF Mesh	52
IV.1.4	Temperature evolution of two points inside the domain	54
IV.1.5	Temperature and velocity fields at steady state (refine mesh)	55
IV.1.6	Comparison of convection schemes for the Temperature ($y = 0.5$)	55
IV.1.7	Comparison of convection schemes for the Temperature ($x = 0.5$)	56
IV.1.8	Comparison of convection schemes for the velocity v ($y = 0.5$)	56
IV.1.9	Comparison of convection schemes for the velocity u ($x = 0.5$)	56
IV.1.10	Comparison of the probe types for an EF_stab convection scheme in the VEF case (velocities at $y = 0.5$)	57
IV.1.11	Comparison of the probe types for an EF_stab convection scheme in the VEF case (velocities at $x = 0.5$)	57
IV.2.1	Dimensions of the domain and boundary conditions for temperature equation.	63

IV.2.2	VDF Mesh	65
IV.2.3	VEF Mesh	65
IV.2.4	Velocity vectors at $t = 800s$ for VEF mesh (Muscl)	67
IV.2.5	y-component of the velocity along the x-axis at $y = 0.5m$, and $t = 800s$	67
IV.2.6	Temperature profile along x axis: $y = 0.5m$	68
IV.2.7	Time evolution of the velocity (Muscl scheme)	68
V.1.1	Diffuser geometry	73
V.1.2	Periodic box: mesh 1 (1104 cells)	74
V.1.3	Periodic box: mesh 2 (440 cells)	75
V.1.4	Diffuser Mesh (36644 cells)	75
V.1.5	Mesh 1 computations convergence: friction velocity evolution	77
V.1.6	Mesh 2 computations convergence: friction velocity evolution	77
V.1.7	Pressure field in the diffuser, Legend	78
V.1.8	Pressure field in the diffuser, mesh1	78
V.1.9	Pressure field in the diffuser, mesh2	78
V.1.10	Velocity field in the diffuser, Legend	78
V.1.11	Velocity field in the diffuser, mesh 1	78
V.1.12	Velocity field in the diffuser, mesh 2	79
V.1.13	Y^+ field in the diffuser, Legend	79
V.1.14	Y^+ field in the diffuser, mesh1	79
V.1.15	Y^+ field in the diffuser, mesh2	79
V.1.16	Longitudinal velocity profile at $x=6$	80
V.1.17	Longitudinal velocity profile at $x=17$	80
V.1.18	Longitudinal velocity profile at $x=20$	81
V.1.19	Longitudinal velocity profile at $x=27$	81
V.1.20	Longitudinal velocity profile at $x=34$	82
V.2.1	3 x 6 in 2D geometry	87
V.2.2	3 x 41 in 2D geometry	87
V.2.3	3 x 6 x 3 in 3D geometry	88
V.2.4	3 x 41 x 6 in 3D geometry	89
V.2.5	Velocity profile	91
V.2.6	Velocity profile U^+	92
V.2.7	Turbulent viscosity	92
V.2.8	Velocity profile	93
V.2.9	Velocity profile U^+	94
V.2.10	Turbulent viscosity	94
V.2.11	Velocity profile	95
V.2.12	Velocity profile U^+	96
V.2.13	Turbulent viscosity	96
V.2.14	Velocity profile comparison with keps	97
V.2.15	Velocity profile U^+ comparison with keps	97
V.2.16	Turbulent viscosity comparison with keps	98
VI.1.1	Geometry	107
VI.1.2	3D mesh	108
VI.1.3	Histogram of angles for 3D mesh	108
VI.1.4	2D mesh	109
VI.1.5	Histogram of angles for 2D mesh	109
VI.1.6	Positions of points for convergence study	111
VI.1.7	Time evolution of V_x on point A	112
VI.1.8	Time evolution of temperature on point B	112
VI.1.9	Time evolution of pressure force on boundary 'Cold'	113
VI.1.10	Evolution of residuals	113
VI.1.11	Profiles of V_x along the P1 line	114

VI.1.12	Profiles of V_x along P4 line	114
VI.1.13	Temperature profiles along P1 line	115
VI.1.14	Temperature profiles along P4 line	115
VI.1.15	Color scale for distribution of Y_+	116
VI.1.16	Distribution of Y_+ for 2D_H	116
VI.1.17	Distribution of Y_+ for 3D_H	116
VI.1.18	Distribution of Y_+ 2D_T	117
VI.1.19	Distribution of Y_+ 3D_T	117
VI.1.20	Velocity field for 2D_H	117
VI.1.21	Velocity field for 3D_H	118
VI.1.22	Velocity field for 2D_T	118
VI.1.23	Velocity field for 3D_T	119
VI.1.24	Color scale for distribution of Temperature	119
VI.1.25	Temperature field for 2D_H	119
VI.1.26	Temperature field for 3D_H	120
VI.1.27	Temperature field for 2D_T	120
VI.1.28	Temperature field for 3D_T	120
VI.2.1	Geometry	124
VI.2.2	Mesh M1	125
VI.2.3	Mesh M1_tetraedrise	126
VI.2.4	Mean axial velocity profiles for different stretch factors	127
VI.2.5	Comparison with mesh M1_tetraedrise	128
VI.2.6	Explanations of M1 result : contribution of transverse velocity	128
VI.2.7	Deviations of transverse velocity V	129
VI.2.8	Deviations of transverse velocity W	129
VI.2.9	Mean temperature profiles for different stretch factors	130
VI.2.10	Comparison with mesh M1_tetraedrise	130
VII.1.1	Bubble in a cubic box : first calculation - mesh at time = 0	138
VII.1.2	Bubble in a cubic box : second calculation - mesh at time = 0	138
VII.1.3	Bubble in a cubic box : first calculation - mesh at time = 0	140
VII.1.4	Bubble in a cubic box : first calculation - oscillations of the interface at t=0.002s	140
VII.1.5	Bubble in a cubic box : first calculation - oscillations of the interface at t=0.004s	141
VII.1.6	Bubble in a cubic box : first calculation - oscillations of the interface at t=0.006s	141
VII.1.7	Bubble in a cubic box : first calculation - oscillations of the interface at t=0.008s	142
VII.1.8	Bubble in a cubic box : first calculation - oscillations of the interface at t=0.01s	142
VII.1.9	Bubble in a cubic box : first calculation - oscillations of the interface at t=0.012s	143
VII.1.10	Bubble in a cubic box : first calculation - oscillations of the interface at t=0.014s	143
VII.1.11	Bubble in a square box - Interfacial area between air and water	144
VII.1.12	Bubble in a cubic box - Pressure difference between the inner and outer fluid	144
VII.1.13	Bubble in a cubic box : second calculation - mesh at time = 0	145
VII.1.14	Bubble in a cubic box : second calculation - oscillations of the interface at t=0.002s	146
VII.1.15	Bubble in a cubic box : second calculation - oscillations of the interface at t=0.004s	146
VII.1.16	Bubble in a cubic box : second calculation - oscillations of the interface at t=0.006s	147
VII.1.17	Bubble in a cubic box : second calculation - oscillations of the interface at t=0.008s	147
VII.1.18	Bubble in a cubic box : second calculation - oscillations of the interface à t=0.01s	148
VII.1.19	Bubble in a cubic box : second calculation - oscillations of the interface à t=0.012s	148
VII.1.20	Bubble in a cubic box : second calculation - oscillations of the interface à t=0.014s	149
VII.1.21	Bubble in a cubic box - Interfacial area between air and water	149
VII.1.22	Bubble in a square box - Interfacial area between air and water - zoom between 0.1 an 0.16 sec	150
VII.1.23	Bubble in a cubic box - Pressure difference between the inner and outer fluid	150
VII.2.1	Profiles of the drop : theoretical data for different amount of water and a contact angle between the tangential curve at the drop close to the wall of 1 radian.	156

VII.2.2 Profiles of the drop : theoretical data for different amount of water and a contact angle between the tangential curve at the drop close to the wall of 1.5 radian.	156
VII.2.3 Profiles of the drop : theoretical data for different amount of water and a contact angle between the tangential curve at the drop close to the wall of 2 radian.	157
VII.2.4 Profiles of the drop : theoretical data for different amount of water and a contact angle between the tangential curve at the drop close to the wall of 2.5 radian.	157
VII.2.5 Profiles of the drop : theoretical data for different amount of water and a contact angle between the tangential curve at the drop close to the wall of 3 radian.	158
VII.2.6 Drop hanged at the top of the box with a contact angle of 1.5 radian - t=0s	160
VII.2.7 Drop hanged at the top of the box with a contact angle of 1.5 radian - t=0.01s	160
VII.2.8 Drop hanged at the top of the box with a contact angle of 1.5 radian - t=0.05s	161
VII.2.9 Drop hanged at the top of the box with a contact angle of 1.5 radian - t=0.1s	161
VII.2.10 Drop hanged at the top of the box with a contact angle of 1.5 radian - t=0.15s	162
VII.2.11 Drop hanged at the top of the box with a contact angle of 1.5 radian - t=0.2s	162
VII.2.12 Drop hanged at the top of the box with a contact angle of 1.5 radian - t=0.35s	163
VII.2.13 Drop hanged at the top of the box with a contact angle of 1.5 radian - t=0.5s	163
VII.2.14 Drop hanged at the top of the box with a contact angle of 1.5 radian - t=0.75s	164
VII.2.15 Drop hanged at the top of the box with a contact angle of 1.5 radian - t=1s	164
VII.2.16 Drop hanged at the top of the box with a contact angle of 1.5 radian - t=1.5s	165
VII.2.17 Drop hanged at the top of the box with a contact angle of 1.5 radian - t=2s	165
VII.2.18 Drop hanged at the top of the box with a contact angle of 1.5 radian - t=2.5s	166
VII.2.19 Drop hanged at the top of the box with a contact angle of 1.5 radian - t=3s	166
VII.2.20 Profils 1.5 radians	167
VII.2.21 Drop hanged at the top of the box with a contact angle of 2.5 radian - t=0s	168
VII.2.22 Drop hanged at the top of the box with a contact angle of 2.5 radian - t=0.01s	168
VII.2.23 Drop hanged at the top of the box with a contact angle of 2.5 radian - t=0.05s	169
VII.2.24 Drop hanged at the top of the box with a contact angle of 2.5 radian - t=0.1s	169
VII.2.25 Drop hanged at the top of the box with a contact angle of 2.5 radian - t=0.15s	170
VII.2.26 Drop hanged at the top of the box with a contact angle of 2.5 radian - t=0.2s	170
VII.2.27 Drop hanged at the top of the box with a contact angle of 2.5 radian - t=0.35s	171
VII.2.28 Drop hanged at the top of the box with a contact angle of 2.5 radian - t=0.5s	171
VII.2.29 Drop hanged at the top of the box with a contact angle of 2.5 radian - t=0.75s	172
VII.2.30 Drop hanged at the top of the box with a contact angle of 2.5 radian - t=1s	172
VII.2.31 Drop hanged at the top of the box with a contact angle of 2.5 radian - t=1.25s	173
VII.2.32 Drop hanged at the top of the box with a contact angle of 2.5 radian - t=1.5s	173
VII.2.33 Drop hanged at the top of the box with a contact angle of 2.5 radian - t=1.75s	174
VII.2.34 Drop hanged at the top of the box with a contact angle of 2.5 radian - t=2s	174
VII.2.35 Profils 2.5 radians	175
VIII.1.1 The domain	183
VIII.1.2 Mesh	184
VIII.1.3 Force per unit length of cylinder	186
VIII.1.4 TrioCFD PRESSION SOM	187
VIII.1.5 TrioCFD VITESSE_magnitude SOM	188
VIII.1.6 TrioCFD Mesh velocity SOM	188
VIII.1.7 TrioCFD Total displacement of the mesh SOM	189
VIII.2.1 The domain	192
VIII.2.2 Force per unit length of cylinder	194
VIII.2.3 TrioCFD PRESSION SOM	195
VIII.2.4 TrioCFD VITESSE_magnitude SOM	196
VIII.2.5 TrioCFD Mesh velocity SOM	197
VIII.3.1 DIVA geometry	201
VIII.3.2 Mesh_1	202
VIII.3.3 Mesh_2	203

VIII.3.4 Mesh_3	203
VIII.3.5 Force per unit length of cylinder	205
VIII.3.6 TrioCFD Mesh_1 PRESSION SOM	208
VIII.3.7 TrioCFD Mesh_1 VITESSE_magnitude SOM	209
VIII.3.8 TrioCFD Mesh_2 PRESSION SOM	209
VIII.3.9 TrioCFD Mesh_2 VITESSE_magnitude SOM	210
VIII.3.10 TrioCFD Mesh_3 PRESSION SOM	210
VIII.3.11 TrioCFD Mesh_3 VITESSE_magnitude SOM	211

List of Tables

I.0.1 Type of flow investigated to each Part.	15
II.1.1 List of folders of TrioCFD test cases.	16
II.1.2 Computer characteristics for running the test cases database.	17
II.2.1 New blocks of instructions in PRM file: content (left) and corresponding keywords (right) in English or French.	20
II.2.2 Keywords that can be used in block Parameters for PRM files.	21
II.2.3 List of keywords for the Problem description block.	22
II.2.4 List of keywords for the Case Setup block.	22
II.3.1 L ^A T _E X files of this report.	23
III.1.1 Physical properties	27
III.1.2 Performance Chart	29
III.2.1 Performance Chart	34
III.2.2 CPU informations for new and reference solutions	36
III.3.1 Physical properties of the fictitious fluid	40
III.3.2 Performance Chart	42
III.3.3 Comparison of Strouhal numbers	45
IV.1.1 Physical properties	51

IV.1.2	Performance Chart	54
IV.1.3	Summary of values from literature	57
IV.1.4	Results for Max(u^*)	58
IV.1.5	Results for Max(v^*)	58
IV.1.6	Relative errors for Max(u^*): ERR[Max(v^*)] in %	58
IV.1.7	Relative errors for Max(v^*): ERR[Max(v^*)] in %	59
IV.2.1	Physical properties	64
IV.2.2	Performance Chart	66
IV.2.3	Oscillation frequency	68
V.1.1	Physical properties	74
V.1.2	Performance Chart	76
V.2.1	Performance Chart	91
V.2.2	2D - $Re_b = 10000$	91
V.2.3	2D - $Re_b = 10^5$	93
V.2.4	3D - $Re_b = 100\ 000$	95
VI.1.1	Performance Chart	110
VI.1.2	Flow balance	111
VI.2.1	Performance Chart	127
VI.2.2	Nusselt Calculation	131
VII.1.1	Performance Chart	139
VII.2.1	Performance Chart	159
VIII.1.1	Meshes properties	185
VIII.1.2	Performance Chart	185
VIII.1.3	Added mass and damping coefficients	186
VIII.2.1	Performance Chart	194
VIII.2.2	Added mass and damping coefficients	195
VIII.3.1	Meshes properties	204
VIII.3.2	Performance Chart	204
VIII.3.3	Added mass coefficients for the Center cylinder	206
VIII.3.4	Added damping coefficients for the Center cylinder	206
VIII.3.5	Added mass coefficients for the Nord cylinder	206
VIII.3.6	Added damping coefficients for the Nord cylinder	206
VIII.3.7	Added mass coefficients for the Sud cylinder	207
VIII.3.8	Added damping coefficients for the Sud cylinder	207
VIII.3.9	Added mass coefficients for the Est cylinder	207
VIII.3.10	Added damping coefficients for the Est cylinder	207
VIII.3.11	Added mass coefficients for the West cylinder	208
VIII.3.12	Added damping coefficients for the West cylinder	208

I. Introduction

THE TrioCFD database contains currently around 160 test cases of validation which are called in this document “validation sheets”. The present report is the result of an inventory work of the most important of these validation sheets to know (non exhaustive list): What type of flow do they simulate? What is the degree of maturity of each validation? What sort of comparison do they exhibit? and so on ...

This validation report has several objectives:

- Help users to identify application areas of TrioCFD code;
- Give users examples of modeling (TrioCFD keywords and boundary conditions) on specific cases;
- Inform users of changes/improvements on the code validation;
- Make an inventory of the code validation for each delivered version;
- Account for physical and/or numerical impacts observed resulting from implementation, corrections or modifications of test cases that have been made between each version;
- Update the validation status of the code.

In previous versions of TrioCFD, each validation sheet has been written by different authors who used their own approach. In order to improve the readability of this report, the content of all these validation sheets has been harmonized by using identical titles and same general organization. For this purpose, a new PRM template has been updated in TrioCFD (v1.8.2). The update has required modifying the Python script and revising all PRM files with the same content. More precisely, new tags have been added and new keywords must be used by authors when writing the PRM file. Details about this new PRM template and keywords are presented in Part II. This new template will be helpful for future versions of this document when a specific study using TrioCFD will lead to write a new PRM sheet or to update an old one. The Part II will also describe the methodology for making this report.

Moreover, until now, all validation sheets were placed in various folders of the TrioCFD package. Hence, some of them could not be found quickly by users who had to browse all directories. This report gathers in one single document some of these sheets classified according the type of flow or physics investigated. The selected test cases are representative of five subdomains summarized in Table I.0.1 and successively presented for flows of increasing complexity: “Laminar flow” (Part III), “Thermal laminar flow” (Part IV), “Turbulent flow” (Part V), “Thermal turbulent flow” (Part VI), “Front Tracking” (Part VII) and “Arbitrary Lagrangian-Eulerian Method” (Part VIII). The first four parts gather the test cases for single phase flow, coupled or not with turbulence and thermal modeling. The last part is dedicated to two-phase flows with interface tracking. Finally Part IX concludes this report and perspectives will be sketched.

Parts	Type of flows
Part III	Laminar Flow
Part IV	Thermal Laminar Flow
Part V	Turbulent Flow
Part VI	Thermal Turbulent Flow
Part VII	Two-phase Flows with Front Tracking
Part VIII	ALE method for fluid/structure interactions

Table I.0.1: Type of flow investigated to each Part.

The sheets appearing in those parts are selected because they separately simulate a particular flow well-known in the CFD literature, such as the “*Poiseuille flow*” and “*lid-driven cavity flow*” which are two examples of “Laminar Flows”. For “Thermal Laminar Flows” the “*Vahl Davis convection flow*” is a standard test case. Other sheets were selected because they compare **TrioCFD** with other CFD results using alternative academic or commercial codes (e.g. **Fluent** or other benchmarks) such as “*OBI diffuser*” (Turbulent flow). When available and representative of flows, experimental data measured on facility tests were included for comparisons and appear on the graphs (e.g. “*Thermal stratification flow in a plenum*”). The number of tests presented in this report will be gradually increased at each new version release of **TrioCFD**. For example, the eighth part which concerns the modeling of the fluid/structure interactions with the ALE method has been added since the last delivery

II. Methodology for building the validation report

II.1

Introduction

In this chapter, the three-stage methodology to build this report is developed as following: 1) inventory and sort of the TrioCFD database ; 2) development of a new PRM template ; 3) running the v1.8.2 of TrioCFD and description of L^AT_EX files. In this first section we present a summary of those three stages before giving accurate instructions and commands in next sections.

1.1 Inventory and sort

Currently, the TrioCFD database contains about 160 test cases archived in different folders (see Table II.1.1). First, an important inventory work was carried out to sort the test cases for targeting quickly the use of TrioCFD in different CFD configurations. The inventory resulted in a single table with plenty information (LibreOffice format), where the test cases are classified into several subdomains of fluid flows. In this document, some of them have been selected and detailed because 1) they are well-known in the literature, 2) they present comparisons with other academic or commercial CFD codes and 3) they present comparisons with experimental data.

Folders	Comments
/validation/share/Validation/Rapports_automatiques/	files validating several baltik
/Front_tracking_discontinu/share/Validation/Rapports_automatiques/	sheets for baltik Front-tracking
/P1NCPORT/share/Validation/Rapports_automatiques/	baltik P1NC0RT
/Rayonnement/share/Validation/Rapports_automatiques/	radiation
/LES/share/Validation/Rapports_automatiques/	LES turbulence
/Schema_Euler_Implicite_Stationnaire/share/Validation/Rapports_automatiques/	Steady state implicit Euler scheme
/ALE/share/Validation/Rapports_automatiques/	ALE method
/Bas_Reynolds/share/Validation/Rapports_automatiques/	Low Reynolds turbulence models
/Turbulence/share/Validation/Rapports_automatiques/	Other turbulence models

Table II.1.1: List of folders of TrioCFD test cases.

This files arrangement of Table II.1.1 is not intuitive and can lose users and sometimes be confusing (e.g. subdirectory names such as "pas_fini", "Fiches_supplementaires", "Bench", and so on ...). For a better understanding of future versions, all files and subfolders will be re-ordered and the directory tree will be simplified.

1.2 Development of a new PRM template

For each datafile of test cases, the PDF file is generated by running a bash script (command `Run_fiche`) which acts on a PRM file. A PRM file is a set of specific instructions for interfacing the L^AT_EX commands with the TrioCFD results post-processed with `Gnuplot` or `Visit`. As its content differs following the test cases, the generated PDF reports may be structured differently, making them hard to read and to understand. Consequently, a new PRM template has been implemented in the present report to harmonize their content for a more homogeneous rendering. Differences between the old and new versions of the PRM template are detailed in Section 2.2. All validation sheets of this report have been revised and enhanced by taking into account the new PRM template.

1.3 Running with v1.8.2 and L^AT_EX files

For all test cases, the datafiles were run with the version 1.8.2 of TrioCFD for checking the achievement of computations. The CPU time required to 1) compile TRUST and TrioCFD and 2) run the 160 validation sheets is 11 days and 12 hours on the computer of characteristics given in Table II.1.2. For each validation sheet, the full documentation is automatically generated via the `Run_fiche` procedure. The validation sheets associated with the daily elementary tests that run daily (not discussed in more detail in this report) allow to obtain a coverage rate of 78.7% of the keywords of TrioCFD. Finally, all selected sheets are gathered in one single document. Precisions will be given on the L^AT_EX files in Section 3.

COMPUTER	OPERATING SYSTEM	COMPILER
is223288@intra.cea.fr		
PC Linux Intel(R) Xeon(R) CPU E5-2620 0@2.00GHz 2 CPU - 6 physical cores per CPU	LINUX Fedora 26 Kernel gcc 7.1.1	GCC7.1.1 MPICH3.2

Table II.1.2: Computer characteristics for running the test cases database.

II.2

Overview of new PRM template

The PRM files are written in a specific template more user-friendly as described in the following. The PRM sheet is then read by Python scripts which convert it to L^AT_EX files.

For a better readability, an enhanced rendering and uniformity of this document, a new PRM template has been implemented. This new template provides a skeleton of the main items one should find in a CFD study. By browsing it, the user will immediately know the system geometry, the physical models, the boundary conditions, the numerical methods and other unavoidable details. Each validation sheet included in this document has been revised and improved with this new PRM template. For some test cases, the physical content has been enriched with an extended analysis and discussion. In subsection 2.1, we remind the structure of an old PRM syntax (until version v1.8.1). The new syntax available with version v1.8.2 is then detail in subsection 2.2.

2.1 Old PRM syntax

In the previous versions of **TrioCFD**, the formalism of a PRM was left to the hand of the writer of the file. The general structure was made up of a first part called **Parameters**. Then the writer could define as many chapters as he wanted via the keyword *Chapter*. The titles of the chapters were left to the discretion of the editor. The methodology for writing the PRM as well as the keywords are explained in the [PRM syntax](#) section after launching "trust-index".

In order to better understand the old structure, we will take the example of the PRM present in Chapter III.3 of this report on a Cylinder in Laminar Cross Flow. The first keyword *Parameters* was structured as follows:

```
Parameters {
    Title "Cir Cyl Re100" % PRM title
    Description "Oscillating flow behind a circular cylinder perpendicular to the flow." % PRM Description
    VersionTrio_U "1.6.1" % Trio-CFD used to establish de TestCase
    ParametersTrio_U Type of problem: 2D laminar hydraulic_problem % definition of different physical and numerical models
    ParametersTrio_U Discretization: VEFPreP1B % used in the modeling
    ParametersTrio_U Time scheme: Euler Explicite for VDF and VEF
    ParametersTrio_U Momentum convection scheme: EF_stab with alpha = 0.2 or Muscl
    ParametersTrio_U Solving of equations: Navier_Stokes_standard

    Reference "#[1] Chabard J.P., Lalanne P., Metivet B., Projet N3S de Mecanique des fluides. Cahier de Validation 2D. EDF/DER HE-41/88.08 1988."
    Reference "#[2] Braza P., Chassang P., H. Ha Minh. Numerical study and physical analysis of pressure and velocity fields in the near wake of a circular cylinder. J. Fluid Mech. 165, 79-130, 1986"

    TestCase EI/Muscl test % Name of generated TestCase with .data file
    TestCase EI/EF_stab02 test

    Author "E. MOREAU (S. VANDROUX)" % Writer(s) of the Test Case and the PRM
    IncludeData 2 % Number of TestCase generated
}
```

Figure II.2.1: Original PRM syntax version - Parameters part

This part generates the first section of the PRM pdf entitede *1. Introduction* as follows:

<p>2 TESTS DESCRIPTION</p> <hr/> <p>Cir Cyl Re100</p> <p>1 Introduction</p> <p>Validation made by : E. MOREAU (S. VANDROUX). Report generated 25/06/2020.</p> <p>1.1 Description Oscillating flow behind a circular cylinder perpendicular to the flow.</p> <p>1.2 Parameters TRUST</p> <ul style="list-style-type: none"> • Version TRUST : 1.6.1 • Binary: /export/home/jd249769/TRIO_CFD/deposits.git/triofd-code/TrioCFD.opt (built on TRUST v/export/home/jd249769/TRIO_CFD/deposits.git/triofd-code/validation/share/Validation/Rapports_au • Type of problem: 2D laminar hydraulic_problem 	<ul style="list-style-type: none"> • Discretization: VEFPreP1B • Time scheme: Euler Explicite for VDF and VEF • Momentum convection scheme: EF_stab with alpha = 0.2 or Muscl • Solving of equations: Navier_Stokes_standard <p>1.3 Test cases</p> <ul style="list-style-type: none"> • EI/Muscl/test.data : • EI/EF_stab02/test.data : <p>1.4 References :</p> <ul style="list-style-type: none"> • [1] Chabard J.P., Lalanne P., Metivet B., Projet N3S de Mecanique des fluides. Cahier de Validation 2D. EDF/DER HE-41/88.08 1988. • [2] Braza P., Chassang P., H. Ha Minh. Numerical study and physical analysis of pressure and velocity fields in the near wake of a circular cylinder. J. Fluid Mech. 165, 79-130, 1986
--	---

Figure II.2.2: Original PRM syntax version - Generated introduction

After this first part, chapters can be freely added via the keyword *Chapter{ ... }* as follows:

```

Chapter {
    Title "Tests Description"                                % Chapter title
    #
    Description "Hydraulic initial conditions: quiescent fluid U = V = 0 m/s"      % chapter redaction
    Description "$bullet$ The velocity is fixed in order to obtain U = 0.03937m/s in such a kind that Re = Ud/$\nu$ = 100 "
    Description "$bullet$ CERCLE paroi_fixe"
    Description "$bullet$ PAROI1 symetrie"
    Description "$bullet$ PAROI2 symetrie"
    Description "$bullet$ SORTIE frontiere_ouverte_pression_imposee Champ_Front_Uniforme 1 0,0"
    Description "$bullet$ SORTIE frontiere_ouverte_vitesse_imposee Champ_Front_Uniforme 2 0,03937 0,0"
    Description ""
    Description "\underline{Validated model:}\underline{Validation with:}\underline{Calculations N3S of Chabard [1] and experiments of Braza et al. [2]} % use of pure latex commands
    #
    Figure {
        Title "Geometry"                                     % insertion of a figure png
        Description "In the following scheme, L = 0.635m ; W = 0.1524m and d = 0,0254m" % figure title -> new subsection creation
        Width 14cm                                         % Text preceding the figure
        picture geometry.png                               % figure dimensions
    }
    #
    visu {
        Title "Mesh overview"                            % insertion of a visu extract from lata
        Description " Mesh build with Gmsh: 9668 elements" % visu title -> new subsection creation
        Width 14cm, viewports: 0 0 1000 550,clip          % Text preceding the visu
        mesh EI/Muscl/test.lata dom                      % figure dimensions and resizing
    }
    # properties Geometry
    Table {
        Title "Physical properties"                     % insertion of a table
        Description ""                                  % table title -> new subsection creation
        nb_columns 1                                    % Text preceding the table
        label Value
        line {
            legend "$\rho$ (kg/m3)"
            file propertiesGeometry.dat
            nb_columns_file 3
            columns ($1)
        }
        line {
            legend "$\mu$ (N/m2/s)"
            file propertiesGeometry.dat
            nb_columns_file 3
            columns ($2)
        }
        line {
            legend "Re"
            file propertiesGeometry.dat
            nb_columns_file 3
            columns ($3)
        }
    }
}

```

Figure II.2.3: Original PRM syntax version - Chapter part

This part generates the second section of the PRM pdf entitled *2. Tests Description* as follows:

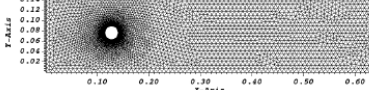
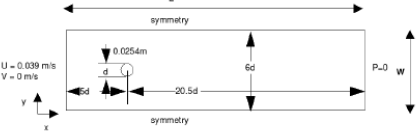
<p>2 Tests Description</p> <p>Hydraulic initial conditions: quiescent fluid $U = V = 0 \text{ m/s}$ Hydraulic boundary condition: <ul style="list-style-type: none"> The velocity is fixed in order to obtain $U = 0.03937\text{m/s}$ in such a kind that $\text{Re} = Ud/\nu = 100$ CERCLE paroi_fixe PAROI1 symetrie PAROI2 symetrie SORTIE frontiere_ouverte_pression_imposee Champ_Front_Uniforme 1 0,0 SORTIE frontiere_ouverte_vitesse_imposee Champ_Front_Uniforme 2 0,03937 0,0 <u>Validated model:</u> <ul style="list-style-type: none"> - No-slip at the wall - 2D channel - Disturbance of a laminar flow <u>Validation with:</u> Calculations N3S of Chabard [1] and experiments of Braza et al. [2] </p>	<p>2.2 Mesh overview Mesh build with Gmsh: 9668 elements</p>  <p>2.1 Geometry In the following scheme, $L = 0.635\text{m}$; $W = 0.1524\text{m}$ and $d = 0.0254\text{m}$</p>  <p>2.3 Physical properties</p> <table border="1"> <thead> <tr> <th></th> <th>Value</th> </tr> </thead> <tbody> <tr> <td>ρ (kg/m³)</td> <td>1.33</td> </tr> <tr> <td>μ (N/m²/s)</td> <td>1e-05</td> </tr> <tr> <td>Re</td> <td>100.0</td> </tr> </tbody> </table>		Value	ρ (kg/m ³)	1.33	μ (N/m ² /s)	1e-05	Re	100.0
	Value								
ρ (kg/m ³)	1.33								
μ (N/m ² /s)	1e-05								
Re	100.0								

Figure II.2.4: Original PRM syntax version - Generated chapter

2.2 New PRM syntax

General improvements

Improvements have been made to the `Run_fiche` procedure (managed by TRUST code) and a new tag, `newvalidTrio`, has been created to activate the new formalism. Some modifications have been made in

this new version for the generation of the L^AT_EX file from the PRM file, without affecting the syntax of the PRM. Thus, the PRM still includes the first block of instructions entitled **Parameters** (see Section 2.1) which is followed by several blocks of instructions entitled by new tags (or keywords). Those new keywords are listed in Section 2.2. The tag **Chapter** appearing in previous versions is removed and replaced by many other tags. An additional improvement concerns the “headers and footers” of PDF files. In earlier versions, the left header stated the number and title of last section whereas the left footer stated the test name. Now, the name is put on the left header, the left footer is empty and the right footer still states the page number. That modification was necessary for the concatenation of L^AT_EX files into one single document and facilitates the readability.

Modification of Python script

As seen in section 2.1, adding a new figure, visu, or table automatically created a new subsection. The title of that subsection is the same as the figure name (respectively visu or table). Therefore, too many irrelevant subsections were created and the title was used as a caption for figures. In this work, the Python scripts have been modified so that the title fields of figures (resp. visu and tables) now correspond to the caption and their creation no longer generates a subsection.

CONTENT OF NEW PRM file	KEYWORDS OF NEW PRM SYNTAX	
1. Purpose	English purpose	French objectif
2. Problem description	pb_description	
2.1 Geometry	geometry	geometrie
2.2 Initial and boundary conditions	icbc	cicl
2.3 Fluid properties	fluidprop	propfluide
2.4 Flow Physics	flowphy	phyecou
3. Case Setup	casesetup	description_cas
3.1 Grid	grid	maillage
3.2 Model options	model_options	options_modele
3.3 Other options (calculations)	other_options	autres_options
4. Results	results	resultats
3.1 Specific information	none	
3.2 Data plots	none	
5. Conclusion	conclusion	
6. References	Reference in block Parameters	
7. Datafile	TestCase in block Parameters (if followed by *)	

Table II.2.1: New blocks of instructions in PRM file: content (left) and corresponding keywords (right) in English or French.

Moreover, the PRM is now interpreted line by line in order to allow better positioning of the figures in the validation sheet. Previously, the Description fields were all displayed together at the start of a section/subsection and the figures afterwards. The Python script has been enhanced with the use of double dictionary to write, in the generated L^AT_EX file, the fields in the same order as that of the PRM. It is therefore now possible to alternate the Description, Figure, Visu or Table fields and their order will be reproduced in the .tex file.

In addition to these modifications, a new PRM syntax has been implemented in order to present an identical content for all validation sheets: now seven sections define all of them. Those sections are listed in Table II.2.1 (left part). When writing one PRM file, a new section corresponds to a new block of instructions which must be declared by its corresponding keyword. The list of keywords is presented in Table II.2.1 (right

part). All instructions inside the block must be enclosed by braces: e.g `objectif {...}`, `pb_description {...}`, `maillage {...}` and so on, where “...” means several instructions on several lines.

Let us remind that in the old PRM syntax, the unique keyword `Chapter` was defined as many times as necessary for defining a new block of instructions. In particular, the number and name of Sections were chosen by the authors (see Section 2.1) and the final rendering was different from one sheet to another. With the new syntax, the blocks of instructions follow the first one called `Parameters`. The second block of instructions is `objective {}`, the third one is `pb_description {...}`, and so on until `conclusion {...}`. The block `Parameters` already existed in previous PRM version but minor modifications have been brought. The commands are listed in Table II.2.2 and an example of use is presented in Alg. 2.1. The first one, `newvalidTrio`, is mandatory because this new flag indicates the new PRM template. `TestCase` and `ParametersTrio_U` can be used multiple times in the block.

Keywords	Use
<code>newvalidTrio</code>	Required keyword to activate the new syntax
<code>Title</code>	Defines title of the validation sheet
<code>VersionTrio_U</code>	First version of TrioCFD that performed validation
<code>ParametersTrio_U</code>	Comments that appear in Section 4.1 of the validation sheet
<code>Reference</code>	References cited in the validation sheet
<code>TestCase</code>	List of test cases run by TrioCFD and included in the validation sheet
<code>Author</code>	First authors who carried out this validation
<code>IncludeData</code>	Command for including the entry datafile of TrioCFD
<code>Description</code>	available in initial formalism, is no longer taken into account.

Table II.2.2: Keywords that can be used in block `Parameters` for PRM files.

Algorithm 2.1 One example of block `Parameters` (for brevity, few instructions are replaced by “...”).

```
Parameters {
    newvalidTrio
    Title "Turbulent flow inside a double-periodic plane channel with heated walls"
    TestCase "Incompressible/Canal_plan_bi_periodique_M1" "Canal_plan_bi_periodique_M1.data" /**
    TestCase "Incompressible/Canal_plan_bi_periodique_M10" "Canal_plan_bi_periodique_M10.data"
    TestCase "Incompressible/Canal_plan_bi_periodique_M100" "Canal_plan_bi_periodique_M100.data"

    TestCase "Incompressible/Canal_plan_bi_periodique_M1_tetraedrise" ...
    TestCase "Incompressible/Canal_plan_bi_periodique_M1bis_tetraedrise" ...

    ParametersTrio_U "Bi-periodic plane channel in X and Z"
    ParametersTrio_U "Convection scheme = EF_stab"
    ParametersTrio_U "k-$\backslash varepsilon$ modelling of turbulence"
    ParametersTrio_U "Wall law = loi_standard_hydr ..."
    ParametersTrio_U "Heat transfer with imposed temperatures"
    ParametersTrio_U "No-slip at the wall"
    Reference "[1] Stanislav N. Danov, Norio Arai and Stuart ..."
    Author "FOURNIER C"
    IncludeData 2
}
```

The keyword `Description`, available in the initial formalism, is no longer taken into account.

In the old formalism, `Chapter` block was defined as many time as necessary with title chosen by the writer of the validation sheet (see Chapter II.1). With this new formalism, predefined blocks can be used after the

block **Parameters**.

The second block is **Purpose** which can be activated by the keyword **purpose** or **objectif**. In the PDF file, the section **Purpose** is then created provided that the author wants to fill it up. It explains which models will be validated in the sheet and what sort of results (numerical, analytical, ...) TricCFD will be compared with.

The third block is **Problem description** which can be activated by the keyword **pb_description**. The section named **Problem description** is then created. In this block, 4 sub-blocks are available for creating 4 subsections which describe the geometry of the physical domain defined to model the phenomenon, the initial and boundary conditions used in the modeling, the fluid properties and the flow physics. They can be activated with the following keywords:

Keyword	Subsection number	Subsection title
geometry or geometrie	2.1	Geometry
icbc or cicl	2.2	Initial Conditions and Boundary Conditions
fluidprop or propfluide	2.3	Fluid Properties
flowphy or phyecou	2.4	Flow Physics

Table II.2.3: List of keywords for the **Problem description** block.

The fourth block entitled **Case Setup** block and activable by the keyword **casesetup** or **description_cas** has 3 available subsections which can be defined by:

Keyword	Subsection number	Subsection title
grid_mesh or maillage	3.1	Grid
model_options or options_modele	3.2	Model Options
other_options or autres_options	3.3	Other Options (calculation)

Table II.2.4: List of keywords for the **Case Setup** block.

The fifth block is an overview of the results of interest from the validation sheet. This block entitled **Results** and activable by the keyword **results** or **resultats** is composed of two subsections. No keyword needed to activate those subsections and the Results block definition is sufficient to create them.

The first, named **Validation Specific Informations** is automatically generated and groups the fields **VersionTrio_U** and **ParametersTrio_U** defined in the **Parameters** block. The performance table for each test case is automatically inserted at the end of this subsection.

The second subsection, entitled **Plot Data** is generated by reading line by line the keywords **Description**, **Figure**, **Visu** or **Table** defined by the author in the block. Respecting this order allows an easier writing and reading of the PRM file.

The **last block** named Conclusion defined by the keyword conclusion has no subsection and is filled by line-by-line reading of the PRM like the other blocks. Here is an assessment of the validation status of the sheet.

The **two last sections** of the validation sheet, **References** and **Data Files**, are automatically generated respectively from keywords Reference and TestCase inside the **Parameters** block.

Four instructions can be used inside all blocks and sub-blocks: **Description**, **Figure**, **Visu** and **Table** that can be repeated as many times as necessary and in the desired writing order.

II.3

L^AT_EX files and report generation

The procedure for generating this report is flexible and automated. As a matter of fact, each author can work independently on each validation sheet with the new PRM template (Section 2.2). Moreover, all parts of this document are written in several L^AT_EX files with clear names (Section 3.1). A new one can easily be added. Finally a shell script automates the following tasks: gathering all L^AT_EX files, cleaning all sheets texfiles (Section 3.2) and making one single PDF document.

3.1 L^AT_EX files

The main L^AT_EX file of this report is named validation_report_TrioCFD.tex. The file contains the standard instructions \documentclass, \usepackage, \begin{document} and \end{document}. The eight parts of this report are written in eight separated L^AT_EX files (see their names in Tab. II.3.1). Those files are included in the main with the command \input{} (e.g. \input{./part1-introduction.tex}).

L ^A T _E X file	Comment
validation_report_TrioCFD.tex	Main file
part1-introduction.tex	File included
part2-methodology.tex	id
part3-laminar.tex	id
part4-thermallaminar.tex	id
part5-turbulent.tex	id
part6-thermalturbulent.tex	id
part7-FT.tex	id
part8-conclusion.tex	id

Table II.3.1: L^AT_EX files of this report.

The validation sheets are also included in the main by the same command. All of them are placed inside the folder ./fiches containing subfolders of all test cases e.g. Poiseuille_flow_2D_VDF_VEF, Cir_Cyl_Re100, OBI_diffuser_VEF_k_eps, and so on ... Inside them, the L^AT_EX file of each validation sheet is called **fic.tex** which can be found in the directory ./build/.tmp/. For instance, instruction for including the validation sheet of “Lid driven cavity flow” is:

\input{./fiches/Lid_driven_cavity/build/.tmp/fic.tex}. All these `fic.tex` files were generated by Python scripts reading the PRM template.

3.2 New shell script for gathering all .tex files

The folder `fiches` and all subfolders of test cases are created by `generer_rapport_valid.unix`. For all test cases, the first task of this shell script is to copy the `build` directory of TrioCFD results in corresponding subfolders. The second task is to clean each `fic.tex` file in order to be included in the main L^AT_EX file. Finally the instruction `pdflatex validation_report_TrioCFD.tex` compiles and generates the PDF file.

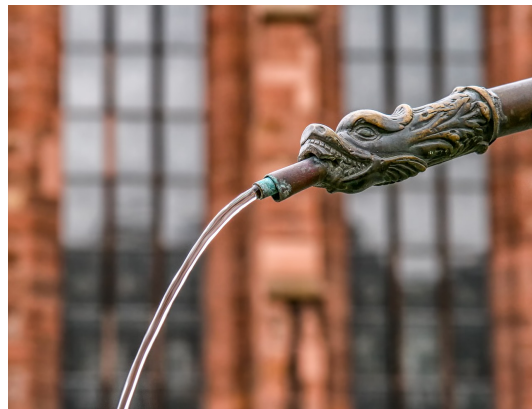
3.3 Enhancement

For future versions of this document, the shell script will be enhanced. Currently, adding a new sheet to the report is carried out manually in the shell script. It would be more comfortable to automate the procedure by copying all PRM files which contains the keyword `newvalidTrio`, copy the build directory and do a loop inside the shell script.

III. Laminar Flow

IN this third part of the document, the test cases with laminar flows are considered. Let us remind that a flow is laminar when the viscous forces dominates the inertial ones. This competition is characterized by the Reynolds number (Re) which is non-dimensional and defined as $Re = LU_0/\nu$, where L is a characteristic linear dimension, ν is the kinematic viscosity and U_0 a characteristic velocity of the system. A flow characterized by a Reynolds number under a critical value of 2000 (approximately) is considered as laminar. Beyond this value, the flow is considered as turbulent. The validation cases of turbulent flows will be considered in Part V of this document. In what follows, three academic cases are detailed:

- Poiseuille flow
- Lid driven cavity flow
- Cylinder in laminar Cross Flow for $Re = 100$



III.1

Poiseuille flow 2D with VDF and VEF meshes

1.1 Purpose

The purpose is to validate the incompressible laminar module of TrioCFD on the well-known analytical solution of Poiseuille flow in a plane channel. Thirteen test cases of Poiseuille flow exist in the TrioCFD database (poiseuille_3D, Poiseuille_flow_2D_VDF_VEF, PoiseuilleInOut2DVDFVEF_prismes, PoiseuilleInOut2DVDFPoiseuilleInOutVDFVEF, Poiseuilleperio2D, and so on ...). Here we present the test corresponding to the Poiseuille_flow_2D_VDF_VEF, for which the analytical solution writes:

$$V_x(H) = -\frac{1}{2}H^2 + 0.125$$

when a pressure drop is applied at inlet and outlet.

Validation made by : E.MOREAU (V.BARTHEL).

Report generated 11/01/2021.

1.2 Problem Description

Geometry

The geometry is a two-dimensional plane channel of dimensions $H = 0.5\text{m}$ and $L = 1\text{m}$ (see Figure)

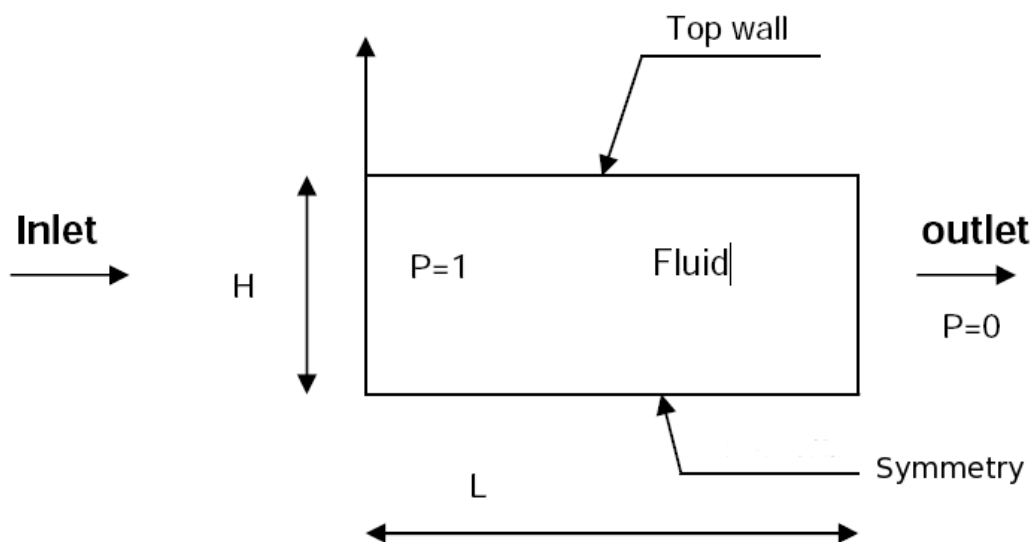


Figure III.1.1: Geometry: Dimensions and domain overview

Initial Conditions and Boundary Conditions

At the beginning of the simulation, the fluid is at rest $V_x = 0$ inside a rectangular domain where the top boundary is a fixed wall, the lower boundary is a symmetry condition and two different values of pressure are applied at the left and the right boundaries. The initial and boundary conditions are summarized below:

- Initial conditions: $V_x = 0$
- Hydraulic boundary conditions:
 - INLET pressure imposed: $P = 1$ bar
 - OUTLET pressure imposed: $P = 0$ bar
 - Top wall: fixed wall
 - Symmetry: symmetry

Fluid Properties

The fluid used in this test is fictive. The two parameters of the model are the dynamic viscosity μ and the density ρ . Their values are summarized in Table 1.

	Value
μ ($N/m^2/s$)	1.0
ρ (kg/m^3)	1.0

Table III.1.1: Physical properties

Flow Physics

At the steady state, the profile of the V_x component must fit the analytical solution (parabolic profile) with a maximum velocity for $H = 0$ and 0 for $H = 0.5$.

1.3 Case Setup

Grid

The calculations are carried out by using two meshes: the first mesh in VDF and the second one in VEF. For the VDF mesh, the 2D grid is composed of 200 cells (20×10) and for the VEF mesh, the grid is composed of 400 cells ($20 \times 10 \times 2$). Both meshes are presented on Fig. 2 (VDF) and Fig. 3 (VEF).

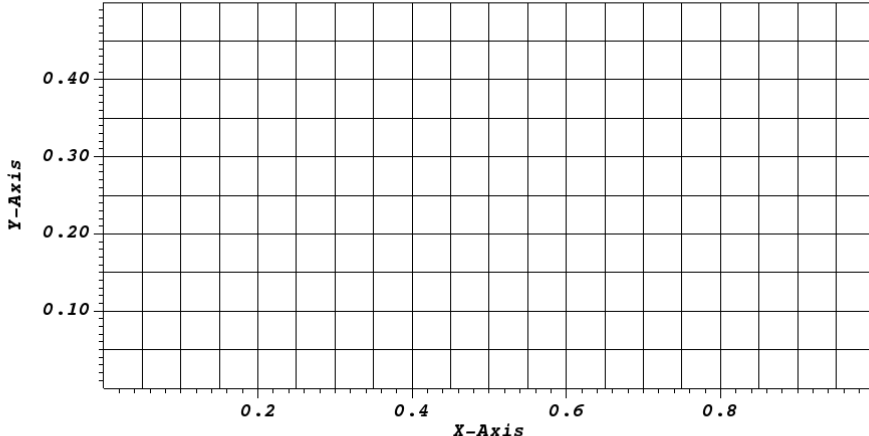


Figure III.1.2: VDF Mesh

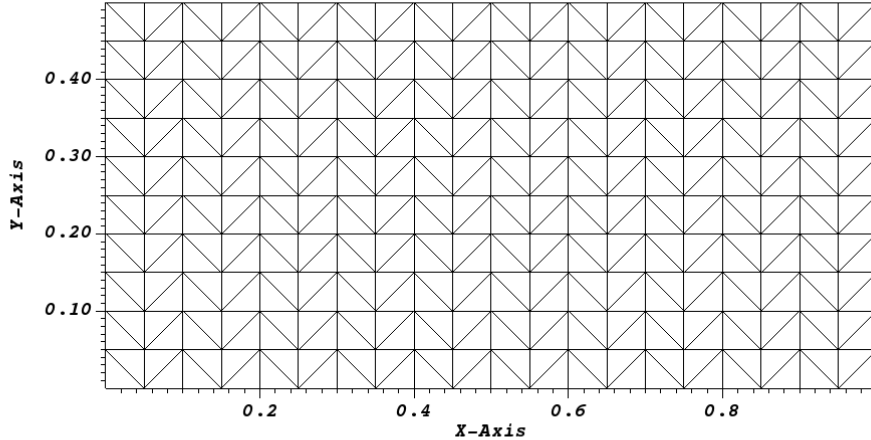


Figure III.1.3: VEF Mesh

Model Options

The case modeled here being a laminar hydraulic problem in 2D, the equations solved are those of standard Navier-Stokes.

Other Options (calculation)

The numerical results are compared with the analytical solution for five spatial discretization schemes implemented in TrioCFD: 'Amont' and 'Quick' for 'VDF' and 'Amont', 'Muscl' and 'stab' for VEF.

1.4 Results

Validation Specific Informations

- Version TRUST : 1.6.1
- Type of probem: 2D hydraulic
- Discretization: VEFPreP1B and VDF
- Time scheme: Explicit Euler
- VDF convection scheme: Quick or Amont
- VEFPreP1B convection scheme: Muscl or Amont or EF_stab ($\alpha = 1$)
- Turbulence model: none
- Type of boundary condition: inlet ; outlet
- Equations being solved: Navier_Stokes_standard
- Master Test case: poiseuille.data
- Location: /validation/share/Validation/Rapports_automatiques/Validant/Fini/Poiseuille_flow_2D_VDF_VEF
- Generated Test cases :
 - VDF/Amont/test.data :
 - VDF/Quick/test.data :
 - VEF/Amont/test.data :

→ VEF/Muscl/test.data :

→ VEF/EF_stab/test.data :

- Performance Chart :

	host	system	Total CPU Time	CPU time/step	number of cell
VDF/Amont/test	is241762.intra.cea.fr	Linux	1.04159	0.000338988	200
VDF/Quick/test	is241762.intra.cea.fr	Linux	1.10344	0.000359253	200
VEF/Amont/test	is241762.intra.cea.fr	Linux	24.9159	0.00104843	400
VEF/Muscl/test	is241762.intra.cea.fr	Linux	26.5423	0.00111611	400
VEF/EF_stab/test	is241762.intra.cea.fr	Linux	26.1092	0.00109784	400
Total			79.7124		

Table III.1.2: Performance Chart

Plot Data

- Transitory calculation time: about 2s of physical time (transitory calculation until a stationnary flow is reached).
- Average time step: $6.2 \cdot 10^{-4}$ s in VDF and $7.8 \cdot 10^{-5}$ s in VEFPreP1B.

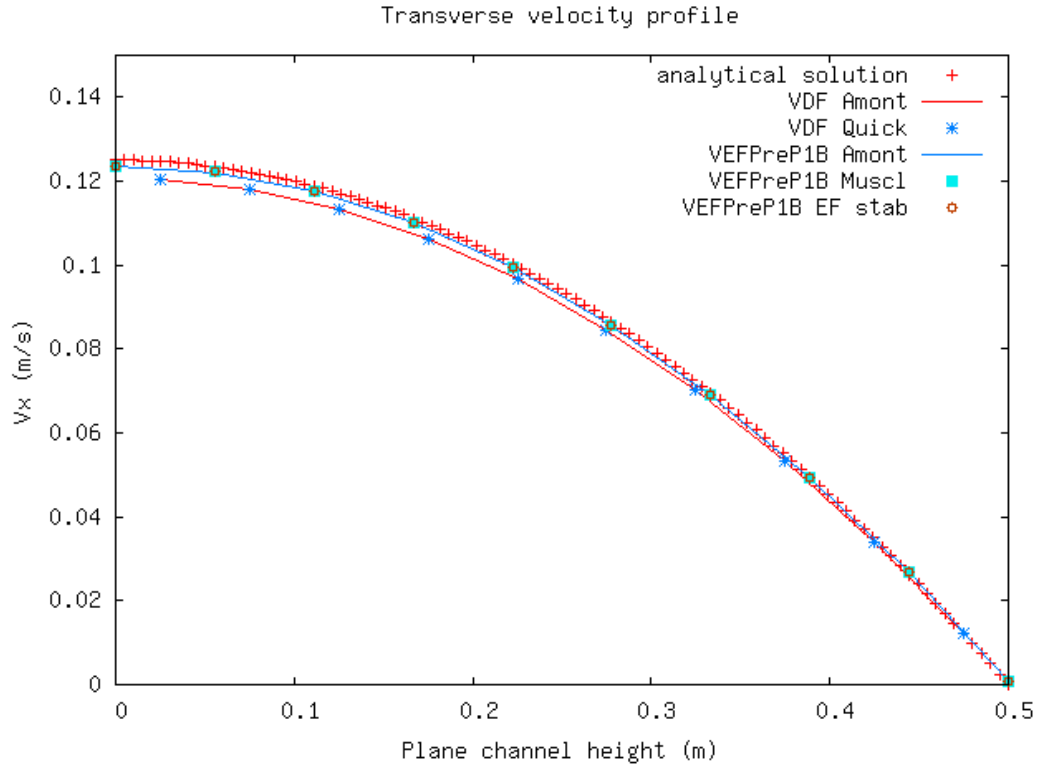


Figure III.1.4: Transverse velocity profile

1.5 Conclusion

In VEFPreP1B discretization (greatest refinement), the analytical solution is well-fitted with TrioCFD, in particular with the EF_stab scheme. The simulations give slightly different results in VDF discretization (less than 3%).

- **Recommendations for users**

The VEFPreP1B discretization associated to an EF_stab scheme gives the best results on the whole domain.

1.6 Data Files

test

```
# Hydraulique 2D : Poiseuille 2D #
# uc=DP/L/8.=0.125 m/s #
# Or a cause de la premiere et derniere demi maille #
# On trouve uc=0.125/0.95=0.131 #
dimension 2
Pb_hydraulique pb
Domaine dom
Mailler dom
{
    Pave Entrée
    {
        Origine 0. 0.
        Nombre_de_Noeuds 21 11
        Longueurs 1 0.5
    }
    {
        bord Entrée X = 0. 0. <= Y <= 0.5
        bord Haut Y = 0.5 0. <= X <= 1.0
        bord Bas Y = 0. 0. <= X <= 1.0
        bord Sortie X = 1.0 0. <= Y <= 0.5
    }
}
# VDF dis #
VDF dis
Schema_Euler_explícite sch
Read sch
{
    tinit 0
    tmax 5000.
    dt_min 0.0001
    dt_max 1.0
    dt_impr 0.0001
    dt_sauv 100
    seuil_statio 1.e-8
}
Fluide_Incompressible fluide
Read fluide
{
    mu Champ_Uniforme 1 1.
    rho Champ_Uniforme 1 1.
}
Champ_Uniforme gravite
Read gravite 2 0 0
Associate pb dom
Associate pb sch
Associate pb fluide
Discretize pb dis
```

```

Read pb
{
  Navier_Stokes_standard
  {
    solveur_pression GCP {
      precond_ssor { omega 1.650000 }
      seuil 1.000000e-16
      impr
    }
    convection { amont }
    diffusion { }
    conditions_initiales {
      vitesse Champ_Uniforme 2 0. 0.
    }
    boundary_conditions {
      Haut paroi_fixe
      Bas symetrie
      Entrée frontiere_ouverte_pression_imposee Champ_Front_Uniforme 1 1.
      Sortie frontiere_ouverte_pression_imposee Champ_Front_Uniforme 1 0.
    }
  }
  Postraitemt
  {
    format lata
    Sondes
    {
      seg_P pression periode 0.1 segment 10 0 0.25 1 0.25
      seg_U1 vitesse periode 0.1 segment 10 0.5 0.025 0.5 0.475
      sonde_pression pression periode 0.1 points 1 0.5 0.425
      sonde_vitesse vitesse periode 0.1 points 1 0.5 0.425
    }
    Champs dt_post 1.0
    {
      pression elem
      pression som
      vitesse elem
      vitesse som
    }
  }
  Solve pb
  Fin
  Fin
}

```

2D Lid driven cavity test

2.1 Purpose

The purpose is to check a new time scheme implementation with the 'implicit_steady' solver using a dual time step in order to reach faster the steady state solution. The new time scheme 'Implicit_Euler_steady_scheme' can be seen as a modification of the 'Euler_Implicit' option (i.e. implicit solver) but with a time step varying inside the domain. The velocity profiles that are obtained with those two time schemes of TrioCFD are superimposed with the Fluent solution and the solutions of references [1] and [2].

Validation made by : MA PUSCAS.

Report generated 11/01/2021.

2.2 Problem Description

The lid-driven cavity test is a well-known benchmark test for checking the incompressible Navier-Stokes solvers in laminar condition.

Geometry

The cavity is a two-dimensional square of size 1m.

Initial Conditions and Boundary Conditions

At initial time, the fluid is at rest inside the cavity (i.e. $\mathbf{V} = \mathbf{0}$). The upper horizontal wall has a non zero x -velocity whereas the 'no-slip boundary condition' is imposed for the three other walls (i.e. the lower horizontal wall and the two vertical ones).

Fluid Properties

Only two parameters are involved in the simulation: the density $\rho = 1$ and the dynamic viscosity $\mu = 0.01$.

Flow Physics

Under the combined influence of the moving upper horizontal wall and the fluid viscosity, the fluid starts to flow inside the cavity. The direction of rotation is clockwise. When the steady state is reached, the V_x and V_y profiles are compared with the reference solutions.

2.3 Case Setup

Grid

The mesh is presented on Fig. 1 (with Visit).

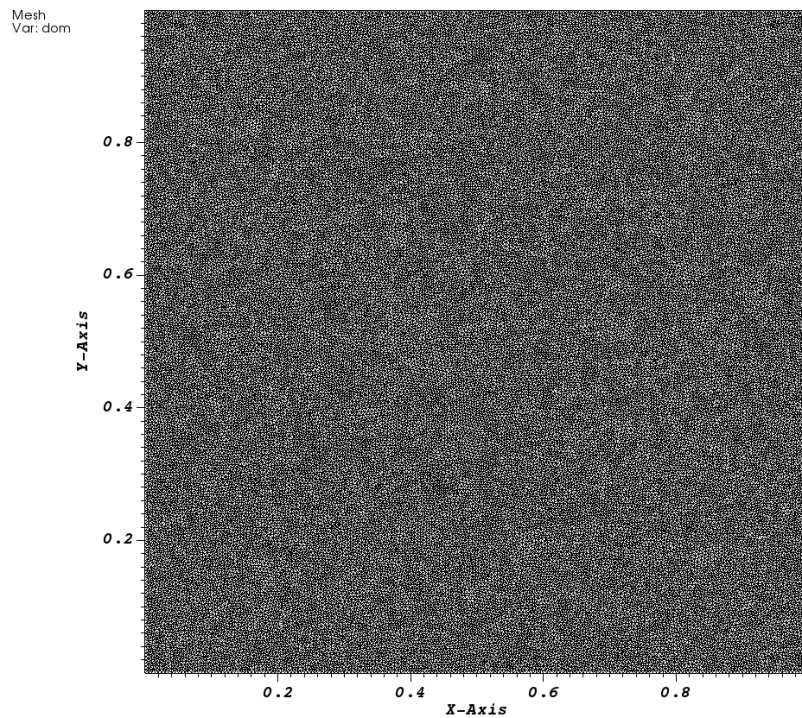


Figure III.2.1: MESH

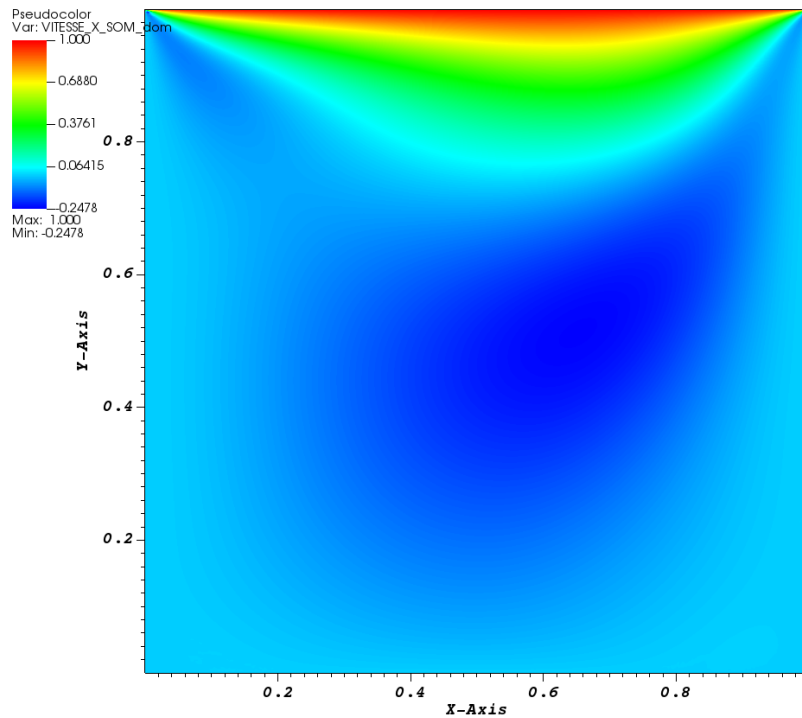


Figure III.2.2: VITESSE_X SOM

Other Options (calculation)

TrioCFD is run with the numerical options that are summarized in Section 4.1.

2.4 Results

Validation Specific Informations

- Version TRUST : 1.7.3
- Type of problem: Steady Navier-Stokes
- Discretizations: VEFPreP1B
- Type of meshes: Triangles
- Pressure solver: GCP with SSOR preconditioneur
- Time scheme: Implicit_Euler_steady_scheme with Solveur implicit_steady
- Convection scheme: amont
- Generated Test cases :
 - Steady/defilante.data : /*jdd en annexe*/
- Performance Chart :

	host	system	Total CPU Time	CPU time/step	number of cell
Steady/defilante	is241762.intra.cea.fr	Linux	3278.71	9.33988	105724

Table III.2.1: Performance Chart

Plot Data

- Convergence

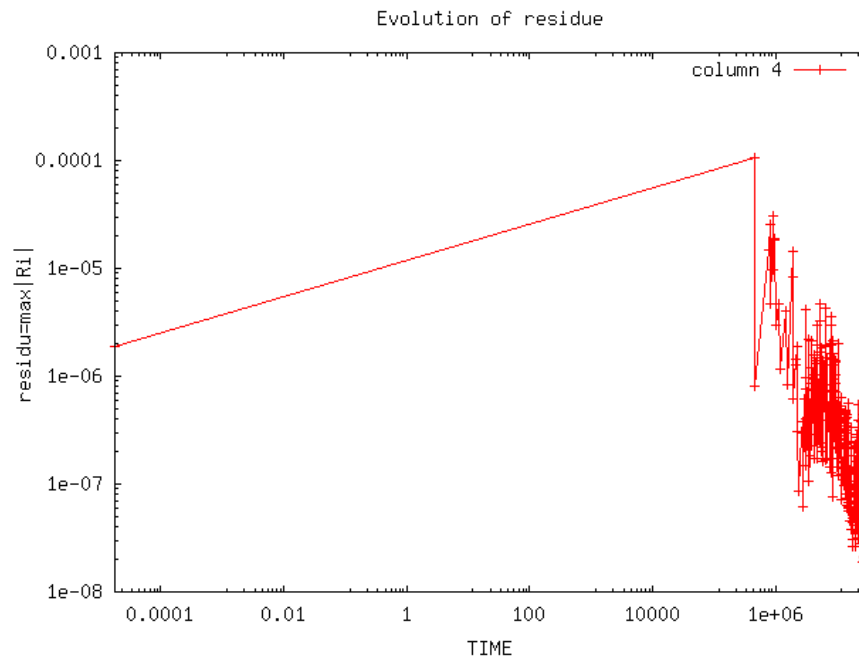


Figure III.2.3: Evolution of residue

- V_x - and V_y -profiles

The V_x - and V_y -profiles are plotted respectively with respect to the y - and x -positions on Figs. 4 and 5. Here after the 'reference solution TrioCFD' is the 'Euler_Implicit' solution.

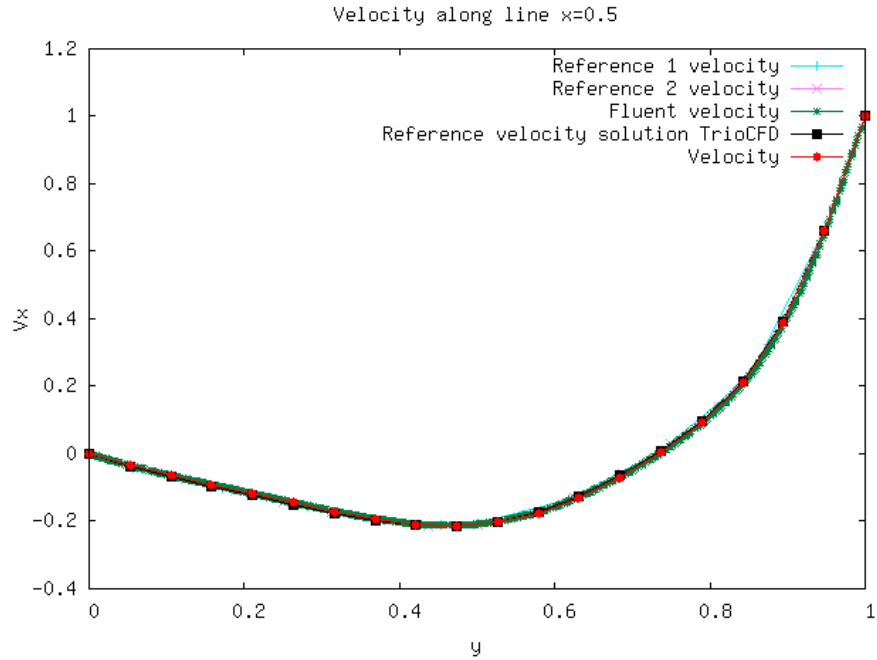


Figure III.2.4: Velocity along line $x=0.5$

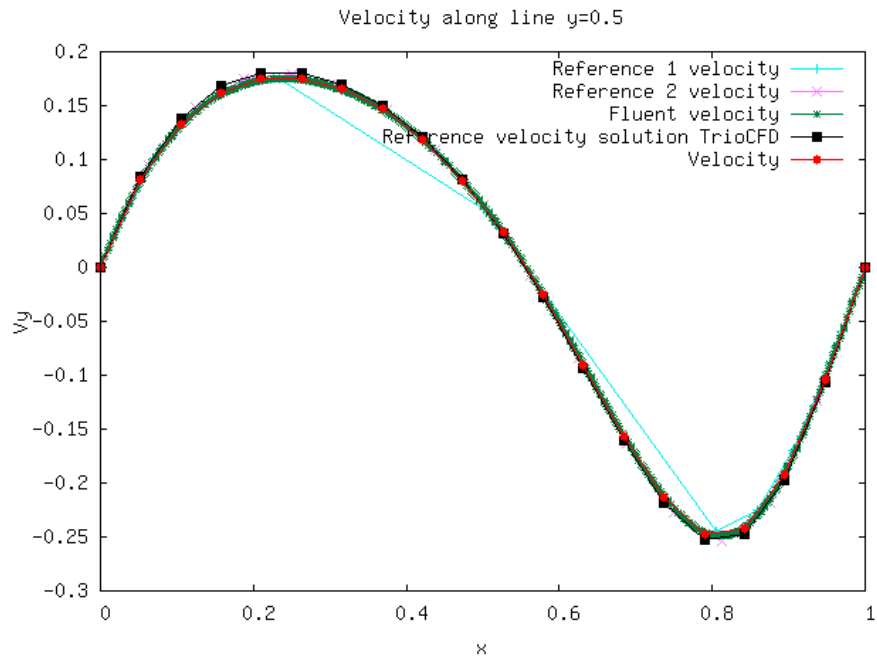


Figure III.2.5: Velocity along line $y=0.5$

- CPU table

	nb_iter
New time scheme	350
Reference solution	3202

Table III.2.2: CPU informations for new and reference solutions

2.5 Conclusion

The time scheme option 'Implicit_Euler_steady_scheme' of TrioCFD reproduces the steady state solution that is obtained with the original time scheme 'Euler_Implicit' but by considerably decreasing the number of time steps required for the transient phase. The both TrioCFD solutions are in perfect agreement with the Fluent solution and with the solutions from two references of the literature. For this test case, the CPU times (in seconds) were equal to 1) 42269s for the 'Euler_Implicit' scheme, 2) 6241s for the 'Implicit_Euler_steady_scheme', and 5196s for Fluent.

2.6 References

- 1 U. Ghia, and K. N. Ghia, and C. Shin, 'High-Re solutions for incompressible flow using the Navier-Stokes equations and a multigrid method', Journal of Computational Physics, 48, pp. 387-411, 1982.
- 2 C. H. Marchi, and R. Suero, and L. K. Araki, 'The lid-driven square cavity flow: numerical solution with a 1024 x 1024 grid', Journal of the Brazilian Society of Mechanical Sciences and Engineering, 3:186-198, 2009.

2.7 Data Files

defilante

```
# Hydraulique 2D : Paroi defilante #
# PARALLEL OK 5 #
dimension 2
Pb_Hydraulique pb
Domaine dom
# BEGIN MESH #
Lire_med family_names_from_group_names dom square square.med
# END MESH #
# BEGIN PARTITION
Partition dom
{
    Partitionneur metis { Nb_parts 4 }
    Larg_joint 2
    Nom_Zones DOM
}
End
END PARTITION #
# BEGIN SCATTER
Scatter DOM.Zones dom
END SCATTER #
VEFpreP1b dis
Implicit_Euler_steady_scheme sch
Read sch
{
    tinit 0.
    nb_pas_dt_max 350
    dt_min 1.e-16
```

```

dt_max 1.e+06
dt_impr 0.01
dt_sauv 1.e+06
seuil_statio 1.e-8
facsec 1
steady_security_facteur 10
steady_global_dt 1
Solveur implicit_steady {
    solveur gmres { diag seuil 1.e-13 controle_residu 1 nb_it_max 3 }
}
}
Fluide_Incompressible fluide
Read fluide
{
    mu Champ_Uniforme 1 0.01
    rho Champ_Uniforme 1 1.
}
Champ_Uniforme gravite
Read gravite 2 0 -9.81
Associate fluide gravite
Associate pb dom
Associate pb sch
Associate pb fluide
Discretize pb dis
Read pb
{
    Navier_Stokes_standard
    {
        solveur_pression GCP {
            precond ssor { omega 1.500000 }
            seuil 1.000000e-16
        }
        convection { amont }
        diffusion { }
        initial_conditions {
            vitesse Champ_Uniforme 2 0. 0.
        }
        boundary_conditions {
            Upper paroi_defilante Champ_Front_Uniforme 2 1. 0.
            Lower paroi_fixe
            Outlet paroi_fixe
            Inlet paroi_fixe
        }
    }
}
Post_processing
{
    Probes
    {
        sonde_pression_1 pression periode 1.e+06 segment 10 0. 0. 1 0.
        sonde_pression_2 pression periode 1.e+06 segment 10 0. 0.5 1 0.5
        sonde_pression_3 pression periode 1.e+06 segment 10 0. 1 1 1
        sonde_pression_4 pression periode 1.e+06 segment 10 0.5 0. 0.5 1
        sonde_vitesse_x_1 vitessex periode 1.e+06 segment 10 0. 0. 1 0.
        sonde_vitesse_x_2 vitessex periode 1.e+06 segment 10 0. 0.5 1 0.5
        sonde_vitesse_x_3 vitessex periode 1.e+06 segment 10 0. 1 1 1
        sonde_vitesse_x_4 vitessex periode 1.e+06 segment 20 0.5 0. 0.5 1
        sonde_vitesse_y_1 vitessey periode 1.e+06 segment 10 0. 0. 1 0.
        sonde_vitesse_y_2 vitessey periode 1.e+06 segment 20 0. 0.5 1 0.5
        sonde_vitesse_y_3 vitessey periode 1.e+06 segment 10 0. 1 1 1
        sonde_vitesse_y_4 vitessey periode 1.e+06 segment 10 0.5 0. 0.5 1
    }
}

```

```
Format lata
fields dt_post 1.e+06
{
    pression elem
    pression som
    vitesse elem
    vitesse som
}
}
sauvegarde_simple binaire Cas.sauv
}
Solve pb
End
End
```

Cylinder in Laminar Cross Flow

3.1 Purpose

The purpose of the validation is to compare numerical values of an oscillating flow behind a circular cylinder perpendicular to the flow with those obtained by calculations and experiments.

Validated model:

- No-slip wall
- 2D channel
- Disturbance of a laminar flow

Validation with: Calculations N3S of Chabard [1] and experiments of Braza et al. [2]

Validation made by : E. MOREAU (S. VANDROUX).

Report generated 11/01/2021.

3.2 Problem Description

In order to observe the disturbances generated by a circular obstacle in an initially laminar flow, we define here a rectangular channel having at mid-height a hole which will correspond to the obstacle. The geometric dimensions of these different elements are given below as well as the conditions necessary for the establishment of the initial laminar flow at the beginning of the transient.

Geometry

In the following scheme, $L = 0.635\text{m}$; $W = 0.1524\text{m}$ and $d = 0.0254\text{m}$

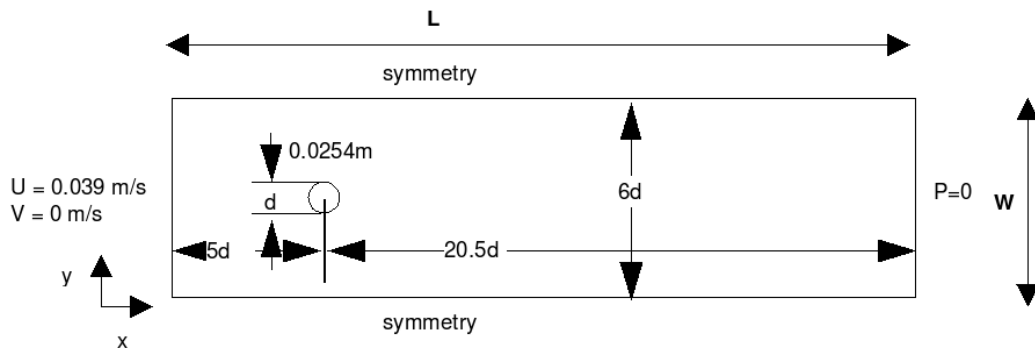


Figure III.3.1: Geometry

Initial Conditions and Boundary Conditions

Hydraulic initial conditions: quiescent fluid $U = V = 0 \text{ m/s}$

Hydraulic boundary condition:

- The X-velocity is imposed in order to obtain $U = 0.03937\text{m/s}$ so that $\text{Re} = Ud/\nu = 100$

- CERCLE : paroi_fixe
- PAROI1 : symetrie
- PAROI2 : symetrie
- SORTIE : frontiere_ouverte_pression_imposee Champ_Front_Uniforme 1 0.0
- SORTIE : frontiere_ouverte_vitesse_imposee Champ_Front_Uniforme 2 0.03937 0.0

Fluid Properties

The fluid used in this test is fictive with the following properties :

	Value
ρ (kg/m^3)	1.33
μ ($\text{N}/\text{m}^2/\text{s}$)	1e-05
Re	100.0

Table III.3.1: Physical properties of the fictitious fluid

Flow Physics

At the beginning of the transient, fluid flow is completely laminar with the Reynolds number equal to 100. In view of the characteristics defined for the fluid, this flow will be quickly disturbed by the obstacle present in the mid-height of the channel.

3.3 Case Setup

Grid

The mesh was built with gmesh and has 9668 elements. It is a tetraedric mesh, homogeneous over most of the domain with a refinement around the central obstacle in order to capture the formation of the boundary layer around the cylinder induced by the adverse pressure gradient. This refinement will optimize the recirculation phenomena around the cylinder and reveal the development of turbulence in an initially laminar flow.

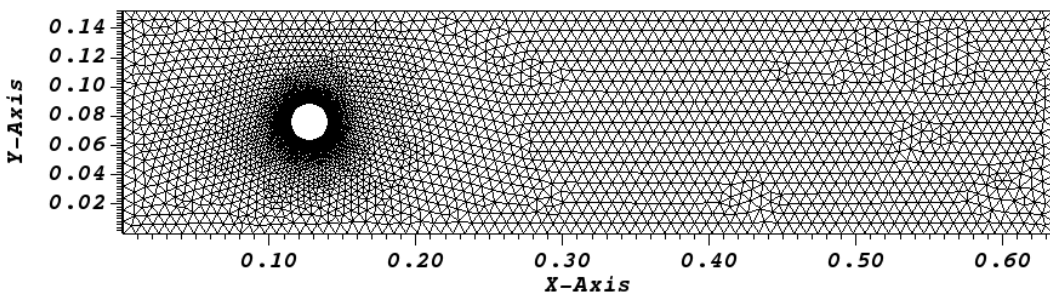


Figure III.3.2: Mesh overview

Triangle layer with 200 points around the circle

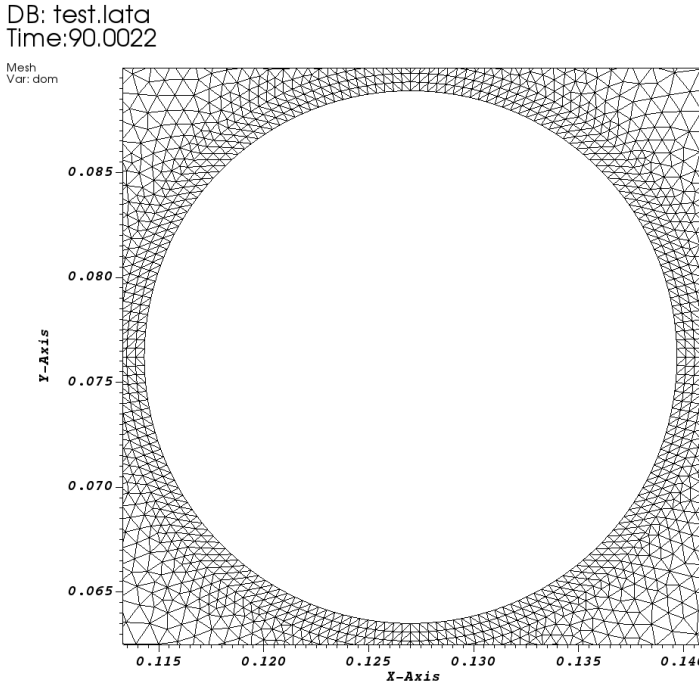


Figure III.3.3: Zoom of the vicinity of the cylinder

Model Options

- The case modeled here being a laminar hydraulic problem, the equations solved are those of standard Navier-Stokes.
- Momentum convection scheme: EF_stab with $\alpha = 0.2$ or Muscl.
- Diffusion scheme: default

Other Options (calculation)

- The time scheme defined in this test case is the Explicit Euler with implicit diffusion. Indeed, **the Euler implicit scheme is not recommended** because, as the calculation presents oscillations, the value of the facsec coefficient must remain small. The calculation time is then increased instead of being improved.
- The pressure variable to be employed in the data file is not 'Pression' but 'Pression_Pa', that gives the pressure in Pa.

3.4 Results

Validation Specific Informations

- Version TRUST : 1.6.1
- Type of problem: 2D laminar hydraulic_problem
- Discretization: VEFPreP1B
- Time scheme: Explicit Euler for VDF and VEF
- Momentum convection scheme: EF_stab with $\alpha = 0.2$ or Muscl
- Solving of equations: Navier_Stokes_standard
- Master Test case: cc_re100.data

- Location: validation/share/Validation/Rapports_automatiques/Validant/Fini/Cir_Cyl_Re100
- Generated Test cases :
 - EI/Muscl/test.data :
 - EI/EF_stab02/test.data :
- Performance Chart :

	host	system	Total CPU Time	CPU time/step	number of cell
EI/Muscl/test	is241762.intra.cea.fr	Linux	3060.54	0.0906818	9668
EI/EF_stab02/test	is241762.intra.cea.fr	Linux	2820	0.08271	9668
Total			5880.54		

Table III.3.2: Performance Chart

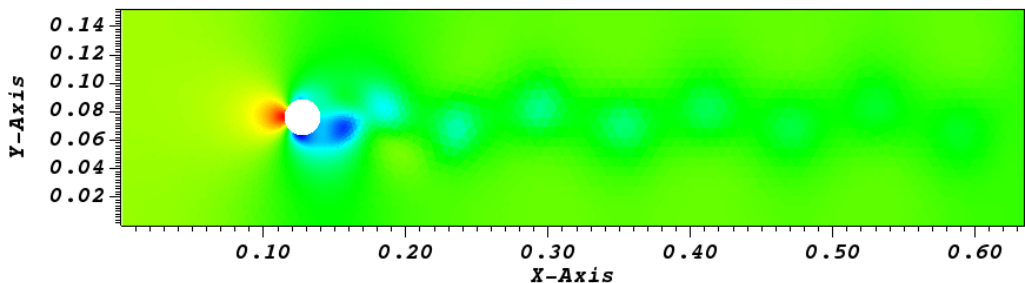
Plot Data

The temporal pressure evolution at two probes located on the cylinder surface ($y = -0.5d$ and $y = +0.5d$) is shown in the following figure for each convection scheme. The simulations have been performed up to 90s of physical time in order to get sufficient cycles allowing the calculation of a frequency.

• Von Karman vortices

When a viscous Newtonian fluid flows around a cylinder, the latter is subjected to forces from the surrounding fluid and complex Reynolds number-dependent phenomena appear. Near the surface of the cylinder wall in contact with the flow, a thin layer of viscous fluid (boundary layer) forms. In this, a speed gradient is established due to viscous stresses which are not negligible. The closer the fluid is to the wall, the more braked, the speed being zero at the surface of the cylinder to satisfy the condition grip. This redistribution in the velocity field leads to a diffusion of the momentum, either by a viscous mechanism or by turbulent movements induced by vortex detachment.

At a specific point, the friction is canceled out and the boundary layer lifts off the wall; this is the point of separation. This separation is not due to the singularity in the geometry, as it would have been the case for a square cylinder, but to the fact that the boundary layer develops in the presence of a pressure gradient that we can observe in the following figure in the pressure field of the domain.

Figure III.3.4: Pressure fields at $t = 90s$

When this pressure gradient is large enough, the speed fluid particles will decrease until they become zero then negative and the separation of the boundary layer occurs.

Behind the cylinder, we can see the development of Karman vortex street caused by a vortex shedding. The characteristics of the fictitious fluid examined here as well as the Reynolds number were established in this academic test case in order to reveal these instabilities.

The boundary layer fluid reaches the detachment area around $\pm \frac{\pi}{2}$ and when its kinetic energy is insufficient to pass further downstream of the cylinder where the pressure is greater, the fluid tends to take off thus

generating a recirculation vortex. This vortex, after reaching a certain size, detaches itself from the layer limit and is convected in the wake. The downstream flow then takes shape of a vortex path and the boundary layer peels off from the cylinder wall.

The wake of the flow will be different depending on the Reynolds number. For $Re = 100$, which will correspond to the case modeled here, the wake of the flow becomes asymmetric and unstable. This gives rise to the phenomenon of vortex detachment: vortices form on each side of the cylinder and are alternately convected in the wake forming a street of laminar vortices, called Von Karman vortices. This detachment is done periodically and two-dimensional, that is to say that the detachment does not take place in the transverse direction (Williamson [3]).

We can observe the establishment of this type of vortex in the figure below.

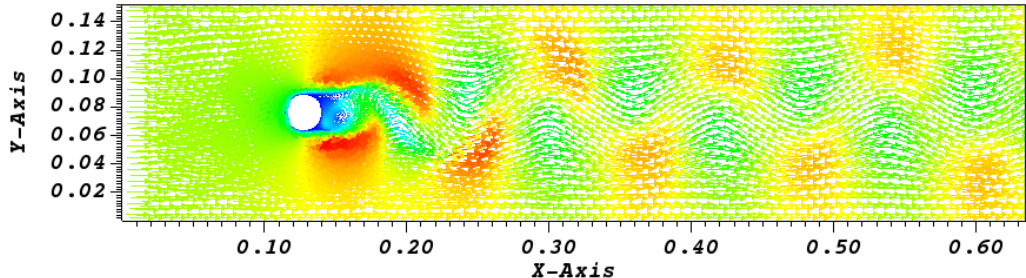


Figure III.3.5: Velocity vectors at $t = 90s$

• Pressure evolution at the cylinder surface

It can be seen that the time of stabilization of the oscillations is of about 40s. From this instant, an oscillation frequency can be determined.

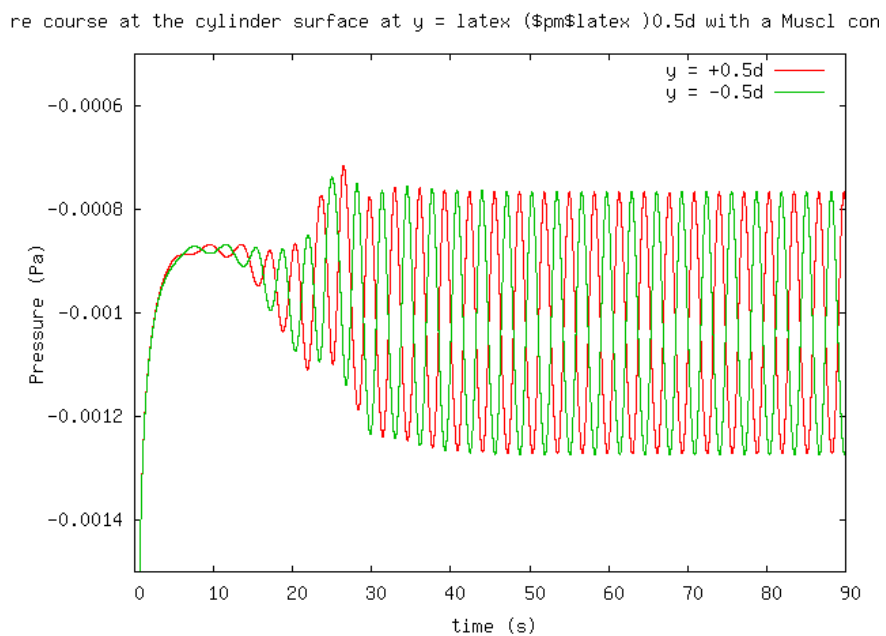


Figure III.3.6: Pressure course at the cylinder surface at $y = \pm 0.5d$ with a Muscl convection scheme

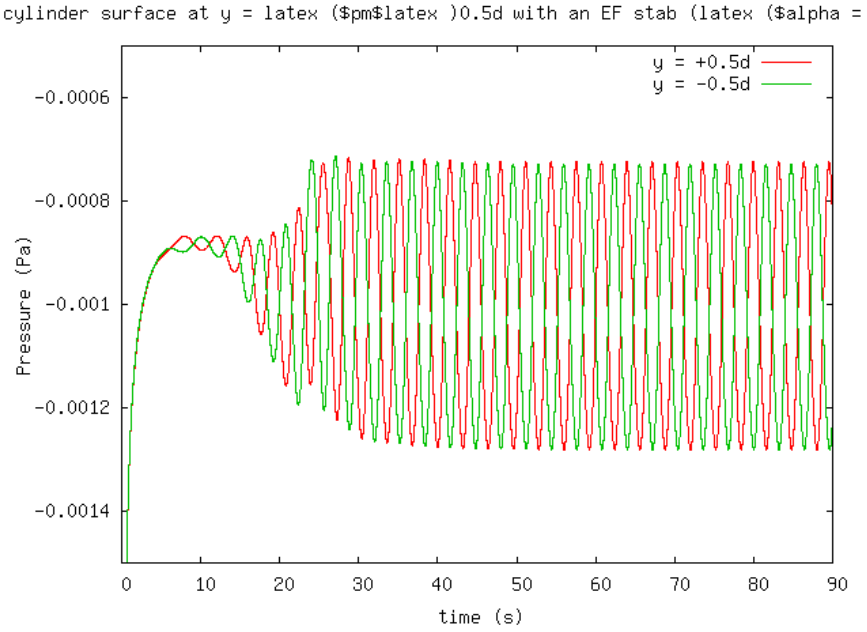


Figure III.3.7: Pressure course at the cylinder surface at $y = \pm 0.5d$ with an EF_stab ($\alpha = 0.2$) convection scheme

The two following figures represent a zoom of the two previous figures from 40 up to 50s. We can notice that oscillations are well established in this time range.

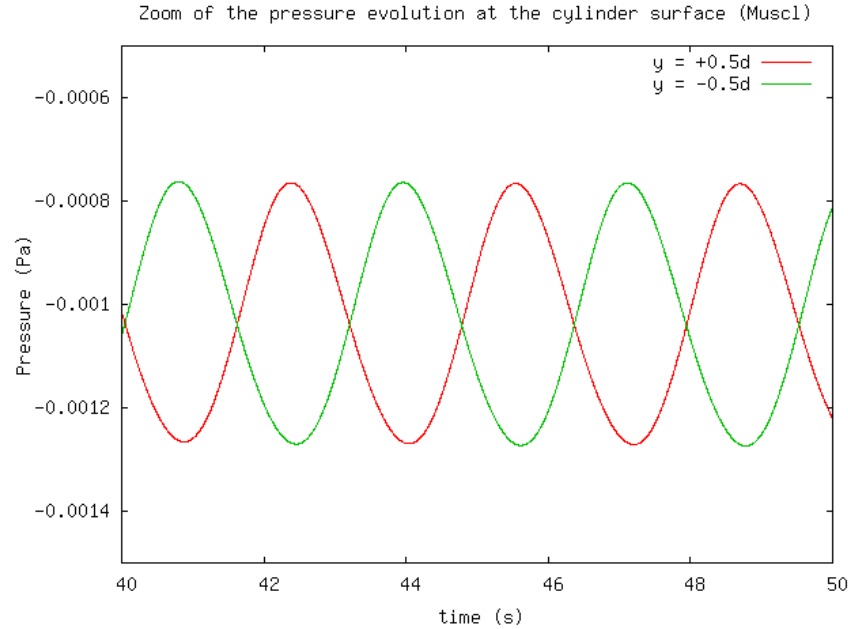


Figure III.3.8: Zoom of the pressure evolution at the cylinder surface (Muscl)

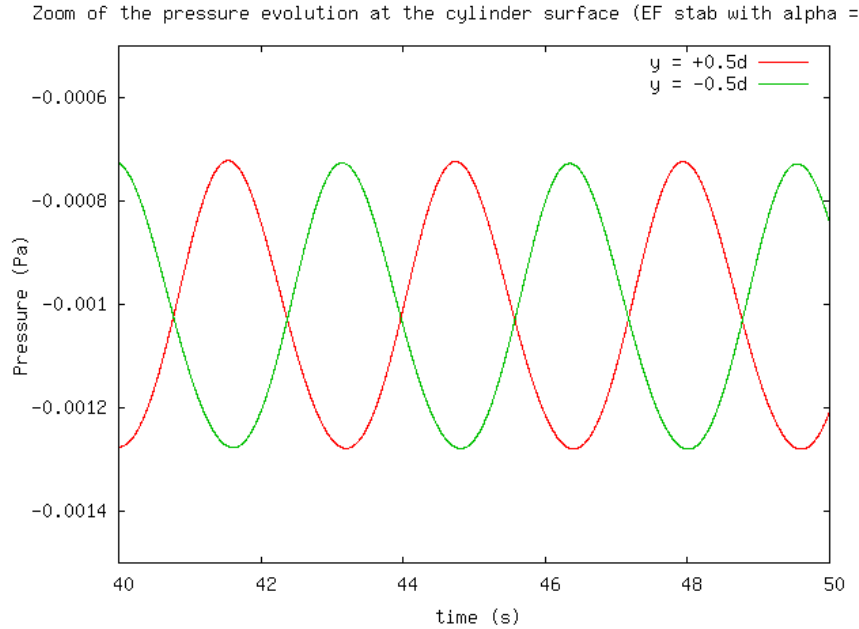


Figure III.3.9: Zoom of the pressure evolution at the cylinder surface (EF_stab with alpha = 0.2)

• Comparison of Strouhal numbers

The temporal pressure evolution in the media allows the determination of the Strouhal number S_t defined as $S_t = \frac{f \cdot d}{U}$, where f stands for the vortices emission frequency, U the undisturbed velocity (in our case the inlet velocity), and d the cylinder diameter. We can in this way compare the simulation values with those of Tritton and Roshko collected by Chabard [1].

	Frequency (Hz)	Strouhal Number	Error % (Tritton)	Error % (Roshko)
Tritton	0.243	0.157	0	6
Roshko	0.259	0.167	6	0
Muscl	0.316	0.204	23.096	18.198
EF_stab ($\alpha = 0.2$)	0.313	0.202	22.13	17.17

Table III.3.3: Comparison of Strouhal numbers

Variations in the Strouhal number are associated with changes in the flow structure as described by Blevins [4]. For flow around a circular cylinder at $Re \sim 40 - 3 \times 10^7$, Williamson [5], Roshko [6] and Schewe [7] observed experimentally that the Strouhal number is close to the value 0.2.

In the case we are modeling here, the value of the Reynolds number is included in this interval ($Re = 100$) and we note that the Strouhal number obtained numerically is equal to 0.2 to 10^{-3} .

• Mean Pressure

The distribution of the mean pressure along the cylinder surface (averaged from 40s up to 90s) is shown and compared to values of N3S [1] and Braza [2]

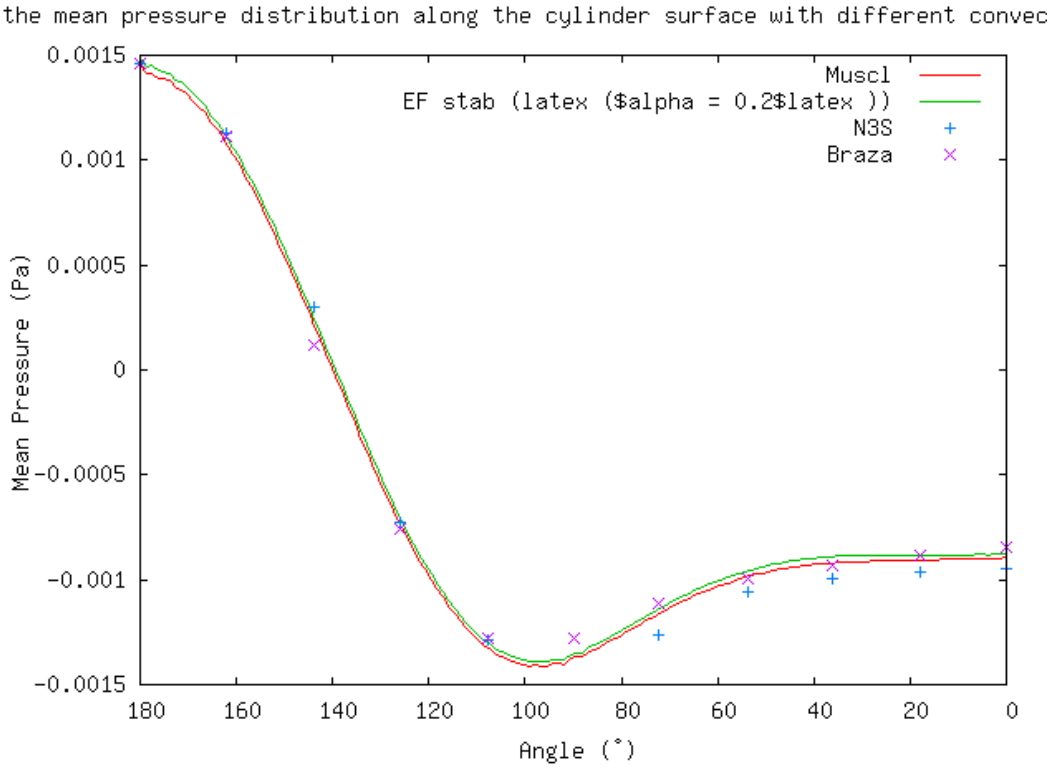


Figure III.3.10: Comparison of the mean pressure distribution along the cylinder surface with different convection and time schemes

3.5 Conclusion

The computation of this test with TrioCFD is satisfactory with a good agreement between calculated results with others numerical results by Chabard [1] and experimental results described by Braza [2].

The calculation ends normally without any particular numerical troubles.

This simulation enables the validation of laminar calculations with Trio-CFD of an oscillating flow behind a cylinder with isothermal fluid and VEF grids.

3.6 References

- [1] Chabard J.P, Lalanne P., Metivet B., Projet N3S de Mecanique des fluides. Cahier de Validation 2D. EDF/DER HE-41/88.08 1988.
- [2] Braza P., Chassaing P., H. Ha Minh, Numerical study and physical analysis of pressure and velocity fields in the near wake of a circular cylinder. J. Fluid Mech. 165, 79-130, 1986
- [3] Williamson C. H. K., Oblique and parallel modes of vortex shedding in the wake of a circular cylinder at low reynolds number. J. of Fluid Mech. 31(11), 3165-3168, 1988
- [4] Blevins R.D., Flow-Induced Vibration, deuxieme edition, 1990
- [5] Williamson C. H. K., Oblique and parallel modes of vortex shedding in the wake of a circular cylinder at low reynolds number. J. of Fluid Mech. 31(11), 3165-3168, 1988
- [6] Roshko A., Experiments on the flow past a circular cylinder at very high reynolds number. J. of Fluid Mech. 10 (3), 345-356, 1961

- [7] Schewe G., On the force fluctuations acting on a circular cylinder in crossflow from subcritical up to transcritical reynolds numbers. J. of Fluid Mech., 133, 265-285, 1995

3.7 Data Files

test

```
# Hydraulique 2D laminaire schema centre #
dimension 2
Pb_hydraulique pb
Domaine dom
# Read_file dom Cir_Cyl.geom #
Read_file dom ../../geometry.geom
VEFPreP1B dis
Schema_Euler_Explicite sch
Read sch
{
    tinit 0.0
    tmax 90.0
    dt_min 1.e-6
    dt_max 1.e-1
    dt_impr 0.1
    dt_sauv 10.0
    seuil_statio 1.e-8
    facsec 1.
    diffusion_ implicite 1
}
Fluide_Incompressible air
Read air
{
    mu Champ_Uniforme 1 1.00e-5
    rho Champ_Uniforme 1 1.33
}
#
# nu = mu/rho = 7.518e-6
# Reynolds 100
#
Associate pb dom
Associate pb sch
Associate pb air
Discretize pb dis
    imprimer_flux dom { CERCLE }
Read pb
{
    Navier_Stokes_standard
    {
        solveur_pression Gcp { precond ssor { omega 1.6 }
                                seuil 1.e-9
                                impr
        }
        convection { muscl }
        diffusion { }
        conditions_initiales
        {
            vitesse Champ_Uniforme 2 0. 0.
        }
        boundary_conditions
        {
            CERCLE paroi_fixe
            PAROI1 symetrie
        }
    }
}
```

```

PAROI2 symetrie
SORTIE frontiere_ouverte_pression_imposee
    Champ_Front_Uniforme 1 0.0
ENTREE frontiere_ouverte_vitesse_imposee
    Champ_front_Uniforme 2 0.03937 0.0
}

{
Postraitemet
{
Definition_champs {
    Pmoy Moyenne {
        t_deb 40 t_fin 89 source refChamp { Pb_champ pb Pression_Pa }
    }
}
Sondes
{
    sonde_pression pression periode 1.e-6 points 4 0.1142 0.0762
                                            0.1398 0.0762
                                            0.1270 0.0890
                                            0.1270 0.0634
    sonde_Pmoy1 Pmoy Periode 10 Circle 150 0.127 0.0762 0.0127 180 0
    sonde_Pmoy2 nodes Pmoy Periode 10 Circle 150 0.127 0.0762 0.0127 180 0
    sonde_Pmoy3 grav Pmoy Periode 10 Circle 150 0.127 0.0762 0.0127 180 0
}
Format lata
    Champs dt_post 30.0
{
    pression som
        Pression_Pa elem
    vitesse som
    vitesse elem
}
}
}
Solve pb
End
sonde_Pmoy Pmoy Periode 10.5 Circle 150 0. 0. 0.0127 0 180
reprise formatte ./sauv/circ_cyl_100_pb.sauv
imprimer_flux dom { CERCLE }
Cholesky { impr }
Gcp { precond ssor { omega 1.5 }
        seuil 1.e-14
        impr
}
GCP_ssor { omega 1.65 seuil 1.e-6 impr }

```

IV. Thermal Laminar Flow

COMPARED to the previous part, the phenomena considered here will involve thermal aspects and, in particular, the flow is still laminar.

The first validation sheet of this category corresponds to the **Vahl Davis** benchmark, which is one of the most known test case for checking the coupling between the convective and thermal phenomena. The second one **Oscillatory convection flow** is very similar to the Vahl Davis test case but this time, the cavity and therefore the flow are no longer symmetrical.



Convection Vahl Davis

1.1 Purpose

The Vahl Davis benchmark is one of the well known test case for checking the coupling between flow and thermics in laminar condition. The coupling between the Navier-Stokes equations and the temperature one is carried out with the Boussinesq approximation.

The validations are presented for three meshes: the first one for the VDF discretization and the two other for the VEF discretization (one coarse and another one fine).

Validation made by : E. MOREAU (S. VANDROUX).

Report generated 11/01/2021.

1.2 Problem Description

Geometry

The geometry is a square domain of dimensions 1mx1m.

Initial Conditions and Boundary Conditions

The initial and boundary conditions must be imposed for temperature equations and fluid flow equations:

- For temperature equation, Dirichlet boundary conditions are applied on the vertical walls $T(x=0)=300.5\text{K}$, $T(x=1)=299.5\text{K}$ and zero flux on the two other boundaries (horizontal walls). As initial condition, a temperature gradient is imposed such as: $T = -x + 300.5$ (in K).
- For fluid flow equations, the initial condition is a uniform velocity $\mathbf{V} = \mathbf{0}$ m/s and no-slip boundary conditions (walls) are applied on all boundaries.

Fluid Properties

In the incompressible Navier-Stokes model, the parameters in the equation of impulsion balance equation are the dynamic viscosity μ , the density ρ and the thermal expansion coefficient β_{th} . In the temperature equation, the parameters are the thermal conductivity and the specific heat C_p . For physical problem involving a coupling between fluid flow and thermics, a dimensionless number, the Rayleigh is defined such as: $Ra = \frac{\rho \beta_{th}}{\nu D} (T_{\Gamma_1} - T_{\Gamma_3}) H^3$ where ν is the kinematic viscosity, D is thermal diffusivity and H is the domain size. The values of those parameters are summarized in Table 1.

	Value
ρ (kg/m^3)	1186.78
μ ($\text{N}/\text{m}^2/\text{s}$)	1.0
λ ($\text{W}/\text{m}/\text{K}$)	1.0
C_p ($\text{J}/\text{kg}/\text{K}$)	0.71
β_{th}	1.0
Ra	1000000.0

Table IV.1.1: Physical properties

Flow Physics

A fluid, initially at rest inside a square box is heated at the left vertical wall and cooled at the right vertical wall. Under the influence of combined effects of the temperature gradient and the gravity, the fluid begins to turn inside the box. The velocity is upward at the left wall and downward at the right.

1.3 Case Setup

Grid

The simulations with TrioCFD are run for three two-dimensional meshes: the first one for the VDF discretization and the two other ones for the VEF discretization (one coarse and another one fine). The VDF mesh, presented on Fig. 1 is composed of 4761 square cells for an area of 1m by 1m. The VEF meshes are respectively composed of 1444 triangular cells, (coarse mesh obtained with option Trianguler_H) and 6084 triangular cells (fine mesh, obtained with option Trianguler_H) for the same area. They are both presented on Figs. 1 and 2.

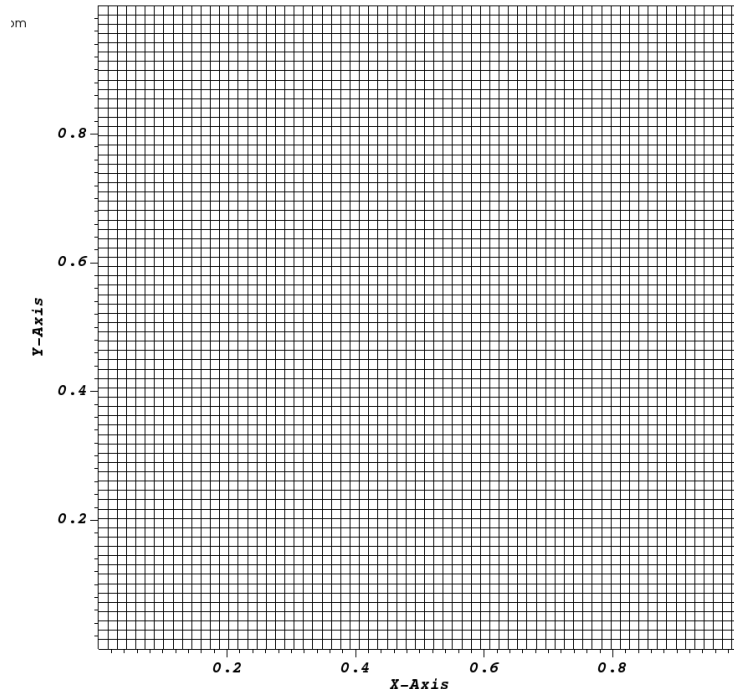


Figure IV.1.1: 2D VDF Mesh

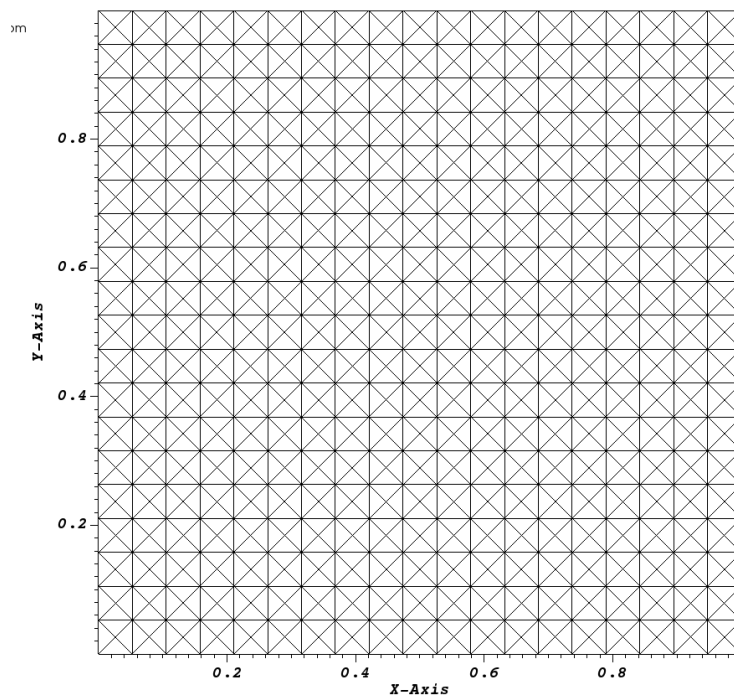


Figure IV.1.2: 2D coarse VEF Mesh

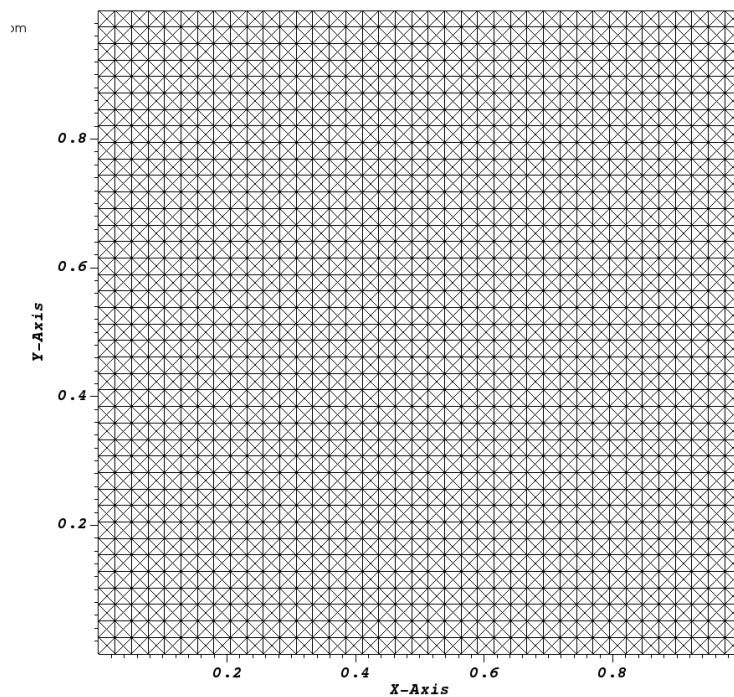


Figure IV.1.3: 2D fine VEF Mesh

Model Options

The gravity is downward.

Other Options (calculation)

TrioCFD simulations are performed with several numerical options for the VDF and VEF discretization. When plotting the temperature and velocity profiles, several curves will be presented, each one of them corresponding to the options 'Amont' or 'Quick' for VDF and 'Muscl', 'Amont', 'EF_stab' (alpha=1) and 'EF_stab (alpha=0.2)' for VEF (for each mesh Coarse/Fine). The options are summarized in section 4.1.

1.4 Results

Validation Specific Informations

- Version TRUST : 1.6.1
- Dimension: 2D
- Discretization: VEFPreP1B or VDF
- Time scheme: Euler Explicite for VDF, and Euler Implicit for VEF
- Momentum convection scheme: EF_stab, Muscl or Amont
- Temperature convection scheme: EF_stab, Muscl or Amont
- Momentum diffusion scheme: Negligible
- Temperature diffusion scheme: Negligible
- Solving of equations: Navier_Stokes_standard and Convection_Diffusion_Temperature
- Master Test case: Vahl-Davis.data
- Location: /validation/share/Validation/Rapports_automatiques/Validant/Fini/Convection_Vahl_Davis
- Generated Test cases :
 - VDF/Amont/test.data :
 - VDF/Quick/test.data :
 - VEF_CoarseMesh/Amont/test.data :
 - VEF_CoarseMesh/Muscl/test.data :
 - VEF_CoarseMesh/EF_stab/test.data :
 - VEF_CoarseMesh/EF_stab0.2/test.data :
 - VEF_FineMesh/Amont/test.data :
 - VEF_FineMesh/Muscl/test.data :
 - VEF_FineMesh/EF_stab/test.data :
 - VEF_FineMesh/EF_stab0.2/test.data :
- Performance Chart :

	host	system	Total CPU Time	CPU time/step	number of cell
VDF/Amont/test	is241762.intra.cea.fr	Linux	16.311	0.00484841	4761
VDF/Quick/test	is241762.intra.cea.fr	Linux	17.0483	0.00510193	4761
VEF_CoarseMesh/Amont/test	is241762.intra.cea.fr	Linux	10.9846	0.00996548	1444
VEF_CoarseMesh/Muscl/test	is241762.intra.cea.fr	Linux	15.3615	0.0108315	1444
VEF_CoarseMesh/EF_stab/test	is241762.intra.cea.fr	Linux	14.1104	0.0107209	1444
VEF_CoarseMesh/EF_stab0.2/test	is241762.intra.cea.fr	Linux	14.5416	0.0104751	1444
VEF_FineMesh/Amont/test	is241762.intra.cea.fr	Linux	178.583	0.0476589	6084

	host	system	Total CPU Time	CPU time/step	number of cell
VEF_FineMesh/Muscl/test	is241762.intra.cea.fr	Linux	225.79	0.0505792	6084
VEF_FineMesh/EF_stab/test	is241762.intra.cea.fr	Linux	209.006	0.049715	6084
VEF_FineMesh/EF_stab0.2/test	is241762.intra.cea.fr	Linux	214.614	0.0490201	6084
Total			916.35		

Table IV.1.2: Performance Chart

Plot Data

The temperature evolution for two points inside the domain (point 1: $x=0.5$, $y = 0.2$; point 2: $x=0.2$, $y=0.5$) shows that, after a few oscillations of weak magnitude (Fig. 4), the steady state is reached after about 60 seconds of physical time. Once the steady state is reached (see the temperature and velocity fields on Fig. 5), the velocity and temperature profiles are compared at $x = 0.5\text{m}$ and $y = 0.5\text{m}$ for various temporal schemes and convection schemes. The results are also presented for coarsened and refined mesh, and compared with values published in the literature.

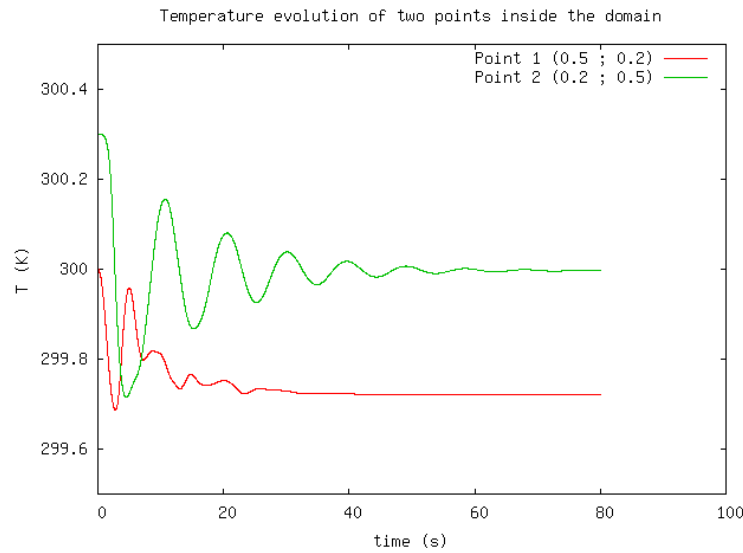


Figure IV.1.4: Temperature evolution of two points inside the domain

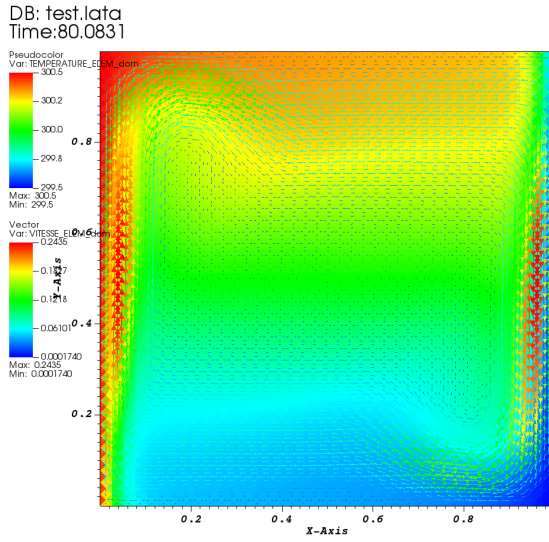


Figure IV.1.5: Temperature and velocity fields at steady state (refine mesh)

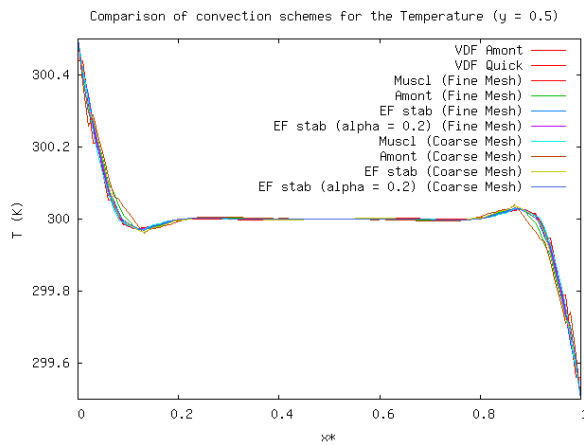


Figure IV.1.6: Comparison of convection schemes for the Temperature ($y = 0.5$)

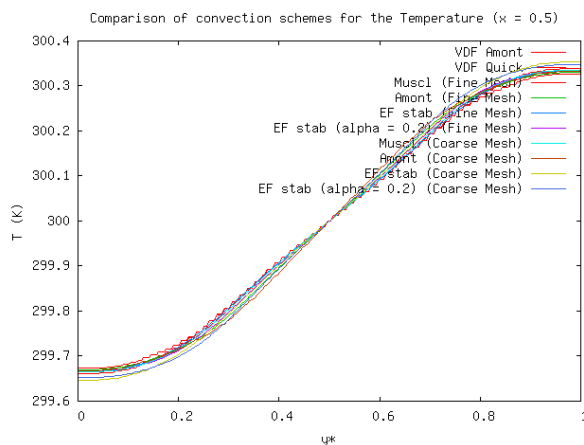
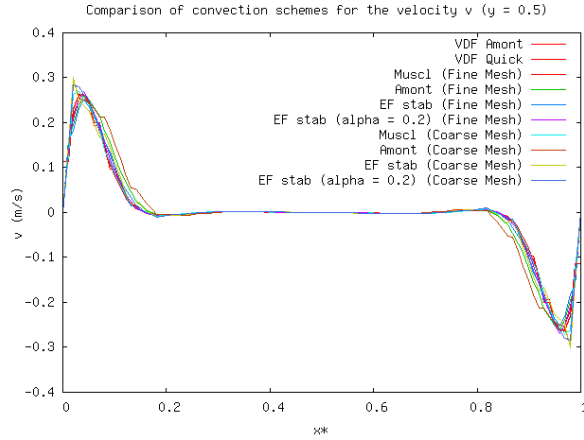
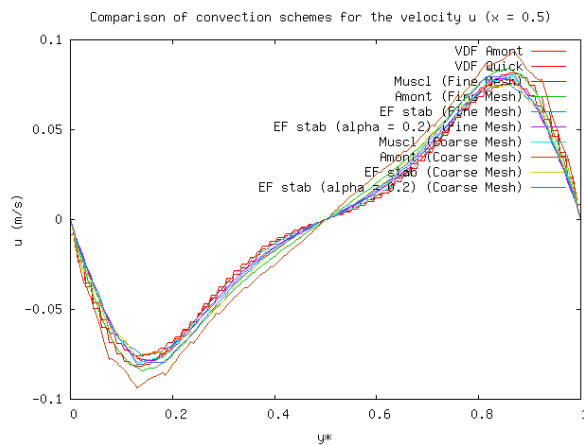


Figure IV.1.7: Comparison of convection schemes for the Temperature ($x = 0.5$)

The Amont, Muscl and EF_stab ($\alpha = 1$ and $\alpha = 0.2$) convection schemes are used either for momentum or for energy equation.

Figure IV.1.8: Comparison of convection schemes for the velocity v ($y = 0.5$)Figure IV.1.9: Comparison of convection schemes for the velocity u ($x = 0.5$)

probe type: standard, grav or nodes.

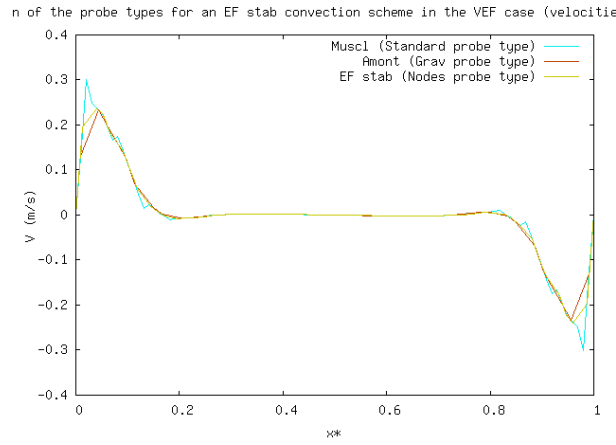


Figure IV.1.10: Comparison of the probe types for an EF_stab convection scheme in the VEF case (velocities at $y = 0.5$)

Probe type: standard, grav or nodes.

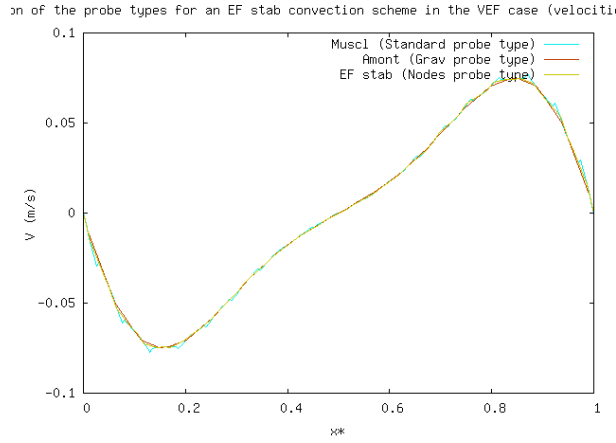


Figure IV.1.11: Comparison of the probe types for an EF_stab convection scheme in the VEF case (velocities at $x = 0.5$)

• Comparison with values from the literature

The following values of u_x^* and u_u^* are given respectively for $x = 0.5\text{m}$ and $y = 0.5\text{m}$, with:
 $u^* = uL\sqrt{Ra \times Pr}$; $v^* = vL\sqrt{Ra \times Pr}$; $y^* = y/L$; $x^* = x/L$

	Max(u^*)	y^*	Max(v^*)	x^*
Vahl_Davis	64.63	0.85	216.36	0.03791
Gresho	64.593	0.888	220.64	0.0237
Winter	63.9	0.85	222	0.039

Table IV.1.3: Summary of values from literature

	Max(u^*)	y^*
VDF (Amont)	68.52983397	0.85929648

	Max(u*)	y*
VDF (Quick)	63.81984907	0.85929648
VEF Coarse Mesh (Amont)	79.04809562	0.86934673
VEF Coarse Mesh (EF_stab)	65.00696018	0.86934673
VEF Coarse Mesh (EF_stab alpha = 0.2)	67.89840452	0.86432161
VEF Coarse Mesh (Muscl)	66.81241427	0.86432161
VEF Fine Mesh (Amont)	70.84564159	0.85929648
VEF Fine Mesh (EF_stab)	63.30202711	0.85929648
VEF Fine Mesh (EF_stab alpha = 0.2)	66.44112896	0.85929648
VEF Fine Mesh (Muscl)	65.7992108	0.85929648

Table IV.1.4: Results for Max(u*)

	Max(v*)	x*
VDF (Amont)	222.3518262	0.03030303
VDF (Quick)	219.48033423	0.03030303
VEF Coarse Mesh (Amont)	251.44078604	0.02020202
VEF Coarse Mesh (EF_stab)	254.09465332	0.02020202
VEF Coarse Mesh (EF_stab alpha = 0.2)	239.22156619	0.02020202
VEF Coarse Mesh (Muscl)	226.68710722	0.03030303
VEF Fine Mesh (Amont)	218.44098804	0.04040404
VEF Fine Mesh (EF_stab)	211.85461139	0.04040404
VEF Fine Mesh (EF_stab alpha = 0.2)	226.40395826	0.04040404
VEF Fine Mesh (Muscl)	222.4034212	0.04040404

Table IV.1.5: Results for Max(v*)

	Vahl-Davis	Gresho	Winter
VDF (Amont)	5.6907098	5.74470088	6.75593928
VDF (Quick)	1.25352148	1.19695777	0.12543182
VEF Coarse Mesh (Amont)	18.23964956	18.2864565	19.16313796
VEF Coarse Mesh (EF_stab)	0.57987665	0.63679363	1.70283333
VEF Coarse Mesh (EF_stab alpha = 0.2)	4.8136691	4.86816228	5.88880482
VEF Coarse Mesh (Muscl)	3.26648019	3.32185912	4.3590915
VEF Fine Mesh (Amont)	8.7734989	8.82572512	9.80390809
VEF Fine Mesh (EF_stab)	2.05473138	1.99862662	0.93579482
VEF Fine Mesh (EF_stab alpha = 0.2)	2.72591539	2.78160379	3.82463242
VEF Fine Mesh (Muscl)	1.77693742	1.8331691	2.88637322

Table IV.1.6: Relative errors for Max(u*): $\text{ERR}[\text{Max}(v^*)]$ in %

	Vahl-Davis	Gresho	Winter
VDF (Amont)	2.69475016	0.76987279	0.15822951
VDF (Quick)	1.42169194	0.52559181	1.13498458
VEF Coarse Mesh (Amont)	13.95190756	12.24971753	11.70883472
VEF Coarse Mesh (EF_stab)	14.85062862	13.16621695	12.63098334
VEF Coarse Mesh (EF_stab alpha = 0.2)	9.55664933	7.76751297	7.19900236
VEF Coarse Mesh (Muscl)	4.55566589	2.66760086	2.06765496
VEF Fine Mesh (Amont)	0.95265456	0.99665154	1.60315854
VEF Fine Mesh (EF_stab)	2.08235746	3.98177511	4.56999487
VEF Fine Mesh (EF_stab alpha = 0.2)	4.43629976	2.54587345	1.94517724
VEF Fine Mesh (Muscl)	2.71732385	0.79289302	0.18139163

Table IV.1.7: Relative errors for Max(v^*): $\text{ERR}[\text{Max}(v^*)]$ in %

1.5 Conclusion

- While the choice of the probe has no effect on the measured maximum velocity u ($x = 0.5$), this is not the case for v . Indeed, as can be seen on the previous arrays, the values of x^* for which v^* is maximal, are located in an area where significant different values of velocities are observed. The use of probes which display the velocity value either at the gravity center of cells (probe grav) or at the cell nodes (probe node), can lead to smoother curves. The information about maximum velocity along the segment profile $y=0.5$, cannot be obtained very precisely. The curves are much smoother however with finer mesh.
- The different time schemes give approximatively the same results for a given set of convection schemes.
- The convection scheme does not influence a lot the temperature profile for $y = 0.5$. The influence of the coefficient scheme is more significant for $x = 0.5$.
- When using the different time schemes, the results obtained appear very closed from each other. There is no clearly visible difference.
- The amont scheme applied to the energy equation leads to higher extremum values of the velocities for $x = 0.5$.
- The temperature profiles are only little influenced by the different convection schemes.
- Regarding the relative errors, the arrays show clearly the influence of the mesh refinement on the results.

Recommendations for users

Check the different profiles with different kinds of post processing probes, in order to ensure that the mesh is fine enough to perform a reliable calculation, especially where the velocity or temperature changes are steeps.

1.6 References

- P.M.GRESHO, C.D. UPSON, R.L. LEE. 'Finite Element Simulations of Thermally Induced Convection in an Enclosed Cavity'. Lawrence Livermore Laboratory Report UCID-18602 (March, 1980).
- G. de VAHL DAVIS. 'Natural Convection in a Square Cavity-A Benchmark Solution'. International Journal for Numerical Methods in Fluids , 3 , 249 - 264.
- K.H. WINTERS. 'A Numerical Study of Natural Convection in a Square Cavity'. United Kingdom Atomic Energy Authority, AERE-R9747 (August, 1980).

1.7 Data Files

test

```
# CAS VAHL DAVIS 2D #
dimension 2
Domaine dom
Mailler dom
{
Pave Cavite
{
    {
        Origine 0. 0.
        Nombre_de_Noeuds 70 70
        Longueurs 1. 1.
    }
    {
        Bord bas      Y = 0.      0. <= X <= 1.
        Bord haut     Y = 1.      0. <= X <= 1.
        Bord gauche   X = 0.      0. <= Y <= 1.
        Bord droit    X = 1.      0. <= Y <= 1.
    }
}
Pb_Thermohydraulique pb
VDF dis
Schema_Euler_Explicite sch
Read sch
{
    tinit 0.
    tmax 80.
    dt_min 1.e-8
    dt_max 1.e2
    dt_impr 1e-1
    dt_sauv 500.
    seuil_statio 1.e-8
    facsec 1.
}
Fluide_Incompressible fluide
Read fluide
{
    mu Champ_Uniforme 1 1.
    rho Champ_Uniforme 1 1186.78
    lambda Champ_Uniforme 1 1.
    Cp Champ_Uniforme 1 0.71
    beta_th Champ_Uniforme 1 1.
}
Champ_Uniforme gravite
Read gravite 2 0 -1.
Associate fluide gravite
Associate pb dom
Associate pb sch
Associate pb fluide
Discretize pb dis
Read pb
{
    Navier_Stokes_standard
    {
        solveur_pression GCP
        {
            precond ssor { omega 1.5 }
            seuil 1e-9
        }
    }
}
```

```

        }
    solveur_bar GCP
    {
        precond_ssor { omega 1.5 }
        seuil 1e-9
    }
sources { Boussinesq_temperature { T0 300. } }
convection { Amont }
diffusion { }
conditions_initiales
{
    vitesse champ_uniforme 2 0. 0.
}
boundary_conditions
{
    haut     paroi_fixe
    bas      paroi_fixe
    gauche   paroi_fixe
    droit    paroi_fixe
}
}
Convection_Diffusion_Temperature
{
    conditions_initiales { Temperature Champ_Fonc_xyz dom 1 -1.*x+300.5 }
    convection { Amont }
    diffusion { }
    boundary_conditions
    {
        haut     paroi_adiabatique
        bas      paroi_adiabatique
        gauche   paroi_temperature_imposee Champ_Front_Uniforme 1 300.5
        droit    paroi_temperature_imposee Champ_Front_Uniforme 1 299.5
    }
}
Postraitemet
{
    format lata
    Sondes
    {
        sonde_temp0 temperature periode 0.001 segment 100
        0. 0.5 1. 0.5
        sonde_temp1 temperature periode 0.001 segment 200 0.5 0. 0.5 1.
        sonde_temppt0 temperature periode 0.01 Points 1 0.5 0.2
        sonde_temppt1 temperature periode 0.01 Points 1 0.2 0.5
        sonde_vit vitesse periode 0.1 Points 1 0.15 0.5
        sonde_vit0 vitesse periode 0.0001 segment 100 0. 0.5 1. 0.5
        sonde_vit1 vitesse periode 0.01 segment 200 0.5 0. 0.5 1.
        sonde_vit0_g grav vitesse periode 0.0001 segment 100 0. 0.5 1. 0.5
        sonde_vit1_g grav vitesse periode 0.01 segment 200 0.5 0. 0.5 1.
        sonde_vit0_n nodes vitesse periode 0.0001 segment 100 0. 0.5 1. 0.5
        sonde_vit1_n nodes vitesse periode 0.01 segment 200 0.5 0. 0.5 1.
    }
    Champs binaire dt_post 10
    {
        vitesse elem
        temperature elem
    }
}
Solve pb
End

```

#####

Oscillatory convection flow

2.1 Purpose

A two-dimensional 'oscillatory convection flow' is studied inside a rectangular heated cavity. The physical test is similar to the previous one, i.e. the 'Convection Vahl Davis' in laminar condition, but the cavity is now non-symmetric. The results are compared with the benchmark of Behnia et al. that is published in the book of reference [1]. The TrioCFD simulations run on VDF and VEF meshes for several options of the convection scheme.

Validation made by : E. MOREAU (S. VANDROUX).
Report generated 11/01/2021.

2.2 Problem Description

Geometry

The test case geometry is a two-dimensional rectangular cavity of dimensions $L=4m \times H=1m$ which is presented on Fig. 1 with the boundary conditions for temperature equation. On that figure the hot wall is on the left side and the cold wall is on the right side.

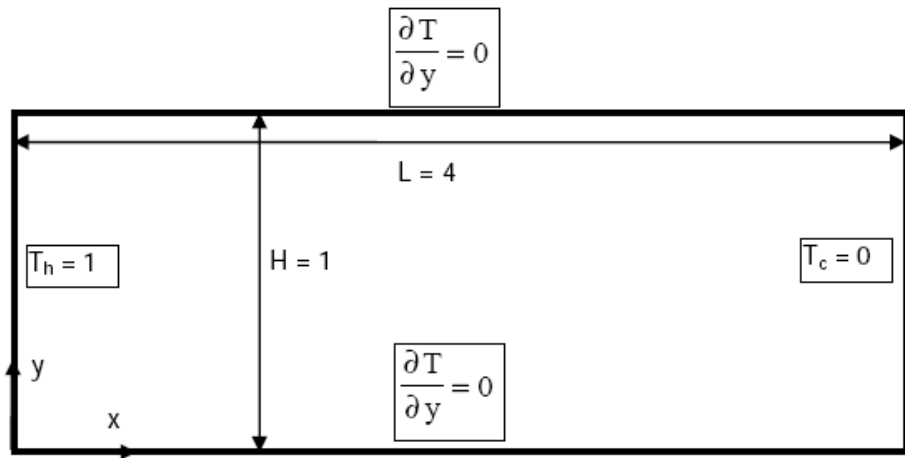


Figure IV.2.1: Dimensions of the domain and boundary conditions for temperature equation.

Initial Conditions and Boundary Conditions

The initial velocity is $U = V = 0$ where U and V are respectively the x -component (horizontal) and the y -component (vertical) of the velocity. At $t=0$, a linear temperature is applied $T(x) = 1 - x \frac{H}{L}$ in the horizontal

direction (zero Prandtl fluid). No-slip boundary conditions are applied for Navier-Stokes equations. For temperature equation, zero flux holds on horizontal walls and Dirichlet boundary conditions hold for vertical ones. The boundary conditions are summarized below with the TrioCFD keywords:

- Hydraulic boundary condition type: 'paroi_fixe'
- The thermal boundary conditons types are as follow:
 - $Y = 0$ (bottom) and $Y = 1$ (top): 'Paroi_adiabatique'
 - $T = 1 \text{ K}$ (hot side: left) and $T = 0 \text{ (cold side: right)}$

The TrioCFD options for the thermal boundary conditions are (respectively for VDF and VEF):

- For VDF calculation:

```
ENTREE paroi_echange_externe_impose T_ext Champ_Front_Uniforme 1 1.00 H_imp
Champ_Front_Uniforme 1 1.e11
SORTIE paroi_echange_externe_impose T_ext Champ_Front_Uniforme 1 0.00 H_imp
Champ_Front_Uniforme 1 1.e11
```

- For VEF calculation:

```
ENTREE paroi_temperature_imposee Champ_Front_Uniforme 1 1.00
SORTIE paroi_temperature_imposee Champ_Front_Uniforme 1 0.00
```

Fluid Properties

The physical parameters are set such as the Grashof number is equal to 3.10^4 . Hence, although the Prandtl number is equal to 200, the fluid may be considered as a zero Prandtl fluid because of a negligible thermal convection scheme. The values of parameters are given in Table 1, where ρ is the density, μ is the dynamic viscosity, λ is the thermal conductivity, C_p is the specific heat and β_{th} is the thermal expansion coefficient.

	Value
$\rho \text{ (kg/m}^3\text{)}$	1.18
$\mu \text{ (N/m}^2\text{/s)}$	0.00062304
$\lambda \text{ (W/m/K)}$	0.00264
$C_p \text{ (J/kg/K)}$	1000.0
β_{th}	0.00341

Table IV.2.1: Physical properties

Flow Physics

Under the influence of the temperature gradient and the Boussinesq approximation, the fluid starts swirling inside the rectangular cavity in the clockwise direction.

2.3 Case Setup

Grid

The VDF and VEF meshes are presented on Figs 2 and 3. The VDF mesh contains 2500 cells which are generated with the 'Pave' option of TrioCFD.

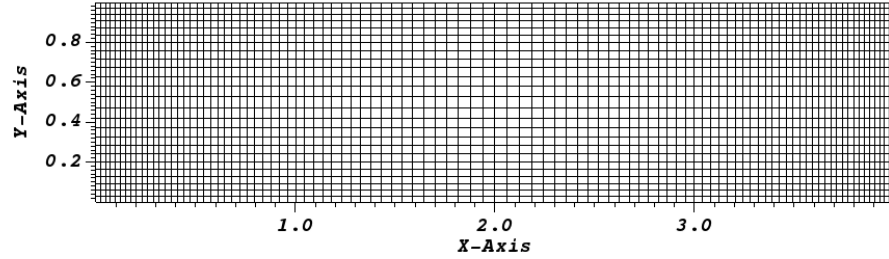


Figure IV.2.2: VDF Mesh

For VEF mesh contains 5040 triangular cells which are obtained with the 'trianguler_H' option of TrioCFD. An expansion has been applied with factors 1.02 along the x-axis, and 1.05 along the y-direction

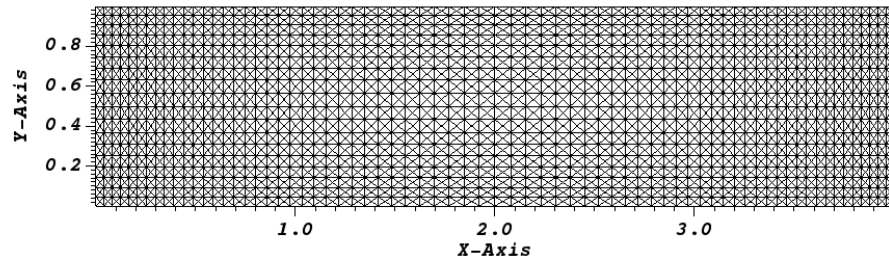


Figure IV.2.3: VEF Mesh

Model Options

The gravity is downward.

Other Options (calculation)

For the VDF scheme, the convection option is 'Quick' or 'Centre' and for the VEF scheme the convection option is 'Muscl', 'EF_stab=0.2' and 'EF_stab=1'. All other numerical options are summarized in Section 4.1.

2.4 Results

Validation Specific Informations

- Version TRUST : 1.6.1
- Dimension: 2D
- Discretization: VDF / VEF
- Thermal hydraulic problem
- Momentum characteristic: Navier_stokes_standard
- Thermal characteristic: Source_Boussinesq_temperature
- Convection_diffusion_temperature not solved (analytical solution known)
- Time scheme: Euler explicite

- VDF Momentum convection scheme: Centre, Quick or Muscl
- VEF Momentum convection scheme: Muscl, EF_stab or EF_stab with alpha = 0.2
- VDF and VEF Temperature convection schemes: Negligible
- Type of fluid: incompressible
- Fluid boundary condition: adhesion on the wall
- Thermal boundary condition: imposed temperature and adiabatic walls
- Location: /validation/share/Validation/Rapports_automatiques/Validant/Fini/Oscillating_Flow
- Master Test case: test_osc_flow.data
- Generated Test cases :
 - VDF/Quick/test.data :
 - VDF/Centre/test.data :
 - VEF/Muscl/test.data :
 - VEF/EF_stab/test.data :
 - VEF/EF_stab02/test.data :
- Performance Chart :

	host	system	Total CPU Time	CPU time/step	number of cell
VDF/Quick/test	is241762.intra.cea.fr	Linux	12.2318	0.00254521	2500
VDF/Centre/test	is241762.intra.cea.fr	Linux	10.9847	0.00226617	2500
VEF/Muscl/test	is241762.intra.cea.fr	Linux	1097.15	0.0444052	5040
VEF/EF_stab/test	is241762.intra.cea.fr	Linux	1090.48	0.0447539	5040
VEF/EF_stab02/test	is241762.intra.cea.fr	Linux	1105.74	0.0449048	5040
Total			3316.59		

Table IV.2.2: Performance Chart

Plot Data

• Grashof number

As a consequence of a zero Prandtl fluid, the temperature field can be determined analytically as the time invariant of a pure conduction solution. Using the thermal boundary conditions shown above, this solution is given by the function $T(x) = 1 - x \frac{H}{L}$. The Grashof number (Gr) is defined by:

$$Gr = \frac{g\rho^2\beta\Delta TH^4}{L\mu^2}$$

Let us notice the presence of the factor H^4/L in the definition (and not L^3) because the domain is rectangular. The desired value of the Grashof Number, 3.10^4 , is obtained by tuning the different parameters of its definition. The temperature scale ΔT is expressed as $\Delta T = (T_h - T_c) = 1K$ and the reference temperature is chosen such as $T_0 = (T_h - T_c)/2 = 0.5K$.

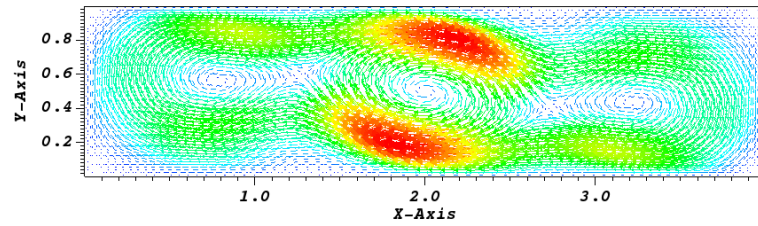
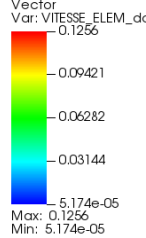
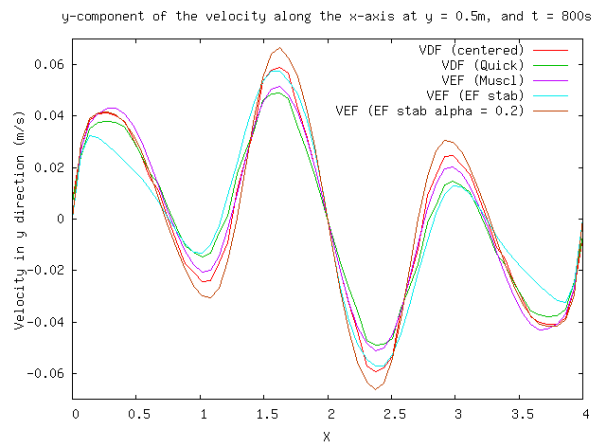
• Velocity and temperature profiles

The velocity vectors are presented on Fig. 4 at the end of simulation. The profiles of the y-component of the velocity are plotted of Fig. 5 at the end of the simulation $t = 800s$. The profiles are presented for VDF and VEF along a horizontal profile for $y=0.5$ (centre of the cavity) i.e. $0 < x < 4$ and $y=0.5$. We can observe

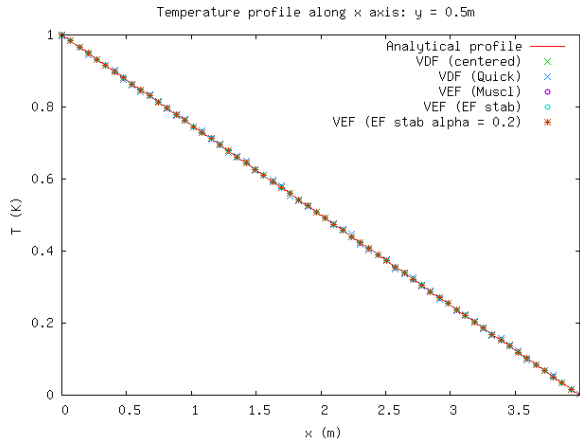
that the three-cells structure of the vortices is calculated correctly for both discretization methods (VDF and VEF).

DB: test.lata

Time:800.015

Figure IV.2.4: Velocity vectors at $t = 800$ s for VEF mesh (Muscl)Figure IV.2.5: y-component of the velocity along the x-axis at $y = 0.5m$, and $t = 800s$

All temperature profiles of TrioCFD, are superimposed to the analytical profile (see Fig. 6).

Figure IV.2.6: Temperature profile along x axis: $y = 0.5\text{m}$

For a Grashof number equal to 3.10^4 , the flow is known to be periodic. In our case, the periodicity is well established near 300s (see Fig. 7). This time is the starting point for the calculation of the oscillation frequency.

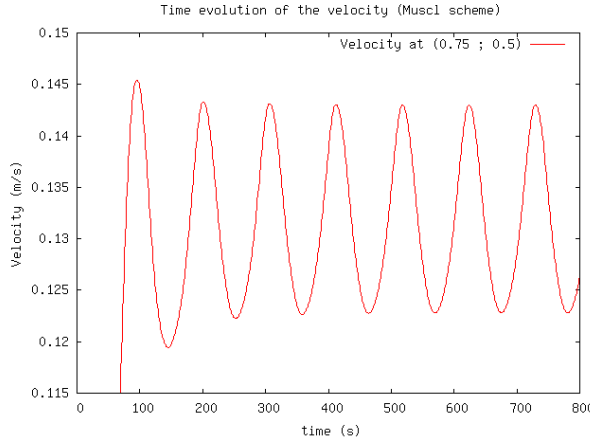


Figure IV.2.7: Time evolution of the velocity (Muscl scheme)

A comparison with the results of Behnia and Vahl Davis (in ref [1]) may be done for a non-dimensional frequency that is scaled with $t_{ref} = H^2/\nu$. The values of the five TrioCFD simulations are presented in Table 3, where the average frequencies are calculated in the range [300s; 800s].

	Period (s)	Non dimensional frequency	Relative error %
Behnia	105.98	17.87	0
VDF (Quick)	104.73	18.08	1.18
VDF (Centered)	106.74	17.74	0.7
VEF (Muscl)	105.75	17.91	0.22
VEF (EF_stab)	115.0	16.47	7.84
VEF (EF_stab alpha = 0.2)	108.75	17.42	2.54

Table IV.2.3: Oscillation frequency

2.5 Conclusion

The simulations validate the laminar fluid flow coupled with the temperature equation with Boussinesq approximation. The TrioCFD simulations are performed in 2D on VDF and VEF grids with several options of convective schemes. The results are in good agreement with those obtained by Behnia, except for the VEF scheme with the 'EF_stab alpha=1' option. For other numerical schemes of TrioCFD, the relative errors vary from 0.22% for 'VEF/Muscl', up to 2.54% for VEF/'EF_stab alpha = 0.2'.

- **Recommendations for users**

The results obtained with the 'EF_stab' scheme are less good than the other ones. However the use of alpha=0.2 instead of alpha=1 improves the result significantly.

2.6 References

- [1] Numerical Simulation of Oscillatory Convection in Low-Pr Flow, Notes in Numerical Fluid Dynamics, A GAMM Workshop, Vol 27, Ed. Bernard ROUX, doi: 10.1007/978-3-322-87877-9, Publisher: Vieweg+Teubner Verlag, 365 p., 1990.

2.7 Data Files

test

```
# Thermohydraulique 2D VDF Boussinesq #
dimension 2
Pb_Thermohydraulique pb
Domaine dom
Mailler dom
{
    Pave Cavite
    {
        Origine 0. 0.
        Nombre_de_Noeuds 101 26
        Longueurs 4.0 1.0
        Facteurs 1.02 1.05
        Symx
        Symy
    }
    {
        Bord ENTREE X = 0. 0. <= Y <= 1.
        Bord HAUT Y = 1. 0. <= X <= 4.
        Bord BAS Y = 0. 0. <= X <= 4.
        Bord SORTIE X = 4. 0. <= Y <= 1.
    }
}
# AA #
VDF dis
Schema_Euler_Explicite sch
Read sch
{
    tinit 0.
    tmax 800.
    dt_min 0.0001
    dt_max 0.2
    dt_impr 0.001
    dt_sauv 100
    seuil_statio 1.e-8
    facsec 1.0
}
Fluide_Incompressible fluide
```

```

Read fluide
{
  mu Champ_Uniforme 1 6.2304e-4
  rho Champ_Uniforme 1 1.18
  lambda Champ_Uniforme 1 2.64e-3
  Cp Champ_Uniforme 1 1000.
  beta_th Champ_Uniforme 1 3.41e-3
}
# Pr = muCp/Lambda = 200 mais schema de convection therm negligable #
Champ_Uniforme gravite
Read gravite 2 0 -9.81
Associate fluide gravite
Associate pb dom
Associate pb sch
Associate pb fluide
Discretize pb dis
Read pb
{
  Navier_Stokes_standard
  {
    solveur_pression GCP { precond ssor { omega 1.5 } seuil 1.e-10 impr }
    convection { quick }
    diffusion { }
    sources { boussinesq_temperature { T0 0.5 } }
    conditions_initiales {
      vitesse Champ_Uniforme 2 0. 0.
    }
    boundary_conditions {
      HAUT paroi_fixe
      BAS paroi_fixe
      ENTREE paroi_fixe
      SORTIE paroi_fixe
    }
  }
  Convection_Diffusion_Temperature
  {
    diffusion { negligable }
    convection { negligable }
    boundary_conditions {
      HAUT Paroi_adiabatique
      BAS Paroi_adiabatique
      ENTREE paroi_echange_externe_impose T_ext Champ_Front_Uniforme 1 1.00
      H_imp Champ_Front_Uniforme 1 1.e11
      SORTIE paroi_echange_externe_impose T_ext Champ_Front_Uniforme 1 0.00
      H_imp Champ_Front_Uniforme 1 1.e11
    }
    conditions_initiales { Temperature champ_fonc_xyz dom 1 1-x/4 }
  }
  Postraitemnt
  {
    Sondes
    {
      sonde_pression pression periode 1. points 1 2.00 0.5
      sonde_vitesse vitesse periode 1. points 5 0.75 0.5
      2.00 0.19
      2.00 0.5
      2.00 0.81
      3.25 0.5
      sonde_temp temperature periode 1. segment 60 0. 0.501 4. 0.501
      sonde_vite vitesse periode 1. segment 60 0. 0.501 4. 0.501
    }
  }
}

```

```
}

Champs dt_post 400.0
{
    pression
    vitesse
}
format lata
Champs dt_post 400. { vitesse elem }
}

Solve pb
End
```

V. Turbulent Flow

In this fifth part of the document, the flow pattern changes completely compared to the two previous parts since here are considered turbulent flows. Let us remind that a flow is considered as turbulent when the Reynolds number is greater than 2000. This critical Reynolds number corresponds to the moment when the viscous forces are no longer strong enough to absorb the vortices. Fluid motion is characterized by chaotic changes in pressure and flow velocity. The flow has a whirlpool character at all points: eddies whose size, location and orientation vary constantly. Turbulent flows are therefore characterized by a very disordered appearance, behavior that is difficult to predict, and the existence of numerous space and time scales.

In this version of the report, two cases are studied:

- Turbulent flow in a 2D diffuser with the $k - \epsilon$ model
- Mixing length in 2D and 3D VEF-plane channel

This part will be enriched in a following version with, in particular, a case in 3D.



Turbulent flow in a 2D diffuser with the $k - \epsilon$ model

1.1 Purpose

This test case aims at validating TrioCFD for a turbulent flow inside a two-dimensional diffuser with the $k - \epsilon$ model and wall functions. The validation are carried out by comparing experimental data and several computational profiles. Experimental results are taken from the ERCOFTAC experiment data base and the CFD profiles are obtained from Fluent and other publications that are listed below. For the test case, the diffuser mesh is generated with ICEM and a fictitious periodic rectangular box is used to provide boundary conditions for the main computational domain (the diffuser). Two different meshes are generated for the periodic box. The goal of the fictitious periodic box is to provide well established values of velocity and $k - \epsilon$ at the inlet boundary conditions of the diffuser. There are two main computations with TrioCFD in this test case since there are two periodic boxes.

Validation made by : A.AUROUSSEAU (S.VANDROUX).
Report generated 11/01/2021.

1.2 Problem Description

Geometry

The diffuser geometry is presented on Fig. 1. All dimensions are expressed by a factor H which is equal to $H = 1\text{m}$.

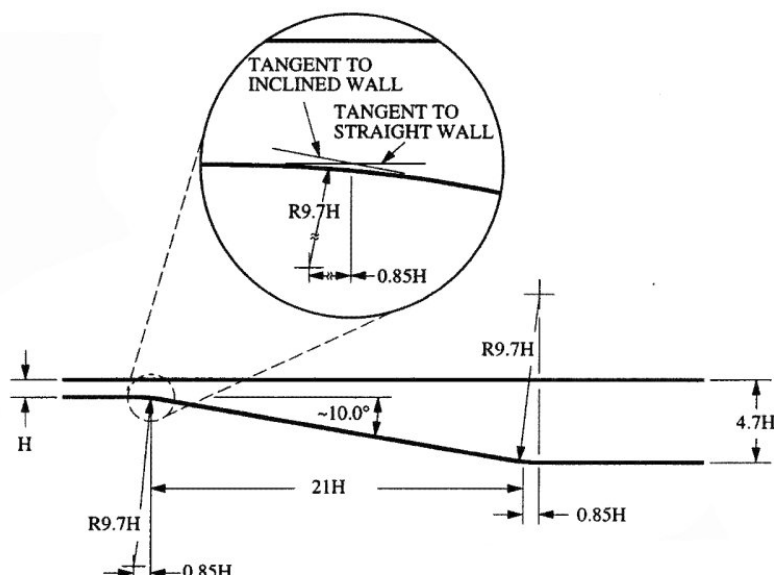


Figure V.1.1: Diffuser geometry.

Initial Conditions and Boundary Conditions

- **Modeling: use of a periodic box**

A periodic rectangular box is introduced for computations on a fictitious periodic domain. That plane channel is used to generate an established velocity and $k - \epsilon$ fields in order to be applied at the inlet of the diffuser (i.e. the main computational domain). Boundary conditions are imposed separately for the periodic box and the main computational domain. For the rectangular box, the periodicity is applied in the x -direction, and no-slip boundary conditions hold in the y -direction. For the diffuser, the values of the periodic box are applied for the $k - \epsilon$ fields and the velocity at inlet and an uniform pressure is applied at outlet. All other boundaries are no-slip conditions. The numerical values of bulk velocity and outlet pressure are given below:

- Velocity inlet: $U = 1$ m/s
- Outlet pressure: $P = 0$

Fluid Properties

Fluid domain: Fictitious fluid for which $Re = 20000$.

	Valeur
Fluid density ρ (kg/m ³)	5.7e-05
Fluid dynamic viscosity μ (Pa.s)	1.0

Table V.1.1: Physical properties

Flow Physics

The objective is to validate the ' $k - \epsilon$ model' with wall function inside a diffuser.

1.3 Case Setup

Grid

Three meshes are presented: two for the periodic box and one additional for the diffuser. The fine mesh of periodic box is presented on Fig. 2 (1104 cells) and the coarse one is presented on Fig.3 (440 cells). For both meshes the dimensions are $[-16, -11] \times [3.7, 4.7]$. The diffuser mesh is presented on Fig. 4 where x varies between 0 and 20. For the actual dimension of the diffuser, x varies between $[-11, 56]$.

Mesh: Extruder en 3 of the inlet face of 3D ICEM mesh

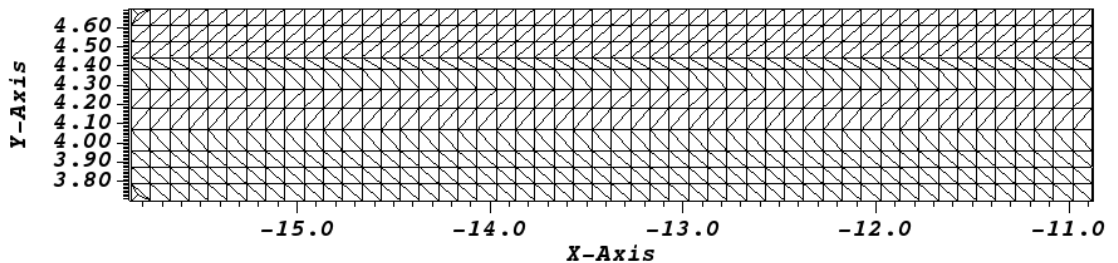


Figure V.1.2: Periodic box: mesh 1 (1104 cells)

Mesh: Extruder_bord of the inlet face of 3D ICEM mesh

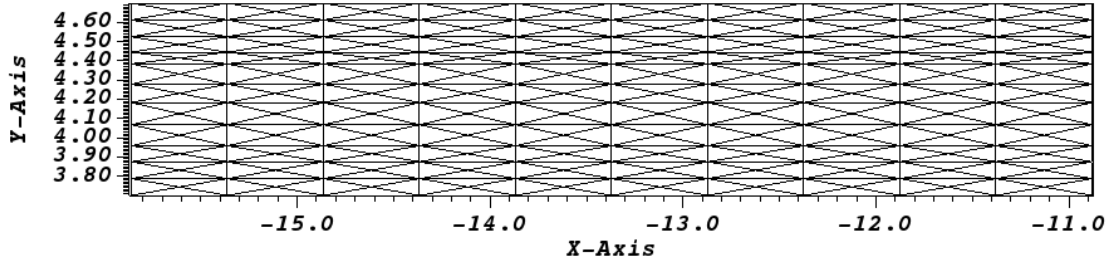


Figure V.1.3: Periodic box: mesh 2 (440 cells)

Mesh: 2D from 3D of ICEM mesh. This figure only shows the divergent part of the diffuser, but the actual domain lies between $x=-10$ and $x=56$.

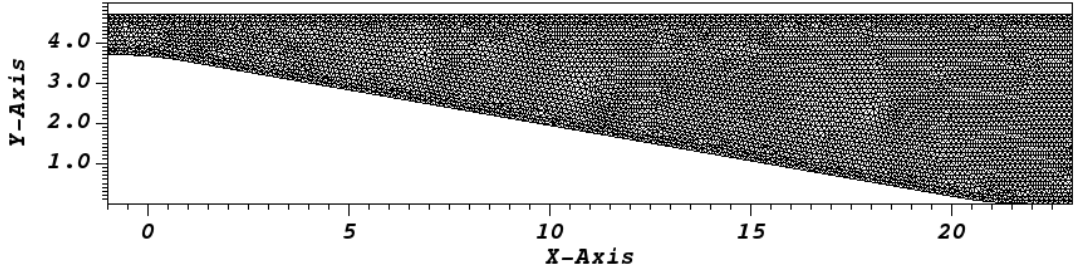


Figure V.1.4: Diffuser Mesh (36644 cells)

Model Options

The Reichardt law is applied near the wall boundary and without gravity effect for this test.

Other Options (calculation)

The 'EF_stab' scheme is applied for convective terms with 'alpha=0.2'. The time scheme is implicit. All numerical options are summarized in Section 4.1.

1.4 Results

Validation Specific Informations

- Version TRUST : 1.6.3
- Type of problem : Hydraulique_Turbulent
- Diffusion scheme : Default{}
- Discretization : VEFPreP1B (ICEM mesh with prisms layer at walls). Two meshes for the periodic box have been generated: one with the extrudeBord keyword, the other one with extruder_en3.
- Time scheme : Euler_implicit - Solveur Implicit
- Solving of equations : Navier Stokes turbulent

- Convection : EF_stab { alpha 0.2 }
- Turbulence model : k- ϵ model
- Wall law : turbulence_paroi_loi_expert_hydr { methode_calcul_face_keps_impose que_les_faces_des_elts_dirichlet }, which is the default option for 3D calculations
- Type of boundary conditions : Periodic box: periodicity in the x -direction, walls in the y -direction. Main computation domain (diffuser): Velocity field and $k - \epsilon$ field (from periodic box) for the inlet, outlet pressure, walls.
- Location : /validation/share/Validation/Rapports_automatiques/Validant/Fini/OBI_diffuser_VEF_k_eps
- Master Test case : Calcul.data - Prepare_extract.data - Prepare_extrude.data
- Generated Test cases :
 - Calcul_fin/Calcul.data : /*see data set in the appendix*/
 - Calcul_gros/Calcul.data :
- Performance Chart :

	host	system	Total CPU Time	CPU time/step	number of cell
Calcul_fin/Calcul	is241762.intra.cea.fr	Linux	1858.34	6.76343	36644
Calcul_gros/Calcul	is241762.intra.cea.fr	Linux	1664.8	6.24008	36644
Total			3523.14		

Table V.1.2: Performance Chart

Plot Data

The next two figures (Figs 5 and 6) show the computations convergence by plotting the evolution of friction velocity versus time for both periodic meshes. The two curves on both figures show the friction evolution in the periodic box computation (red curve) and in the main computation (green curve). The two domains are different so the friction velocity is computed on different surfaces, Reynolds numbers are different, and the ways the friction velocity is averaged are different too. That is why the values of U_τ are different. For both meshes, the main computation reaches convergence after about 250s of physical time, and the periodic computation after 75s. The periodic computation stops around 200s since the convergence criteria (seuil_statio) is met.

Main computation values are increased on purpose to allow plotting both curves on the same figure

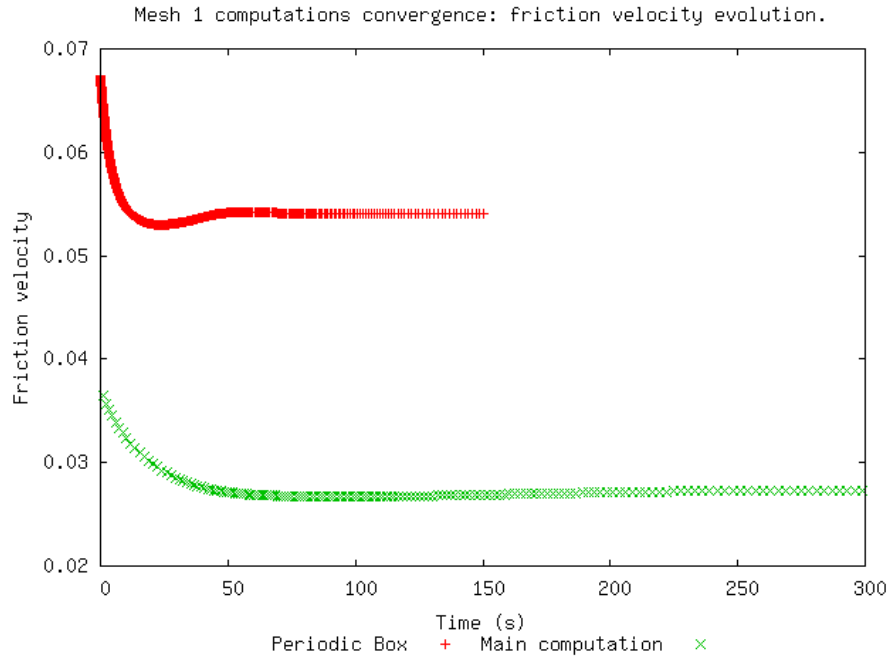


Figure V.1.5: Mesh 1 computations convergence: friction velocity evolution.

The convergence criteria on the periodic computation is met after 200s

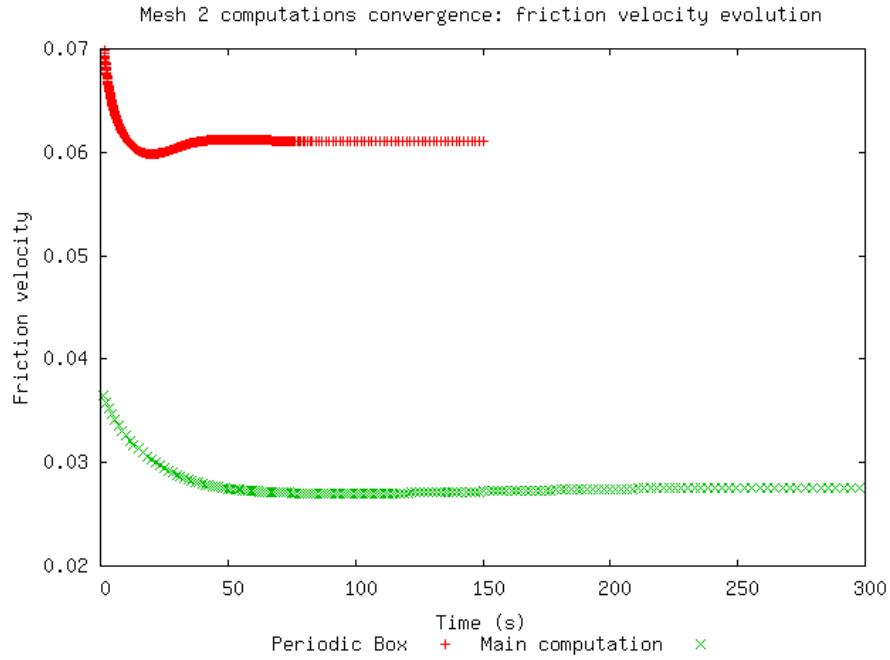


Figure V.1.6: Mesh 2 computations convergence: friction velocity evolution

- **Fields of pressure, velocity and $Y+$**

For each periodic mesh, the pressure field in the diffuser is presented on Figs. 8 and 9 (Fig. 7 is for the color scale) the velocity field in the diffuser is presented on Figs. 11 and 12 (Fig. 10 for the color scale). Finally the $Y+$ fields are presented on Figs. 14 and 15 (color scale on Fig. 13).

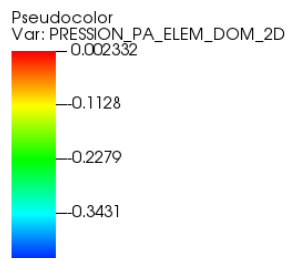


Figure V.1.7: Pressure field in the diffuser, Legend

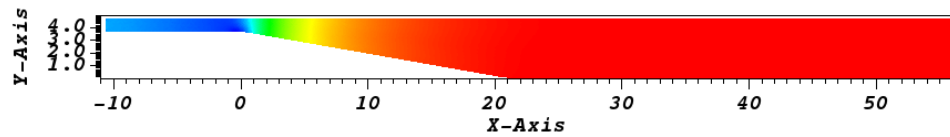


Figure V.1.8: Pressure field in the diffuser, mesh1.

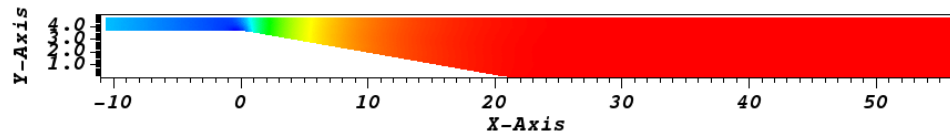


Figure V.1.9: Pressure field in the diffuser, mesh2.

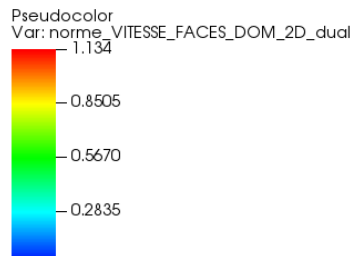


Figure V.1.10: Velocity field in the diffuser, Legend.

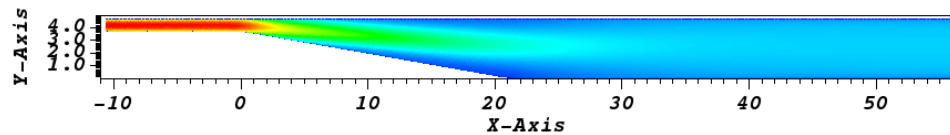


Figure V.1.11: Velocity field in the diffuser, mesh 1.

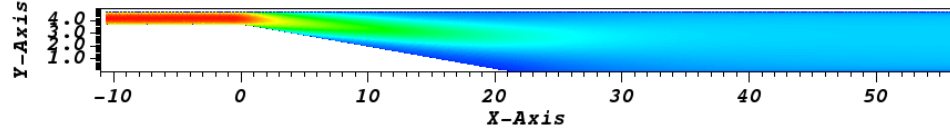
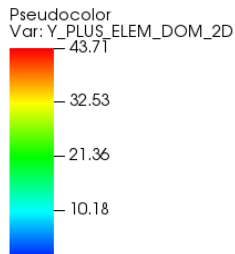
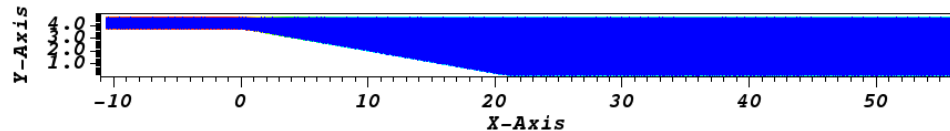
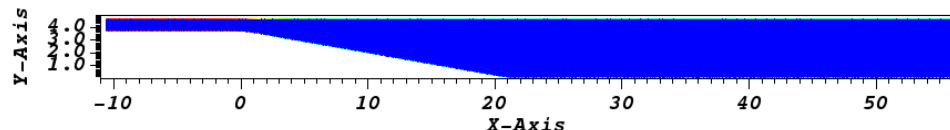
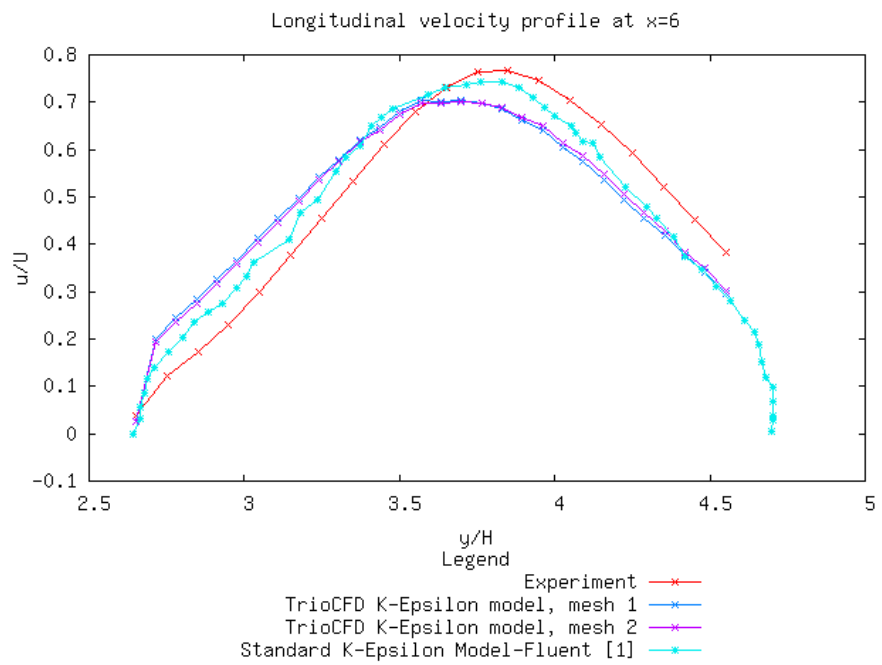
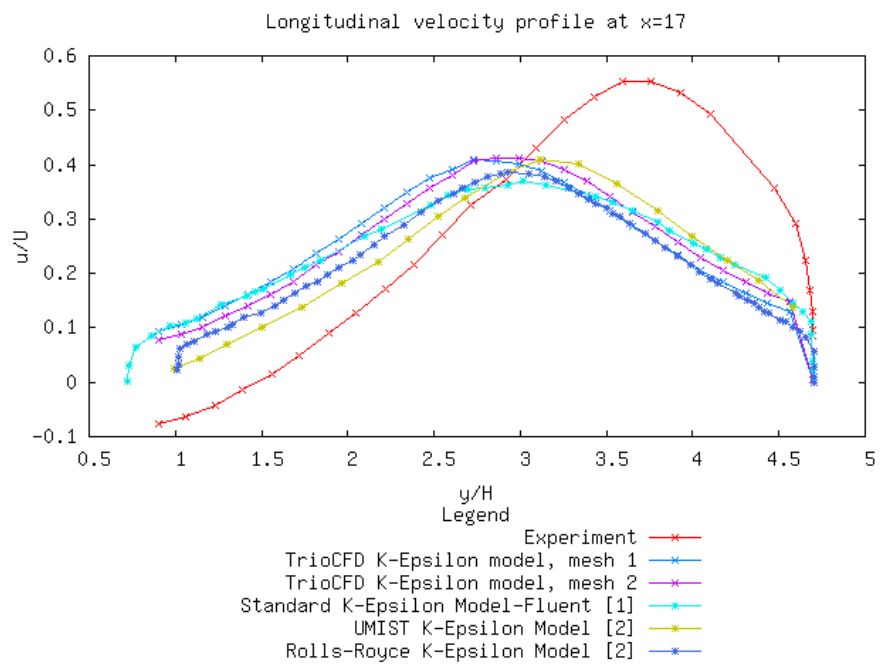


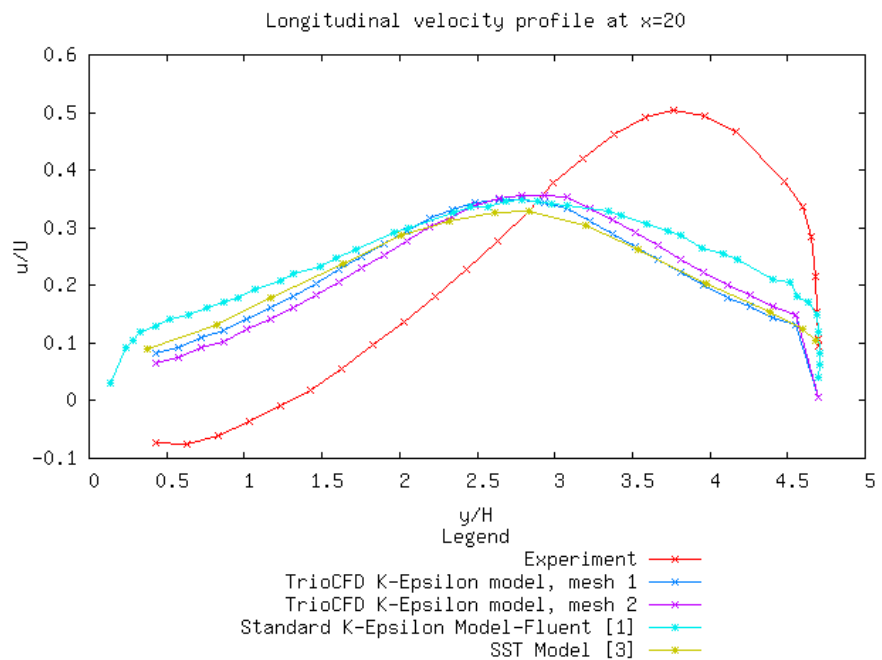
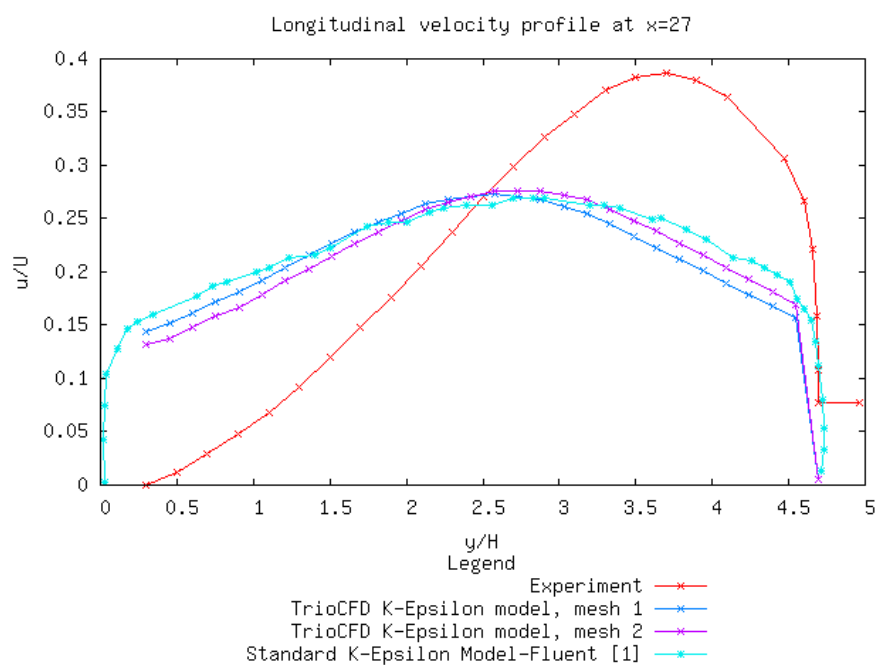
Figure V.1.12: Velocity field in the diffuser, mesh 2.

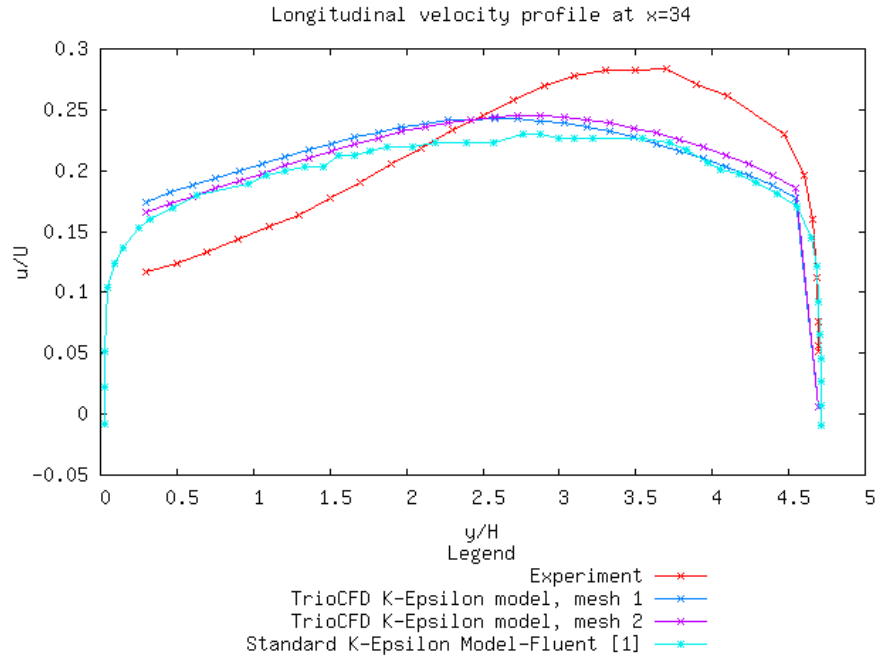
Figure V.1.13: Y^+ field in the diffuser, Legend.Figure V.1.14: Y^+ field in the diffuser, mesh1.Figure V.1.15: Y^+ field in the diffuser, mesh2.

- Comparisons of TrioCFD profiles

The y -profiles of velocity are compared at several x -positions in the diffuser. The position $x = 0$ corresponds to the point where the divergent part of the diffuser begins. The position $x = 20$ is the end of the divergent part. Beyond this point, the domain is a plane channel. The y -profiles are presented for $x = 6$ (Fig. 16), $x = 17$ (Fig. 17), $x = 20$ (Fig. 18), $x = 27$ (Fig. 19) and $x = 34$ (Fig. 20). For those graphs, the red curve is the experimental one and the cyan curve is the 'standard $k - \epsilon$ model of Fluent'. The TrioCFD results are colored in blue (mesh 1) and magenta (mesh2).

Figure V.1.16: Longitudinal velocity profile at $x=6$ Figure V.1.17: Longitudinal velocity profile at $x=17$

Figure V.1.18: Longitudinal velocity profile at $x=20$ Figure V.1.19: Longitudinal velocity profile at $x=27$

Figure V.1.20: Longitudinal velocity profile at $x=34$

1.5 Conclusion

- The pressure fields that are obtained by both meshes are similar. There is a low pressure zone at the beginning of the diffuser divergent part. The velocity fields are also similar in both computations. The divergent part of the diffuser is a low velocity zone.
- Comparisons of several y -profiles of velocity are carried out between 1) the $k - \epsilon$ model of TrioCFD, 2) the 'Standard $k - \epsilon$ model' of Fluent and 3) the experimental results from Ercoftac experiment. For few x values, other results are also available in the literature and used for comparisons.

At $x=6$ (beginning of the divergent part), the profiles are relatively similar. The Fluent results are slightly closest to the experimental curve. This experimental profile is a little shifted toward larger y/H values. The computational curves are closest to the experimental one for that x -position. For other velocity profiles (larger x values: 17, 20, 27 and 34) all computational results are relatively similar but far from the experimental results. The experimental profiles are not symmetric, whereas the CFD profiles have a near symmetrical behavior.

- We note that the TrioCFD profiles are very close to each other, showing that the method used to generate the periodic mesh has a little influence on the final computation results. In conclusion, it is well-known that the $k - \epsilon$ model of turbulence yields bad results for such a configuration, the TrioCFD results are not an exception and give similar results. A more promising $k - \epsilon$ model, better suited for simulating this type of phenomenon will be proposed in a future version of this validation sheet.

1.6 References

- [1] A Comparative Study of Turbulence Models Performance for Turbulent Flow in a Planar Asymmetric Diffuser, Samy M. El-Behery and Mofreh H. Hamed. International Journal of Aerospace and Mechanical Engineering 5:2 2001.
- [2] Advanced Turbulence Modelling of Separated Flow in a Diffuser, D.D Apsley and M.A Leschziner. Flow, Turbulence and Combustion 63:81-112,1999.

- [3] Ten Years of Industrial Experience with the SST Turbulence Model, F.R Menter and M. Kuntz and R. Langtry. Turbulence, Heat and Mass Transfer 4. K. Hanjalic, Y. Nagano and M. Tummers (Editors), Begell House, Inc. 2003.

1.7 Data Files

Calcul

```
# Hydraulique 3 #
# lance_test 3 ecart #
dimension 3
Domaine DOM_DOM
Read_unsupported_ASCII_file_from_ICEM DOM_DOM trio_DOM_geo.asc
Domaine DOM_2D
Extract_2D_from_3D DOM_DOM left DOM_2D
dimension 2
Pb_Hydraulique_Turbulent pb
VerifierCoin DOM_2D { }
Ecrire_fichier DOM_2D OBI_2D.geom
VEFPreP1B dis
Read dis { P0 P1 Changement_de_base_P1bulle 1 Modif_div_face_dirichlet 1 }
Schema_Euler_ implicite sch
Read sch
{
  tinit 0.0
  tmax 600.
  dt_min 1.e-10
  dt_max 3.0
  dt_impr 1.0
  dt_sauv 1000.
  seuil_statio 1.e-8
  facsec 50.
  facsec_max 2000
  periode_sauvegarde_securite_en_heures 5
  solveur implicite
  {
    seuil_convergence_solveur 1.e-12
    solveur gmres { diag seuil 1.e-12 impr controle_residu 1 }
  }
}
Fluide_Incompressible fluide
Read fluide
{
  mu Champ_Uniforme 1 5.7e-5
  rho Champ_Uniforme 1 1.
}
Associate pb DOM_2D
Associate pb fluide
Associate pb sch
Discretize pb dis
Read pb
{
  Navier_Stokes_Turbulent
  {
    solveur_pression Cholesky { }
    convection { EF_stab { alpha 0.2 } }
    diffusion { }
    conditions_initiales {
      vitesse Champ_Uniforme 2 1. 0.
    }
  }
}
```

```

boundary_conditions
{
    in      frontiere_ouverte_vitesse_imposee champ_front_recyclage { pb_champ_evaluateur pb
                        moyenne_imposee connexion_approchee fichier FICHIER_V_PREPARE
                        ampli_moyenne_imposee 2 1. 1.
                        ampli_moyenne_recyclee 2 0. 0.
                        ampli_fluctuation 2 0. 0. }
    out     frontiere_ouverte_pression_imposee champ_front_Uniforme 1 0.
    wall    paroi_fixe
}
modele_turbulence K_Epsilon
{
    Transport_K_Epsilon
    {
        convection { EF_stab { alpha 0.2 } }
        diffusion { }
        boundary_conditions
        {
            in frontiere_ouverte_K_eps_impose champ_front_recyclage { pb_champ_evaluateur
                        moyenne_imposee connexion_approchee fichier FICHIER_K_PREPARE
                        ampli_moyenne_imposee 2 1. 1.
                        ampli_moyenne_recyclee 2 0. 0.
                        ampli_fluctuation 2 0. 0. }
            out frontiere_ouverte K_EPS_EXT Champ_Front_Uniforme 2 0.125e-2 0.492e-2
            wall paroi
        }
        conditions_initiales
        {
            k_Eps Champ_Uniforme 2 1.6e-7 1.6e-8
        }
    }
    turbulence_paroi loi_expert_hydr { methode_calcul_face_keps_impose que_les_faces_des_elt
    }
    Traitement_particulier { Canal
    {
        dt_impr_moy_spat 50.
    }
}
Postraitemt
{
    Sondes
    {
        sonde_V03 vitesse periode 0.01 segment 30 3. 3.25 3. 4.55
        sonde_V06 vitesse periode 0.01 segment 30 6. 2.65 6. 4.55
        sonde_V14 vitesse periode 0.01 segment 30 14. 1.50 14. 4.698
        sonde_V17 vitesse periode 0.01 segment 30 17. 0.90 17. 4.698
        sonde_V21 vitesse periode 0.01 segment 30 20. 0.43 20. 4.698
        sonde_V24 vitesse periode 0.01 segment 30 24. 0.30 24. 4.698
        sonde_V27 vitesse periode 0.01 segment 30 27. 0.30 27. 4.698
        sonde_V30 vitesse periode 0.01 segment 30 30. 0.30 30. 4.698
        sonde_V34 vitesse periode 0.01 segment 30 34. 0.30 34. 4.698
    }
    Format lata
    Champs binaire dt_post 100.
    {
        pression_pa elem
        vitesse faces
        k elem
        eps elem
        viscosite_turbulente elem
    }
}

```

```
y_plus elem
}
}
Sauvegarde binaire OBI.sauv
}
Solve pb
End
```

Mixing length in 2D and 3D VEF-plane channel

2.1 Purpose

The purpose is to validate one particular model of turbulence in TrioCFD, the 'mixing length' model. Comparisons are carried out in two and three dimensions with the analytical law of Reichardt [1] on several VEF meshes. The system is a plane channel in 2D and a parallelepipedal box in 3D, with periodic boundary conditions except in y -direction. The wall function of Reichardt is applied for the TrioCFD computations. The relative errors of the Re_τ number are given for two values of the Re_b number, where the reference is obtained from the Dean's correlation. The comparisons are also carried out with TrioCFD simulations with the $k - \epsilon$ model.

Validation made by : R. PAILLE.
Report generated 11/01/2021.

2.2 Problem Description

Geometry

The geometry is a two-dimensional plane channel of dimensions $L_y = h = 2$, $L_x = 0.2$ or 0.8 . For three-dimensional simulations, the geometry is a parallelepipedal box of same dimensions with $L_z = L_x$.

Initial Conditions and Boundary Conditions

A non-null velocity $U_x=10$ is initialized inside the domain. Periodic boundary conditions are applied in x - and z -directions and no-slip boundary conditions are applied on top and bottom y -walls. A source term is added in order to maintain a constant flow.

Fluid Properties

Incompressible case:

The fluid is incompressible of constant density $\rho = 1$. Two values of viscosity are used for simulations: $\mu = 0.001$ or 0.0001 such as $Re_b = (U_b l)/\nu = 10\ 000$ or $100\ 000$ where $l = 1$ is the half-height $h/2$.

2.3 Case Setup

Grid

Four VEF meshes are used for the simulations: two 2D meshes (Figs 1 and 2) with option 'trianguler_fin' and two 3D meshes (Fig 3 and 4) with option 'tetraedriser_homogene_fin' (3D). The number of cells are $N_y = 6 - 11 - 21 - 41$, and $N_x = N_z = 3$ with options 'trianguler_fin' (2D) or 'tetraedriser_homogene_fin' (3D)

Canal_perio { bord periox }

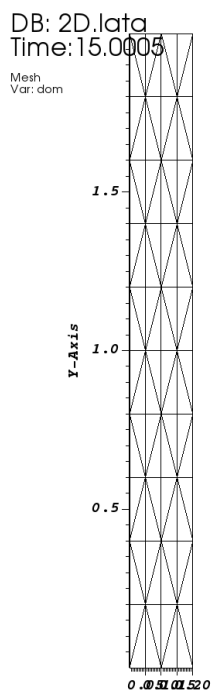


Figure V.2.1: 3 x 6 in 2D geometry

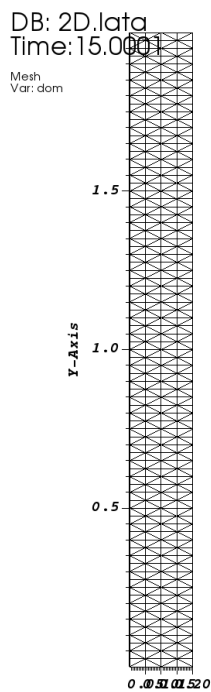


Figure V.2.2: 3 x 41 in 2D geometry

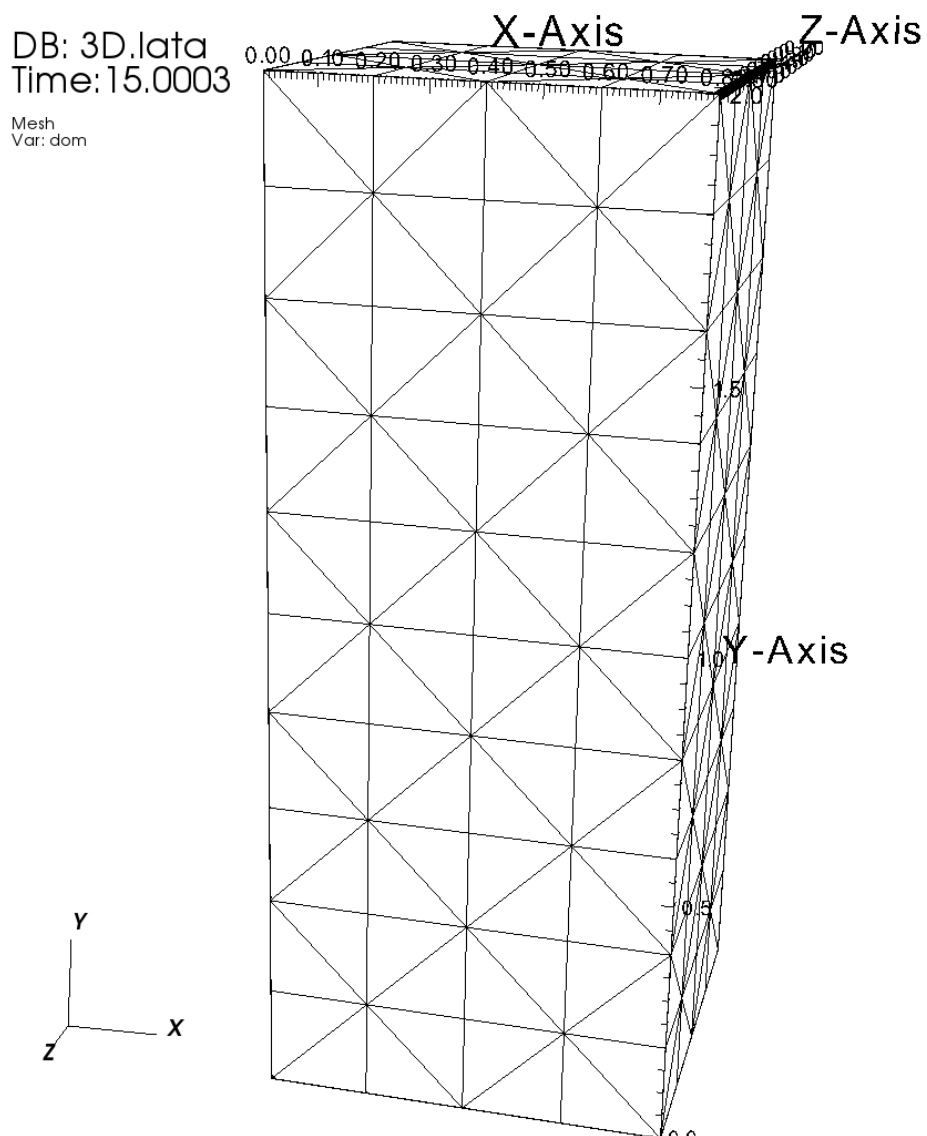


Figure V.2.3: 3 x 6 x 3 in 3D geometry

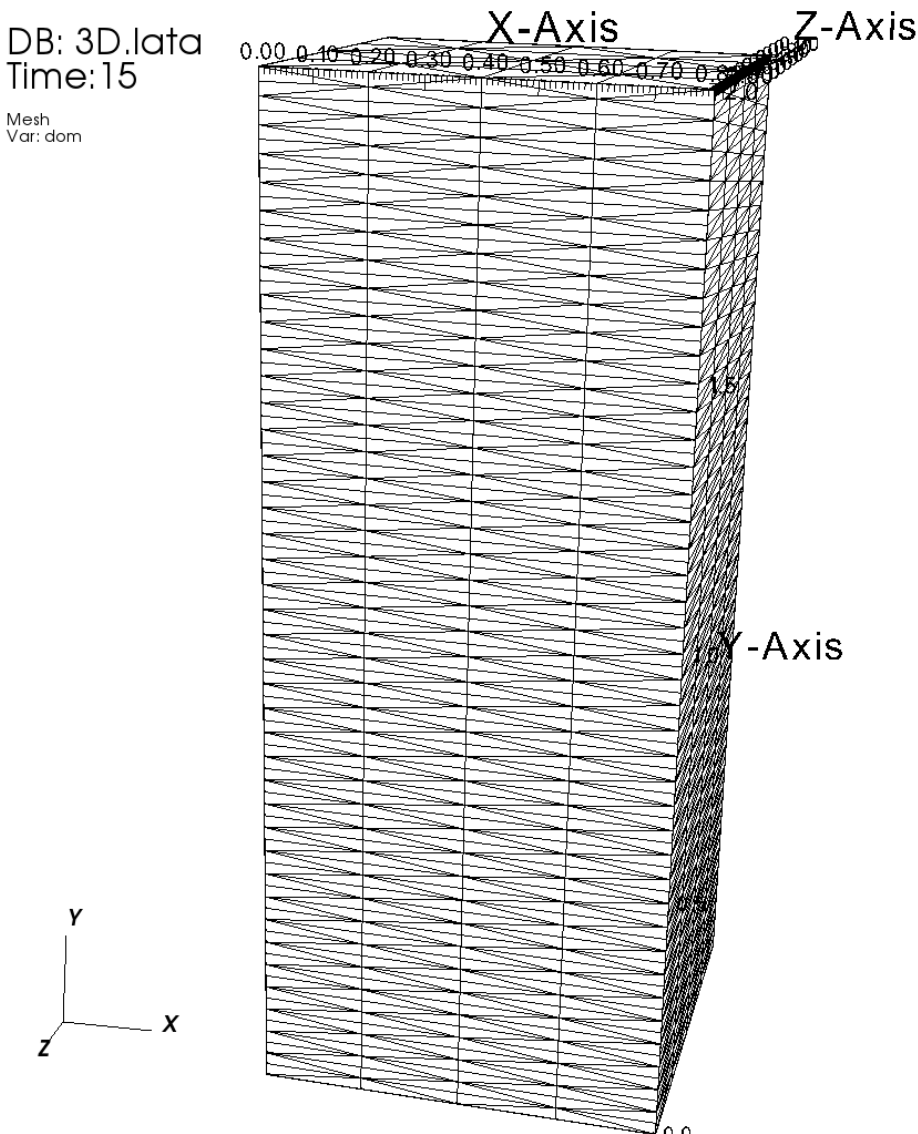


Figure V.2.4: 3 x 41 x 6 in 3D geometry

Model Options

The 'mixing length' model of turbulence is applied inside a double-periodic plane channel. The flow is forced by adding a source term in the impulsion balance equation.

Other Options (calculation)

The convection scheme is 'EF_stab'. All other numerical options are summarized in section 4.1.

2.4 Results

Validation Specific Informations

- Version TRUST : 1.5.5
- Type of problem : Hydraulique_Turbulent

- Diffusion scheme : Default{}
- Discretization : VEFPreP1B
- Time scheme : Euler_explicite (fac_sec 0.9)
- Solving of equations : Navier Stokes turbulent with Modele_turbulence Longueur_melange
- Solving of equations : Turbulence_paroi_loi_standard_hydr (new ones)
- Convection : EF_stab
- Turbulence model : Mixing Length (compared with k- ϵ)
- Type of boundary conditions : Periodicity in x (and z for 3D) direction, wall for y boundaries
- Location: /validation/share/Validation/Rapports_automatiques/Validant/Fini/Mixing_length_VEF_WF
- Master Test case: 2D.data - 3D.data - 3D_keps.data
- Generated Test cases :
 - 2D_100000_11/2D.data :
 - 2D_100000_21/2D.data :
 - 2D_100000_41/2D.data :
 - 2D_100000_6/2D.data :
 - 2D_10000_11/2D.data :
 - 2D_10000_21/2D.data :
 - 2D_10000_41/2D.data :
 - 2D_10000_6/2D.data : /**/
 - 3D_11/3D.data :
 - 3D_21/3D.data :
 - 3D_21_keps/3D_keps.data :
 - 3D_41/3D.data :
 - 3D_6/3D.data : /**/
 - 3D_6_keps/3D_keps.data : /**/
- Performance Chart :

	host	system	Total CPU Time	CPU time/step	number of cell
2D_100000_11/2D	is241762.intra.cea.fr	Linux	9.40639	0.000477272	160
2D_100000_21/2D	is241762.intra.cea.fr	Linux	15.435	0.000630364	320
2D_100000_41/2D	is241762.intra.cea.fr	Linux	52.5335	0.00118327	640
2D_100000_6/2D	is241762.intra.cea.fr	Linux	8.50823	0.000447995	80
2D_10000_11/2D	is241762.intra.cea.fr	Linux	11.0194	0.000486191	160
2D_10000_21/2D	is241762.intra.cea.fr	Linux	19.8518	0.000683158	320
2D_10000_41/2D	is241762.intra.cea.fr	Linux	62.4064	0.0011983	640
2D_10000_6/2D	is241762.intra.cea.fr	Linux	9.15485	0.000427046	80
3D_11/3D	is241762.intra.cea.fr	Linux	70.8697	0.00424826	1920
3D_21/3D	is241762.intra.cea.fr	Linux	317.766	0.00981064	3840
3D_21_keps/3D_keps	is241762.intra.cea.fr	Linux	524.347	0.0178621	3840
3D_41/3D	is241762.intra.cea.fr	Linux	5774.09	0.0512184	7680

	host	system	Total CPU Time	CPU time/step	number of cell
3D_6/3D	is241762.intra.cea.fr	Linux	30.3662	0.00181968	960
3D_6_keps/3D_keps	is241762.intra.cea.fr	Linux	48.3333	0.00289752	960
Total			6954.09		

Table V.2.1: Performance Chart

Plot Data

- **2D results for $Re_b = 10^4$**

The Re_τ number of TrioCFD is compared to the Dean's correlation ($Re_\tau = 0.175(Re_b)^{7/8}$) for two values of Re_b . For 2D simulations the relative errors are given in Table 2 for $Re_b = 10^4$ and Table 3 for $Re_b = 10^5$. For $Re_b = 10^4$ the velocity profiles along the y -direction are presented on Fig. 5 for four values of N_y and the comparison with the Reichardt analytical solution (red line) is presented on a graph $U+$ with respect to $y+$ in logscale (Fig. 6). The y -profile of ν_t is presented on Fig. 7.

	N_y	$y+$	Re_τ	Relative error
Theoretical(*)			554.7	
6	56.0	559.9	0.9	
11	28.2	563.5	1.6	
21	14.1	564.1	1.7	
41	6.6	524.7	5.4	

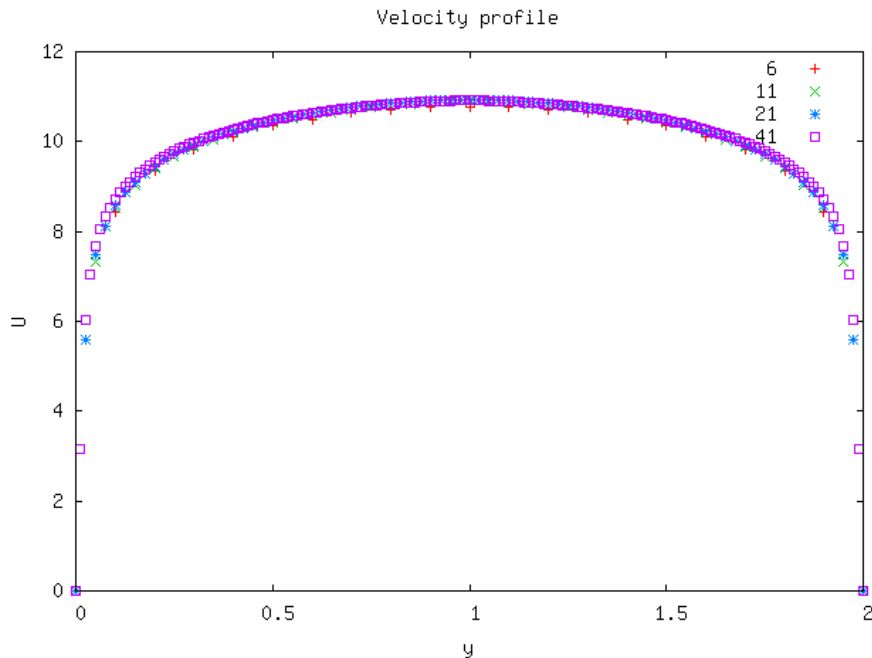
Table V.2.2: 2D - $Re_b = 10000$ 

Figure V.2.5: Velocity profile

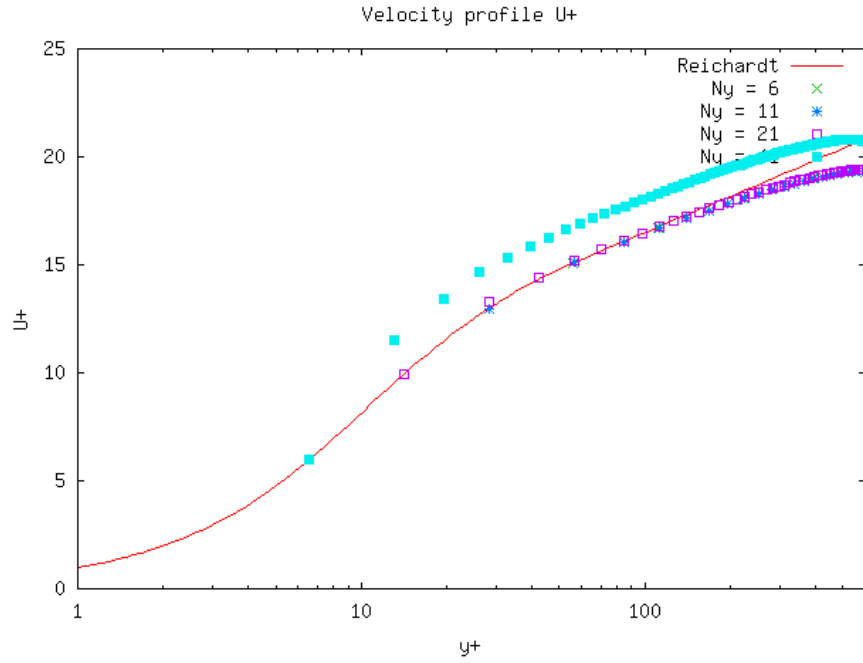
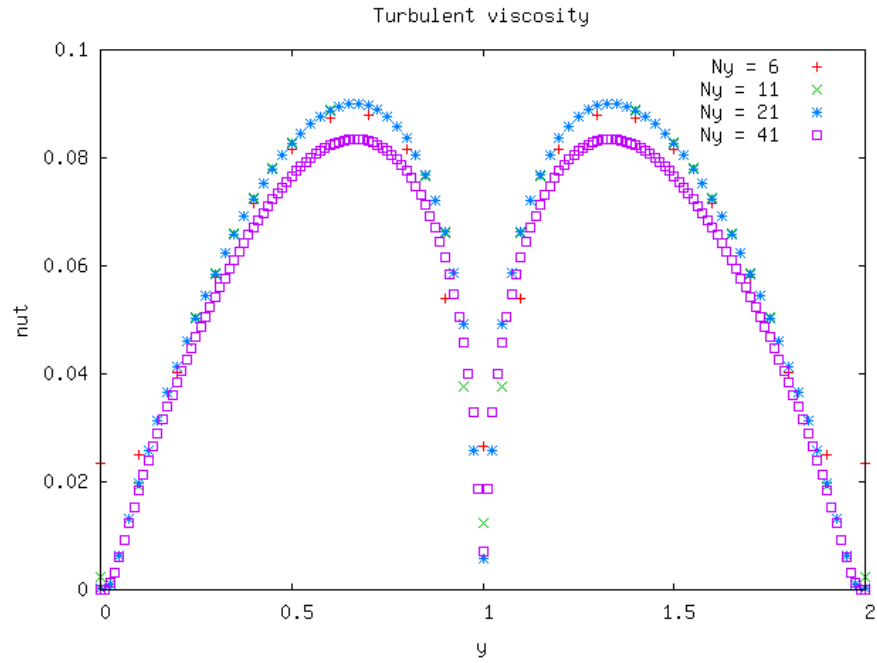
Figure V.2.6: Velocity profile $U+$ 

Figure V.2.7: Turbulent viscosity

- **2D results for $Re_b = 10^5$**

For the two-dimensional simulation with $Re_b = 10^5$, the relative errors on the Re_τ number (still compared to the Dean's correlation) are given in Table 3 and the same graphs are presented respectively on Fig. 8 for U , on Fig. 9 for $U+$ and Fig. 10 for ν_t . The Reichardt law is compared on Fig. 9.

	Ny	y+	Re_τ	Relative error
Theoretical(*)			4159.4	
6	439.9	4399.4	5.8	
11	220.3	4406.4	5.9	
21	110.3	4413.0	6.1	
41	55.2	4414.8	6.1	

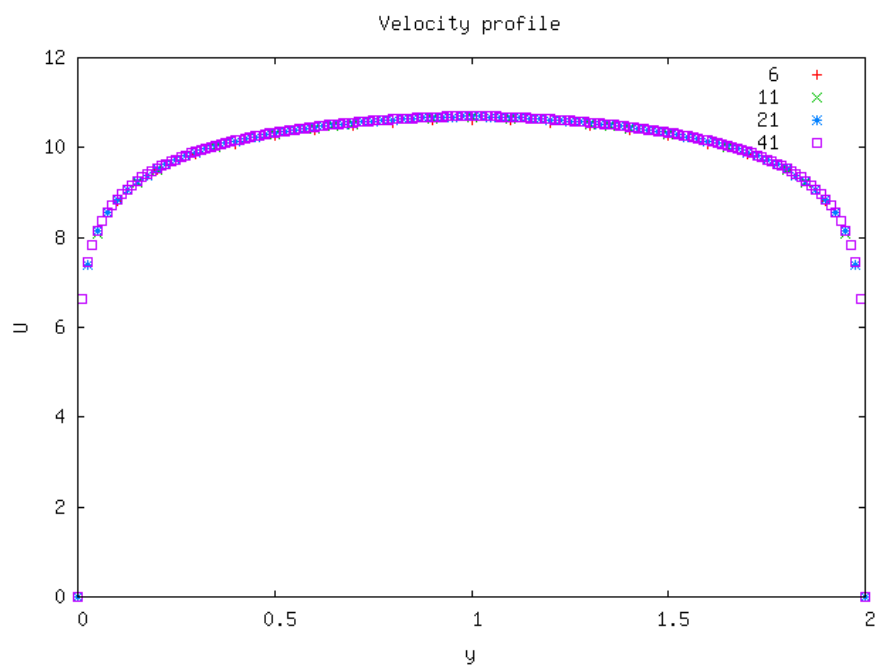
Table V.2.3: 2D - $Re_b = 10^5$ 

Figure V.2.8: Velocity profile

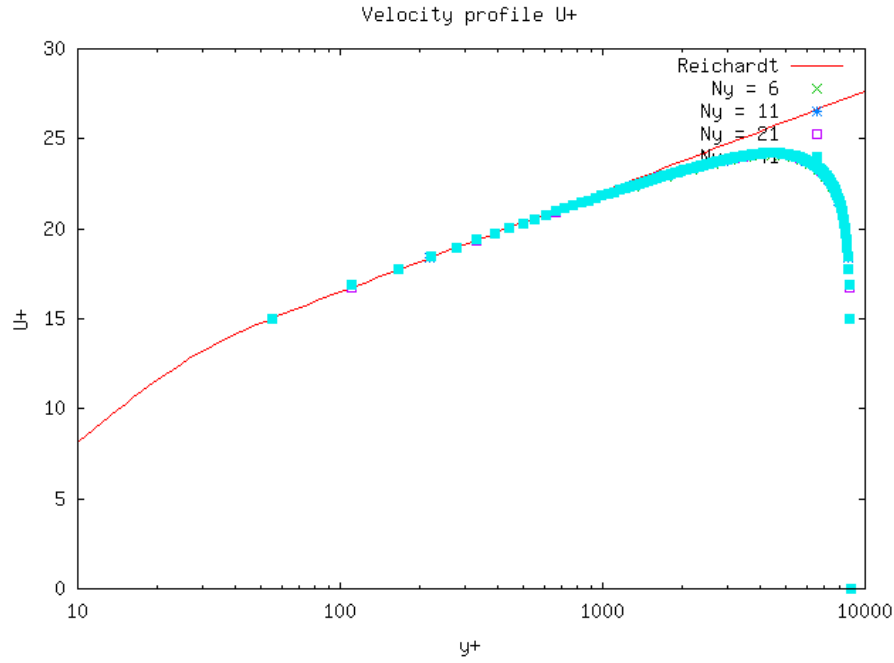
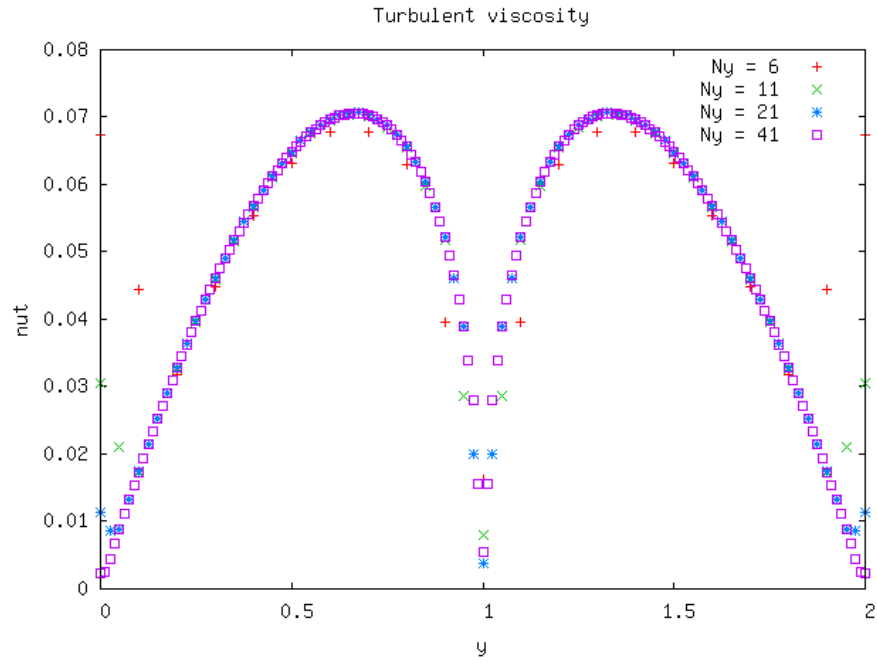
Figure V.2.9: Velocity profile $U+$ 

Figure V.2.10: Turbulent viscosity

- **3D results for $Re_b = 10^5$**

For 3D simulation, the relative errors are given in Table 4 for $Re_b = 10^5$. The profiles of U , $U+$ and ν_t are presented on Figs 11, 12 and 13. For the same physical quantities, three additional graphs appear for comparing the TrioCFD profiles of 'Mixing length'-model and ' $k - \epsilon$ '-model for several meshes (Figs 14, 15 and 16).

	Ny	y+	Re_τ	Relative error
Theoretical(*)			4159.4	
6	313.1	4696.2	12.9	
11	157.1	4711.6	13.3	
21	77.4	4645.7	11.7	
41	38.1	4571.4	9.9	
6keps	286.2	4292.9	3.2	
21keps	70.3	4215.4	1.3	

Table V.2.4: 3D - Reb = 100 000

NB : The use of 'tetraedriser_homogene mesh' for Ny=21 and k-eps model leads to higher relative error

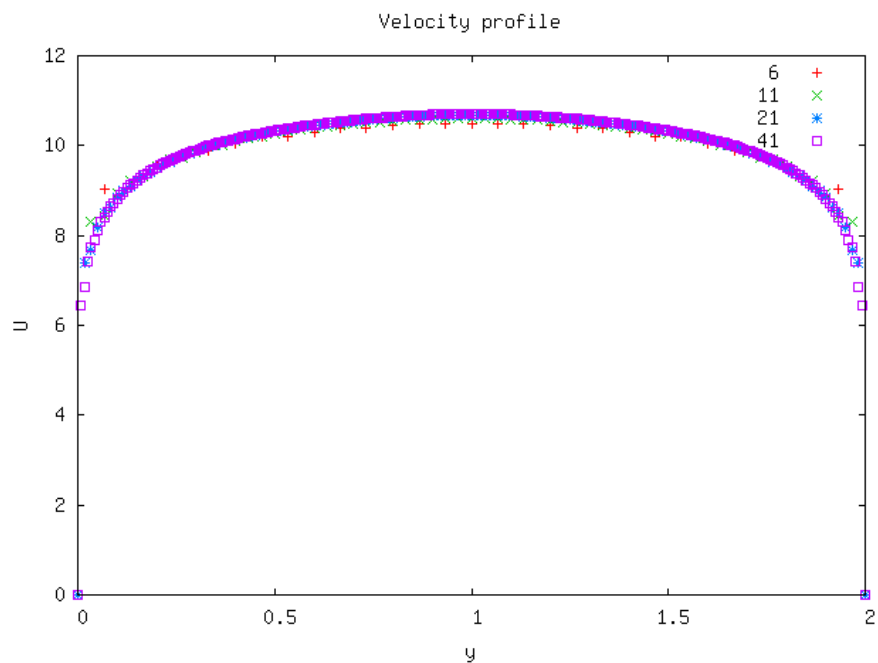


Figure V.2.11: Velocity profile

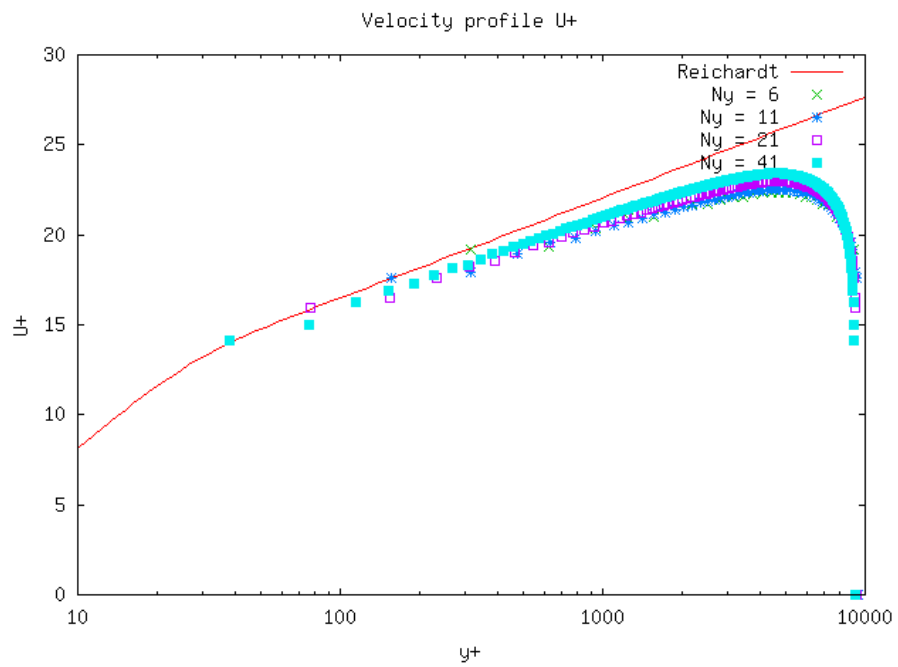
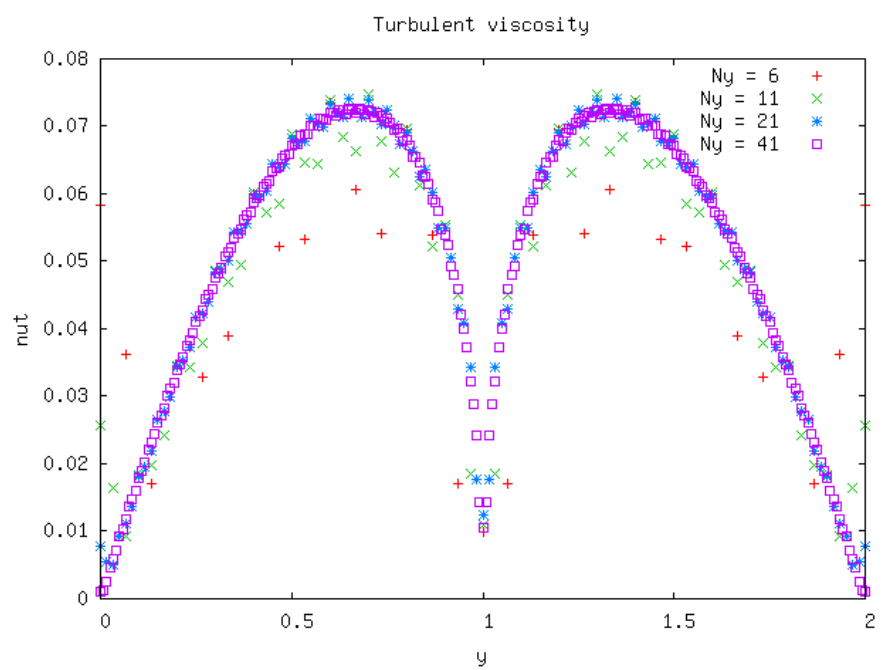
Figure V.2.12: Velocity profile $U+$ 

Figure V.2.13: Turbulent viscosity

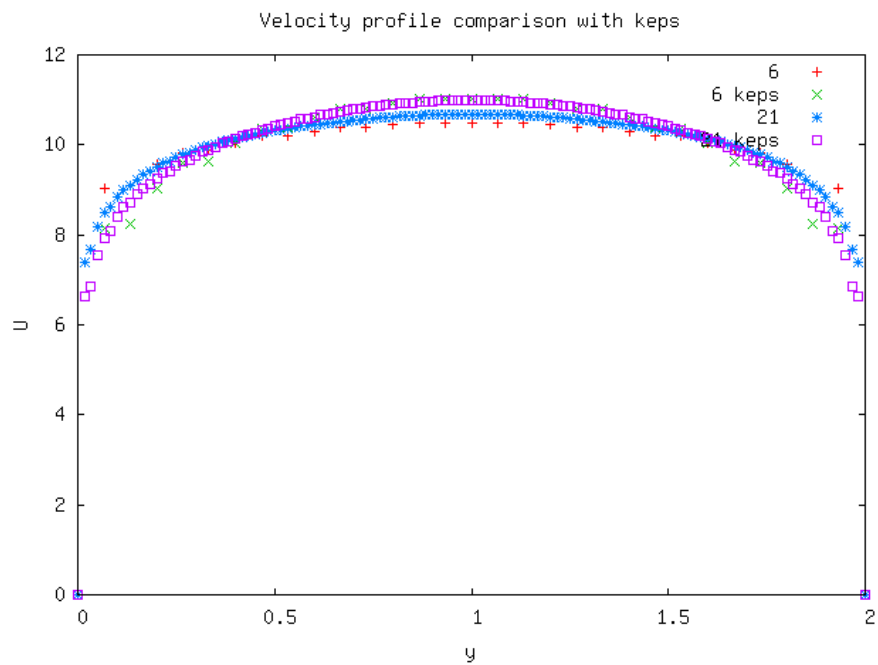
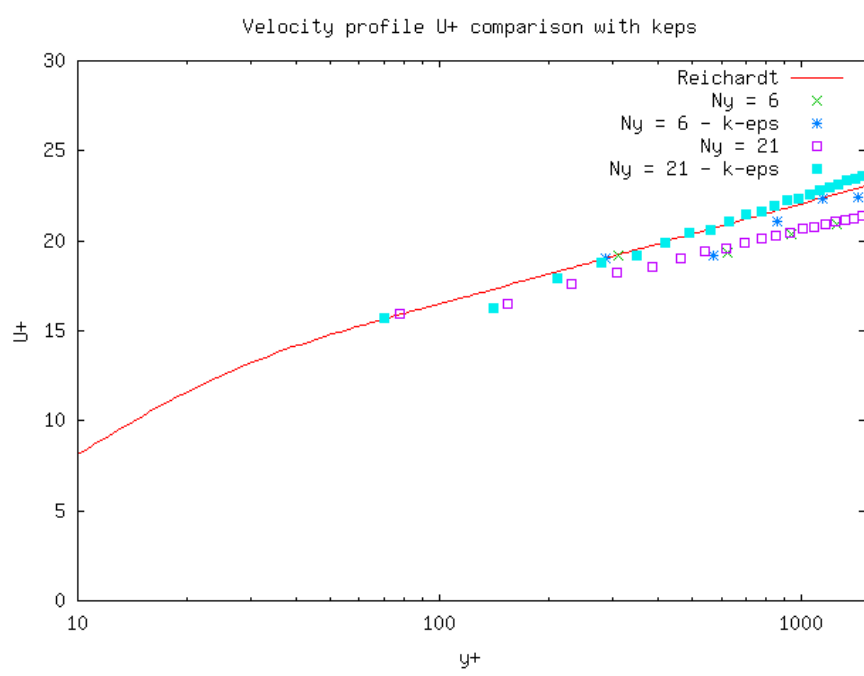


Figure V.2.14: Velocity profile comparison with keps

Figure V.2.15: Velocity profile U^+ comparison with keps

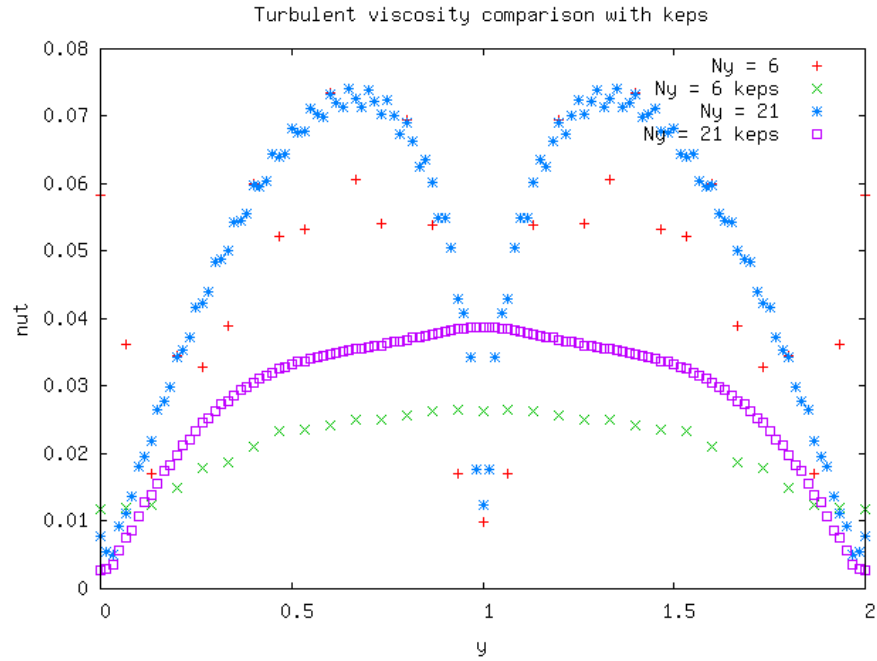


Figure V.2.16: Turbulent viscosity comparison with keps

2.5 Conclusion

With the 'Mixing length'-model, compared to the Dean's correlation, the 2D relative errors on Re_τ is about 2% when $Re_b = 10^4$ and 6% when $Re_b = 10^5$. For the 3D simulations with $Re_b = 10^5$, the relative error is about 10% with the 'Mixing length'-model whereas better results are obtained with the ' $k - \epsilon$ '-model (near 2%). Most of comparisons with the Reichardt analytical law are well-fitted except for the 2D case with $N_y = 41$ and $Re_b = 10^5$.

2.6 References

- [1] Reichardt H. : Vollstaendige Darstellung der turbulenten Geschwindigkeitsverteilung in glatten Leitungen. ZAMM 31, 208-219 (1951)
- [2] <http://www.sla.maschinenbau.tu-darmstadt.de/lehre/tms/Turbulence-TUDarmstadt-Pt2-6.pdf>

2.7 Data Files

2D

```
# SIMULATION D UN CANAL PLAN 2D avec modele Longueur de melange #
# PARALLEL NOT postraitemet #
# Tests du modele Longueur de Melange et de la procedure de calcul du frottement parietal (Paro
dimension 2
Pb_Hydraulique_Turbulent pb
Domaine dom
# BEGIN MESH #
Mailler dom
{
Pave Cavite
{
```

```

        Origine 0. 0.
        Nombre_de_Noeuds 3 6
        Longueurs 0.2 2.
    }
{
    Bord periox X = 0. 0. <= Y <= 2.
    Bord periox X = 0.2 0. <= Y <= 2.
    Bord bas Y = 0. 0. <= X <= 0.2
    Bord haut Y = 2. 0. <= X <= 0.2
}
}
Trianguler_fin dom
# END MESH #
# BEGIN PARTITION
Partition dom
{
    Partitionneur tranche { tranches 1 2 }
    Larg_joint 2
    Nom_Zones DOM
    periodique 1 periox
}
End
END PARTITION #
# BEGIN MESH #
Distance_paroi dom 2 haut bas binaire
# END MESH #
# BEGIN SCATTER
Scatter DOM.Zones dom
END SCATTER #
VEFPreP1b dis
Schema_Euler_explicite sch
Read sch
{
    tinit 0.
    tmax 15.
    dt_min 1.e-7
    dt_max 1.e-3
    dt_start dt_calc
    dt_impr 0.1
    dt_sauv 10.
    seuil_statio 1.e-8
    facsec 0.9
}
Fluide_Incompressible fluide
Read fluide
{
    mu Champ_Uniforme 1 0.001
    rho Champ_Uniforme 1 1
}
Associate pb dom
Associate pb sch
Associate pb fluide
Discretize pb dis
Read pb
{
    Navier_Stokes_Turbulent
    {
        solveur_pression GCP { precond ssor { omega 1.5 } seuil 1e-8 }
        convection { EF_stab { } }
        diffusion { }
        Sources { Canal_perio { bord periox } }
    }
}

```

```

conditions_initiales
{
    vitesse Champ_fonc_xyz dom 2 10. 0
}
boundary_conditions
{
    periox periodique
    haut paroi_fixe
    bas paroi_fixe
}
Modele_turbulence Longueur_Melange
{
    turbulence_paroi loi_standard_hydr dt_impr_ustar 10
    dmax 1000. fichier dom_Wall_length.xyz
}
Traitement_particulier { Canal
{
    dt_impr_moy_spat 5.
}
}
Postraitemet
{
    Sondes
    {
        sonde_vit vitesse periode 5. segment 50 0.05 0. 0.05 2.
        sonde_viscturb viscosite_turbulente periode 5. segment 50 0.05 0. 0.05 2.
    }
    format lata
    Champs dt_post 10
    {
        vitesse elem
        viscosite_turbulente elem
        pression elem
        y_plus elem
    }
}
Solve pb
End

```

3D

```

# SIMULATION D UN CANAL PLAN 2D avec modele Longueur de melange #
# PARALLEL NOT postraitemet #
# Tests du modele Longueur de Melange et de la procedure de calcul du frottement parietal (Paro
dimension 3
Pb_Hydraulique_Turbulent pb
Domaine dom
# BEGIN MESH #
Mailler dom
{
Pave Cavite
{
    Origine 0. 0. 0.
    Nombre_de_Noeuds 3 6 3
    Longueurs 0.8 2. 0.8
}
{
    Bord periox X = 0. 0. <= Y <= 2. 0. <= Z <= 0.8
    Bord periox X = 0.8 0. <= Y <= 2. 0. <= Z <= 0.8
}

```

```

        Bord bas      Y = 0. 0. <= X <= 0.8 0. <= Z <= 0.8
        Bord haut     Y = 2. 0. <= X <= 0.8 0. <= Z <= 0.8
        Bord perioz   Z = 0. 0. <= X <= 0.8 0. <= Y <= 2.
        Bord perioz   Z = 0.8 0. <= X <= 0.8 0. <= Y <= 2.
    }
}
Tetraedriser_homogene_fin dom
Corriger_frontiere_periodique { Domaine dom Bord periox }
Corriger_frontiere_periodique { Domaine dom Bord perioz }
# END MESH #
# BEGIN PARTITION
Partition dom
{
    Partitionneur_tranche { tranches 1 1 2 }
    Larg_joint 2
    Nom_Zones DOM
    periodique 2 periox perioz
}
End
END PARTITION #
# BEGIN MESH #
Distance_paroi dom 2 haut bas binaire
# END MESH #
# BEGIN SCATTER
Scatter DOM.Zones dom
END SCATTER #
VEFPreP1b dis
Schema_Euler_explicie sch
Read sch
{
    tinit 0.
    tmax 15.
    dt_min 1.e-7
    dt_max 1.e-3
    dt_start dt_calc
    dt_impr 1.
    dt_sauv 5.0
    seuil_statio 1.e-8
    facsec 0.9
}
Fluide_Incompressible fluide
Read fluide
{
    mu Champ_Uniforme 1 0.0001
    rho Champ_Uniforme 1 1
}
Associate pb dom
Associate pb sch
Associate pb fluide
Discretize pb dis
Read pb
{
    Navier_Stokes_Turbulent
    {
        solveur_pression GCP { precond ssor { omega 1.5 } seuil 1e-8 }
        convection { EF_stab { } }
        diffusion { }
        Sources { Canal_perio { bord periox } }
    }
    conditions_initiales
    {
        vitesse Champ_fonc_xyz dom 3 10. 0. 0.
    }
}

```

```

        }
    boundary_conditions
    {
        periox    periodique
        perioz    periodique
        haut      paroi_fixe
        bas       paroi_fixe
    }
Modele_turbulence Longueur_Melange
{
    turbulence_paroi loi_standard_hydr dt_impr_ustar 5.
    dmax 1000. fichier dom_Wall_length.xyz
}
Traitement_particulier { Canal
{
    dt_impr_moy_spat 5.
}
}
Postraitemet
{
    Sondes
    {
        sonde_vit vitesse periode 5. segment 50 0.05 0. 0.05 0.05 2. 0.05
        sonde_viscturb viscosite_turbulente periode 5. segment 50 0.05 0. 0.05
        0.05 2. 0.05
    }
    format lata
    Champs dt_post 10
    {
        vitesse elem
        viscosite_turbulente elem
        pression elem
        y_plus elem
    }
}
Solve pb
End

```

3D_keps

```

# SIMULATION D UN CANAL PLAN 2D avec modele Longueur de melange #
# PARALLEL NOT postraitemet #
# Tests du modele Longueur de Melange et de la procedure de calcul du frottement parietal (Paro
dimension 3
Pb_Hydraulique_Turbulent pb
Domaine dom
# BEGIN MESH #
Mailler dom
{
Pave Cavite
{
    Origine 0. 0. 0.
    Nombre_de_Noeuds 3 6 3
    Longueurs 0.8 2. 0.8
}
{
    Bord periox X = 0. 0. <= Y <= 2. 0. <= Z <= 0.8
    Bord periox X = 0.8 0. <= Y <= 2. 0. <= Z <= 0.8
    Bord bas Y = 0. 0. <= X <= 0.8 0. <= Z <= 0.8
}

```

```

        Bord haut      Y = 2. 0. <= X <= 0.8 0. <= Z <= 0.8
        Bord perioz   Z = 0. 0. <= X <= 0.8 0. <= Y <= 2.
        Bord perioz   Z = 0.8 0. <= X <= 0.8 0. <= Y <= 2.
    }
}
Tetraedriser_homogene_fin dom
Corriger_frontiere_periodique { Domaine dom Bord periox }
Corriger_frontiere_periodique { Domaine dom Bord perioz }
# END MESH #
# BEGIN PARTITION
Partition dom
{
    Partitionneur_tranche { tranches 1 1 2 }
    Larg_joint 2
    Nom_Zones DOM
    periodique 2 periox perioz
}
End
END PARTITION #
# BEGIN MESH #
Distance_paroi dom 2 haut bas binaire
# END MESH #
# BEGIN SCATTER
Scatter DOM.Zones dom
END SCATTER #
VEFPreP1b dis
Schema_Euler_explicite sch
Read sch
{
    tinit 0.
    tmax 15.
    dt_min 1.e-7
    dt_max 1.e-3
    dt_start dt_calc
    dt_impr 1.
    dt_sauv 5.0
    seuil_statio 1.e-8
    facsec 0.9
}
Fluide_Incompressible fluide
Read fluide
{
    mu Champ_Uniforme 1 0.0001
    rho Champ_Uniforme 1 1
}
Associate pb dom
Associate pb sch
Associate pb fluide
Discretize pb dis
Read pb
{
    Navier_Stokes_Turbulent
    {
        solveur_pression GCP { precond ssor { omega 1.5 } seuil 1e-8 }
        convection { EF_stab { } }
        diffusion { }
        Sources { Canal_perio { bord periox } }
    }
    conditions_initiales
    {
        vitesse Champ_fonc_xyz dom 3 10. 0. 0.
    }
}

```

```

boundary_conditions
{
periox    periodique
perioz    periodique
haut      paroi_fixe
bas       paroi_fixe
}
modele_turbulence_K_Epsilon {
    Transport_K_Epsilon
    {
        convection { EF_stab { } }
        diffusion { }
        boundary_conditions {
            periox    periodique
            perioz    periodique
            haut      paroi
            bas       paroi
        }
        conditions_initiales { k_eps Champ_Uniforme 2 0.45 0.075 }
    }
    turbulence_paroi loi_standard_hydr dt_impr_ustar 5.
}
Traitement_particulier { Canal
{
    dt_impr_moy_spat 5.
}
}
Postraitemet
{
    Sondes
    {
        sonde_vit   vitesse periode 5. segment 50 0.05 0. 0.05 0.05 2. 0.05
        sonde_viscturb viscosite_turbulente periode 5. segment 50 0.05 0. 0.05
0.05 2. 0.05
    }
    format lata
    Champs dt_post 10
    {
        vitesse elem
        viscosite_turbulente elem
        pression elem
        y_plus elem
    }
}
Solve pb
End

```

VI. Thermal Turbulent Flow

LIKE for laminar flows, in this section, thermal aspects are added to turbulent flows. In this version of the report, two cases are studied:

- Thermal stratification flow in a plenum
- Turbulent flow inside a double-periodic plane channel with heated walls

These two cases both use $k - \epsilon$ model for turbulence and 3D modeling.



Thermal stratification flow in a plenum

1.1 Purpose

The purpose of this test case is to compare TrioCFD with an experiment carried out by Kamide et al. (see reference [1]). In that experiment, the geometry is a plenum with an inlet channel representing the upper part of a neutron shield of a fuel assembly. The experiment is performed in water and the right vertical wall of the cavity (see Fig. 1 below) is cooled to simulate the cooling liquid metal. The aim of this experiment is to highlight the thermal stratification of flow and the establishment of a phenomenon of natural convection in the upper plenum. The turbulence model of TrioCFD is based on the ' $k - \epsilon$ ' one which is coupled with the temperature equation and a wall function for modeling the thin boundary layer. The simulations are carried out in 2D and 3D by considering two types of boundary condition at the cold vertical wall: Neumann and Dirichlet.

Validation made by : MALOD C., VANDROUX S., BARTHEL V.
Report generated 12/01/2021.

1.2 Problem Description

Geometry

The geometry (see Fig. 1) reproduces a plenum with an inlet channel representing the upper part of a neutron shield of a fuel assembly (see reference [1]). The inlet is located at the lower part of the system and the outlet is located at the upper part. Comparisons with experimental data will be performed on the two dashed vertical lines P1 and P4. Neumann and Dirichlet boundary conditions will be considered on the cold wall (right side of Fig. 1).

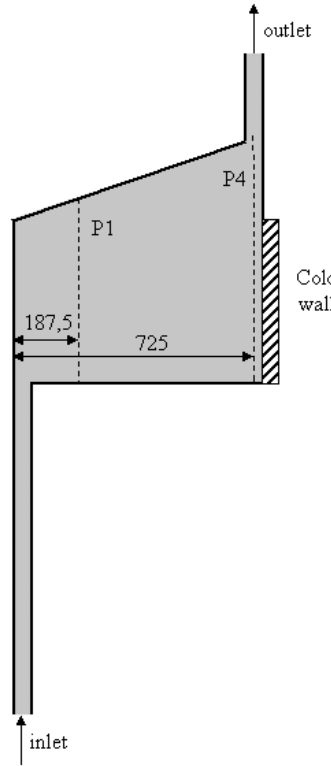


Figure VI.1.1: Geometry

Initial Conditions and Boundary Conditions

The initial velocity is set equal to 0 m/s in all the domain. Symmetry is applied in z -direction. The boundary conditions are velocity imposed at inlet to 0.0415 m/s, and pressure imposed to 0 Pa at outlet. The turbulent kinetic energy is set to $1.6e-7 \text{ m}^2/\text{s}^2$ on inlet and outlet, and the turbulent dissipation rate set to $1.6e-8 \text{ m}^3/\text{s}^2$ on inlet and outlet. Thin boundary layer equations model are solved on all wall boundaries with 50 nodes in the TBLE grid and a stretching ratio equal to 1.

Fluid Properties

The physical properties of water at 48.9°C are set equal to $\rho = 988.03 \text{ kg/m}^3$ for density, $\mu = 5.49e-4 \text{ kg/m/s}$ for dynamic viscosity, $\lambda = 0.59 \text{ W/m/K}$ for thermal conductivity, $C_p = 4180 \text{ J/kg/K}$ for specific heat, and $\beta = 3.9e-4 \text{ 1/K}$ for thermal expansion coefficient.

Flow Physics

It is expected to observe a thermal stratification of flow and the establishment of natural convection phenomenon in the upper plenum. A turbulence model is taken into account as well as buoyancy force with the Boussinesq approximation and wall function.

1.3 Case Setup

Grid

The 3D mesh, made with Icem, contains 27 252 tetrahedral cells and 6 546 nodes (Fig. 2). The histogram of largest angles of 3D mesh is also presented on Fig. 3.

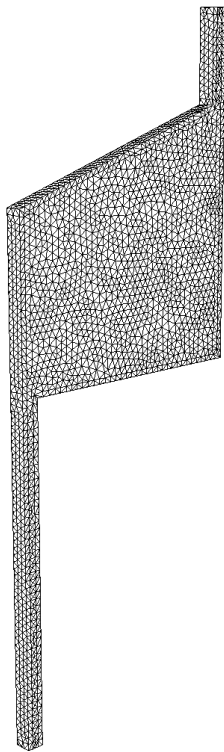


Figure VI.1.2: 3D mesh

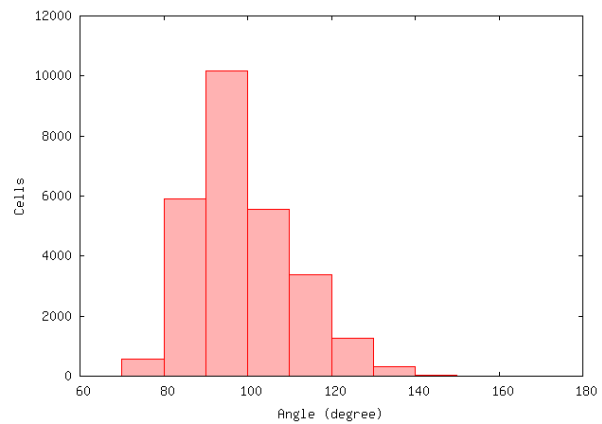


Figure VI.1.3: Histogram of angles for 3D mesh

The 2D mesh is obtained by slicing the 3D one (Fig. 4). It contains 2 968 triangular cells and 1 619 nodes. The histogram of largest angles of 2D mesh is presented on Fig. 5.

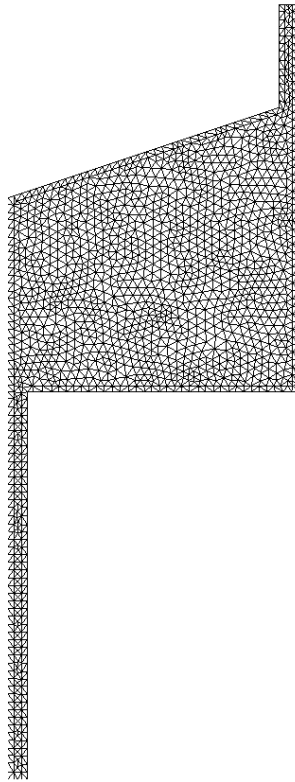


Figure VI.1.4: 2D mesh

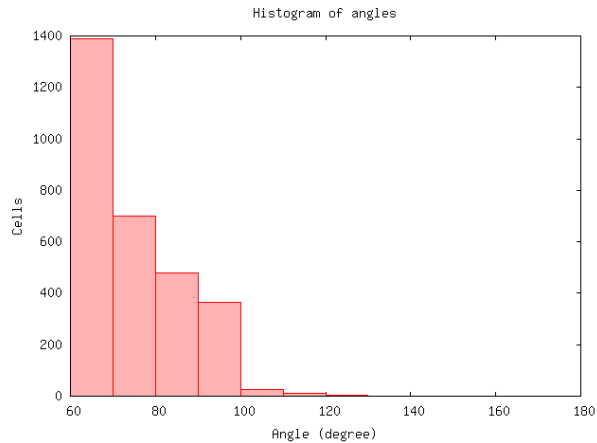


Figure VI.1.5: Histogram of angles for 2D mesh

Model Options

Four simulations are carried out in order to study the influence of two types of boundary condition for temperature on the cold wall (see Fig. 1): either Neumann in 2D and 3D or Dirichlet in 2D and 3D. For imposed flux, the results will be referenced by the labels '2D_H' and '3D_H', and for temperature, the labels will be '2D_T' and '3D_T'. The gravity is considered through the Boussinesq buoyancy force in the impulsion balance equation.

Other Options (calculation)

The time scheme is implicit and the convection schemes are respectively 'EF_stab' for momentum and energy equations and 'Amont' for turbulence model. All other details of numerical schemes and model options are summarized in section 4.1. The parameters values related to the numerical methods are given in the datafile of Section 7.

1.4 Results

Validation Specific Informations

- Version TRUST : 1.6.2
- Type of problem : Pb_Thermohydraulique_Turbulent
- Discretization : VEFPreP1B
- Time scheme : Euler_Implicite with Solver Implicite
- Solving of equation : Navier_Stokes_turbulent with Modele_turbulence K_Epsilon and Turbulence_paroi Paroi_TBle, and Convection_Diffusion_Temperature_Turbulent with Modele_turbulence Prandtl and Turbulence_paroi Paroi_TBle_scal
- Convection scheme : Ef_Stab for Momentum and Energy, and Amont for Turbulence
- Diffusion scheme : default for all equations
- Boundary condition : Velocity inlet, Pressure outlet, Symmetry and Wall
- Wall condition : Imposed heat flux (for test cases 2D_H and 3D_H) or temperature (for test cases 2D_T and 3D_T)
- Location: /validation/share/Validation/Rapports_automatiques/Validant/Fini/Thermal_stratification_flow
- Master Test case: Plenum.data
- Generated Test cases :
 - ./2D_H/Plenum.data :
 - ./2D_T/Plenum.data :
 - ./3D_H/Plenum.data : /* jdd attached */
 - ./3D_T/Plenum.data :
- Performance Chart :

	host	system	Total CPU Time	CPU time/step	number of cell
./2D_H/Plenum	is241762.intra.cea.fr	Linux	690.16	0.0624166	2968
./2D_T/Plenum	is241762.intra.cea.fr	Linux	1248.08	0.0559659	2968
./3D_H/Plenum	is241762.intra.cea.fr	Linux	26785.6	1.10389	27252
./3D_T/Plenum	is241762.intra.cea.fr	Linux	26397.4	1.06949	27252
Total			55121.2		

Table VI.1.1: Performance Chart

Plot Data

- Time iterations until steady state

This section presents the time evolution of physical quantities until the steady state is reached (after about 2000 s of physical time). The evolutions are presented on points A, B and line C (see Fig. 6) for velocity (Fig. 7), temperature (Fig. 8) and pressure (Fig. 9). On the graphs four curves are plotted, corresponding to each simulation '2D_H' (red), '3D_H' (blue), '2D_T' (green) and '3D_T' (magenta). Those physical quantities were chosen because they are the least well-converged. The residuals of each calculation are also plotted on Fig. 10.

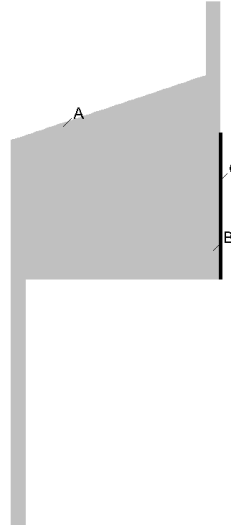


Figure VI.1.6: Positions of points for convergence study

In order to ensure that the calculations are correct, the table 2 below presents the flow balance for each simulation.

	IN	OUT	Total
2D_H	-0.002075	0.002075	-4.33680869e-19
2D_T	-0.002075	0.002075	-8.67361738e-19
3D_H	-0.000103750024	0.000103750024	-6.77626358e-20
3D_T	-0.000103750024	0.000103750024	4.06575815e-20

Table VI.1.2: Flow balance

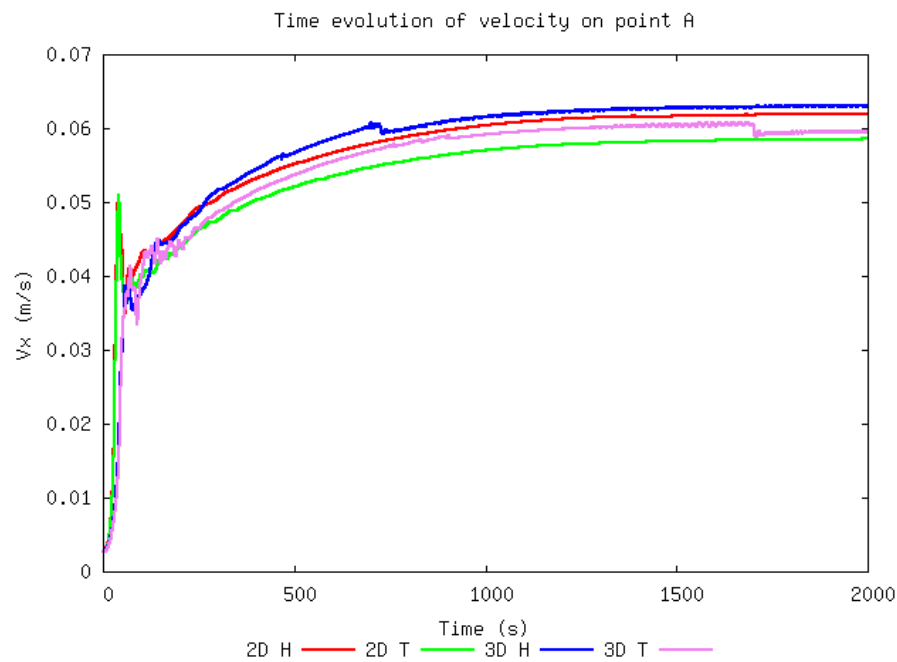
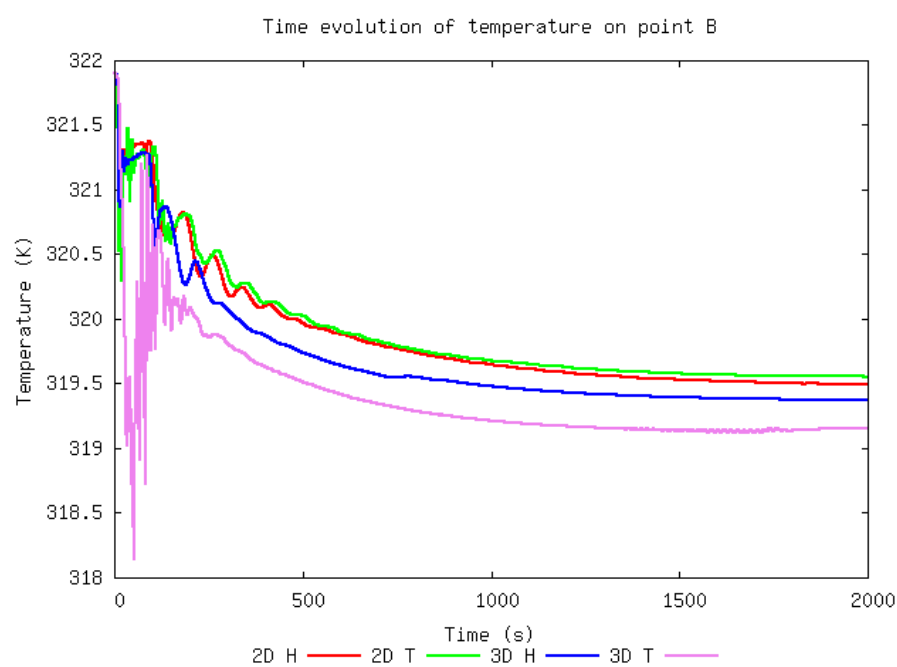
Figure VI.1.7: Time evolution of V_x on point A

Figure VI.1.8: Time evolution of temperature on point B

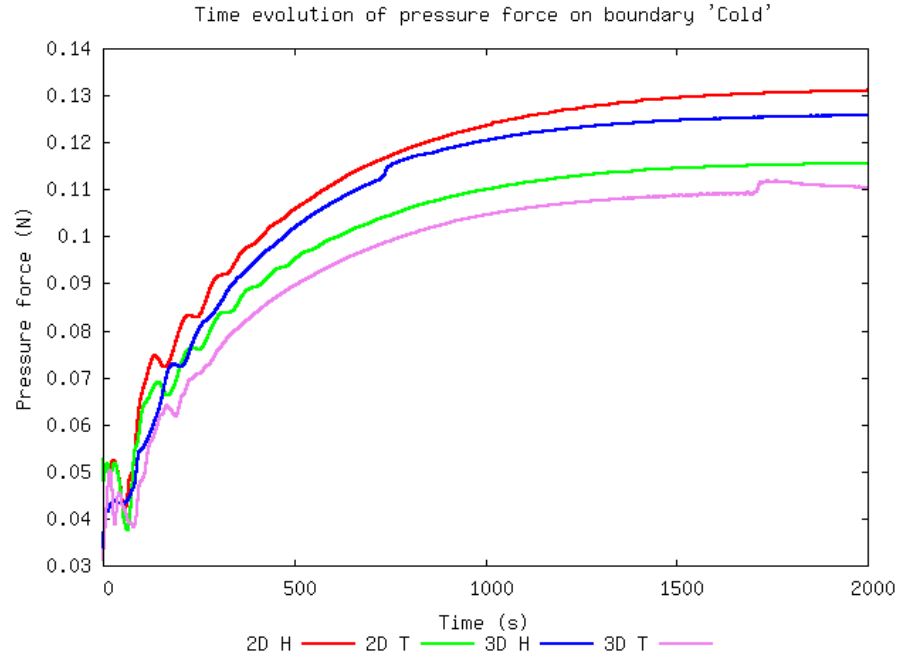


Figure VI.1.9: Time evolution of pressure force on boundary 'Cold'

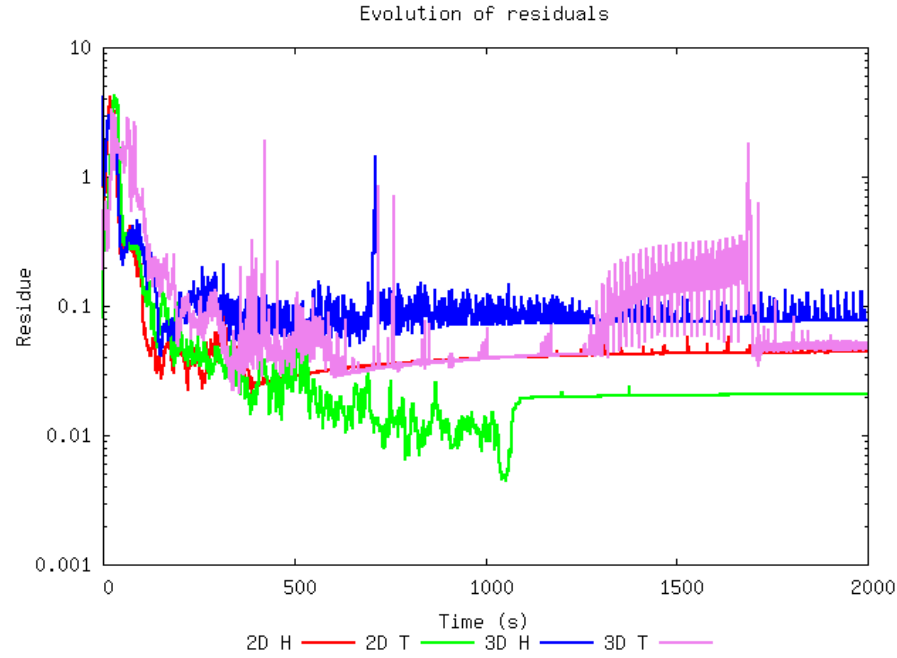
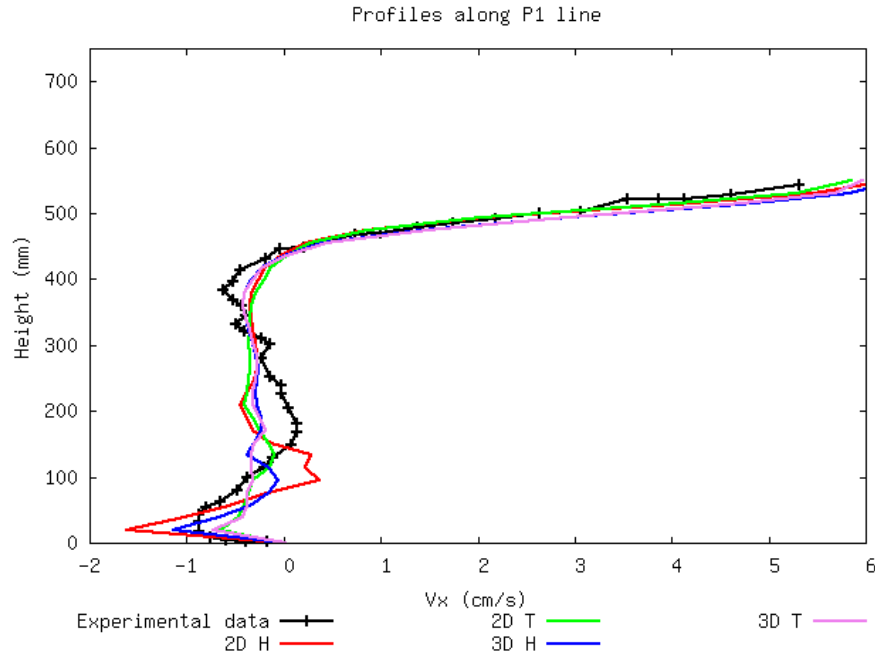
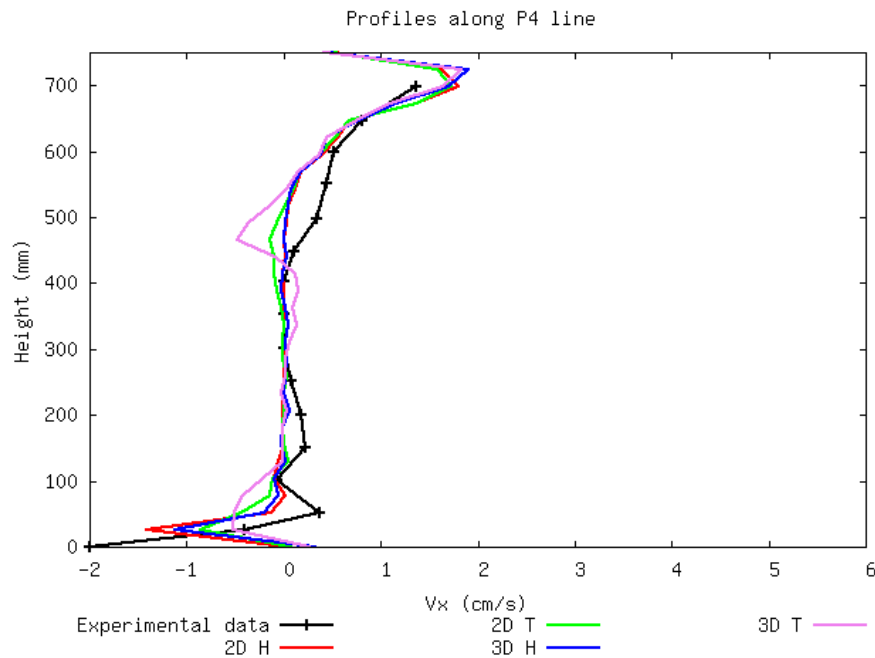


Figure VI.1.10: Evolution of residuals

- **Velocity profiles (V_x -component)**

In this part we present the velocity profiles along the lines P1 and P4, compared to experimental data (black lines). The other curves correspond to 2D_H (red), 3D_H (blue), 2D_T (green) and 3D_T (magenta). For P1 line, the velocity profiles are plotted on Fig. 11, and for P4 line they appear on Fig. 12. The experimental velocity profiles are quite well reproduced by the simulations.

Figure VI.1.11: Profiles of V_x along the P1 lineFigure VI.1.12: Profiles of V_x along P4 line

- Temperature profiles

The temperature profiles are plotted on Fig. 13 (P1 line) and Fig. 14 (P4 line). On both graphs we can observe that the temperatures are over-estimated for height 0mm. The experimental temperature is about 40°C wheras the numerical temperatures are near 44°C. When the height increases ($H > 100$ mm) the numerical temperatures are under-estimated compared to the experimental profile.

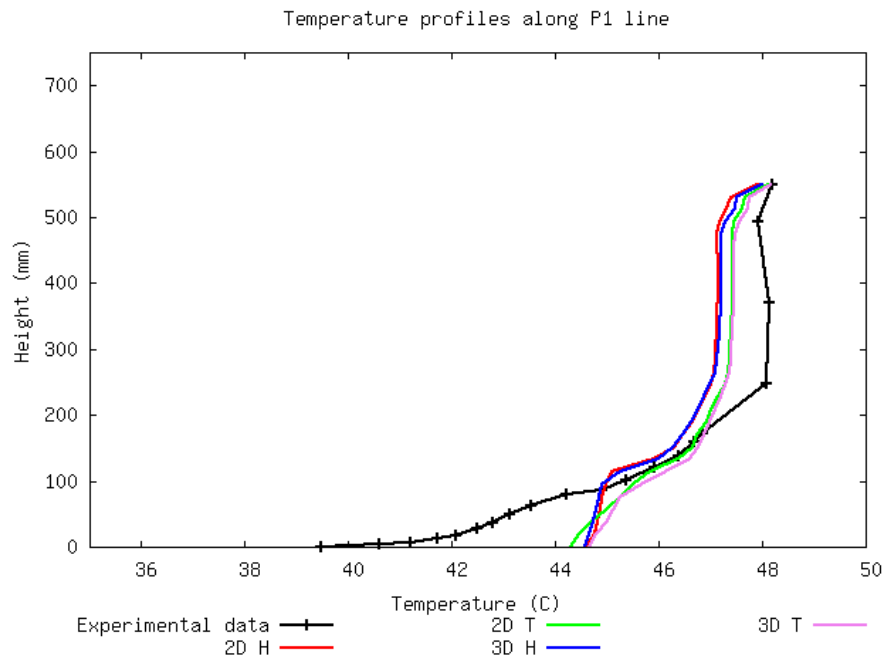


Figure VI.1.13: Temperature profiles along P1 line

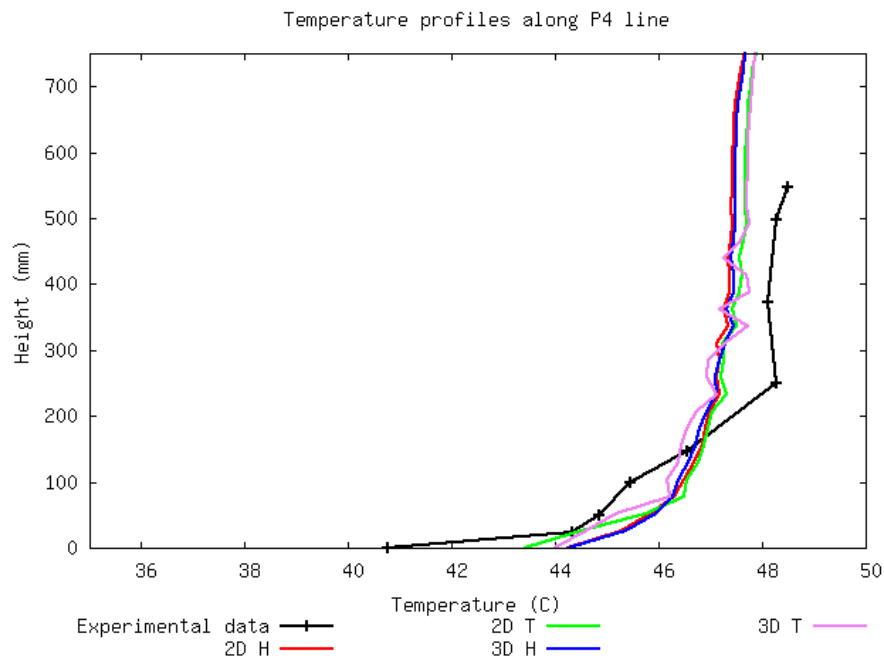
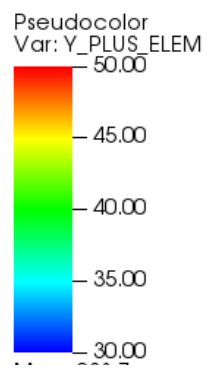
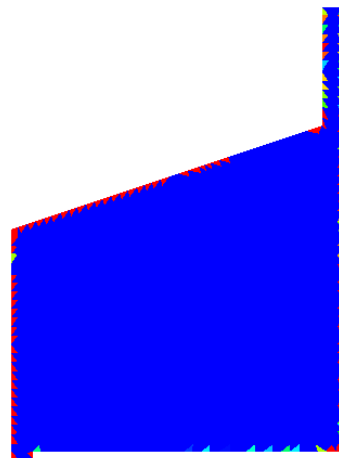
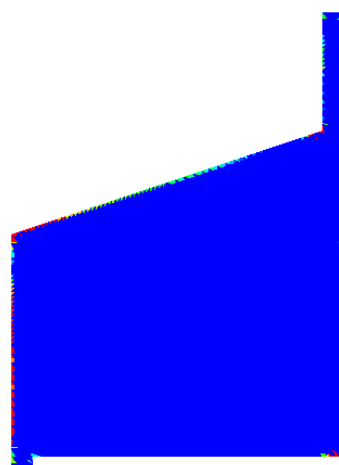


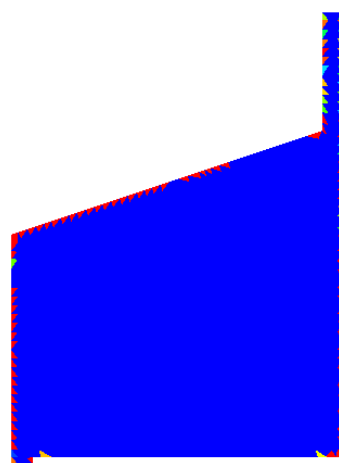
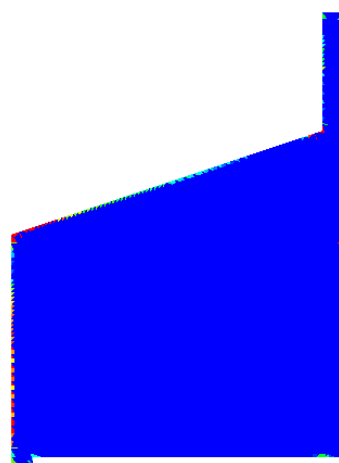
Figure VI.1.14: Temperature profiles along P4 line

The fields of Y_+ , velocity and temperature are shown in the rest of this document for illustration.

- **Distribution of Y_+**

In that section the color scale of Y_+ is first presented on Fig. 15, next the Y_+ fields are presented for 2D_H (Fig. 16), 3D_H (Fig. 17), 2D_T (Fig. 18) and 3D_T (Fig. 19).

Figure VI.1.15: Color scale for distribution of $Y+$ Figure VI.1.16: Distribution of $Y+$ for 2D_HFigure VI.1.17: Distribution of $Y+$ for 3D_H

Figure VI.1.18: Distribution of $Y+$ 2D_TFigure VI.1.19: Distribution of $Y+$ 3D_T

- Velocity fields

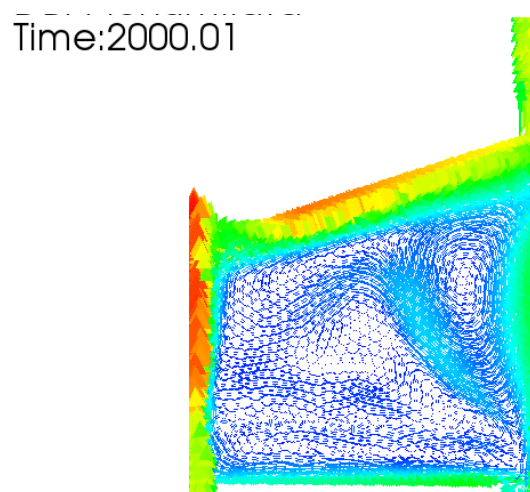


Figure VI.1.20: Velocity field for 2D_H

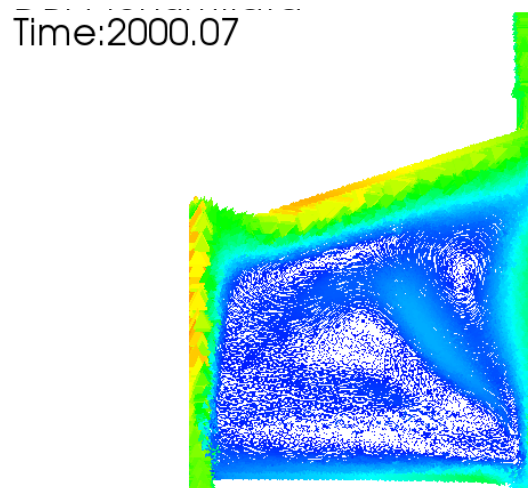


Figure VI.1.21: Velocity field for 3D_H

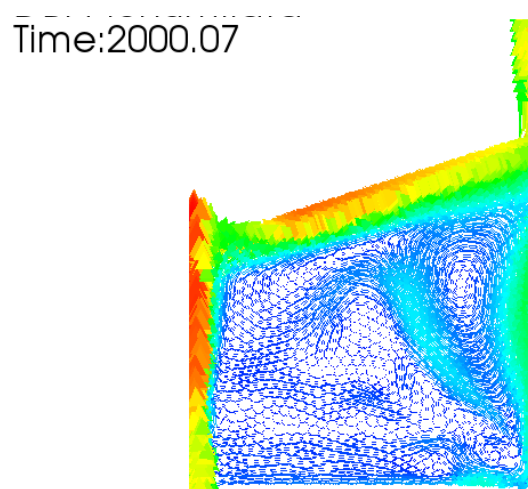


Figure VI.1.22: Velocity field for 2D_T

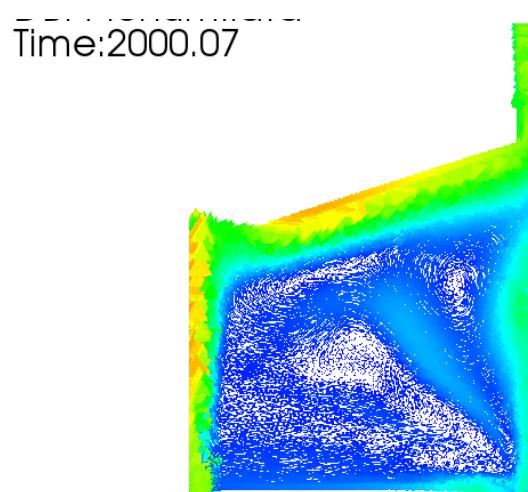


Figure VI.1.23: Velocity field for 3D_T

- Temperature fields

When flux is imposed on the wall, the temperature fields are presented on Figs. 25 (2D) and 26 (3D). When Dirichlet boundary condition is applied on the wall the temperature fields are presented on Figs. 27 (2D) and 28 (3D).

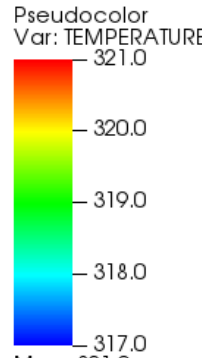


Figure VI.1.24: Color scale for distribution of Temperature

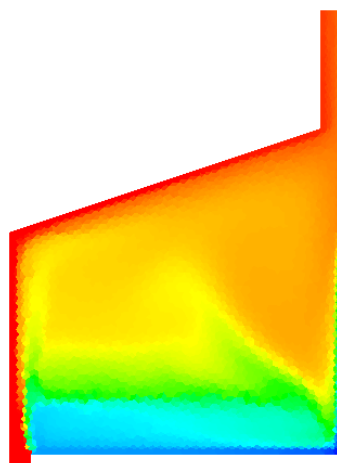


Figure VI.1.25: Temperature field for 2D_H

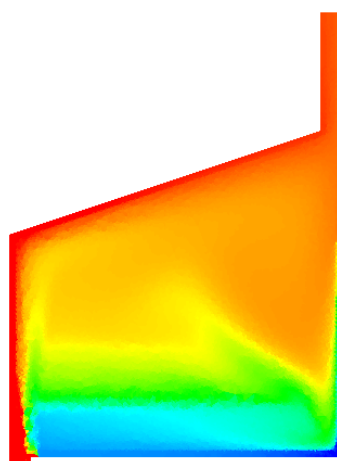


Figure VI.1.26: Temperature field for 3D_H

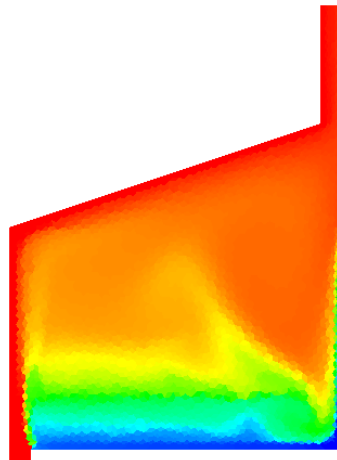


Figure VI.1.27: Temperature field for 2D_T

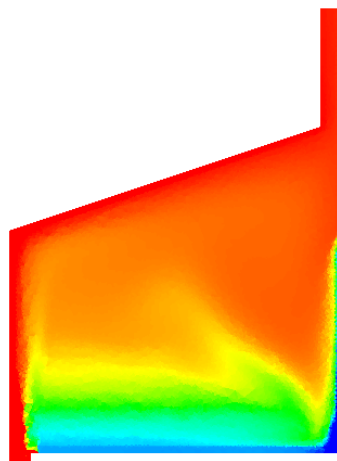


Figure VI.1.28: Temperature field for 3D_T

1.5 Conclusion

The non-isothermal flow in a plenum was simulated using the ' $k - \epsilon$ ' turbulence model in a plenum by considering two types of boundary conditions for temperature: imposed flux and imposed temperature. The TrioCFD results were quantitatively compared with experimental profiles of velocity and temperature. The fits are quite good for velocity along P1 and P4 profiles and TrioCFD gives similar results to other studies in reference.

• Recommendations for users

The time step and the cell size must be chosen small enough to ensure convergence of computations.

1.6 References

- [1] H. Kamide, J. Kobayashi, Y. Leda, H. Ninokata : Benchmark exercise for multi-dimensional thermohydraulic analysis codes. Journal of Hydraulic research vol.34, 1996, n°3.
- [2] E. Krepper, H-G Willschutz, F-P Weiss : Solution of a mixed convection flow benchmark using computational fluid dynamic codes. Technical report FZR-268, 47-55, 1999. <https://www.osti.gov/etdeweb/biblio/20053064>

1.7 Data Files

Plenum

```

dimension 3
Domaine dom_3D
Read_unsupported_ASCII_file_from_ICEM dom_3D ... / Plenum3D.asc
dilate dom_3D 1.e-3
#
Domaine dom_2D
Extract_2D_from_3D dom_3D SYMZ0 dom_2D
dimension 2
VerifierCoin dom_2D { }
#
Pb_Thermohydraulique_Turbulent pb
VEFPreP1B dis
Schema_Euler_implicite sch
Read sch
{
  tinit 0.
  tmax 2000.
  dt_min 1.e-6
  dt_max 1.5
  dt_impr 0.001
  dt_sauv 1000.
  dt_start dt_calc
  facsec 10
  facsec_max 20
  seuil_statio 1.e-8
  solveur implicite
  {
    seuil_convergence_solveur 1.e-13
    solveur gmres { diag seuil 1.e-13 impr controle_residu 1 nb_it_max 5 }
  }
}
Fluide_Incompressible fluide
Read fluide
{
  mu Champ_Uniforme 1 5.49e-4
  rho Champ_Uniforme 1 988.03
  lambda Champ_Uniforme 1 0.59
  Cp Champ_Uniforme 1 4180.
  beta_th Champ_Uniforme 1 3.9e-4
}
Champ_Uniforme gravite
Read gravite 3 0 -9.81 0
Associate fluide gravite
Associate pb dom_3D
Associate pb sch
Associate pb fluide
Discretize pb dis

```

```

Read pb
{
  Navier_Stokes_Turbulent
  {
    solveur_pression Cholesky { }
    convection { ef_stab { } }
    diffusion { }
    sources { boussinesq_temperature { T0 321.9 } }
    conditions_initiales { vitesse Champ_Uniforme 3 0. 0. 0. }
    boundary_conditions
    {
      IN frontiere_ouverte_vitesse_imposee champ_front_Uniforme 3 0. 0.0415 0.
      OUT frontiere_ouverte_pression_imposee champ_front_Uniforme 1 0.
      WALL paroi_fixe
      COLD paroi_fixe
      SYMZ0 symetrie
      SYMZ1 symetrie
    }
    modele_turbulence K_Epsilon
    {
      Transport_K_Epsilon
      {
        parametre_equation parametre_implicit { resolution_explicite }
        convection { amont }
        diffusion { }
        boundary_conditions
        {
          IN frontiere_ouverte_K_eps_impose Champ_Front_Uniforme 2 1.6e-7 1.6e-8
          OUT frontiere_ouverte K_EPS_EXT Champ_Front_Uniforme 2 1.6e-7 1.6e-8
          WALL paroi
          COLD paroi
          SYMZ0 symetrie
          SYMZ1 symetrie
        }
        conditions_initiales { k_Eps Champ_Uniforme 2 1.6e-7 1.6e-8 }
      }
      turbulence_paroi Paroi_TBLE { N 50 facteur 1 }
    }
  }
  Convection_Diffusion_Temperature_Turbulent
  {
    diffusion { }
    convection { ef_stab { } }
    boundary_conditions
    {
      IN frontiere_ouverte_temperature_imposee champ_front_uniforme 1 321.9
      OUT frontiere_ouverte T_ext champ_front_uniforme 1 321.9
      WALL paroi_adiabatique
      COLD paroi_flux_impose champ_Front_Uniforme 1 -2.13e+4
      SYMZ0 symetrie
      SYMZ1 symetrie
    }
    conditions_initiales { Temperature Champ_Uniforme 1 321.9 }
    modele_turbulence Prandtl
    {
      turbulence_paroi Paroi_TBLE_scal { N 50 facteur 1. }
    }
  }
  Postraitemet
  {
    Sondes
  }
}

```

```

{
  sonde_T1  temperature periode 0.01 segment 30 0.1875 0. 0. 0.1875 0.55 0.
  sonde_T2  temperature periode 0.01 segment 30 0.375 0. 0. 0.375 0.62 0.
  sonde_T3  temperature periode 0.01 segment 30 0.5625 0. 0. 0.5625 0.68 0.
  sonde_T4  temperature periode 0.01 segment 30 0.725 0. 0. 0.725 0.75 0.
  sonde_V1  vitesse   periode 0.01 segment 30 0.1875 0. 0. 0.1875 0.55 0.
  sonde_V2  vitesse   periode 0.01 segment 30 0.375 0. 0. 0.375 0.62 0.
  sonde_V3  vitesse   periode 0.01 segment 30 0.5625 0. 0. 0.5625 0.68 0.
  sonde_V4  vitesse   periode 0.01 segment 30 0.725 0. 0. 0.725 0.75 0.
  sonde_Ventree vitesse   periode 0.01 segment 10 0. -0.2 0. 0.05 -0.2
0.
}
Format lata
Champs binaire dt_post 100.
{
  pression elem
  vitesse   faces
  temperature faces
  k   elem
  eps   elem
  y_plus   elem
  viscosite_turbulente elem
}
}
Solve pb
End

```

Turbulent flow inside a double-periodic plane channel with heated walls

2.1 Purpose

The purpose of this test case is to check TrioCFD on a thermal turbulent flow inside a double-periodic plane channel. The fluid is assumed to be Incompressible and the turbulence model is the $k - \epsilon$ one. A temperature gradient is imposed at fixed walls where the Reichardt law function is applied. In this test, the effect of several meshes is compared. The validations are carried out between the Nusselt number computed by TrioCFD and an analytical expression that is derived in reference [1]. The comparisons are also presented for the mean velocity profile with the logarithmic law. Moreover, the mean temperature profile is compared to the linear law $T^+ = PrY^+$ and the Kader's law. We remind the definitions of the Dean's correlation $Re_\tau = 0.175.Re_{bulk}^{7/8}$ and the bulk Reynolds number $Re_{bulk} = \frac{\rho(T_b).U_b.(h/2)}{\mu(T_b)}$ where h is the distance between both walls and ρ , μ and U_b are the density, the dynamic viscosity and the bulk velocity.

Validation made by : FOURNIER C.

Report generated 11/01/2021.

2.2 Problem Description

Geometry

The geometry is a double-periodic plane channel of Dimensions : $h = 4$ mm, $L = 4$ mm, $P = 2$ mm as sketched on Fig. 1.

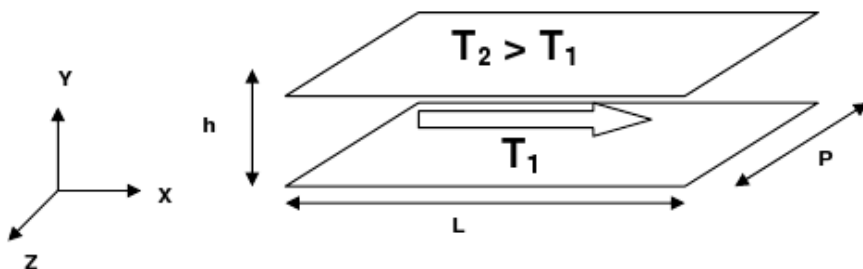


Figure VI.2.1: Geometry

Initial Conditions and Boundary Conditions

- **Boundary conditions**

For Navier-Stokes equations, periodic boundary conditions hold in x - and z -directions and a no-slip boundary condition is applied for both walls. For temperature equation, Dirichlet boundary conditions are applied on both walls. The walls temperatures are set such as $\frac{T_2}{T_1} = 1.01$ where T_2 and T_1 are the temperatures of hot and cold walls respectively. For simulations, they are set equal to, $T_2 = 680$ K and $T_1 = 673$ K.

- **Initial conditions**

The flow initial condition imposes a uniform velocity equal to 80 m/s in the x -direction. For temperature, the initial condition is a linear profile between T_2 and T_1 .

Fluid Properties

Inside the domain the fluid is Helium at 70 bars and 676 K with $\rho = 3.824 \text{ kg/m}^3$, $\mu = 3.475310^{-7} \text{ N/m}^2/\text{s}$, $\lambda = 2.5638910^{-3} \text{ W/m/K}$, $C_p = 5193 \text{ J/kg/K}$ and $\beta_{th} = 0 \text{ K}^{-1}$. The Reynold numbers are $Re_{bulk} = 17605$ and $Re_\tau = 908$.

Flow Physics

The flow is turbulent inside de double-periodic domain and heated with a temperature gradient between both walls.

2.3 Case Setup

Grid

3 meshes (tetrahedral elements) are made by stretching the mesh below, by a factor 1, 10 or 100 in X direction.

Number of cells : 2214

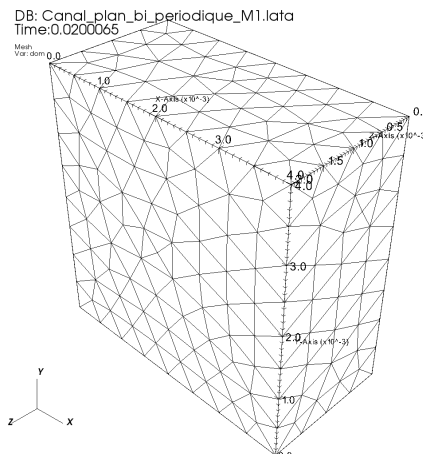


Figure VI.2.2: Mesh M1

2 meshes (tetrahedral elements) generated from cartesian hexahedral elements are used

Number of cells: mesh M1_tetraedrise (drawn below) : 1536

Number of cells: mesh M1bis_tetraedrise : 5184

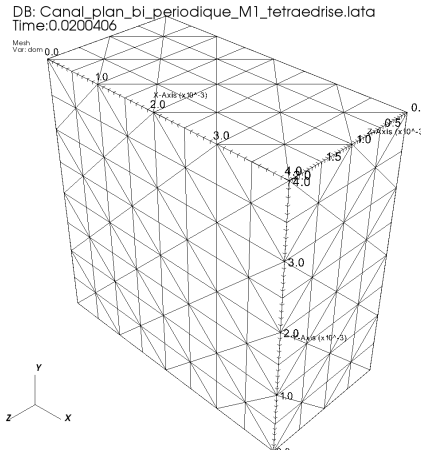


Figure VI.2.3: Mesh M1_tetraedrise

Model Options

The TrioCFD keywords are 'Pb_Thermohydraulique_Turbulent' with 'Fluide_Incompressible' with constant properties. The turbulence models are taken into account by the keywords 'Navier_Stokes_Turbulent' with 'Modele_Turbulence K_Epsilon'. As the periodic and no-slip boundary conditions are considered, a force term is applied in the impulsion balance equation with the keyword 'Sources { Canal_perio { bord Periox } }'. Finally for the temperature equation 'Convection_Diffusion_Temperature_Turbulent', the keyword 'Modele_Turbulence Prandtl' is used in the datafile. Finally the wall function is the Reichardt law with the option " loi standard hydr " (which is similar to 'loi expert hydr').

Other Options (calculation)

The numerical options are 'Schema_Euler_Implicite - Solveur Implicit' with the 'EF_stab' scheme for Navier-Stokes and temperature equation. For the latter 'EF_stab { alpha 0.2 }'.

2.4 Results

Validation Specific Informations

- Version TRUST :
- Bi-periodic plane channel in X and Z
- Convection scheme = EF_stab
- k- ε modelling of turbulence
- Wall law = loi_standard_hydr (similar to loi_expert_hydr { methode_calcul_face_keps_impose que_les_faces_des_elts_dirichlet })
- Heat transfer with imposed temperatures
- No-slip at the wall
- Location: validation/share/Validation/Rapports_automatiques/Validant/Fini/Channel_T1_T2_incompressible
- Master Test Case: Canal_plan_bi_periodique_M1.data - Canal_plan_bi_periodique_M1_tetraedrise.data

- Generated Test cases :

```

→ Incompressible/Canal_plan_bi_periodique_M1/Canal_plan_bi_periodique_M1.data : /**
→ Incompressible/Canal_plan_bi_periodique_M10/Canal_plan_bi_periodique_M10.data :
→ Incompressible/Canal_plan_bi_periodique_M100/Canal_plan_bi_periodique_M100.data :
→ Incompressible/Canal_plan_bi_periodique_M1_tetraedrise/Canal_plan_bi_periodique_M1_tetraedrise.data :
→ Incompressible/Canal_plan_bi_periodique_M1bis_tetraedrise/Canal_plan_bi_periodique_M1bis_tetraedrise :

```

- Performance Chart :

Incompressible/Canal_plan_bi_periodique_M1/Canal_plan_bi_periodique_M1		is2417
Incompressible/Canal_plan_bi_periodique_M10/Canal_plan_bi_periodique_M10		is2417
Incompressible/Canal_plan_bi_periodique_M100/Canal_plan_bi_periodique_M100		is2417
Incompressible/Canal_plan_bi_periodique_M1_tetraedrise/Canal_plan_bi_periodique_M1_tetraedrise		is2417
Incompressible/Canal_plan_bi_periodique_M1bis_tetraedrise/Canal_plan_bi_periodique_M1bis_tetraedrise		is2417
Total		

Table VI.2.1: Performance Chart

Plot Data

• Velocity results

The mean axial velocity profiles at outlet ($U^+ = U/U_\tau$; $Y^+ = Y.U_\tau/\nu$) are compared to the wall function: $U^+ = 1/0.415 \times \ln(Y^+) + 5.32$. On Fig. 4 the comparisons are done for three meshes 'M1', 'M10' and 'M100'. For Fig. 5, the comparisons are done for 'M1' and 'M1 tetrahedrise'.

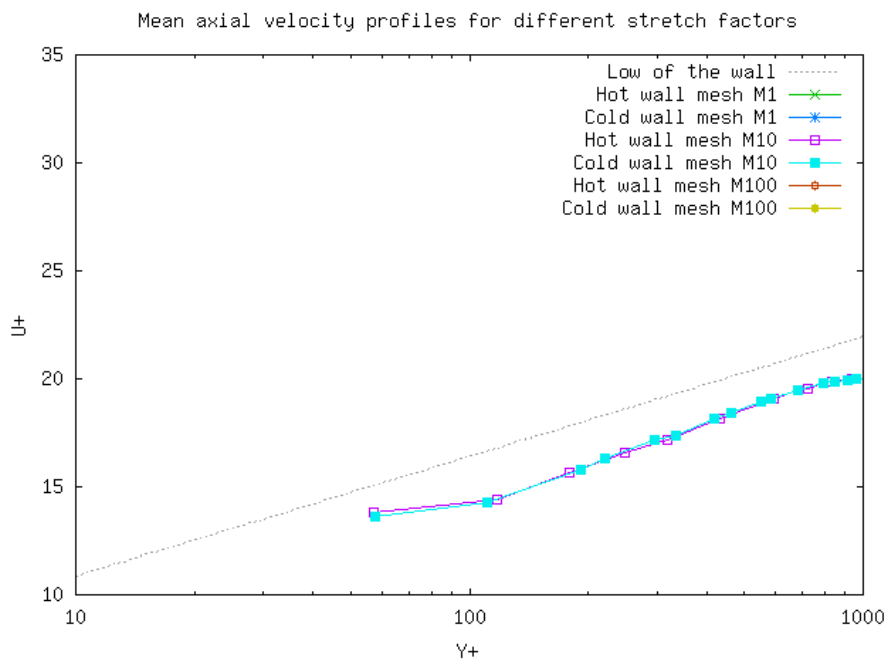


Figure VI.2.4: Mean axial velocity profiles for different stretch factors

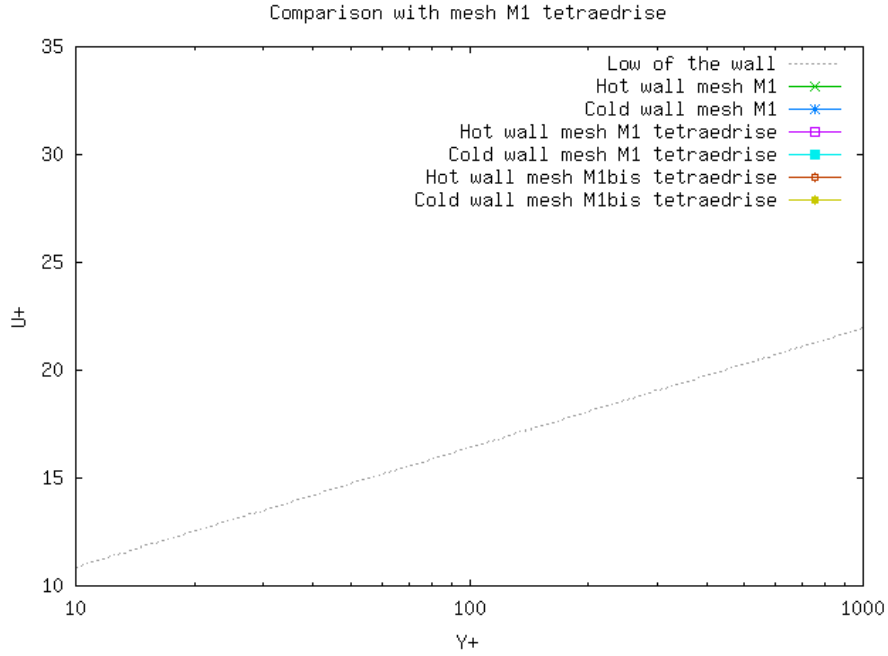
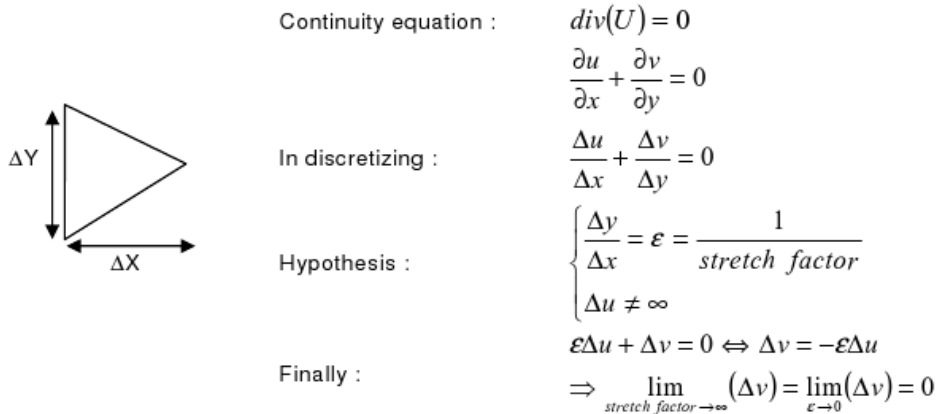


Figure VI.2.5: Comparison with mesh M1_tetraedrise



When the stretch factor increases, the contribution of the deviation of transverse velocity decreases and the flow becomes one-dimensional.

Figure VI.2.6: Explanations of M1 result : contribution of transverse velocity

The deviations of transverse velocities V and W are respectively presented on Figs. 7 and 8. On those two figures, we can observe that the results obtained with the mesh M1 are not conclusive and can be interpreted as a non-negligible contribution of the deviation of transverse velocities. However the two other meshes M10 and M100 (made by stretching the mesh M1) and the meshes generated from cartesian hexahedral elements (M1_tetraedrise and M1bis_tetraedrise) give better results.

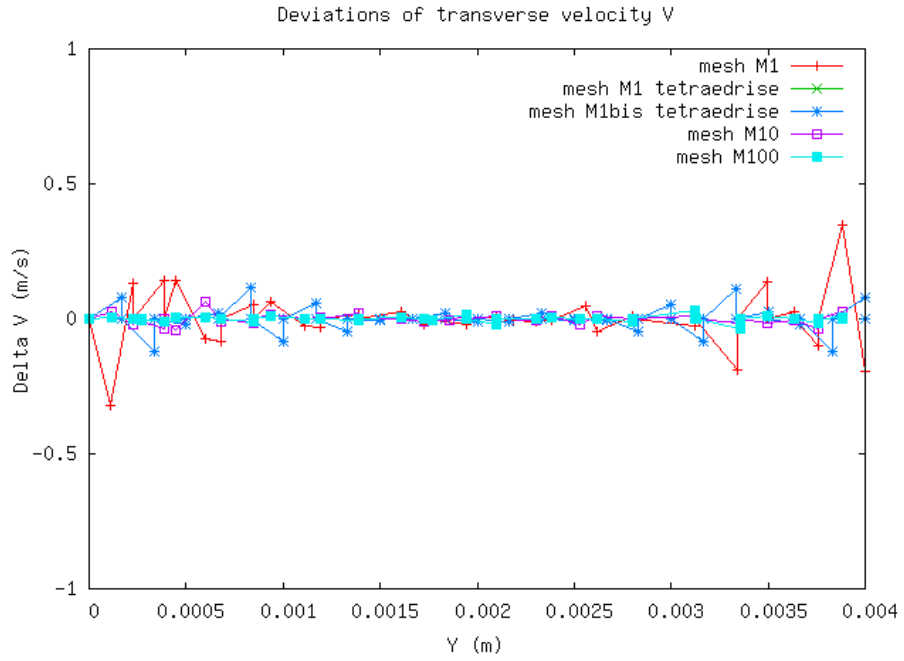


Figure VI.2.7: Deviations of transverse velocity V

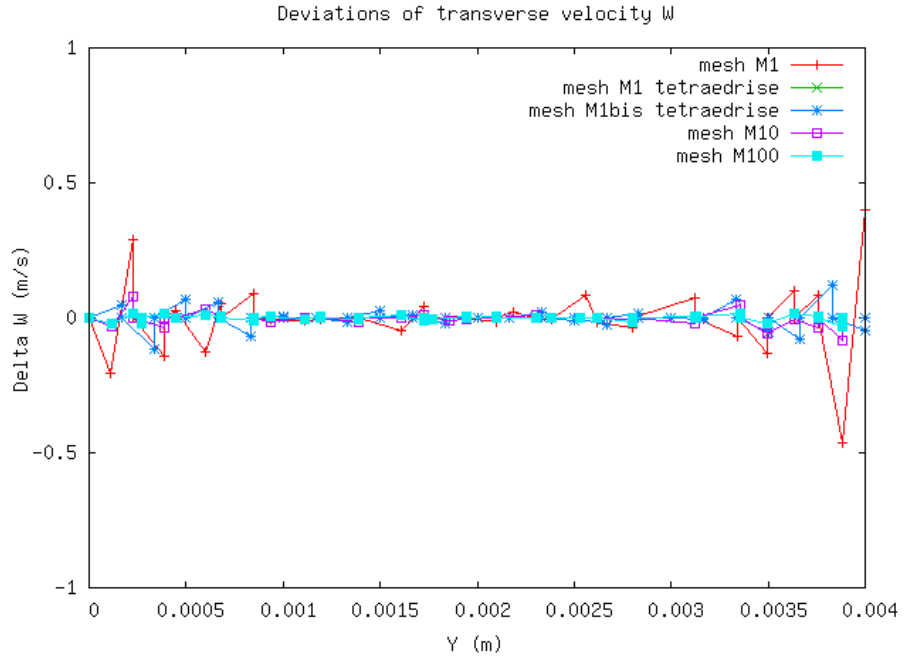


Figure VI.2.8: Deviations of transverse velocity W

• Temperature results

The mean temperature profiles at outlet ($T^+ = T/T_\tau; T_\tau = \varphi/(\rho C_p U_\tau); Y^+ = YU_\tau/\nu$) are compared to the linear law $T^+ = \text{Pr}Y^+$ and the Kader's law on Figs. 9 and 10. The Kader's law is defined by:
 $T^+ = \text{Pr}Y^+ \exp(-\Gamma) + [2.12 \ln(1+Y^+) + \beta(\text{Pr})] \exp(-1/\Gamma)$
 With $\Gamma = 0.01(\text{Pr}Y^+)^4 / (1+5Y^+\text{Pr}^3)$ and $\beta(\text{Pr}) = (3.85\text{Pr}^{1/3} - 1.3)^2 + 2.12 \ln(\text{Pr})$

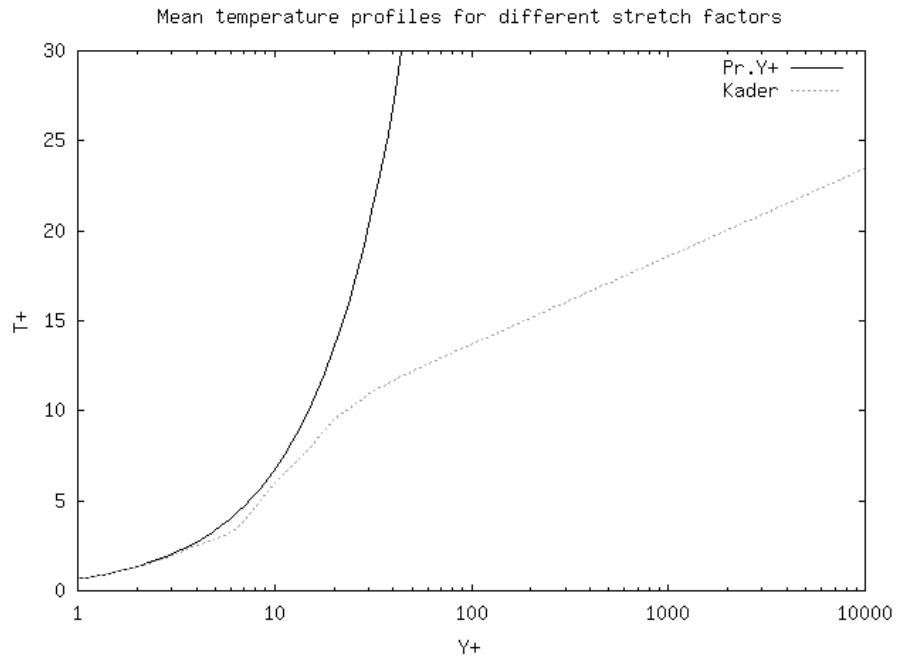


Figure VI.2.9: Mean temperature profiles for different stretch factors

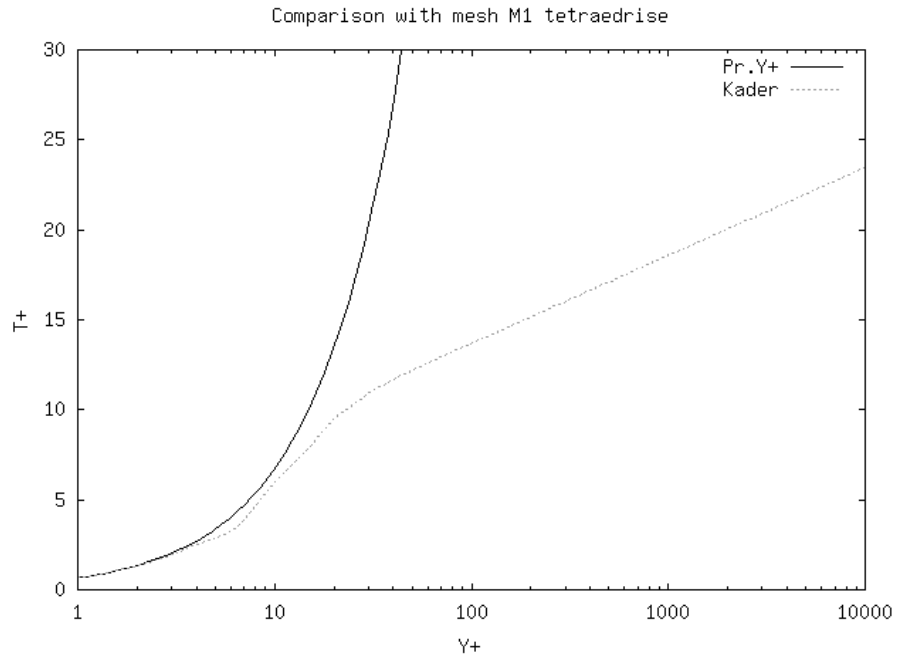


Figure VI.2.10: Comparison with mesh M1_tetraedrise

- **Nusselt Calculation**

$$Nu = \frac{D_h \cdot \left(\frac{dT}{dy} \right)}{\Delta T} ; D_h = \text{hydraulic diameter}$$

Classical correlations found in the literature (like the correlation of Colburn or Dittus Boelter) were derived in cases where the walls are subjected to an imposed flux or the same temperature. None of them seem

applicable in this case because both walls are subjected to different temperatures. In order to validate TrioCFD, we compare the results with numerical solutions corresponding to the convection in turbulent flow between parallel plates with unequal uniform temperature of reference [1]. The authors propose the following formulation for Nusselt number :

$$Nu_{Ref} = \frac{1}{4 * \int_0^1 \frac{dy^+}{1 + \frac{Pr}{Pr_t} \left(\frac{(u'v')^{++}}{1 - (u'v')^{++}} \right)}}$$

with $(u'v')^{++} = -\rho \bar{u}' \bar{v}' / \tau$. We need an evaluation of the turbulent shear stress to calculate the Nusselt number numerically. In reference [1], the author uses a correlation based on experimental data for a round tube and supposed to be valid for a flow between parallel plates. This correlation writes:

$$(u'v')^{++} = \left(\left[0.7 \left(\frac{y^+}{10} \right)^3 \right]^{-8/7} + \left[\exp \left(\frac{-1}{0.436y^+} \right) - \frac{1}{0.436Re_\tau} \left(1 + \frac{6.95y^+}{Re_\tau} \right) \right]^{-8/7} \right)^{-7/8}$$

In our case, $Pr = 0.667$, $Pr_t = 0.9$, $Re_\tau = 908$ and $Nu_{Ref} = 93$. The TrioCFD Nusselt number and the relative errors are given in Table 2 where we observe that the TrioCFD results are very close to the analytical ones.

	$Nu_{TrioCFD}$	$\Delta Nu_{Ref} (\%)$
M1	0.06	-99.94
M10	0.6	-99.35
M100	6.01	-93.54
M1_tetraedrise	0.06	-99.94
M1bis_tetraedrise	0.06	-99.94

Table VI.2.2: Nusselt Calculation

2.5 Conclusion

The thermal turbulent flow has been validated in this test case. The flow is considered inside a double-periodic plane channel with the ' $k - \epsilon$ ' model of turbulence. At fixed walls, the Reichardt law function is considered and a temperature gradient is applied. The temperature profiles were compared with the Kader's law and the linear one. Finally the Nusselt number that are computed by TrioCFD are close to those calculated in reference [1].

2.6 References

- [1] Stanislav N. Danov, Norio Arai and Stuart W. Churchill, Exact formulations and nearly exact numerical solutions for convection in turbulent flow between parallel plates, International Journal of Heat and Mass Transfer, Number 43, pp. 2767-2777, 2000.

2.7 Data Files

Canal_plan_bi_periodique_M1

```
# SIMULATION D'UN CANAL PLAN 3D VEF EN THERMOHYDRAULIQUE INCOMPRESSIBLE #
dimension 3
Pb_Thermohydraulique_turbulent pb
Domaine dom
# BEGIN MESH #
Lire_Tgrid dom Canal_plan_bi_periodique_M1.msh
Transformer dom x y z
# END MESH #
```

```

# BEGIN PARTITION
Partition dom
{
    Partitionneur metis { Nb_parts 2 }
    Larg_joint 2
    Nom_Zones DOM
}
End
END PARTITION #
# BEGIN SCATTER
Scatter DOM.Zones dom
END SCATTER #
VEFPreP1B dis
Schema_Euler_implicite sch
Read sch
{
    tinit 0.
    tmax 0.02
    dt_min 1.e-10
    dt_max 1.e-1
    dt_impr 1.e-5
    dt_sauv 0.01
    seuil_statio 1.e-8
    facsec 10
        facsec_max 500
        Solveur
            Implicite
            {
                seuil_convergence_solveur 1.e-10
            }
}
Fluide_incompressible fluide
Read fluide
{
    mu Champ_Uniforme 1 3.4753e-5
    rho Champ_Uniforme 1 3.824
    lambda Champ_Uniforme 1 0.256389
    Cp Champ_Uniforme 1 5193.
        beta_th Champ_Uniforme 1 0.
}
Champ_Uniforme gravite
Read gravite 3 0 0
Associate fluide gravite
Associate pb dom
Associate pb sch
Associate pb fluide
Discretize pb dis
Read pb
{
    Navier_Stokes_turbulent
    {
        solveur_pression GCP { precond ssor { omega 1.5 } seuil 1e-8 }
        convection { EF_stab { } }
        diffusion { }
        Sources { Canal_perio { bord Periox } }
        conditions_initiales { vitesse champ_uniforme 3 80. 0. 0. }
        boundary_conditions
        {
            Periox periodique
            Perioz periodique
            Bas Paroi_fixe
    }
}

```

```

        Haut  Paroi_fixe
    }
        Modele_turbulence K_Epsilon
{
    Transport_K_Epsilon
    {
        convection { EF_stab { } }
                    diffusion { }
                    boundary_conditions
    {
        Periox periodique
        Perioz periodique
        Bas Paroi
        Haut Paroi
    }
        parametre_equation parametre_implicite
    {
        resolution_explicite
    }
                    conditions_initiales { k_Eps Champ_Uniforme 2 64. 1.4e6 }
    }
        turbulence_paroi loi_standard_hydr dt_impr_ustar 0.001
}
}
Convection_Diffusion_Temperature_turbulent
{
    diffusion { }
    convection { EF_stab { alpha 0.2 } }
    boundary_conditions
    {
        Periox periodique
        Perioz periodique
        Bas paroi_temperature_imposee Champ_Front_Uniforme 1 673.
        Haut paroi_temperature_imposee Champ_Front_Uniforme 1 680.
    }
    conditions_initiales { Temperature Champ_fonc_xyz dom 1 1750.*y+673. }
    Modele_turbulence Prandtl
    {
        Turbulence_paroi loi_standard_hydr_scalaire
dt_impr_nusselt 0.001
    }
}
Postraitemet
{
    Sondes
    {
        sonde_pression pression periode 0.0001 segment 50
0.00025 0.0 0.00025 0.00025 0.004 0.00025
        sonde_vitesse nodes vitesse periode 0.0001 segment 50
0.00025 0.0 0.00025 0.00025 0.004 0.00025
        sonde_temperature nodes temperature periode 0.0001 segment 50
0.00025 0.0 0.00025 0.00025 0.004 0.00025
        sonde_y_plus nodes y_plus periode 0.0001 segment 50
0.00025 0.0 0.00025 0.00025 0.004 0.00025
        sonde_k nodes k periode 0.0001 segment 50 0.00025 0.0 0.00025 0.00025 0.004 0.000
        sonde_eps nodes eps periode 0.0001 segment 50
0.00025 0.0 0.00025 0.00025 0.004 0.00025
        sonde_visco_turb nodes viscosite_turbulente periode 0.0001 segment 50
0.00025 0.0 0.00025 0.00025 0.004 0.00025
    }
    format lata Champs dt_post 0.01

```

```
{  
    pression      elem  
    pression      som  
    vitesse       elem  
    vitesse       som  
    temperature   elem  
    temperature   som  
    y_plus        elem  
    y_plus        som  
    Viscosite_turbulente elem  
    Viscosite_turbulente som  
    k             elem  
    k             som  
    eps           elem  
    eps           som  
}  
}  
}  
}  
Solve pb  
End
```

VII. Two-phase Flows with Front-Tracking

IN this last part, the test cases correspond to two-phase flows at local scale. Direct numerical simulations of such flows consist in modeling two incompressible and immiscible fluids separated by a mobile interface. The mass and impulsion balance equations hold for each bulk phase with the viscosity and density of each fluid. The temperature equation is neglected as well as phase change but the gravity is considered. In such an approach, bubbles or drops are described individually with their surface tension and the main difficulty is to follow accurately interfaces that evolve in space and time. Several numerical methods are dedicated to such interface tracking. They can be gathered into two main families: “diffuse interface method” and “sharp interface method”. In **TrioCFD**, interfaces are tracked by “Front-Tracking”, a sharp interface method, for which the surface of separation between both fluids is discretized by an additional lagrangian mesh. A re-meshing is required during the calculation with a fine adjustment of numerical parameters. In this part, the method is used for simulating problems of **oscillating bubble** and **hanging drop**.



Oscillation of a bubble

1.1 Purpose

The aim of this test is to check the capability of the Front Tracking algorithm to describe the oscillations of the interface between an air bubble and the surrounding water.

In the current state, this sheet is not really a validation sheet strictly speaking. Indeed, no advanced comparison, whether with other CFD codes or analytical results, is made. Rather, it is a sheet which demonstrate the capabilities of TrioCFD for the modeling of this type of phenomenon. No reference is therefore given in this sheet.

By version v1.8.4, validation will be redone on this sheet in order to:

- Check the convergence of the results,
- Resdefine the mesh if it turns out that the simulation was not converged into a mesh,
- Validate the numerical results obtained with theoretical and experimental ones or those of other CFD codes,
- Update the Test case and the PRM accordingly.

Validation made by : S.Pigny.

Report generated 11/01/2021.

1.2 Problem Description

The test deals with the presence of a bubble in a box filled of liquid. Initially, the liquid is at rest. No gravity forces are taken into account. In the calculation, the initial shape of the bubble is slightly an ellipsoidal one. It makes it be out of equilibrium, concerning surface tension forces. Its free surface is subject to oscillations. Their wavelengths are directly connected to the mass balance. To investigate their frequencies, the analytical results to be used as reference are relative to inviscid fluids. Therefore, this test-case is intended to provide a verification of the correct balance between surface tension and inertial effects which are the only effects which control the fluid motion. In addition, since the analytical results are non-dissipative, this test-case provides a tool to estimate the rate of the energy dissipation due to the modeling method. This is connected to the problem of numerical diffusion.

In this two-fluid problem, the following notations are introduced to describe the fluids and interface physical and transport properties. The two fluids are considered as non-miscible. The inclusion equivalent diameter is defined as the diameter of the sphere which volume is equal to that of the actual inclusion. Let D be this diameter and R the corresponding radius. The test makes sense if the physical properties correspond roughly to an inertia dominated flow with a very low viscosity for the gas and the liquid. This means that the capillary numbers based on the physical properties of each phase are very small. They are defined by:

$$C_{a_k} = \frac{\rho_k}{\mu_k} \sqrt{\frac{D\sigma}{\rho_k}}$$

where the subscript $k = L;G$ denotes respectively the liquid or the gas phase, ρ_k , μ_k is the dynamical viscosity and σ is the surface tension between the gas and the liquid. Therefore, it is assumed that viscosity effects vanish when the following condition is fulfilled:

$$C_{a_k} \gg 1$$

Rayleigh in 1879 derived the frequency of oscillations of such an inclusion. This derivation is based on the potential flow theory and is valid for any arbitrary inner and outer values of the density. This is shown for example by Lamb [1], (p. 475, equation 10). The angular frequency of the oscillations is obtained for each mode by using the linearized momentum jump at the interface; it is given by:

$$\omega_n^2 = \frac{n(n+1)(n-2)(n+2)}{(n+1)\rho_I + n\rho_O} \frac{\sigma}{R^3}$$

We focus on the main oscillation mode $n = 3$, which correspond to the slowest dissipation of kinetic energy. It leads to the theoretical value of 50 Hz, for the interface oscillation

Two calculations are made in this sheet. The differences between these 2 calculations relate only to the parameters of meshing used which will be explained in the paragraph **Mesh**.

Geometry

The problem is solved in a cubic field of 0.01 meter side. A spherical bubble is initially positionned in its center.

Initial Conditions and Boundary Conditions

Different initial and boundary conditions are applied between the domain and the water-air interface.

- **For the domain:**

→ *Initial condition*: zero uniform velocity field for the 3 directions

→ *Boundary conditions*: at the top of the domain, an outlet boundary condition is defined with an uniform field for P/ρ equal to 0 (Pa/kg.m³). For the 5 other borders, a situation of adherence is defined.

- **For the interface:**

→ *Initial condition*: the following function is applied to define the initial shape of the bulle : $0.0016 * 0.0016 - ((x - 0.005) * (x - 0.005) / 1.21 + (y - 0.005) * (y - 0.005) * 1.21 + (z - 0.005) * (z - 0.005))$

→ *Boundary conditions*: a specific boundary condition for discontinuous Front_Tracking problem is defined *paroi_ft_disc* with a symetrie condition.

Fluid Properties

In order to construct the diphasic fluid, two incompressible fluids, water and air, are defined by the usual keyword *Fluide_Incompressible*. Then, they are associated to create the two-phase fluid via the keyword *Fluide_Diphasique*.

1.3 Case Setup

Grid

Regarding the general domain (the cube), the mesh is regular and consists of 61 meshes in each direction.

Regarding the interface between air and water (bubble surface), a specific mesh adapted to Front-Tracking problem has been defined. 2 simulations with different parameters are performed:

- **First calculation:**

→ *lissage_courbure_iterations* = 0

→ *facteur_longueur_ideale* = 2

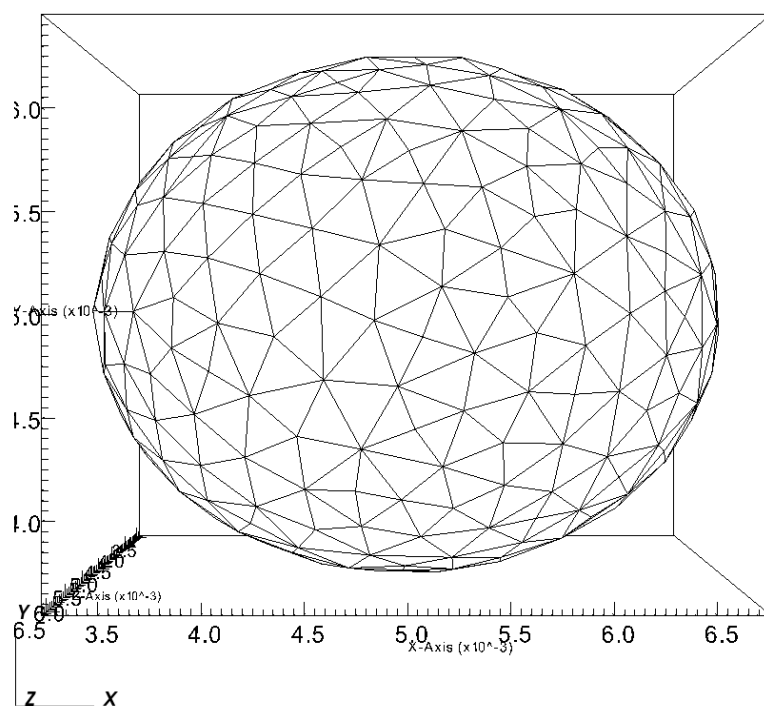


Figure VII.1.1: Bubble in a cubic box : first calculation - mesh at time = 0

- Second calculation:

↪ *lissage_courbure_iterations* = 10
 ↪ *facteur_longueur_ideale* = 0.8

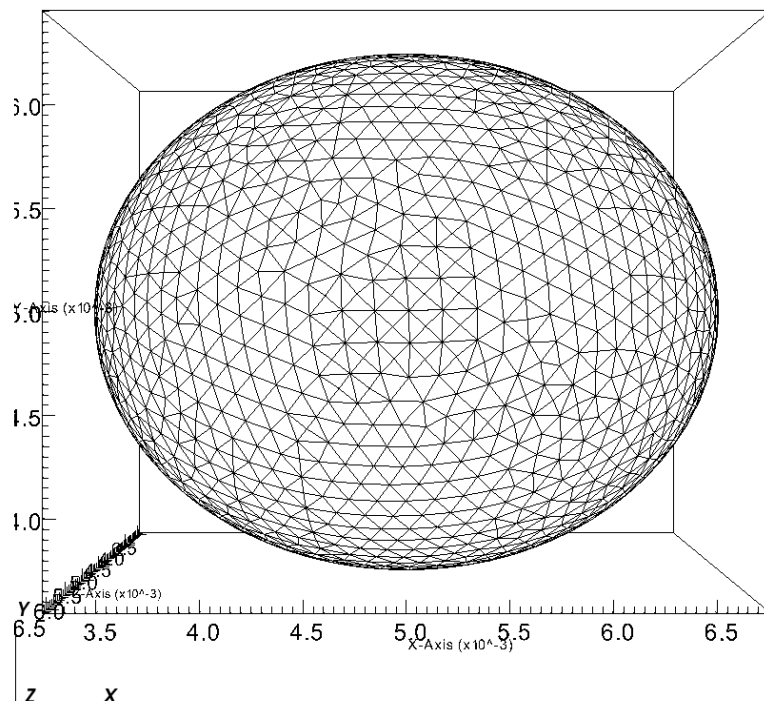


Figure VII.1.2: Bubble in a cubic box : second calculation - mesh at time = 0

Model Options

This sheet deals with a generic Front-Tracking problem in the discontinuous version. It differs from others TrioCFD test cases : The problem does not state the number of equations that are enclosed in the problem. Two equations are compulsory : a momentum balance equation (alias Navier-Stokes equation) and an interface tracking equation. The list of equations to be solved is declared in the beginning of the data file. Another difference with more classical TRUST data file, lies in the fluids definition. The two-phase fluid (Fluide_Diphasique) is made with two usual single-phase fluids (Fluide_Incompressible). As the list of equations to be solved in the generic Front-Tracking problem is declared in the data file and not predefined in the structure of the problem, each equation has to be distinctively associated with the problem with the Associer keyword.

Other Options (calculation)

The time scheme defined in this test case is the Explicit Euler scheme.

1.4 Results

Validation Specific Informations

- Version TRUST : 1.6.1
- Type of problem: Front Tracking problem
- Discretization: VDF
- Convection scheme : Schema_Euler_explicite
- Type of fluid : air and water
- Location: Front_tracking_discontinu/share/Validation/Rapports_automatiques/FTD_oscillating_bubble
- Master Test case: Bulle/FTD_Oscillation_Bulle_3D_VDF.data
- Generated Test cases :
 - Bulle/Cas_01/FTD_Oscillation_Bulle_3D_VDF.data : /* data file in appendix */
 - Bulle/Cas_02/FTD_Oscillation_Bulle_3D_VDF.data :
- Performance Chart :

	host	system	Total CPU Time	CPU time/step	nu
Bulle/Cas_01/FTD_Oscillation_Bulle_3D_VDF	is241762.intra.cea.fr	Linux	296.434	0.33095	
Bulle/Cas_02/FTD_Oscillation_Bulle_3D_VDF	is241762.intra.cea.fr	Linux	154.983	0.381857	
Total			451.417		

Table VII.1.1: Performance Chart

Plot Data

• First calculation:

Here are the profiles of the oscillating bubble every 0.002 second with the first remeshing options a described in paragraph **Mesh**.

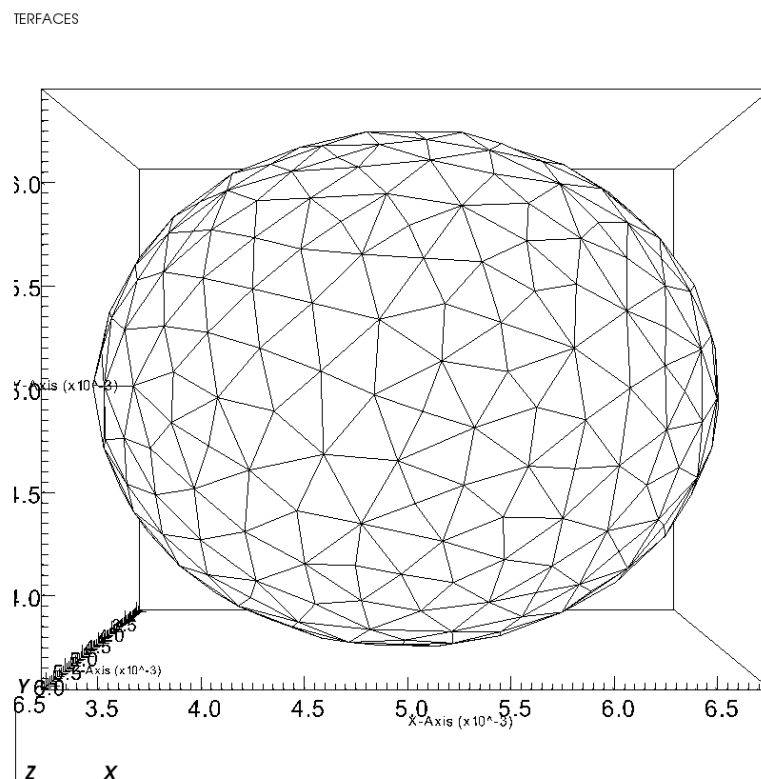


Figure VII.1.3: Bubble in a cubic box : first calculation - mesh at time = 0

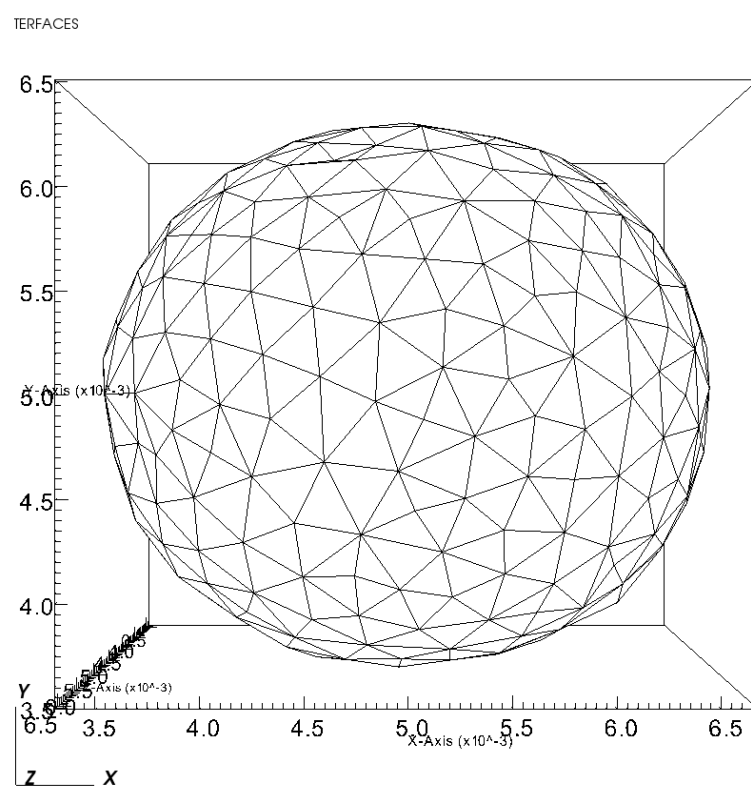


Figure VII.1.4: Bubble in a cubic box : first calculation - oscillations of the interface at $t=0.002s$

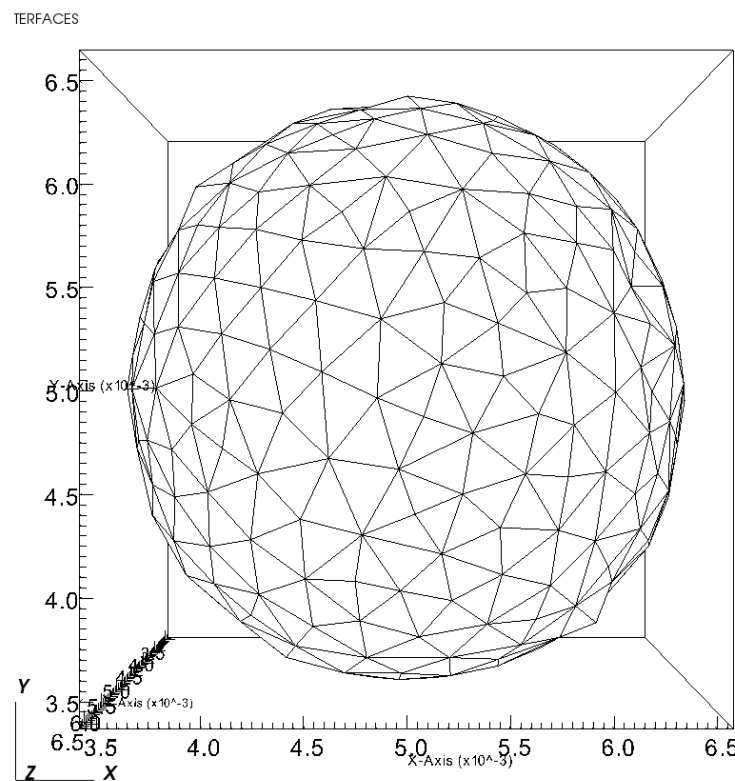


Figure VII.1.5: Bubble in a cubic box : first calculation - oscillations of the interface at $t=0.004\text{s}$

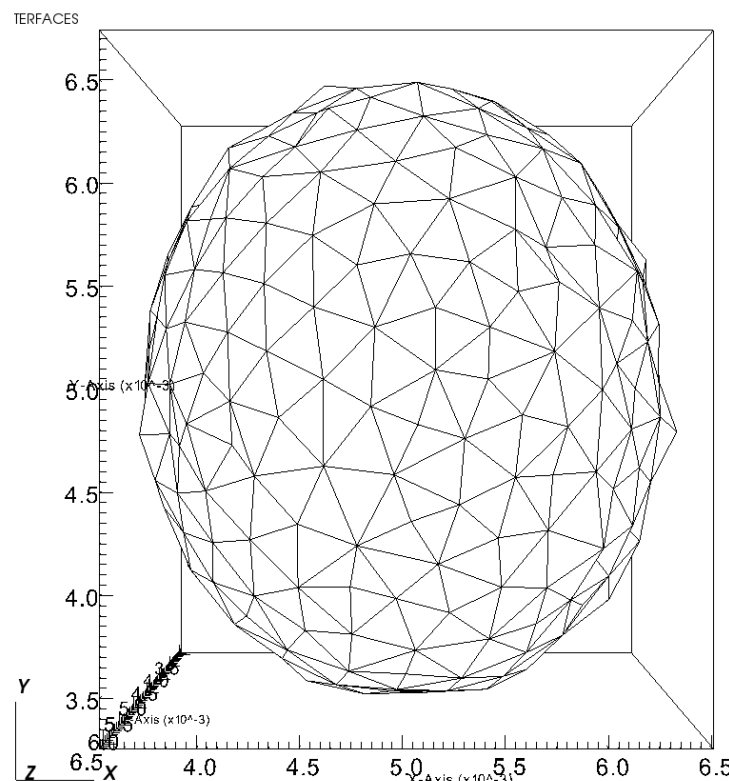


Figure VII.1.6: Bubble in a cubic box : first calculation - oscillations of the interface at $t=0.006\text{s}$

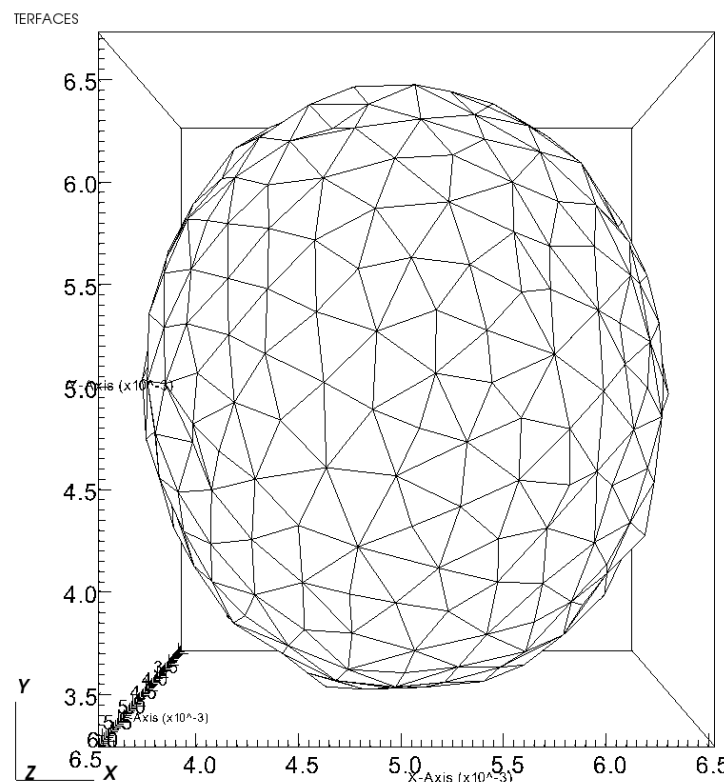


Figure VII.1.7: Bubble in a cubic box : first calculation - oscillations of the interface at $t=0.008\text{s}$

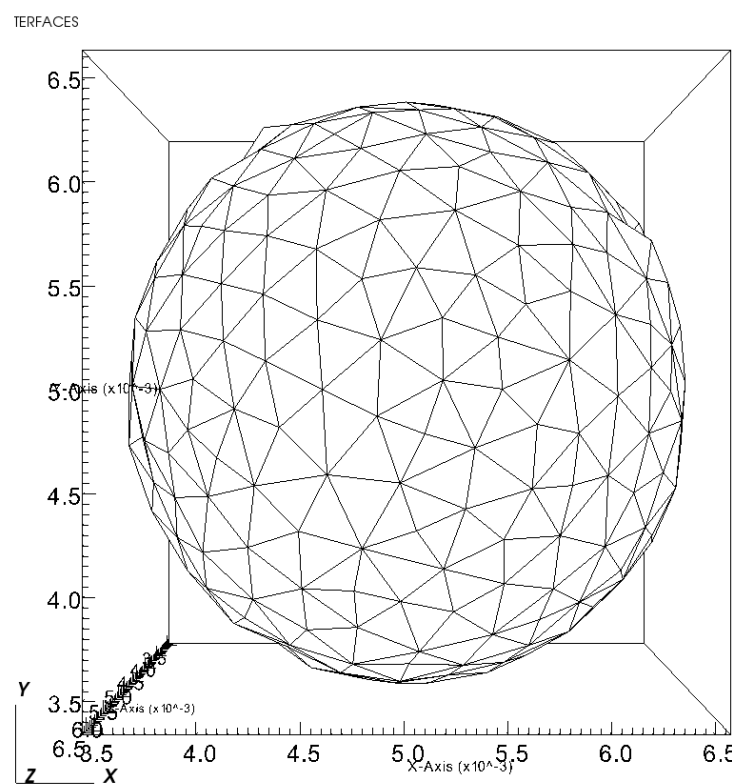


Figure VII.1.8: Bubble in a cubic box : first calculation - oscillations of the interface at $t=0.01\text{s}$

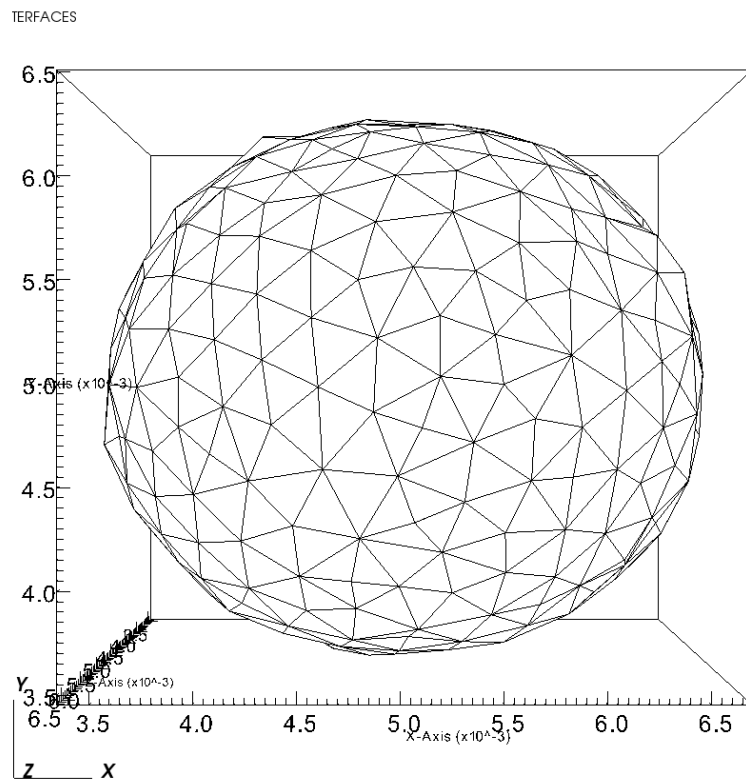


Figure VII.1.9: Bubble in a cubic box : first calculation - oscillations of the interface at $t=0.012s$

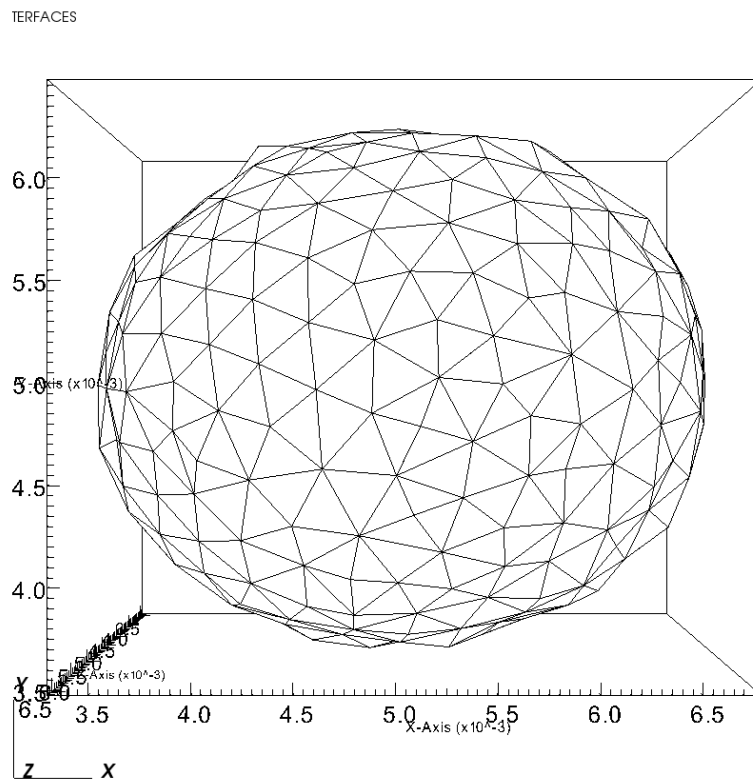


Figure VII.1.10: Bubble in a cubic box : first calculation - oscillations of the interface at $t=0.014s$

We compare the value of the frequency of the oscillation obtained in the calculation to the theoretical one. One can see in the figures below that results are not satisfactory. The oscillations of free surface do not correspond to the theoretical value of 50 Hz.

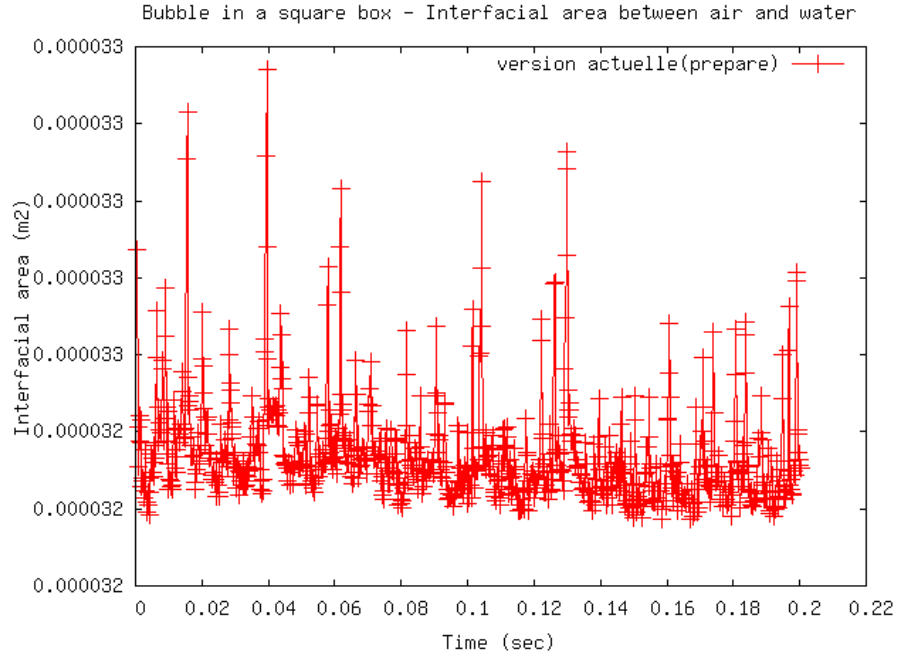


Figure VII.1.11: Bubble in a square box - Interfacial area between air and water

Moreover, the pressure difference between inner and outer fluid suddenly decreases after 0.13 second. The theoretical value is 88 Pa.

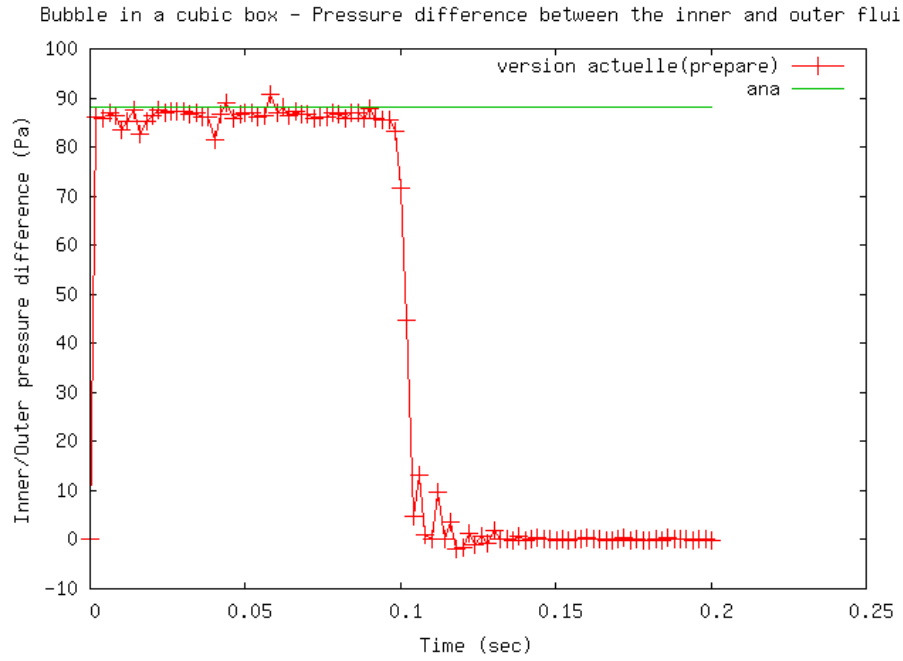


Figure VII.1.12: Bubble in a cubic box - Pressure difference between the inner and outer fluid

This first calculation shows the ability of the Front-Tracking baltik of TrioCFD to simulate an oscillating interface. However, the interface area is too disturbed from one time step to another to check that the frequency of the oscillations with the theoretical value.

To reduce these instabilities, a second calculation was carried out with finer parameterization of the Front-Tracking algorithm, in particular for the remeshing of the interface during the calculation.

- **Second calculation:**

The settings of the Front-Tracking algorithm for this second calculation are given in paragraph **Mesh**. Here are the profiles of the oscillating bubble every 0.002 second with the second remeshing options.

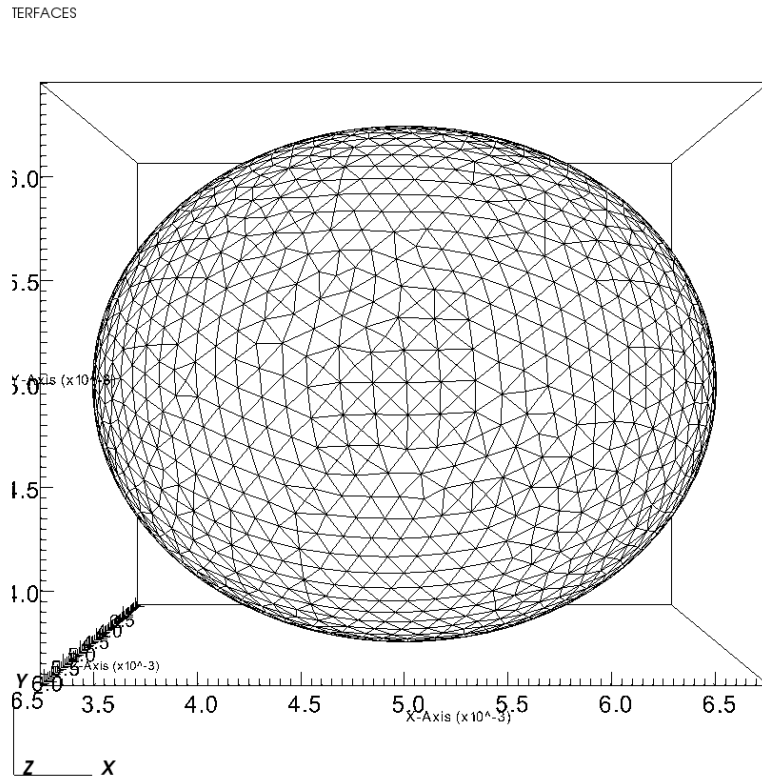


Figure VII.1.13: Bubble in a cubic box : second calculation - mesh at time = 0

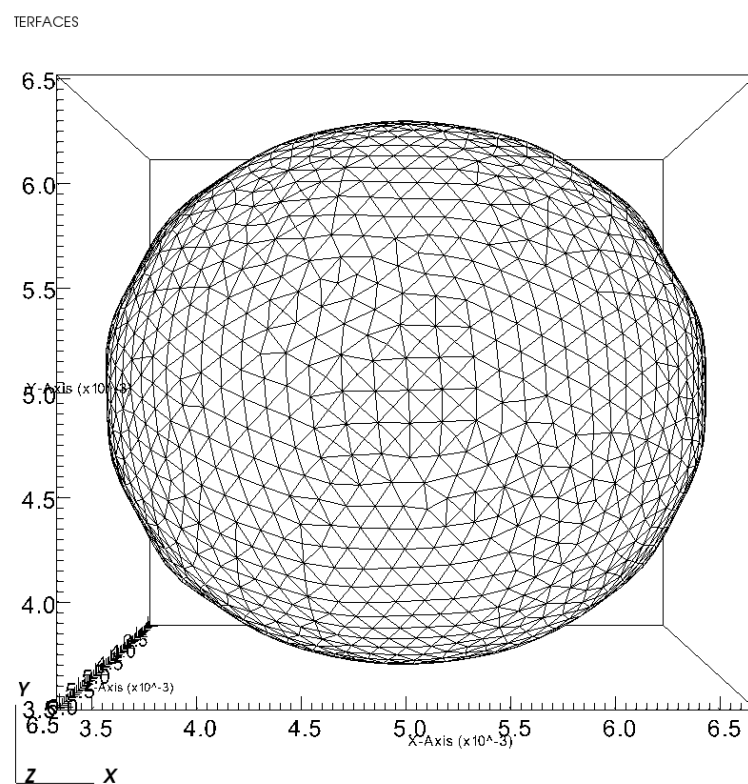


Figure VII.1.14: Bubble in a cubic box : second calculation - oscillations of the interface at $t=0.002s$

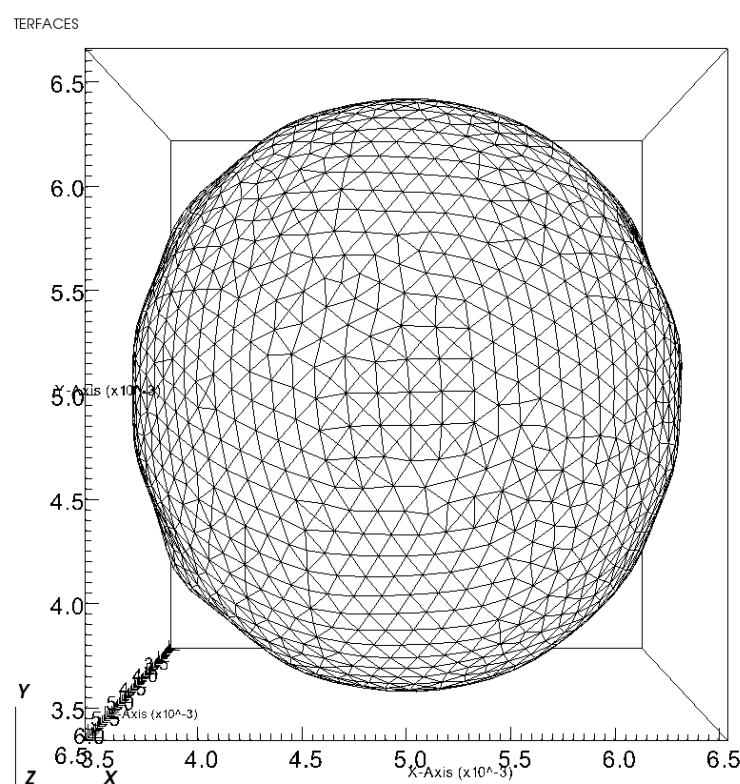


Figure VII.1.15: Bubble in a cubic box : second calculation - oscillations of the interface at $t=0.004s$

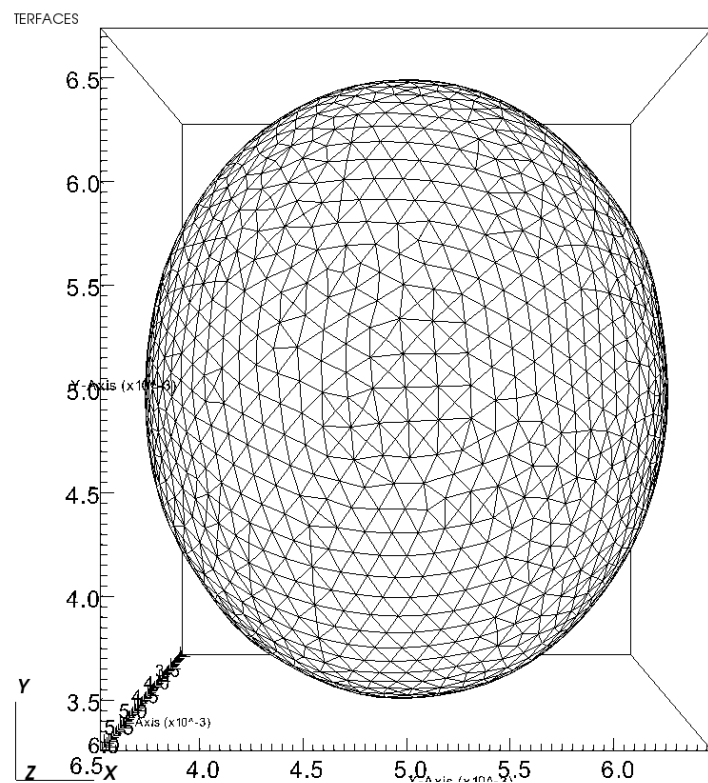


Figure VII.1.16: Bubble in a cubic box : second calculation - oscillations of the interface at $t=0.006s$

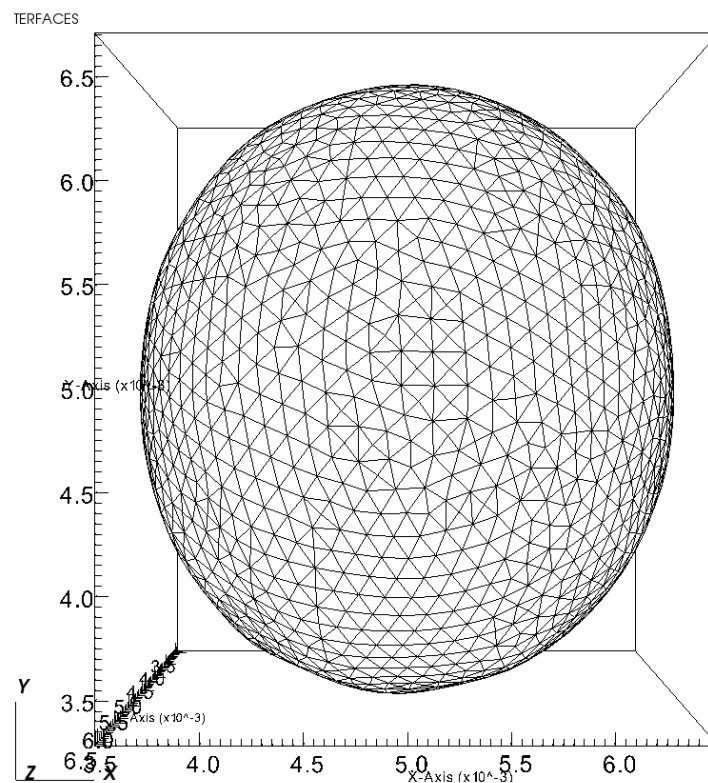


Figure VII.1.17: Bubble in a cubic box : second calculation - oscillations of the interface at $t=0.008s$

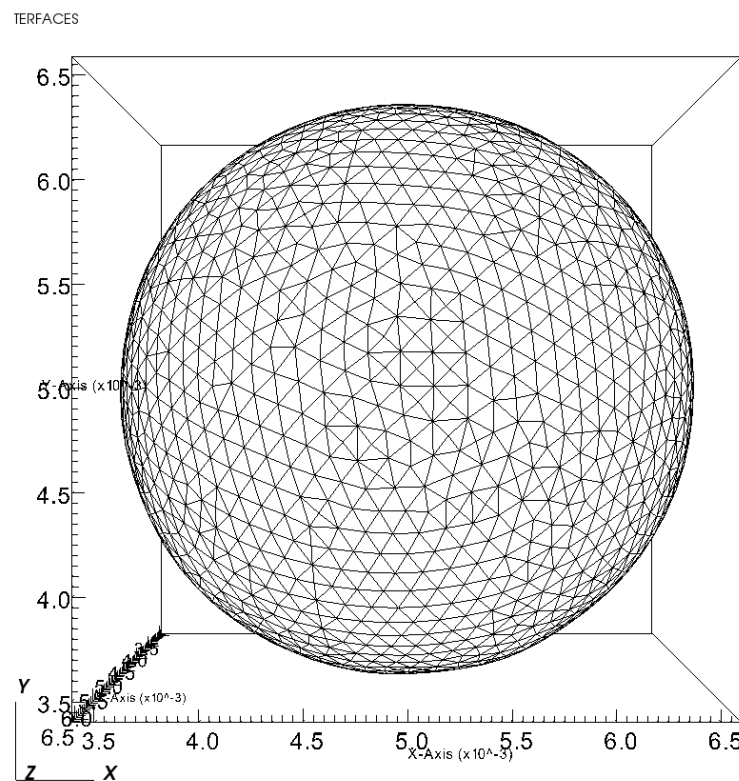


Figure VII.1.18: Bubble in a cubic box : second calculation - oscillations of the interface à $t=0.01s$

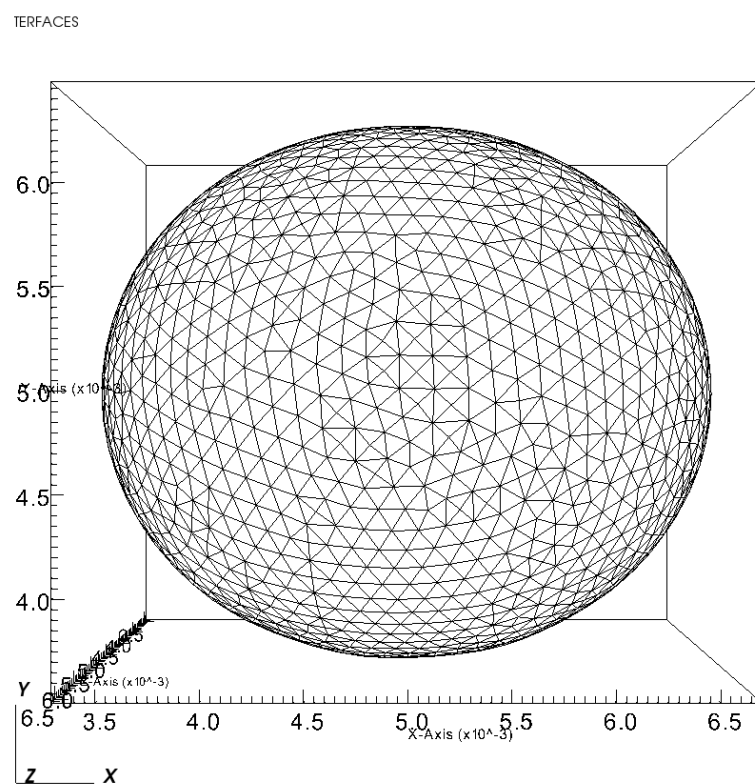


Figure VII.1.19: Bubble in a cubic box : second calculation - oscillations of the interface à $t=0.012s$

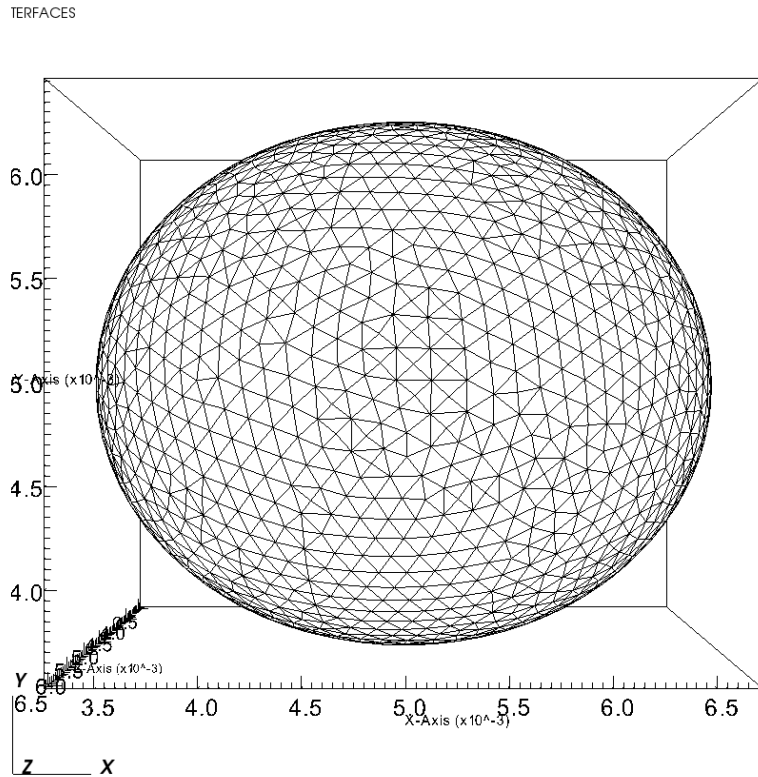


Figure VII.1.20: Bubble in a cubic box : second calculation - oscillations of the interface à $t=0.014s$

One can see in figures below that results are improved with regard to the previous case. The oscillations of free surface correspond to the theoretical value of 50 Hz. The pressure difference between inner and outer fluid is also correctly reproduced. It seems this result could be considered as a reference calculation. One can see a time damping of oscillations. This effect is due to numerical diffusion.

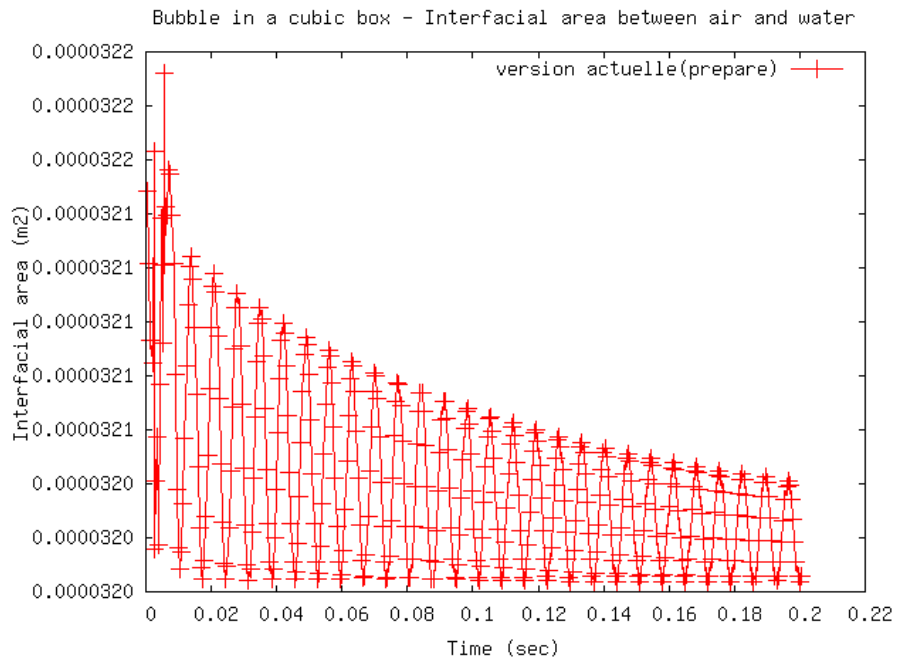


Figure VII.1.21: Bubble in a cubic box - Interfacial area between air and water

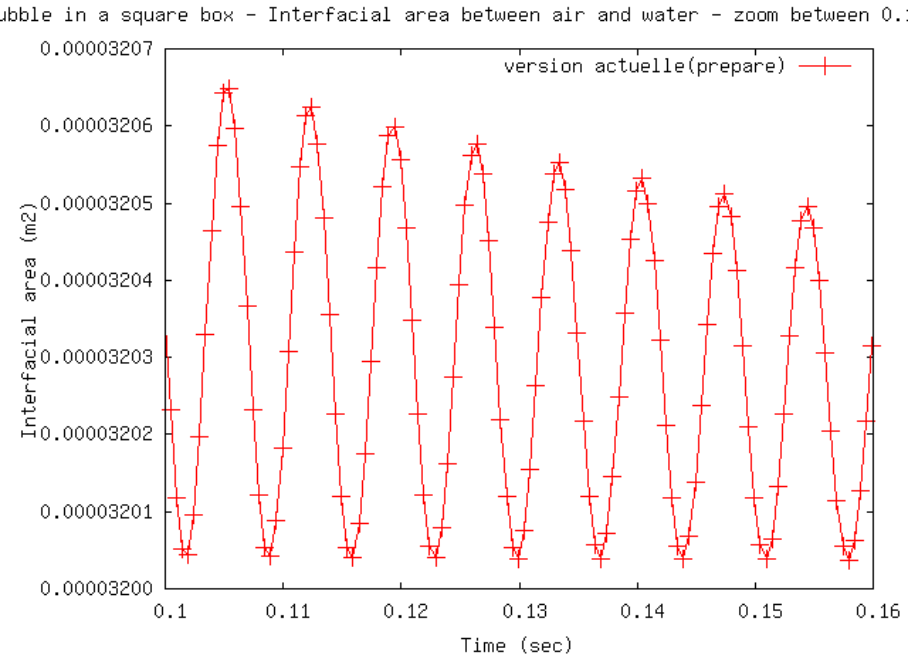


Figure VII.1.22: Bubble in a square box - Interfacial area between air and water - zoom between 0.1 and 0.16 sec

The theoretical value for pressure difference is 88 Pa.

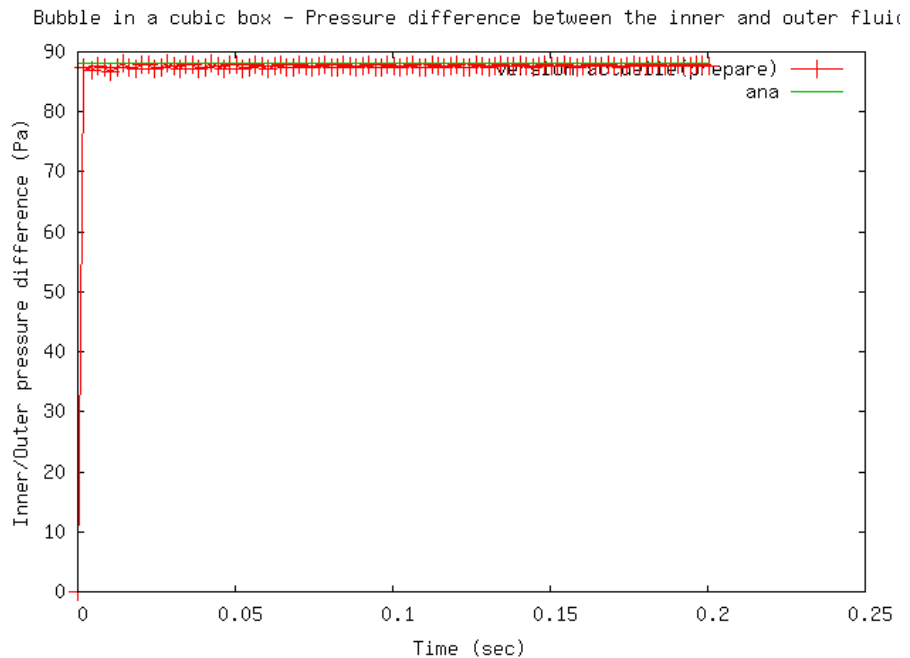


Figure VII.1.23: Bubble in a cubic box - Pressure difference between the inner and outer fluid

1.5 Conclusion

A too coarse lagrangian mesh to describe interface leads to wrong results. On the contrary, providing an accurate enough mesh is chosen, one can obtain results in agreement with theoretical data. The choice can be done via some options chosen in the input data.

If a first comparison with the theory allowed to show that the baltik Front-Tracking of TrioCFD is able to simulate an oscillating bubble in a promising way with the appropriate configuration, this sheet does not yet want to constitute the validation of the code.

To reach the validation stage, it is necessary to:

- check the convergence in mesh of the test case
- validate the numerical results obtained with more advanced theoretical results, experimental ones or those of other CFD codes,
- update the Test case and the PRM accordingly.

This work is planned by version v1.8.4 (end 2021) of TrioCFD.

1.6 References

- [1] Lamb. Year 1975

1.7 Data Files

FTD_Oscillation_Bulle_3D_VDF

```
# Hydraulique 3D laminaire : schema upwind #
# PARALLEL ONLY 4 #
dimension 3
Probleme_FT_Disc_gen pb
Domaine dom
Scatter dom.Zones dom
VDF dis
Schema_Euler_explícite sch
Read sch
{
    tinit 0.0
    tmax 0.2
    dt_min 1.e-10
    dt_max 5.e-4
    dt_impr 0.2
    dt_sauv 0.1
    seuil_statio -1.e-8
    facsec 1.
}
Fluide_Incompressible eau
Read eau
{
    mu Champ_Uniforme 1 1.e-5
    rho Champ_Uniforme 1 1000.
}
Fluide_Incompressible air
Read air
{
    mu Champ_Uniforme 1 1.e-7
    rho Champ_Uniforme 1 1.
}
Fluide_Diphasique fluide
Read fluide
{
    fluide0 eau
```

```

        fluide1 air
        sigma Champ_Uniforme 1 0.07
    }
Champ_Uniforme gravite
Read gravite 3 0. 0. 0.
Associate fluide gravite
Navier_Stokes_FT_Disc          hydraulique
Transport_Interfaces_FT_Disc   interf
Associate pb hydraulique
Associate pb interf
Associate pb dom
Associate pb sch
Associate pb fluide
System "mkdir -p lata"
Discretize pb dis
Read pb
{
hydraulique
{
    modele_turbulence sous_maille_wale
    {
        Cw           0.
        turbulence_paroi negligable
    }
    solveur_pression GCP { precond ssor { omega 1.6 } seuil 1.e-10 impr }
    convection      { amont }
    diffusion       { }
    conditions_initiales { vitesse champ_uniforme 3 0. 0. 0. }
    equation_interfaces proprietes_fluide interf
    boundary_conditions
    {
        haut Sortie_libre_rho_variable champ_front_uniforme 1 0.
        gauche paroi_fixe
        droite paroi_fixe
        bas paroi_fixe
        devant paroi_fixe
        fond paroi_fixe
    }
    terme_gravite rho_g
}
interf
{
    conditions_initiales {
        fonction 0.0016*0.0016 -((x-0.005)*(x-0.005)/1.21+(y-0.005)*(y-0.005)*1.21+(z-0.005)*(z-0.005)/1.21)
    }
methode_transport vitesse_interpolee hydraulique
    iterations_correction_volume 2
    n_iterations_distance 2
remaillage {
    pas 1e-8
    nb_iter_remaillage 5
    criterie_arete 0.35
    criterie_remaillage 0.20
    pas_lissage 1e-8
    lissage_courbure_iterations 0
    lissage_courbure_coeff -0.1
    nb_iter_barycentrage 5
    relax_barycentrage 1.
    facteur_longueur_ideale 2.
    nb_iter_correction_volume 1
    seuil_dvolume_residuel 1e-15
}

```

```

}
boundary_conditions
{
    gauche Paroi_FT_disc symetrie
    droite Paroi_FT_disc symetrie
    haut Paroi_FT_disc symetrie
    bas Paroi_FT_disc symetrie
    devant Paroi_FT_disc symetrie
    fond Paroi_FT_disc symetrie
}
}
postraitements {
    Sondes
    {
        sonde_pression nodes pression periode 2.e-3 Points 2 0.005 0.005 0.005 0.009 0.009 0.009
    }
    champs dt_post 1. {
        vitesse elem
        indicatrice_interf
    }
}
liste_postraitements {
    postraitements_ft_lata post1 {
        dt_post 0.002
        nom_fichier lata/post
        format binaire
        print
        champs elements {
            indicatrice_interf
        }
        interfaces interf {
            champs sommets { courbure }
        }
    }
}
sauvegarde binaire Oscillation_bulle3.rep
}
Solve pb
End
postraitements {
    Sondes
    {
        sonde_vitesse nodes vitesse           periode 2.e-3 Segment 51 0. 0.005 0.0025 0.0025
        sonde_pression nodes pression         periode 2.e-3 Segment 51 0. 0.005 0.0025 0.0025
        sonde_rho     nodes indicatrice_interf periode 2.e-3 Segment 51 0. 0.005 0.0025 0.0025
    }
    champs dt_post 1. {
        vitesse elem
        indicatrice_interf
    }
}
liste_postraitements {
    postraitements_ft_lata post1 {
        dt_post 0.002
        nom_fichier lata/post2DVDF
        format binaire
        print
        champs elements {
            indicatrice_interf
        }
        champs sommets {
    }
}

```

```
    pression
}
champs faces {
    vitesse
}
    interfaces interf {
        champs sommets {
            pe
        courbure
    }
}
}
```

Drop hanged at the ceiling

2.1 Purpose

The aim of this test is to check the capability of the Front Tracking algorithm to model the deformations of the free surface of a drop hanging in the air.

In the current state, this sheet is not really a validation sheet strictly speaking. Indeed, no advanced comparison, whether with other CFD codes or analytical results, is made. Some comparisons are nevertheless made on the evolution of the profile of the drop during the calculation with theoretical values but no reference is given.

By version v1.8.4, validation will be redone on this sheet in order to improve the stability of the test case as well as the validation of this phenomenon with other codes, theoretical and/or analytical results.

Validation made by : S.Pigny.

Report generated 11/01/2021.

2.2 Problem Description

A water drop is present at the upper frontier of a closed box. Despite the presence of gravity effects, its position can be maintained hanged close to a solid wall, by the action of surface tension forces. Phenomena related to the contact angle close to the solid wall play an important role. The contact angle is the angle between the surface where is hanged the drop and the tangent at the meridians of the drop close to the solid wall. It is measured on the external face of the drop. Its value leads to the determination of the amount of water that can be present in the drop, before it falls. The present test case is useful to analyse the way the surface tension forces are taken into account in the presence of contact angle. An emphasis is laid on the importance of parasitic currents. During the calculation, the bubble grows due to low velocity water injection. Water is injected at the center of the drop, via a boundary condition located in the wall. The surface involved in the boundary condition is much lower than the surface wetted by the drop. At the beginning of the process, the volume of the drop has a small value. Its shape tends to be a part of a sphere. Thereafter, it changes, due to hydrostatic pressure. The computationally obtained profile of the drop is compared to an analytical reference solution. Its shape is supposed to follow a cylindrical symmetry. It is given by the integration of the following equation :

$$-\frac{\partial \theta}{\partial s} - \frac{\sin \theta}{x} = \frac{g(\rho_l - \rho_g)}{\sigma} (y - y_0)$$

The parameter y_0 is determined so that the contact angle at the top frontier keeps a fixed, constant, given value. The entire profile of the drop is determined via a classical iteration Runge-Kutta method.

In the case modeled here, the following assumptions are taken:

- The drop is hanged close to a solid support;
- The gravity is upwardly oriented;
- The y-axis is the axis of symmetry of the drop.

Solving the integral of the above equation with the previously mentioned hypotheses makes it possible to predict the theoretical profiles of a water drop in air, for different sizes, i.e for different amounts of water involved in it. Different contact angles with solid wall are also presented. Contact angle values are accounted

in the air. The numerical accuracy is satisfactory, since the curvature and the contact angle are second order calculated.

Two calculations are made in this sheet. The differences between them relate only to the contact angle between the tangential curve at the drop close to the wall. In the first case, this one measures 1.5 radian and 2.5 radians in the second case (these values are accounted in the air). This value will be defined in the boundary conditions of the testcase (see sub-section 2.2).

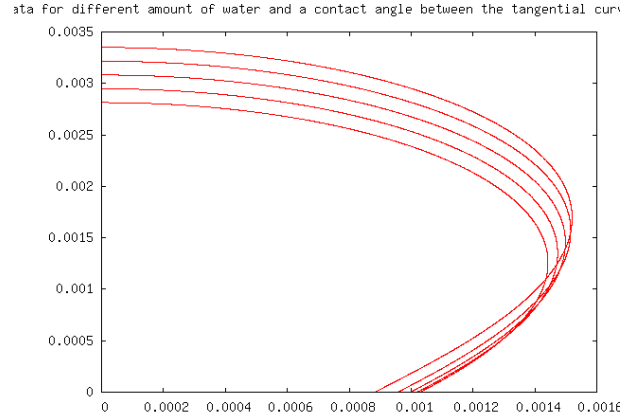


Figure VII.2.1: Profiles of the drop : theoretical data for different amount of water and a contact angle between the tangential curve at the drop close to the wall of 1 radian.

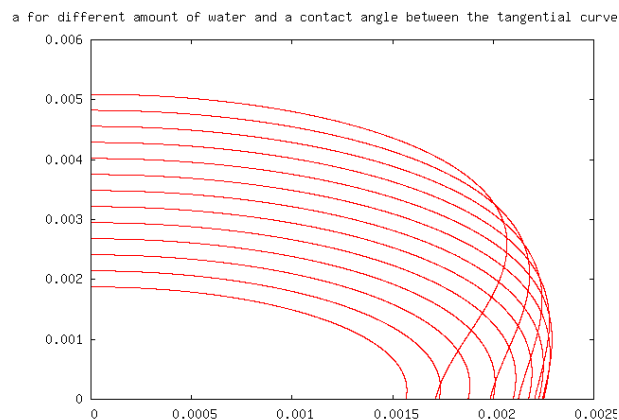


Figure VII.2.2: Profiles of the drop : theoretical data for different amount of water and a contact angle between the tangential curve at the drop close to the wall of 1.5 radian.

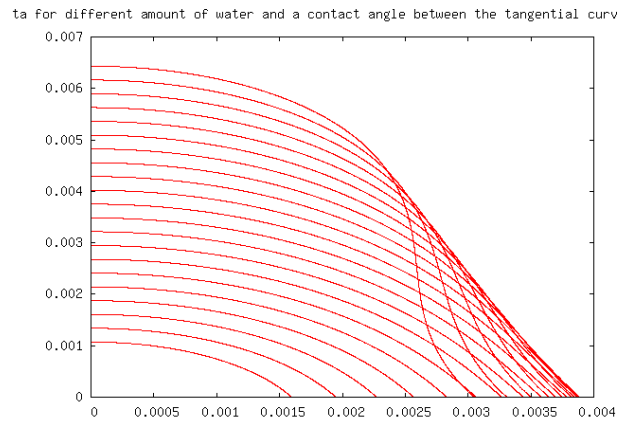


Figure VII.2.3: Profiles of the drop : theoretical data for different amount of water and a contact angle between the tangential curve at the drop close to the wall of 2 radian.

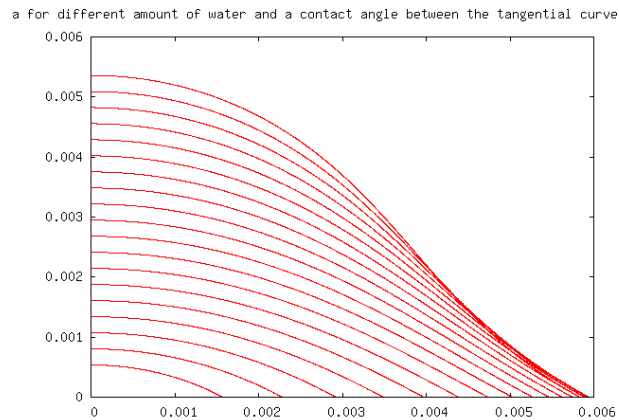


Figure VII.2.4: Profiles of the drop : theoretical data for different amount of water and a contact angle between the tangential curve at the drop close to the wall of 2.5 radian.

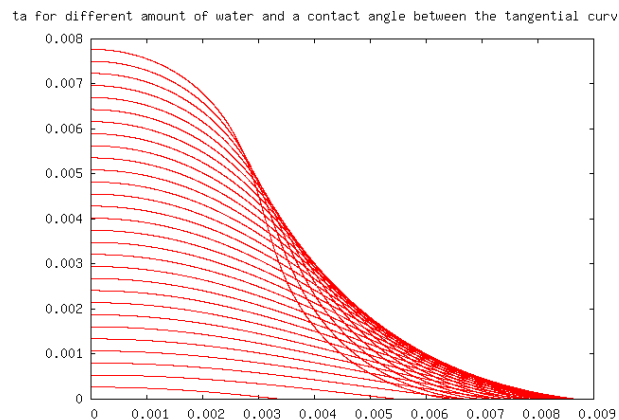


Figure VII.2.5: Profiles of the drop : theoretical data for different amount of water and a contact angle between the tangential curve at the drop close to the wall of 3 radian.

Geometry

The problem is solved in a cuboid field with dimensions $0.021 \times 0.012 \times 0.021$ meter according X, Y and Z directions. A drop initially hangs in the center of the top face of the cuboid. The angle formed between the free surface of the drop and the upper face of the domain is 1.5 radian (first case - accounted in the air) or 2.5 radians (second case - accounted in the air).

Initial Conditions and Boundary Conditions

Different initial and boundary conditions are applied between the domain and the water-air interface.

- **For the domain:**

→ *Initial condition*: zero uniform velocity field for the 3 directions

→ *Boundary conditions*: at the top of the domain, a velocity boundary condition of -0.1m.s^{-1} is applied to give a boost to the drop. At the top of the domain, an outlet boundary condition is defined with an uniform field for P/ρ equal to 0 (Pa/kg.m^3). For the 4 vertical borders, a situation of adherence is defined.

- **For the interface:**

→ *Initial condition*: the following function is applied to define the initial shape and position of the bubble : $-(x - 0.0105) * (x - 0.0105) - (z - 0.0105) * (z - 0.0105) - (y - 0.012) * (y - 0.012) + 0.0005 * 0.0005$

→ *Boundary conditions*: a specific boundary condition for discontinuous Front_Tracking problem is defined *paroi_ft_disc*. The boundary condition is used to define the initial contact angle formed by the drop on the upper wall. The defined function is of the form $\alpha + \sqrt{((x - 0.0105) * (x - 0.0105) + (z - 0.0105) * (z - 0.0105))) * 1000}$, where α represents the contact angle on the liquid side. This value of α will therefore be different for the 2 calculations: 94° in the liquid part to represent 1.5 radians in air (1st case) and 37° in the liquid part to represent 2.5 radians in air (2nd case).

Fluid Properties

In order to construct the diphasic fluid, two incompressible fluids, water and air, are defined by the usual keyword *Fluide_Incompressible*. Then, they are associated to create the two-phase fluid via the keyword *Fluide_Diphasique*.

2.3 Case Setup

Grid

Regarding the interface between air and water (drop surface), a specific mesh adapted to Front-Tracking problem has been defined.

The re-meshing criteria defined to model this phenomenon are relatively high with *lissage_courbure_iterations* = 20, *lissage_courbure_coeff* = -0.05 and *facteur_longueur_ideale* = 1.

Indeed, in Front-Tracking calculations, one can notice that the accuracy does not depend on the eulerian mesh only : the equilibrium profile is fully determinated via the geometrical curvature of interfaces and the gravity potentiel, which is evaluated at the interfacial nodes. It does not depend on discretised quantities related to the fixed mesh but to discretized quantities at the interface. Thus, to properly capture the profile of the drop, it is necessary to define an effective remeshing.

In the next version of this sheet, a study will be carried out on these parameters and recommendations adapted to the modeling of this phenomenon will be given to reach a good compromise between the CPU time and the fineness of the results.

Model Options

This sheet deals with a generic Front-Tracking problem in the discontinuous version. It differs from others TrioCFD test cases : The problem does not state the number of equations that are enclosed in the problem. Two equations are compulsory : a momentum balance equation (alias Navier-Stokes equation) and an interface tracking equation. The list of equations to be solved is declared in the beginning of the data file. Another difference with more classical TRUST data file, lies in the fluids definition. The two-phase fluid (Fluide_Diphasique) is made with two usual single-phase fluids (Fluide_Incompressible). As the list of equations to be solved in the generic Front-Tracking problem is declared in the data file and not predefined in the structure of the problem, each equation has to be distinctively associated with the problem with the Associer keyword.

2.4 Results

Validation Specific Informations

- Version TRUST : 1.6.1
- Type of problem: Front Tracking problem
- Discretization: VDF
- Convection scheme: Schema_Euler_explicite
- Type of fluid: air and water at 293K
- Location: Front_tracking_discontinu/share/Validation/Rapports_automatiques/FTD_hanging_drop
- Generated Test cases :
 - pendante_1p5/goutte.data : /* data file in annex */
 - pendante_2p5/goutte.data : /* data file in annex */
- Performance Chart :

	host	system	Total CPU Time	CPU time/step	number of cell
pendante_1p5/goutte	is241762.intra.cea.fr	Linux	356.149	0.116558	67240
pendante_2p5/goutte	is241762.intra.cea.fr	Linux	1927.71	0.192692	67240
Total			2283.86		

Table VII.2.1: Performance Chart

Plot Data

- **First Calculation: contact angle of 1.5 radian between the tangential curve at the drop close to the wall**

The following figures show the growth of the hanging drop at the top of the box for different times.

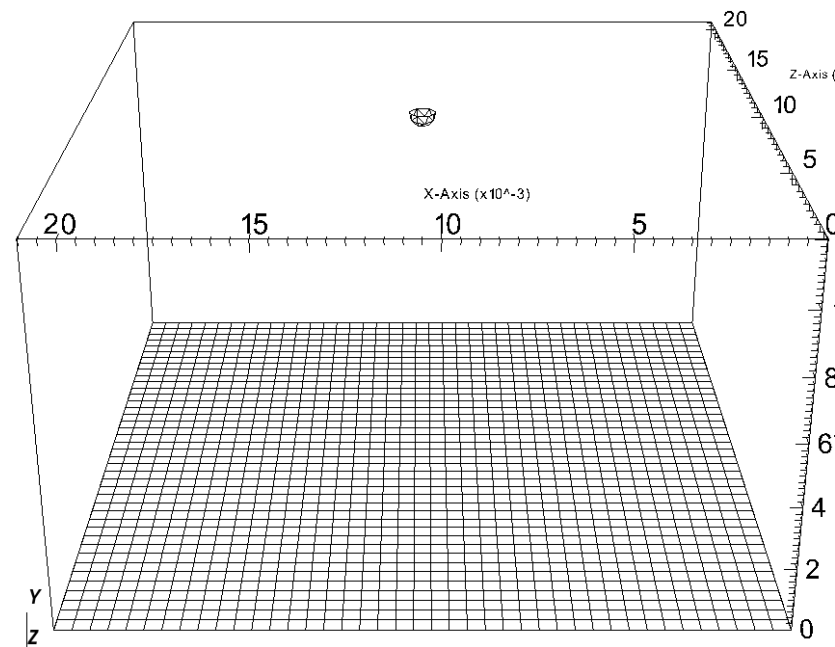


Figure VII.2.6: Drop hanged at the top of the box with a contact angle of 1.5 radian - $t=0s$

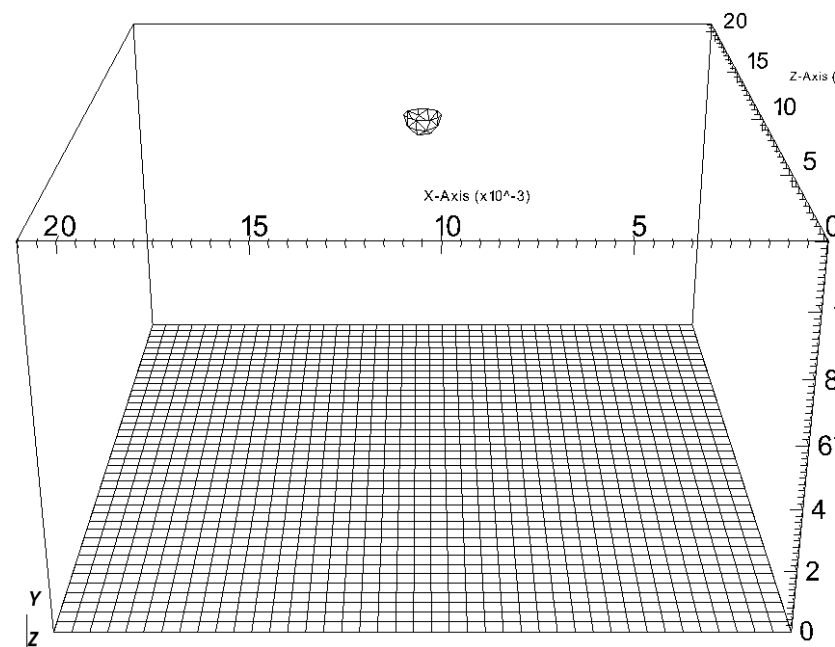


Figure VII.2.7: Drop hanged at the top of the box with a contact angle of 1.5 radian - $t=0.01s$

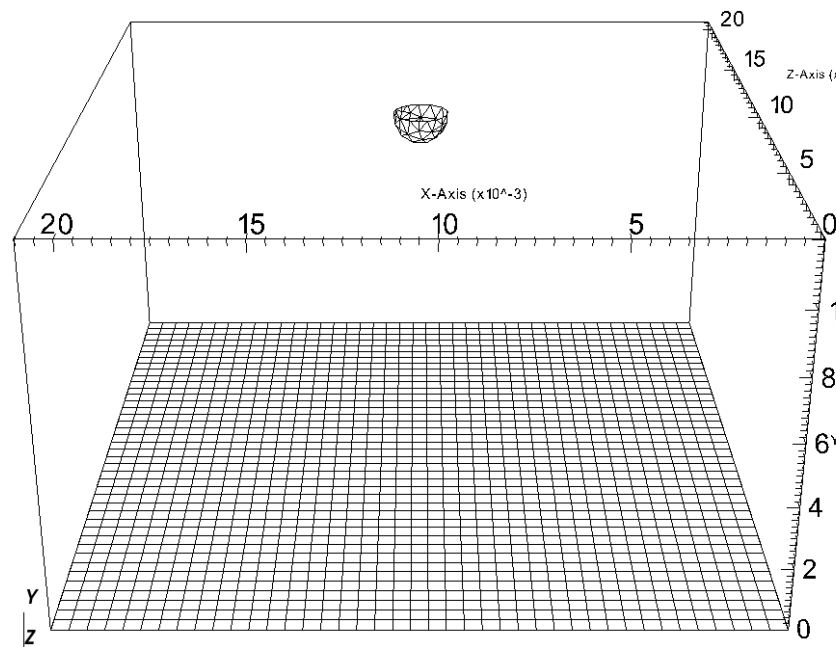


Figure VII.2.8: Drop hanged at the top of the box with a contact angle of 1.5 radian - $t=0.05s$

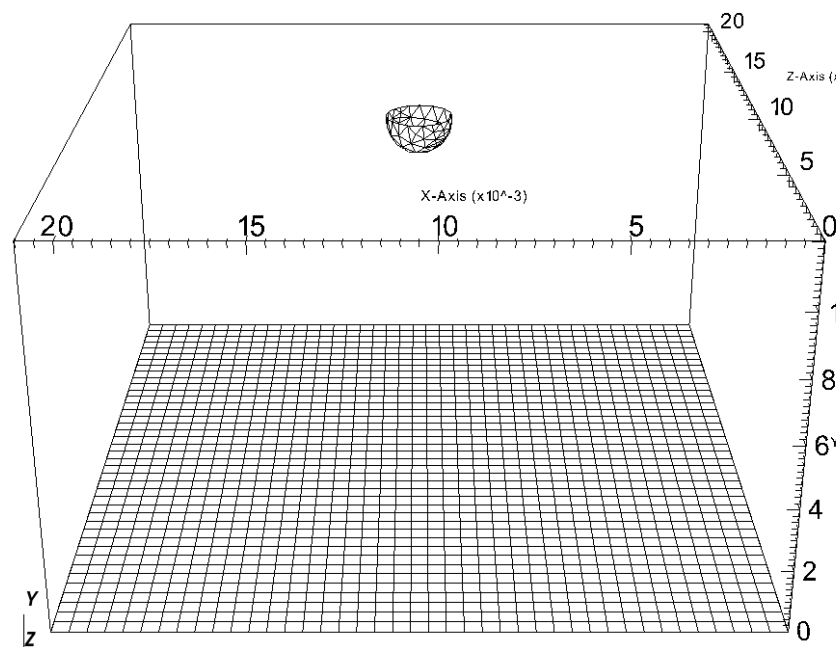


Figure VII.2.9: Drop hanged at the top of the box with a contact angle of 1.5 radian - $t=0.1s$

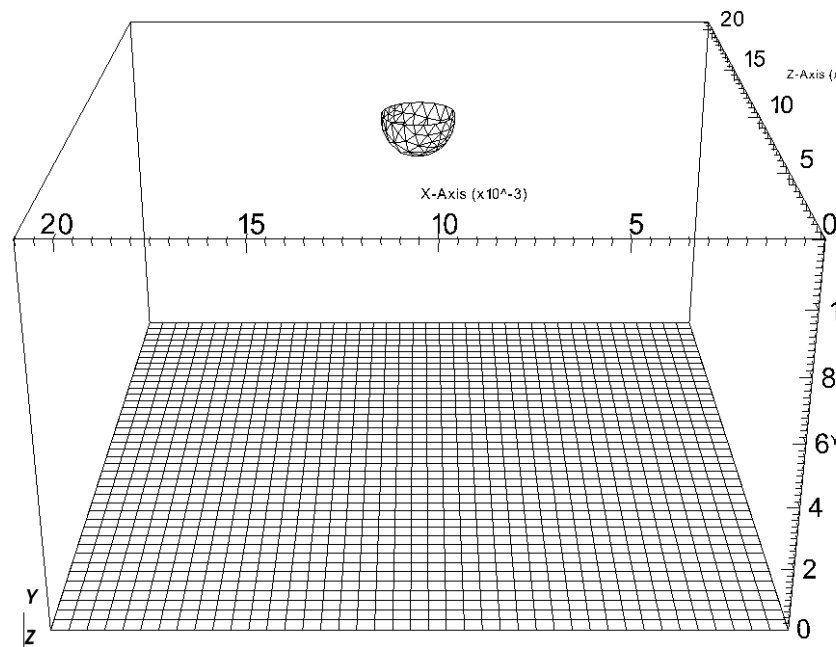


Figure VII.2.10: Drop hanged at the top of the box with a contact angle of 1.5 radian - $t=0.15\text{s}$

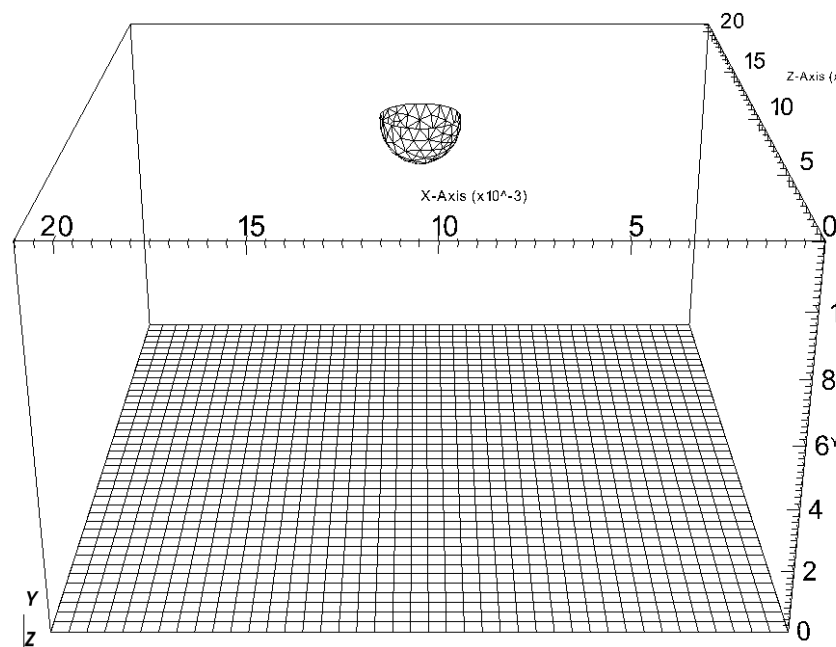


Figure VII.2.11: Drop hanged at the top of the box with a contact angle of 1.5 radian - $t=0.2\text{s}$

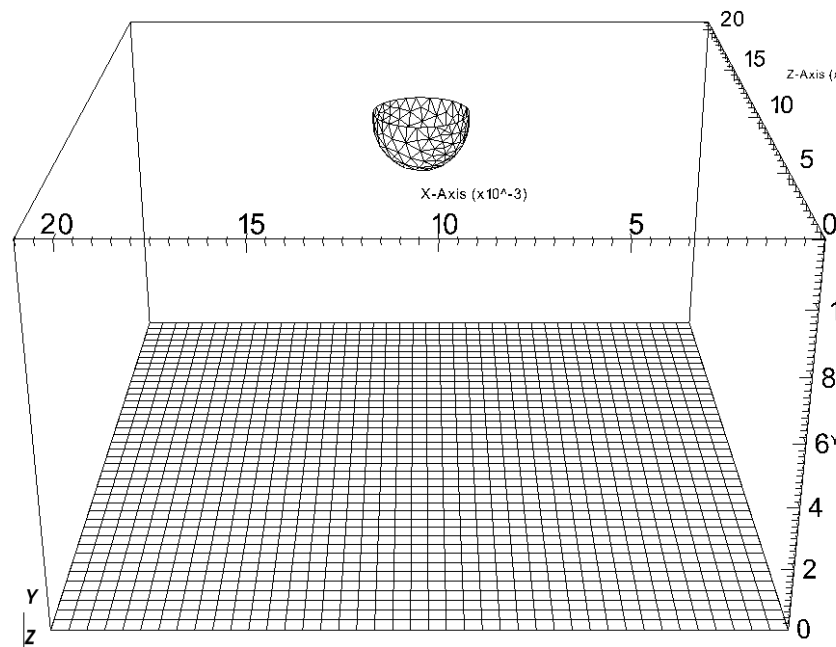


Figure VII.2.12: Drop hanged at the top of the box with a contact angle of 1.5 radian - $t=0.35\text{s}$

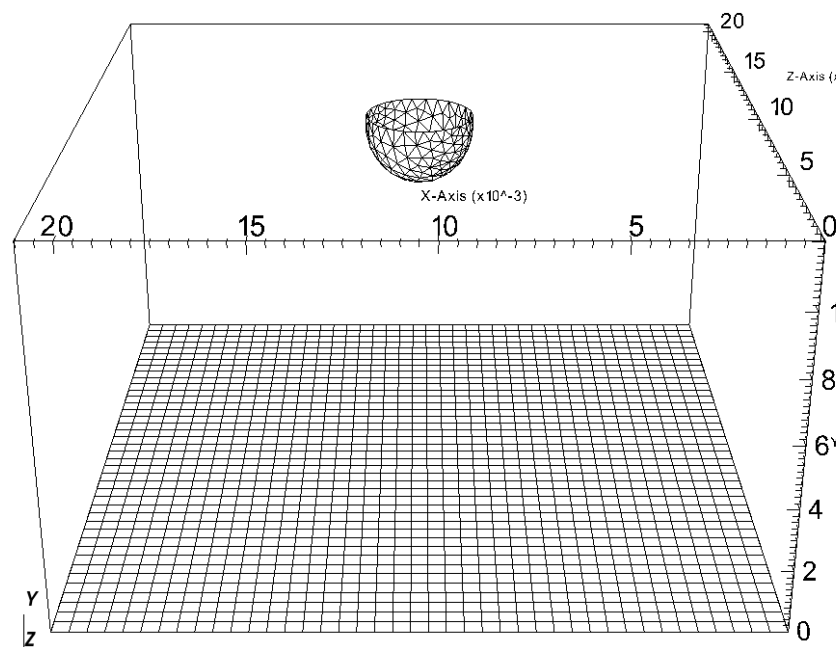


Figure VII.2.13: Drop hanged at the top of the box with a contact angle of 1.5 radian - $t=0.5\text{s}$

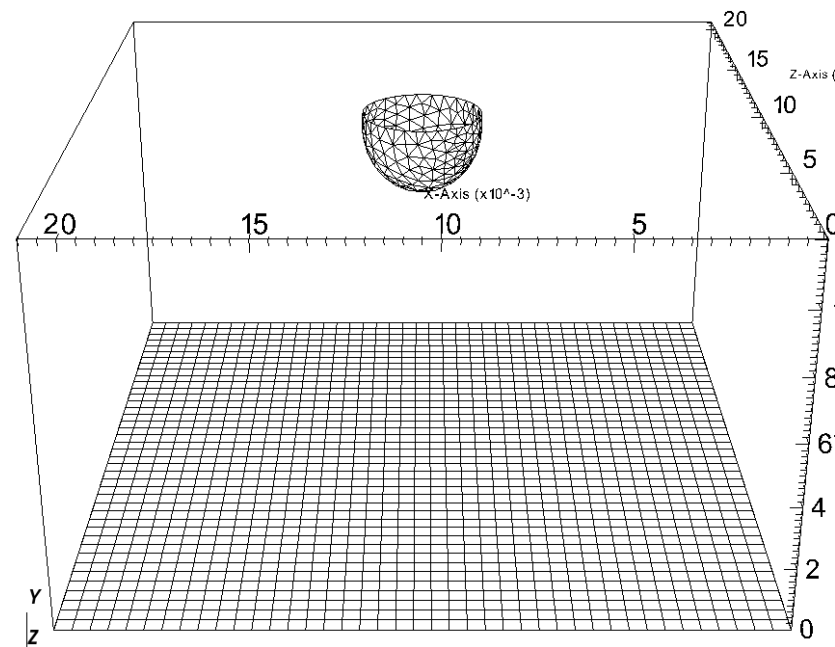


Figure VII.2.14: Drop hanged at the top of the box with a contact angle of 1.5 radian - $t=0.75\text{s}$

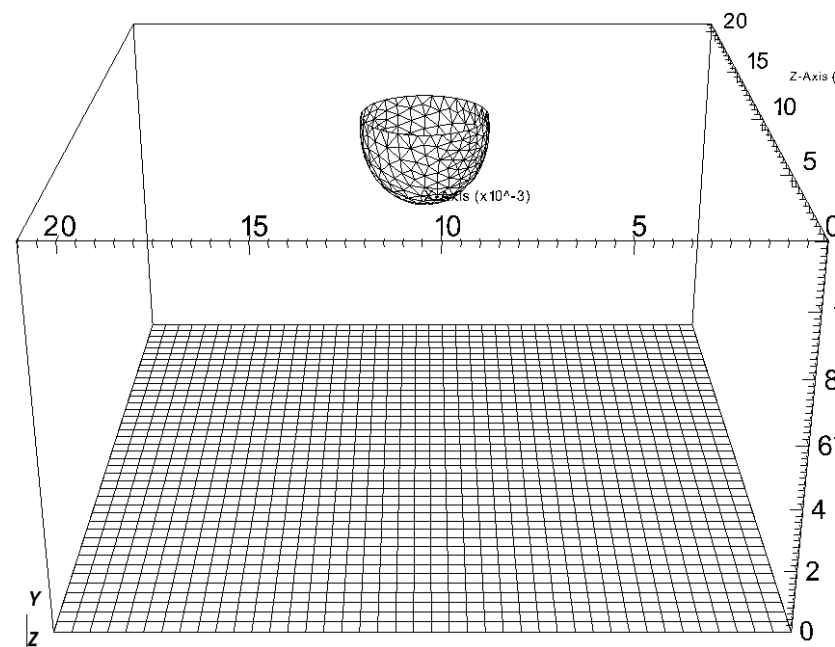


Figure VII.2.15: Drop hanged at the top of the box with a contact angle of 1.5 radian - $t=1\text{s}$

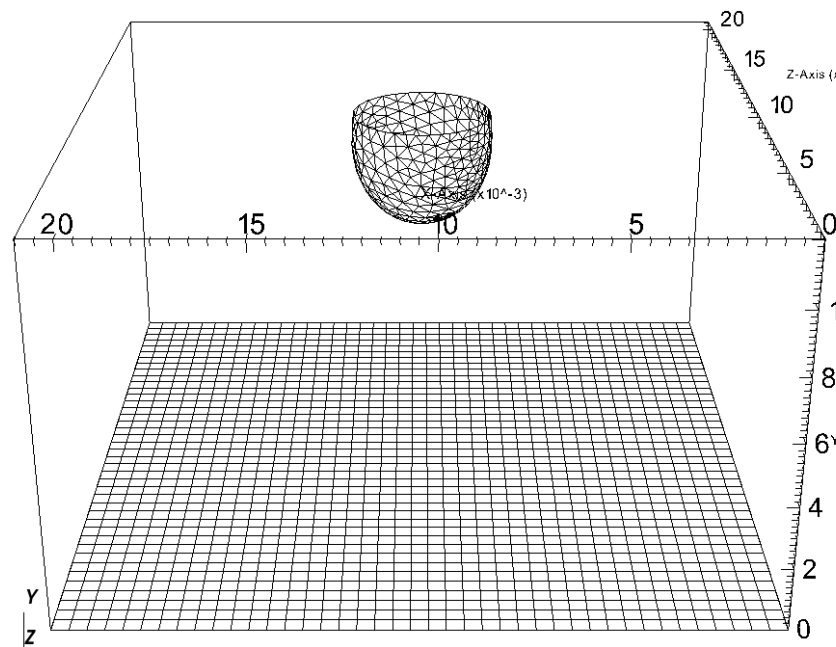


Figure VII.2.16: Drop hanged at the top of the box with a contact angle of 1.5 radian - $t=1.5\text{s}$

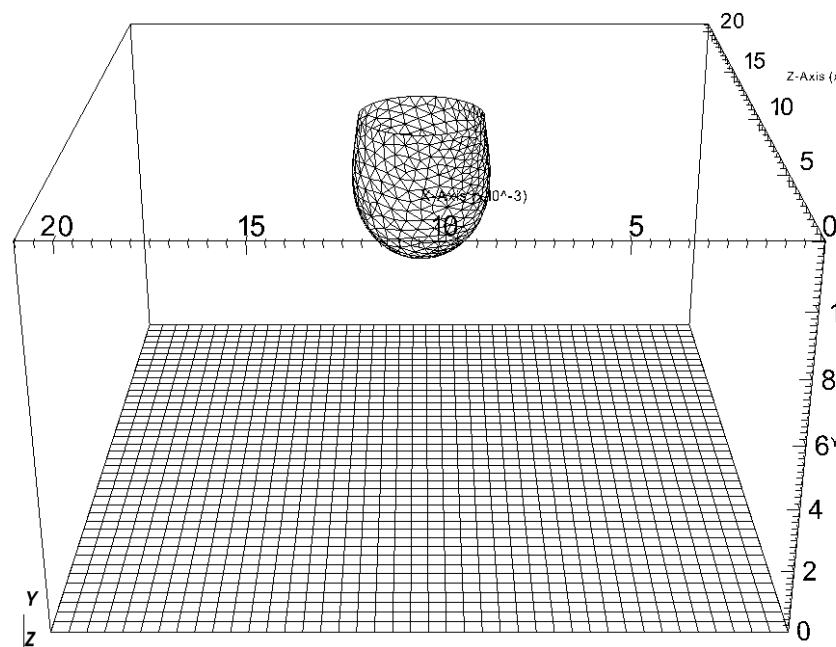


Figure VII.2.17: Drop hanged at the top of the box with a contact angle of 1.5 radian - $t=2\text{s}$

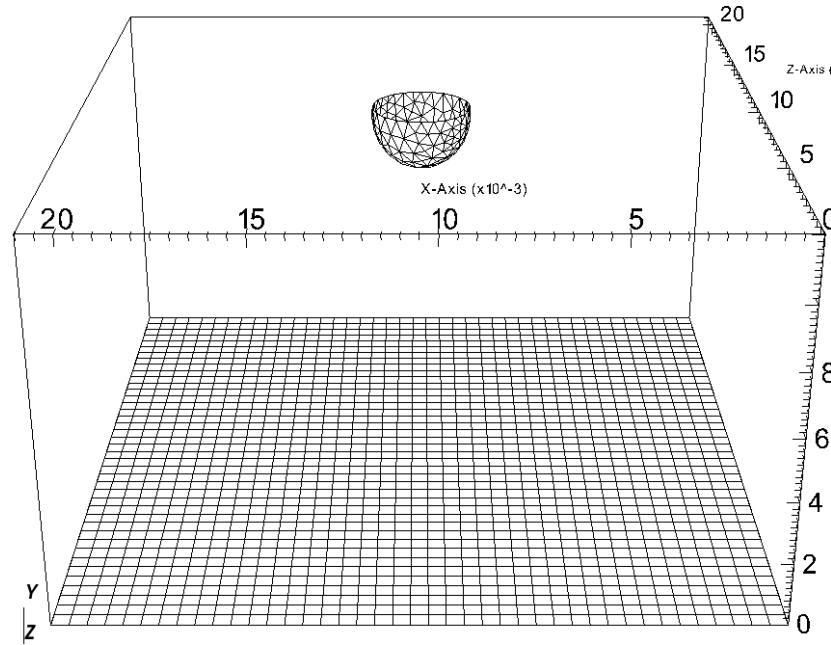


Figure VII.2.18: Drop hanged at the top of the box with a contact angle of 1.5 radian - $t=2.5\text{s}$

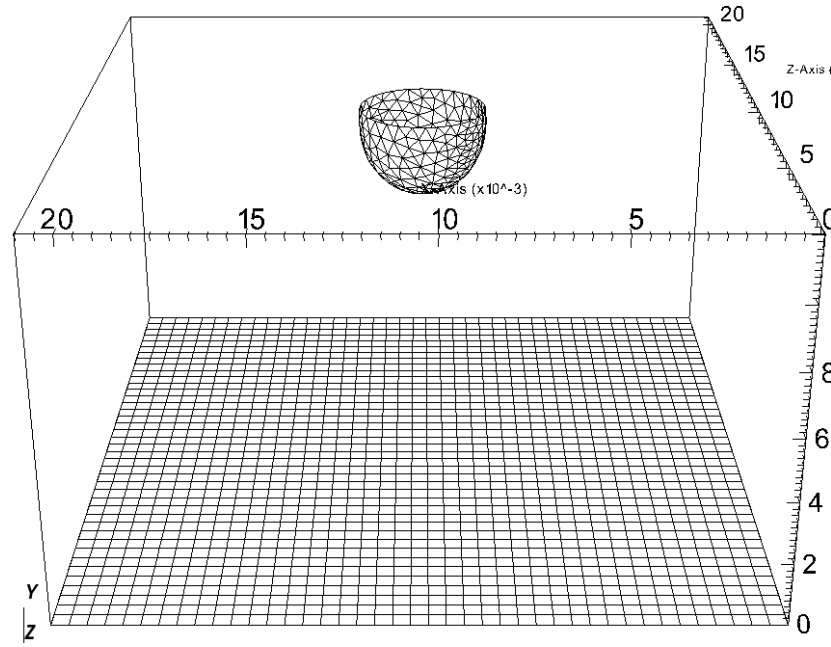


Figure VII.2.19: Drop hanged at the top of the box with a contact angle of 1.5 radian - $t=3\text{s}$

The following graph represents the profile of the drop at different moments : $t_1 = 0.45\text{s}$, $t_2 = 1.15\text{s}$ and $t_3 = 2.05\text{s}$ and comparisons of positions of nodes of lagrangian mesh points and theoretical profiles. The contact angle of the drop become quickly greater than 90° and one can notice that the numerical accuracy degrades for high contact angle values.

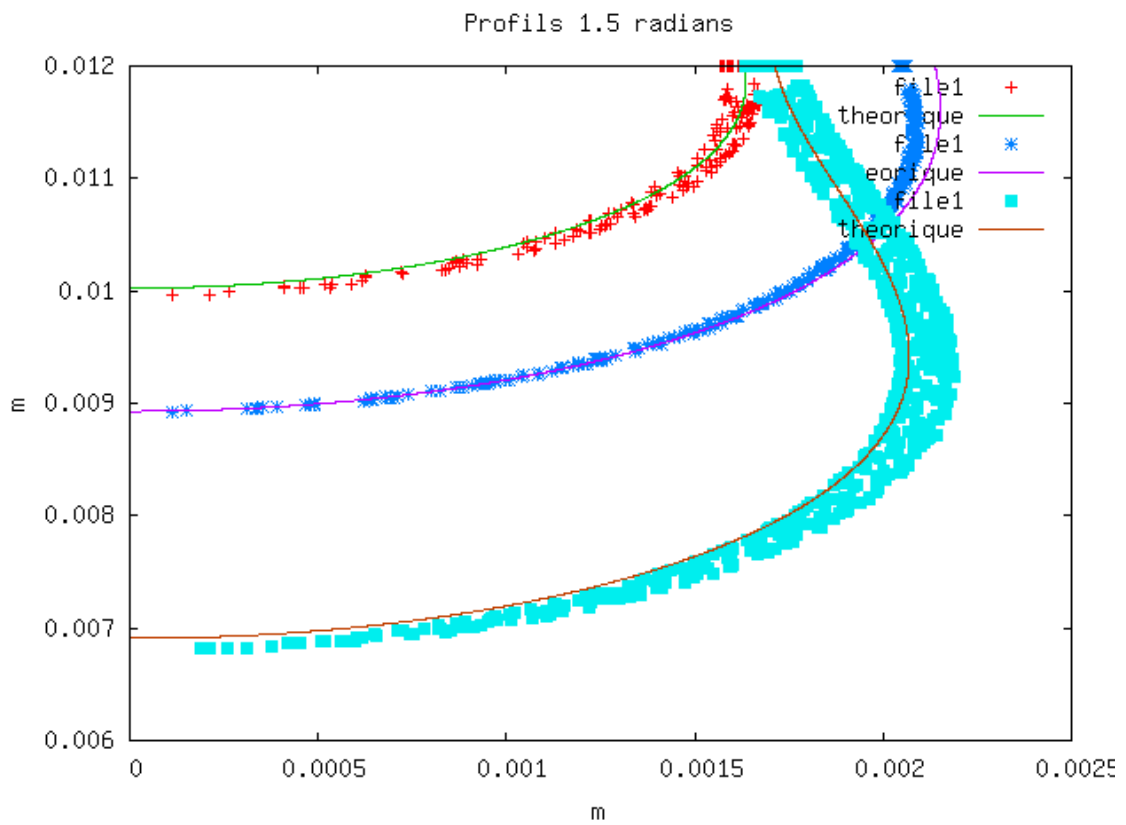


Figure VII.2.20: Profils 1.5 radians

Description des courbes de la figure fic019.png:

- file1 : Trio_U
fichier ./pendante_1p5/profil_trio_u_t1.txt
 - theoreque : trio_u
fichier ./profil/nouv_1.5_0.737
 - file1 : Trio_U
fichier ./pendante_1p5/profil_trio_u_t2.txt
 - theoreque : trio_u
fichier ./profil/nouv_1.5_1.146
 - file1 : Trio_U
fichier ./pendante_1p5/profil_trio_u_t3.txt
 - theoreque : trio_u
fichier ./profil/nouv_1.5_1.9
- **Second Calculation: contact angle of 2.5 radian between the tangential curve at the drop close to the wall**

The following figures show the growth of the hanging drop at the top of the box for different times.

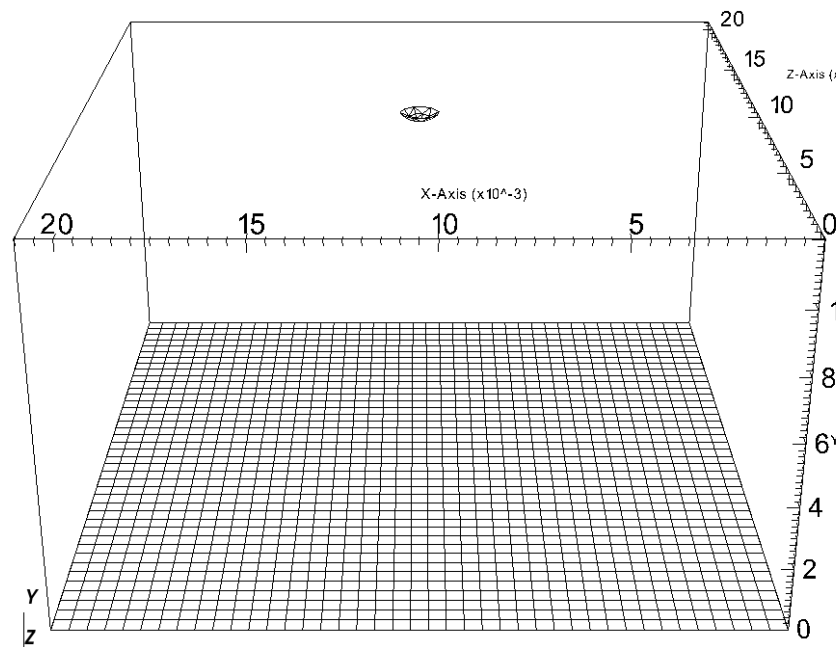


Figure VII.2.21: Drop hanged at the top of the box with a contact angle of 2.5 radian - $t=0$ s

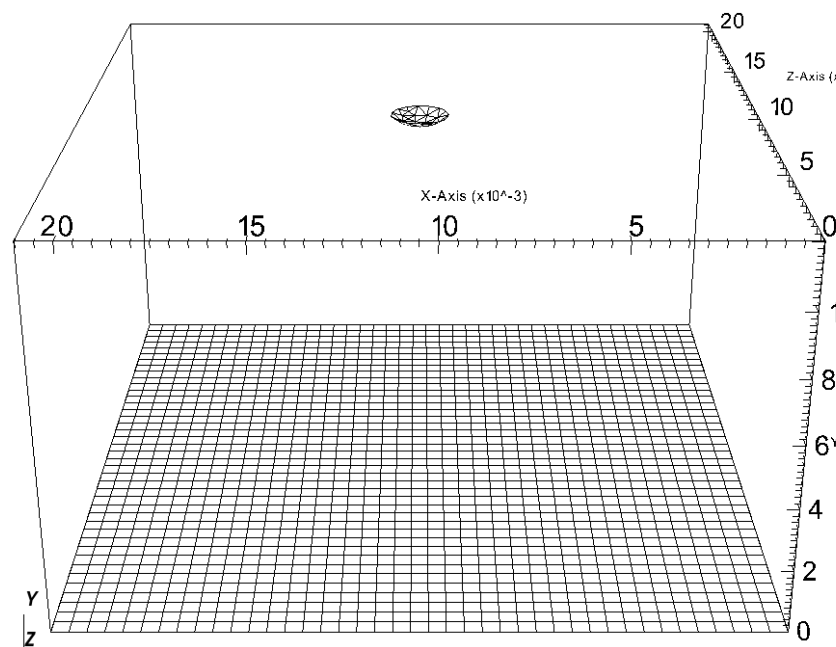


Figure VII.2.22: Drop hanged at the top of the box with a contact angle of 2.5 radian - $t=0.01$ s

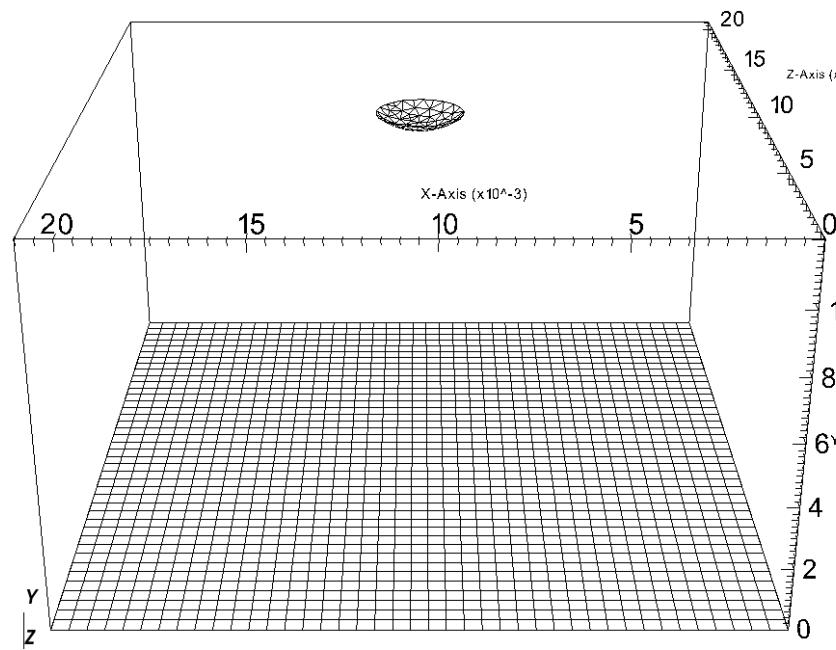


Figure VII.2.23: Drop hanged at the top of the box with a contact angle of 2.5 radian - $t=0.05\text{s}$

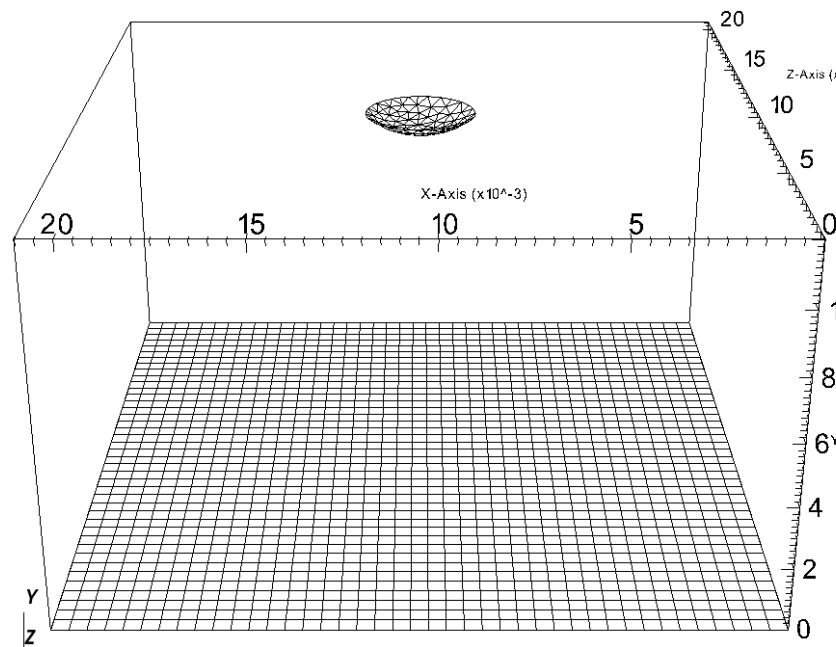


Figure VII.2.24: Drop hanged at the top of the box with a contact angle of 2.5 radian - $t=0.1\text{s}$

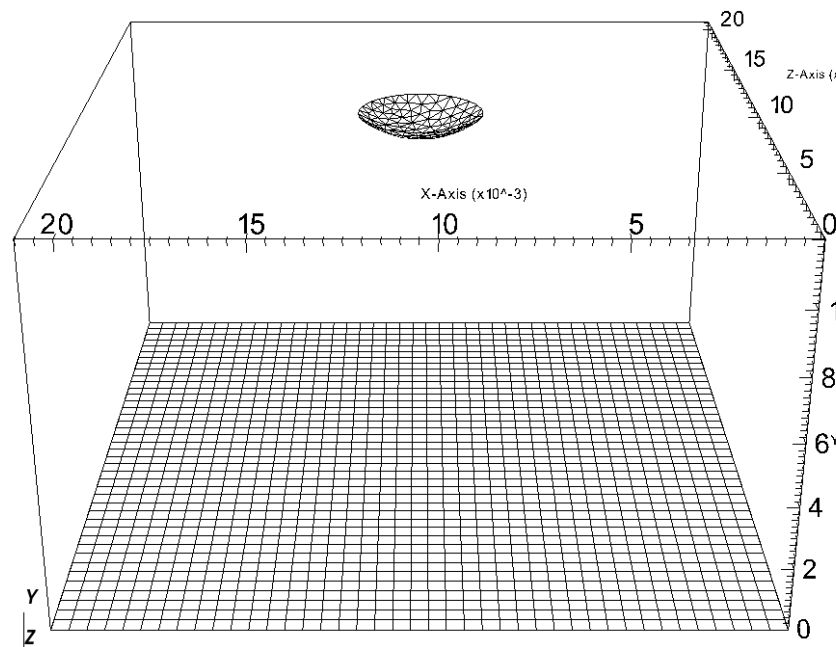


Figure VII.2.25: Drop hanged at the top of the box with a contact angle of 2.5 radian - $t=0.15\text{s}$

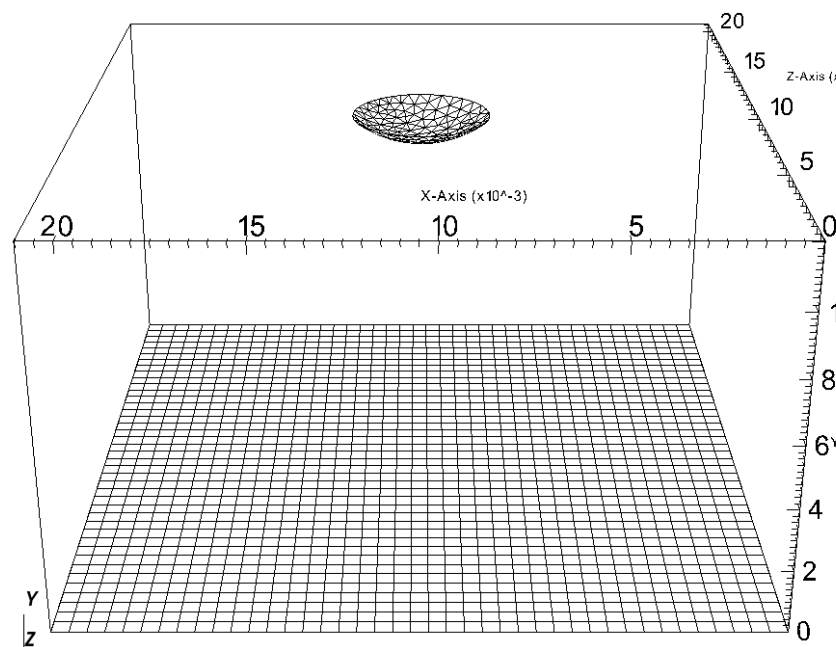


Figure VII.2.26: Drop hanged at the top of the box with a contact angle of 2.5 radian - $t=0.2\text{s}$

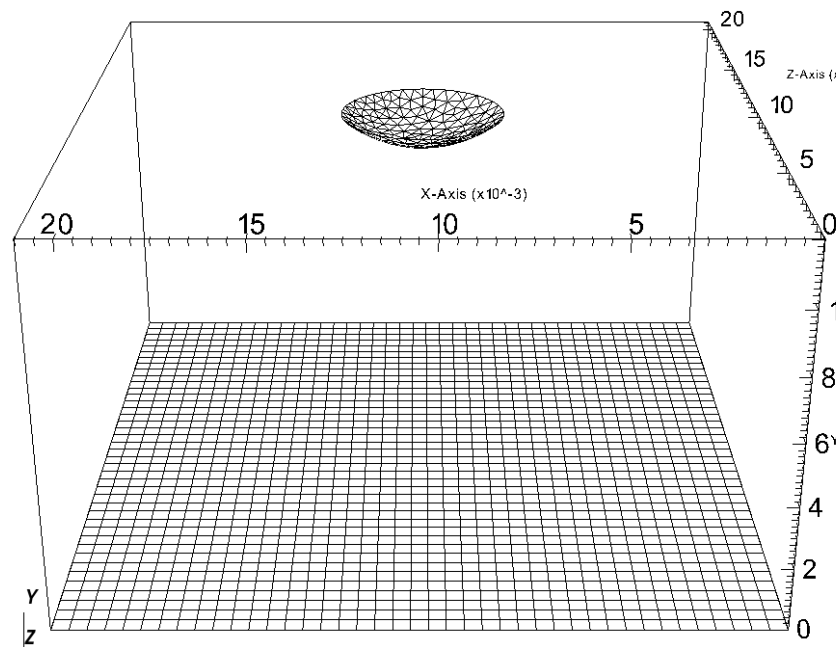


Figure VII.2.27: Drop hanged at the top of the box with a contact angle of 2.5 radian - $t=0.35s$

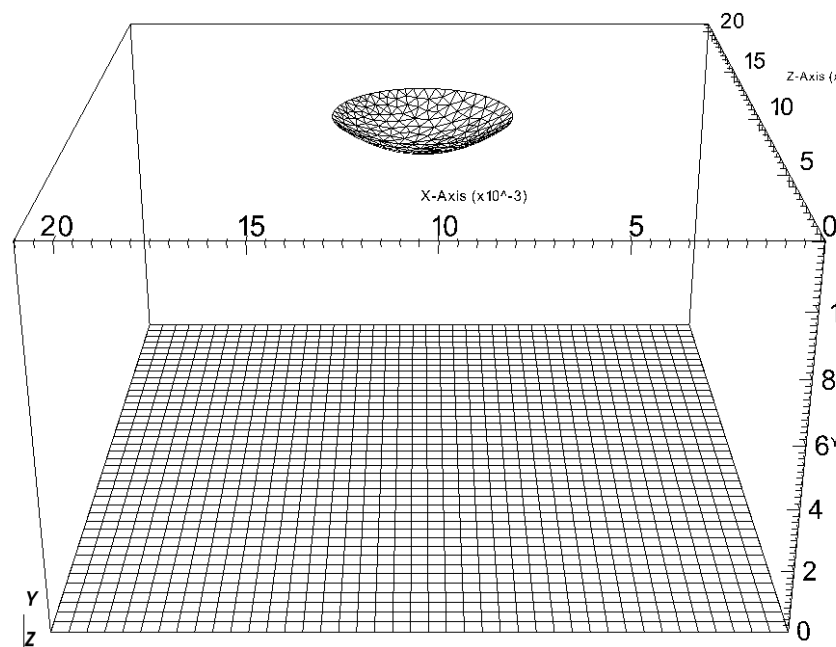


Figure VII.2.28: Drop hanged at the top of the box with a contact angle of 2.5 radian - $t=0.5s$

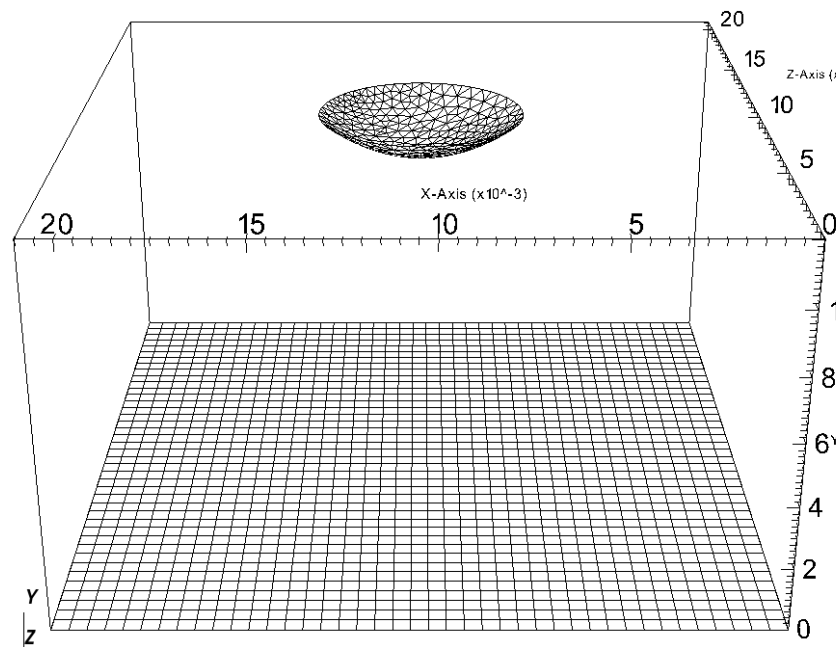


Figure VII.2.29: Drop hanged at the top of the box with a contact angle of 2.5 radian - $t=0.75\text{s}$

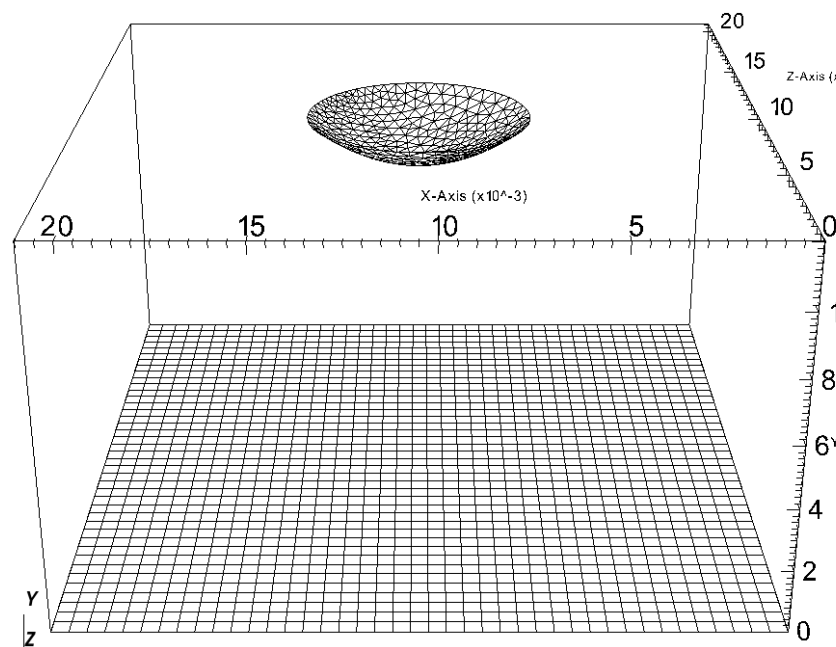


Figure VII.2.30: Drop hanged at the top of the box with a contact angle of 2.5 radian - $t=1\text{s}$

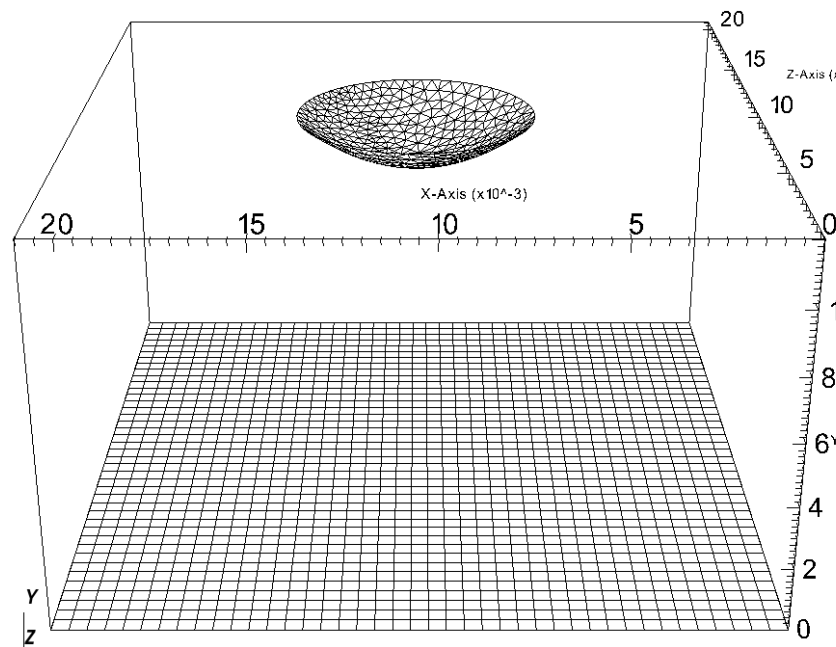


Figure VII.2.31: Drop hanged at the top of the box with a contact angle of 2.5 radian - $t=1.25s$

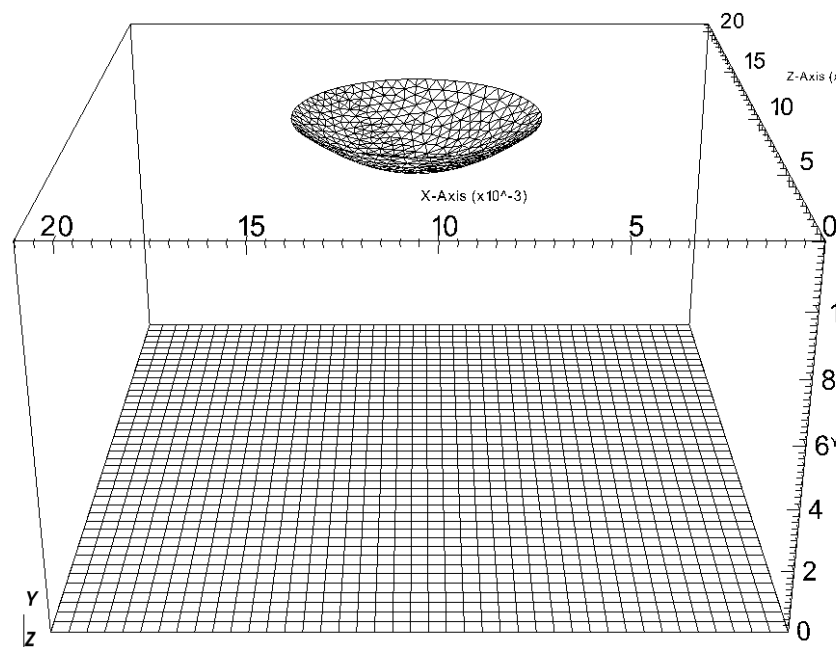


Figure VII.2.32: Drop hanged at the top of the box with a contact angle of 2.5 radian - $t=1.5s$

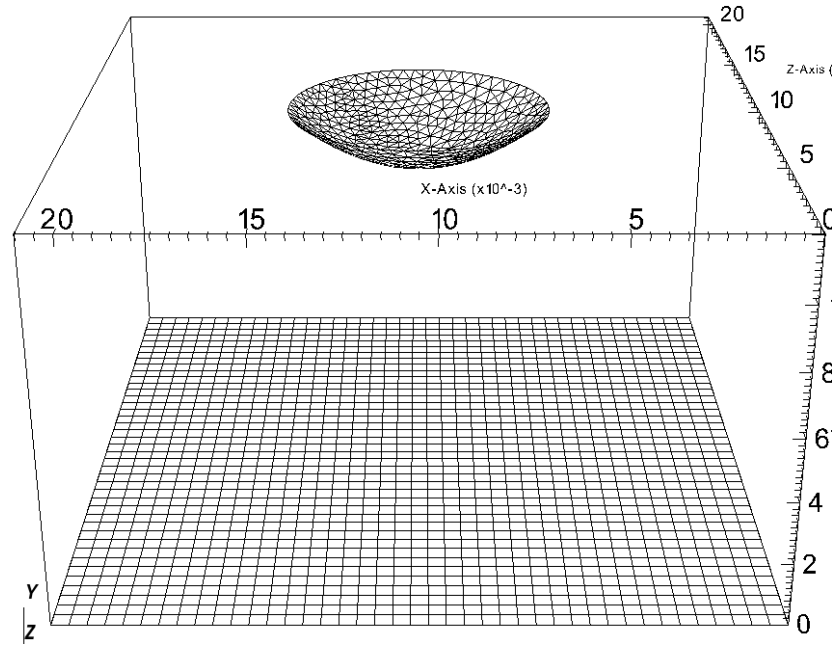


Figure VII.2.33: Drop hanged at the top of the box with a contact angle of 2.5 radian - $t=1.75s$

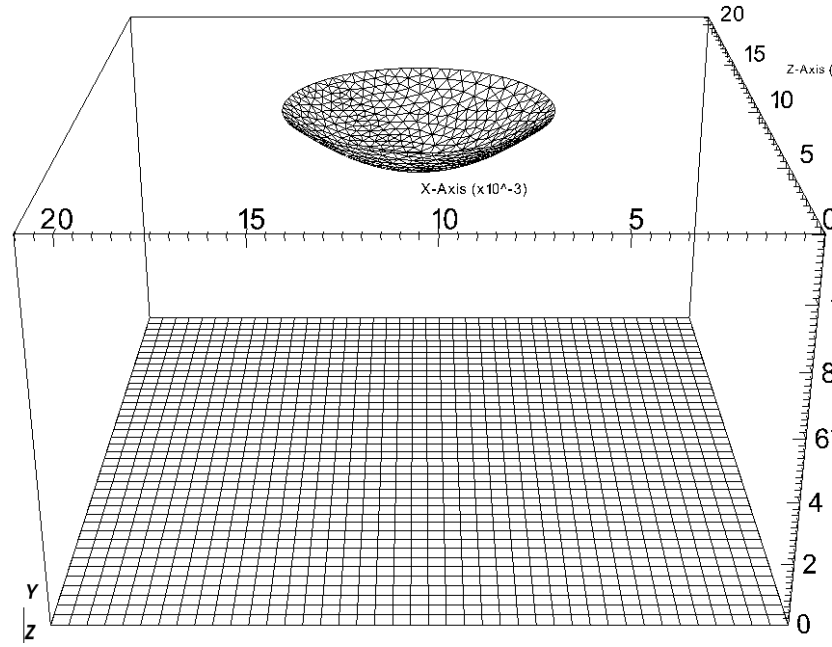


Figure VII.2.34: Drop hanged at the top of the box with a contact angle of 2.5 radian - $t=2s$

The following graph the profile of the drop at different moment : $t_1 = 2.4s$, $t_2 = 3.65s$ and $t_3= 6.45s$ and comparisions of positions of nodes of lagrangian mesh points and theoretical profiles.

Regarding profiles for 1.5 and 2.5 radians, one can notice that for low values of contact angle, the profile is less stable in time. Some spurious oscillations of the interface take place.

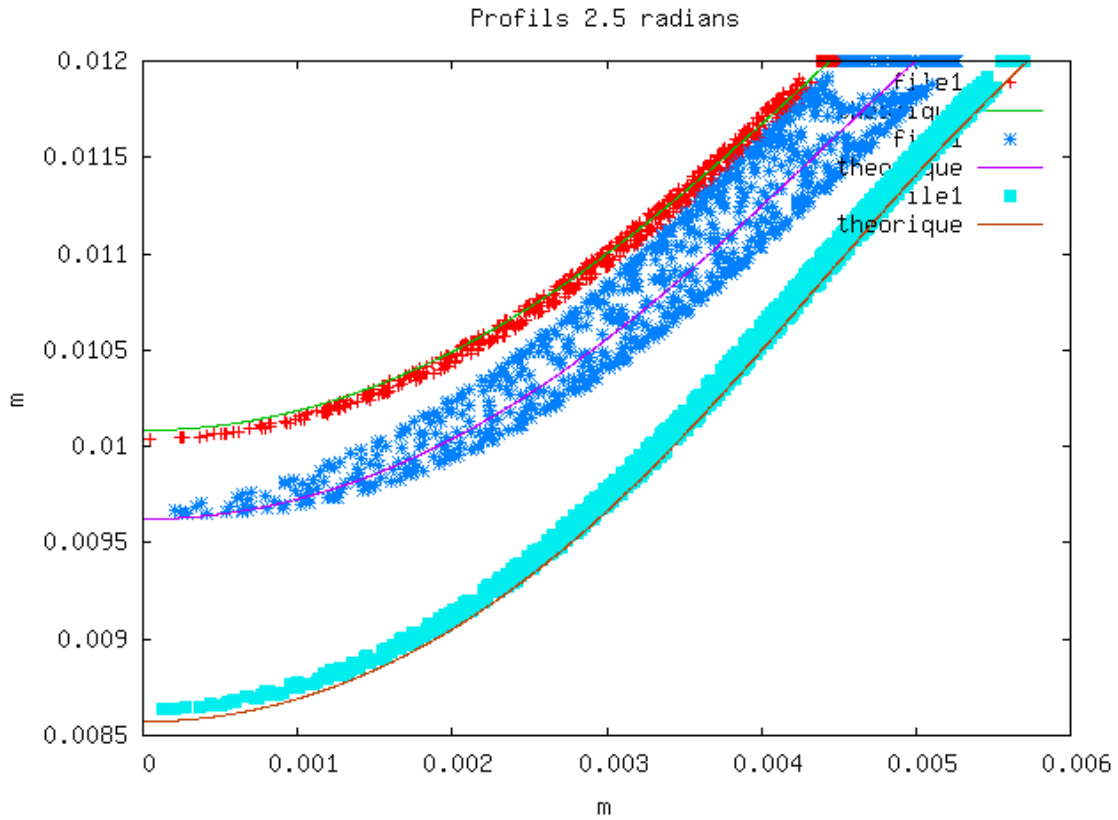


Figure VII.2.35: Profils 2.5 radians

Description des courbes de la figure fic034.png:

- file1 : Trio_U
fichier ./pendante_2p5/profil_trio_u_t1.txt
- theorique : trio_u
fichier ./profil/nouv_2.5_0.715
- file1 : Trio_U
fichier ./pendante_2p5/profil_trio_u_t2.txt
- theorique : trio_u
fichier ./profil/nouv_2.5_0.887
- file1 : Trio_U
fichier ./pendante_2p5/profil_trio_u_t3.txt
- theorique : trio_u
fichier ./profil/nouv_2.5_1.279

2.5 Conclusion

This sheet demonstrate the capabilities of TrioCFD for the modeling of this type of phenomenon. A first comparison with the theory shows a good prediction of the shape of the drop over time. However, for drop contact angles greater than 90° , the accuracy is deteriorated. A study will be carried out between now and v1.8.4 in order to understand the origin of these oscillations, reduce them and give recommendations for a good parameterization of Front-Tracking remeshing.

2.6 Data Files

goutte

```
# Hydraulique 3D laminaire : schema upwind #
dimension 3
Probleme_FT_Disc_gen pb1
Domaine dom_pb1
Read_file dom_pb1 Pb1_44_44_43.geom
VDF dis
schema_euler_explcit sch
Read sch
{
    tinit 0.0
    tmax 3.
    dt_min 1.e-10
    dt_max 0.001
    dt_impr 0.2
    dt_sauv 10.
    seuil_statio -1.e-8
    facsec 1
}
Fluide_Incompressible eau
Read eau
{
    mu Champ_Uniforme 1 2.82e-4
    rho Champ_Uniforme 1 1000.
}
Fluide_Incompressible air
Read air
{
    mu Champ_Uniforme 1 2.82e-5
    rho Champ_Uniforme 1 10.
}
Fluide_Diphasique fluide
Read fluide
{
    fluide0 air
    fluide1 eau
    sigma Champ_Uniforme 1 0.07
}
Champ_Uniforme gravite
Read gravite 3 0. -9.81 0.
Associate fluide gravite
Navier_Stokes_FT_Disc          hydraulique
Transport_Interfaces_FT_Disc   interf
Associate pb1 hydraulique
Associate pb1 interf
Associate pb1 dom_pb1
Associate pb1 sch
Associate pb1 fluide
System "mkdir -p lata"
Discretize pb1 dis
Read pb1
{
    hydraulique
{
    modele_turbulence sous_maille_wale
    {
        Cw           0.
    }
}
```

```

        turbulence_paroi_negligeable
    }
solveur_pression GCP { optimized precond ssor { omega 1.6 } seuil 1.e-11 impr }
convection { quick }
diffusion { }
conditions_initiales { vitesse champ_uniforme 3 0. 0. 0. }
equation_interfaces proprietes_fluide interf
conditions_limites
{
    injection frontiere_ouverte_vitesse_imposee champ_front_uniforme 3 0. -0.1 0.
    paroi paroi_fixe
    ouverte Sortie_libre_rho_variable champ_front_uniforme 1 0.
}
terme_gravite grad_I
}
interf
{
    conditions_initiales {
        fonction
-(x-0.0105)*(x-0.0105)-(z-0.0105)*(z-0.0105)-(y-0.012)*(y-0.012)+0.0005*0.0005
    }
methode_transport vitesse_interpolee hydraulique
    iterations_correction_volume 0
    n_iterations_distance 2
remaillage {
    pas 1.e-4
    nb_iter_remaillage 2
    criterie_arete 0.5
    criterie_remaillage 0.1
    pas_lissage 1.e-5
    lissage_courbure_iterations 20
    lissage_courbure_coeff -0.05
    nb_iter_barycentrage 3
    relax_barycentrage 1.
    facteur_longueur_ideale 1.
    nb_iter_correction_volume 5
    seuil_dvolume_residuel 1e-15
}
collisions {
    active
    juric_pour_tout
    type_remaillage
    Thomas { distance_interface_element_max 1 }
}
conditions_limites
{
#    injection Paroi_FT_disc Constant Champ_Front_Uniforme 1 120 #
#    Pour un angle de contact de 1 radian compte dans le gaz on a 57
degres comptes dans le gaz et 123 degres comptes dans le liquide #
#    Pour un angle de contact de 1.5 radian compte dans le gaz on a 86
degres comptes dans le gaz et 94 degres comptes dans le liquide #
#    Pour un angle de contact de 2 radian compte dans le gaz on a 115 degres comptes dans le g
degres comptes dans le liquide #
#    Pour un angle de contact de 2.5 radian compte dans le gaz on a 143 degres comptes dans le g
degres comptes dans le liquide #
#    Pour un angle de contact de 3 radian compte dans le gaz on a 172 degres comptes dans le g
degres comptes dans le liquide #
    injection Paroi_FT_disc Constant Champ_Front_Fonc_xyz 1 94.+sqrt(((x-0.0105)*(x-0.0105)+(z-0.0105)*(z-0.0105)))
    paroi Paroi_FT_disc Constant Champ_Front_Fonc_xyz 1 94.+sqrt(((x-0.0105)*(x-0.0105)+(z-0.0105)*(z-0.0105)))
    ouverte Paroi_FT_disc Constant Champ_Front_Fonc_xyz 1 94.+sqrt(((x-0.0105)*(x-0.0105)+(z-0.0105)*(z-0.0105)))
}

```

```

}

postraitements {
    Definition_champs {
        hauteur1 Reduction_0D {
            methode moyenne_ponderee
            source Transformation {
                methode formule
                expression 1 exp(-(x*x+z*z)*1000)*(1-indicatrice_interf_natif_dom_pb1)
                source refChamp { Pb_champ pb1 indicatrice_interf }
            }
        }
        hauteur2 Reduction_0D {
            methode moyenne_ponderee
            source Transformation {
                methode formule
                expression 1 exp(-(x*x+z*z)*10000)*(1-indicatrice_interf_natif_dom_pb1)
                source refChamp { Pb_champ pb1 indicatrice_interf }
            }
        }
        hauteur3 Reduction_0D {
            methode moyenne_ponderee
            source Transformation {
                methode formule
                expression 1 exp(-(x*x+z*z)*100000)*(1-indicatrice_interf_natif_dom_pb1)
                source refChamp { Pb_champ pb1 indicatrice_interf }
            }
        }
    }
    Sondes {
        hauteur1 hauteur1 periode 0.02 points 1 0. 0.1 0.
        hauteur2 hauteur2 periode 0.02 points 1 0. 0.1 0.
        hauteur3 hauteur3 periode 0.02 points 1 0. 0.1 0.
    }
    champs dt_post 1e3
    {
        indicatrice_interf elem
    }
}
liste_postraitements {
    postraitements_ft_lata post1 {
        dt_post 0.01
        nom_fichier lata/post
        format binaire
        champs elements { indicatrice_interf }
        champs faces { vitesse }
            interfaces interf { champs sommets { courbure } }
    }
}
sauvegarde binaire Oscillation_bulle3.rep
}
Solve pb1
Fin

```

goutte

```

# Hydraulique 3D laminaire : schema upwind #
dimension 3
Probleme_FT_Disc_gen pb1
Domaine dom_pb1
Read_file dom_pb1 Pb1_44_44_43.geom
VDF dis

```

```

schema_euler_explcite sch
Read sch
{
  tinit 0.0
  tmax 10.
  dt_min 1.e-10
  dt_max 0.001
  dt_impr 0.2
  dt_sauv 10.
  seuil_statio -1.e-8
  facsec 1
}
Fluide_Incompressible eau
Read eau
{
  mu Champ_Uniforme 1 2.82e-4
  rho Champ_Uniforme 1 1000.
}
Fluide_Incompressible air
Read air
{
  mu Champ_Uniforme 1 2.82e-5
  rho Champ_Uniforme 1 10.
}
Fluide_Diphasique fluide
Read fluide
{
  fluide0 air
  fluide1 eau
  sigma Champ_Uniforme 1 0.07
}
Champ_Uniforme gravite
Read gravite 3 0. -9.81 0.
Associate fluide gravite
Navier_Stokes_FT_Disc      hydraulique
Transport_Interfaces_FT_Disc interf
Associate pb1 hydraulique
Associate pb1 interf
Associate pb1 dom_pb1
Associate pb1 sch
Associate pb1 fluide
System "mkdir -p lata"
Discretize pb1 dis
Read pb1
{
hydraulique
{
  modele_turbulence sous_maille_wale
  {
    Cw          0.
    turbulence_paroi negligable
  }
  solveur_pression GCP { optimized precond ssor { omega 1.6 } seuil 1.e-11 impr }
  convection      { quick }
  diffusion       { }
  conditions_initiales { vitesse champ_uniforme 3 0. 0. 0. }
  equation_interfaces proprietes_fluide interf
  conditions_limites
  {
    injection frontiere_ouverte_vitesse_imposee champ_front_uniforme 3 0. -0.1 0.
    paroi paroi_fixe
  }
}

```

```

        ouverte Sortie_libre_rho_variable champ_front_uniforme 1 0.
    }
    terme_gravite grad_I
}
interf
{
    conditions_initiales {
        fonction
        -(x-0.0105)*(x-0.0105)-(z-0.0105)*(z-0.0105)-(y-0.012)*(y-0.012)+0.0005*0.0005
    }
    methode_transport vitesse_interpolee hydraulique
        iterations_correction_volume 0
        n_iterations_distance 2
    remaillage {
        pas 1.e-4
        nb_iter_remaillage 2
        criteres_arete 0.5
        criteres_remaillage 0.1
        pas_lissage 1.e-5
        lissage_courbure_iterations 20
        lissage_courbure_coeff -0.05
        nb_iter_barycentrage 3
        relax_barycentrage 1.
        facteur_longueur_ideale 1.
        nb_iter_correction_volume 5
        seuil_dvolume_residuel 1e-15
    }
    collisions {
        active
        juric_pour_tout
        type_remaillage
        Thomas { distance_interface_element_max 1 }
    }
    conditions_limites
    {
#     injection Paroi_FT_disc Constant Champ_Front_Uniforme 1 120 #
#     Pour un angle de contact de 1 radian compte dans le gaz on a 57
degres_comptes dans le gaz et 123 degres_comptes dans le liquide #
#     Pour un angle de contact de 1.5 radian compte dans le gaz on a 86
degres_comptes dans le gaz et 94 degres_comptes dans le liquide #
#     Pour un angle de contact de 2 radian compte dans le gaz on a 115 degres_comptes dans le
degres_comptes dans le liquide #
#     Pour un angle de contact de 2.5 radian compte dans le gaz on a 143 degres_comptes dans le
degres_comptes dans le liquide #
#     Pour un angle de contact de 3 radian compte dans le gaz on a 172 degres_comptes dans le
degres_comptes dans le liquide #
        injection Paroi_FT_disc Constant Champ_Front_Fonc_xyz 1 37.+sqrt(((x-0.0105)*(x-0.0105)+(z-
paroi Paroi_FT_disc Constant Champ_Front_Fonc_xyz 1 37.+sqrt(((x-0.0105)*(x-0.0105)+(z-0.
        ouverte Paroi_FT_disc Constant Champ_Front_Fonc_xyz 1 37.+sqrt(((x-0.0105)*(x-0.0105)+(z-0.
    }
}
postraitements {
    Definition_champs {
        hauteur1 Reduction_0D {
            methode moyenne_ponderee
            source Transformation {
                methode formule
                expression 1 exp(-(x*x+z*z)*1000)*(1-indicatrice_interf_natif_dom_pb1)
                source refChamp { Pb_champ pb1 indicatrice_interf }
            }
        }
    }
}

```

```

hauteur2 Reduction_0D {
    methode moyenne_ponderee
    source Transformation {
        methode formule
        expression 1 exp(-(x*x+z*z)*10000)*(1-indicatrice_interf_natif_dom_pb1)
        source refChamp { Pb_champ pb1 indicatrice_interf }
    }
}
hauteur3 Reduction_0D {
    methode moyenne_ponderee
    source Transformation {
        methode formule
        expression 1 exp(-(x*x+z*z)*100000)*(1-indicatrice_interf_natif_dom_pb1)
        source refChamp { Pb_champ pb1 indicatrice_interf }
    }
}
Sondes {
    hauteur1 hauteur1 periode 0.02 points 1 0. 0.1 0.
    hauteur2 hauteur2 periode 0.02 points 1 0. 0.1 0.
    hauteur3 hauteur3 periode 0.02 points 1 0. 0.1 0.
}
champs dt_post 1e3
{
    indicatrice_interf elem
}
liste_postraitements {
    postraitement_ft_lata post1 {
        dt_post 0.01
        nom_fichier lata/post
        format binaire
    champs elements { indicatrice_interf }
    champs faces { vitesse }
        interfaces interf { champs sommets { courbure } }
    }
}
sauvegarde binaire Oscillation_bulle3.rep
}
Solve pb1
Fin

```

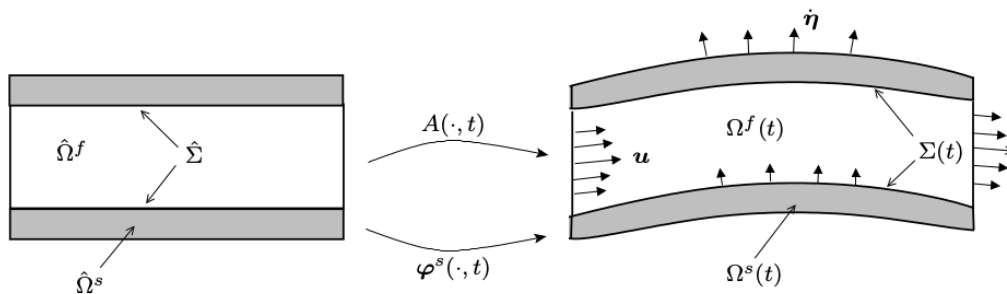
VIII. Fluid-structure interactions with ALE

To determine the flow of a fluid, it is necessary to describe the kinematics of all its material particles throughout time. To do so, one can adopt either an Euler description of motion, in which a fluid particle is identified by its initial position, or a Lagrange description of motion, in which a fluid particle is identified by its instantaneous position. Both descriptions are totally equivalent, leading to different forms of the Navier-Stokes equations that can be discretized on a stationary mesh grid (Euler) or a mesh grid that follows the motion of the fluid particles (Lagrange). In both cases, the mesh nodes do not account for the motion of the boundaries, which makes the numerical simulations of the related Navier-Stokes equations delicate. To overcome this problem, several approaches, such as the immersed boundary methods, or the Arbitrary Lagrangian-Eulerian (ALE) method have been developed.

Here, we rely on the ALE method. In the ALE approach, the fluid flow is computed in a domain that is deformed in order to follow the movement of the fluid-solid interface. It provides a hybrid description not associated with the fluid particles and the laboratory coordinates. We associate the description with a moving imaginary mesh that follows the fluid domain. The motion of the ALE computational mesh is independent of the material motion, the approach treats the mesh as a frame that moves with an arbitrary velocity. In the Eulerian approach, this velocity is zero, whereas it is equal to the velocity of the fluid particles in the Lagrangian approach. But in the ALE method, this velocity is equal to neither zero nor the velocity of the fluid particles; it varies smoothly and arbitrarily between both of them. This method is a Lagrangian description in zones and directions near a solid interface and Eulerian elsewhere.

In that part, three cases used ALE method are detailed:

- Single-phase flow around a vibrating cylindrical tube
- Hydrodynamic interaction of two cylinders subjected to small oscillations
- Vibrations of a cylinder in a square tube bundle immersed in a viscous fluid (DIVA experiments)



extract from Donea J., Huerta A., Ponthot J. Ph. and Rodriguez-Ferran A., Encyclopedia of Computational Mechanic, American Cancer Society, Arbitrary Lagrangian-Eulerian Methods, 2004

VIII.1

Single-phase flow around a vibrating cylindrical tube

1.1 Purpose

A 2D fluid annulus region, confined between an inner wall moving with an harmonic motion and an outer wall fixed, has been numerically simulated.

This validation test case has been created to compare TrioCFD ALE results with the analytical solution of such a problem [1].

We investigate the force exerted by the fluid on the cylindrical tube subjected to a transverse excitation. We will seek, in particular, on the characteristics of the fluid force, represented by the added mass and damping coefficients.

A detailed analysis of the present test case is presented in [2].

Validation made by : M. A. Puscas and D. Panunzio.

Report generated 12/01/2021.

1.2 Problem Description

The domain used for the numerical simulations is the one in Figure 1.

Geometry

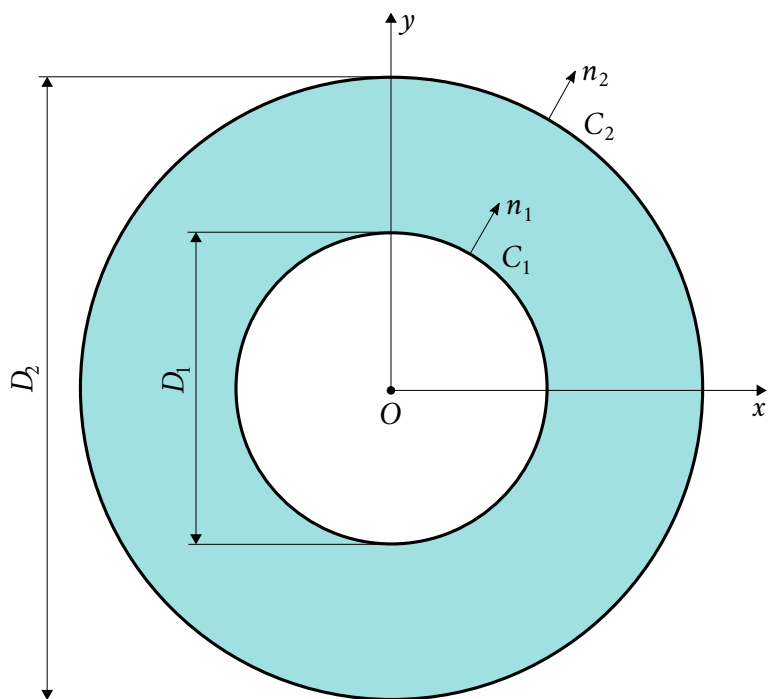


Figure VIII.1.1: The domain

Initial Conditions and Boundary Conditions

The inner moves with an harmonic motion: $\mathbf{u} = U * \sin(\omega * t) \mathbf{e}_x$, where U : amplitude of displacement and ω : angular frequency of displacement.

The outer cylinder fixed.

Initially, the fluid is at rest.

Fluid Properties

The tube bundle is immersed in a Newtonian and homogeneous fluid, with mass density ρ (1000 Kg/m^3) and kinematic viscosity ν ($1.007 * 10^{-6} \text{ m}^2/\text{s}$). The fluid flow generated by the oscillation of the central cylinder is assumed as incompressible and two-dimensional.

1.3 Case Setup

In this section is reported the mesh used during the simulations.

Numerical simulations have been carried out on a set of adaptive meshes. Two local sizes have been defined: a smaller one at the inner wall (min_size) and a larger one at the outer wall (max_size). By this way, a refined mesh is used in the regions with large gradient fields whereas a loose mesh is used in the areas with low gradient fields. The main properties are summarized in the table below.

Grid

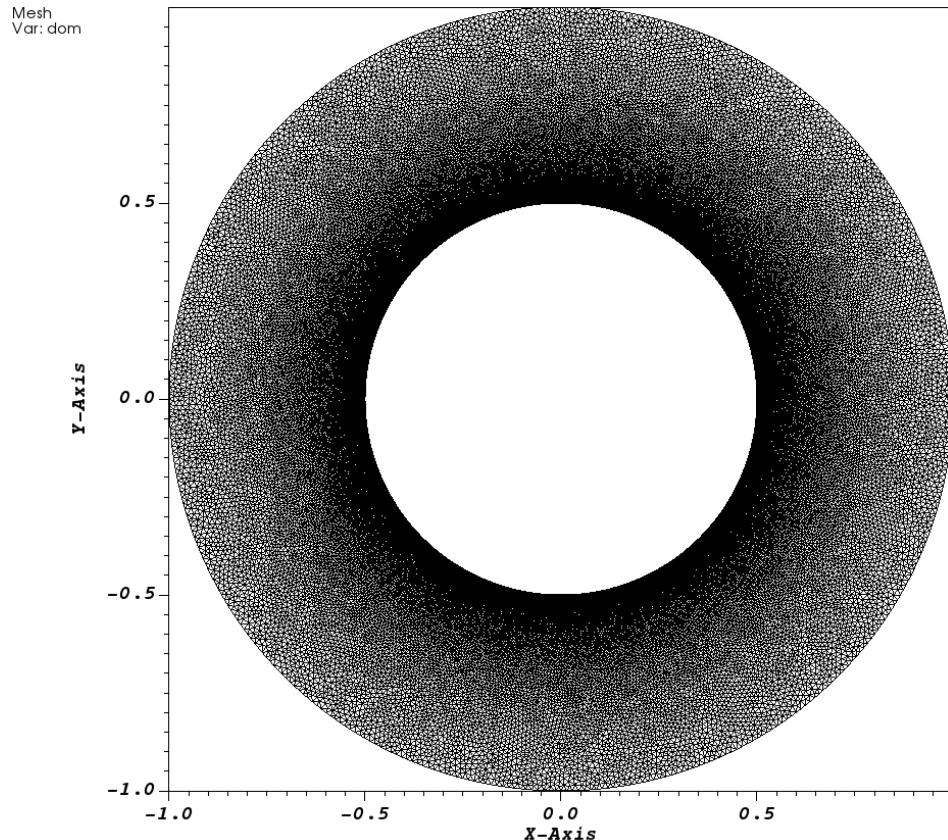


Figure VIII.1.2: Mesh

	Nb_elements	Nb_processors	max_size	min_size
Mesh	110466	4	0.015	0.003

Table VIII.1.1: Meshes properties

Model Options

The fluid problem with moving boundaries is handled by the Arbitrary Lagrangian-Eulerian (ALE) method. In the ALE approach, the fluid flow is computed in a domain that is deformed in order to follow the movement of the fluid-solid interface. It provides a hybrid description not associated with the fluid particles and the laboratory coordinates. We associate the description with a moving imaginary mesh that follows the fluid domain.

1.4 Results

Validation Specific Informations

- Version TRUST :
- Problem: Pb_hydraulique_ALE
- Dimension: 2D
- Domain: Domaine_ALE
- Pressure solver: Solver_moving_mesh_ALE PETSC Cholesky
- Discretization: VEFPre1B
- Time scheme: Scheme_euler_implicit with solver implicite_ALE GMRES
- Medium: Fluide_Incompressible
- Hydraulic problem: Navier_Stokes_standard_ALE
- Convection scheme: ALE muscl
- Location: ALE/share/Validation/Rapports_automatiques/TwoCylindersALE
- Generated Test cases :
 - ./TwoCylinders.data : /*jdd en annexe*/
- Performance Chart :

	host	system	Total CPU Time	CPU time/step	number of cell
./TwoCylinders	is241762.intra.cea.fr	Linux	24618.4	4.58583	110466

Table VIII.1.2: Performance Chart

Plot Data

In this section the analytical solution [1] for the force per unit length exerted by the fluid over the inner cylinder and the added coefficients are compared with the TrioCFD results.

According to Chen et al. [1], the analytical solution of the fluid force per unit length acting on the inner cylinder is:

$$\mathbf{F} = \rho\pi \left(\frac{D_1}{2}\right)^2 u D_1 \omega^2 \left[m_{self} \sin(\omega t) - c_{self} \cos(\omega t) \right] \mathbf{e}_x \quad (1.1)$$

where $\rho = 1 \text{ kg/m}^3$, $D_1 = 1 \text{ m}$ (diameter of the inner cylinder), $u = 10^{-2}$ (dimensionless displacement respect to D_1), $\omega = 0.06327 \text{ rad/s}$ (angular frequency of motion) and m_{self} and c_{self} the added mass and damping coefficients, respectively.

The analytical solution (Chen et al. [1]) is here depicted and compared with the numerical one, obtained by the sum of the pressure and viscous force acting on the inner cylinder along x. Simulations have been performed for $t = [0, 5T]$ where $T = 2\pi/\omega$.

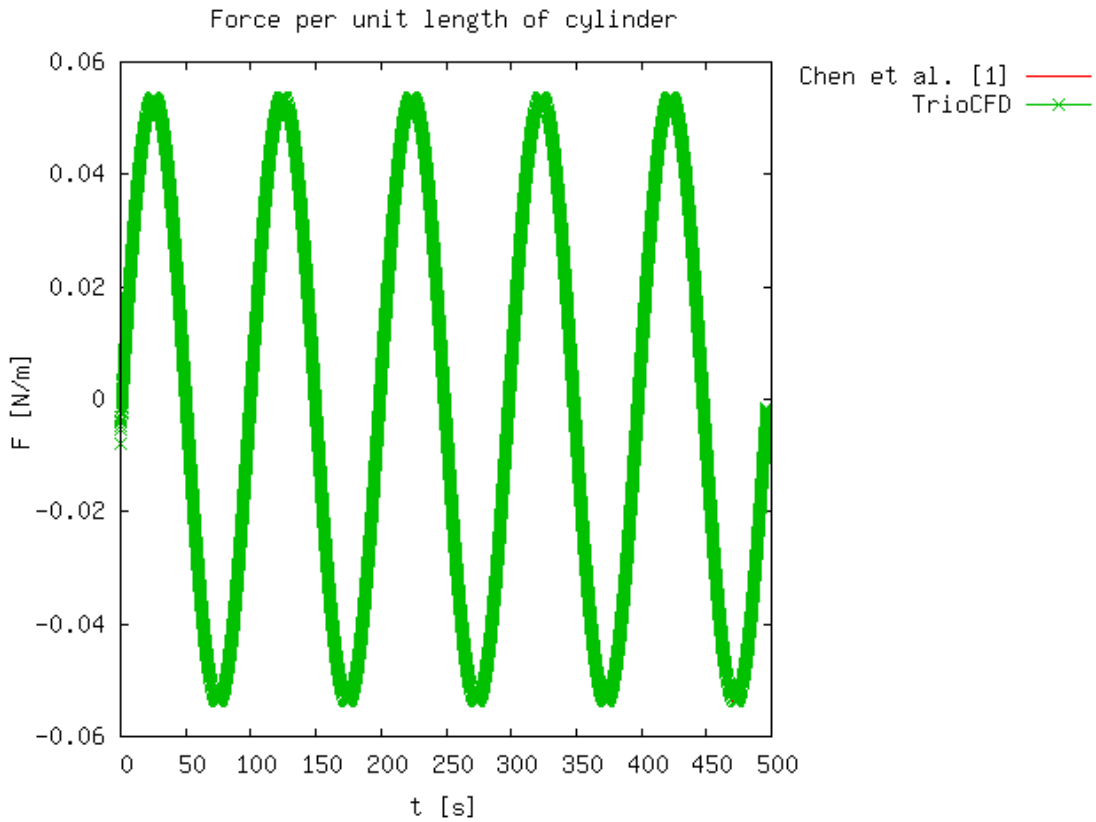


Figure VIII.1.3: Force per unit length of cylinder

For the analytical calculation of the added coefficients, the reader is referred to [1]. Numerically, the added coefficients are computed with a Fourier product as:

$$\begin{aligned} m_{self} &= \frac{\langle \sin(\omega t), F(t) \rangle}{\rho\pi(D_1/2)^2uD_1\omega^2} \quad \text{with} \quad \langle \sin(\omega t), F(t) \rangle = \frac{2}{5T} \int_0^{5T} \sin(\omega t)F(t)dt \\ c_{self} &= \frac{\langle \cos(\omega t), F(t) \rangle}{\rho\pi(D_1/2)^2uD_1\omega^2} \quad \text{with} \quad \langle \cos(\omega t), F(t) \rangle = \frac{2}{5T} \int_0^{5T} \cos(\omega t)F(t)dt \end{aligned} \quad (1.2)$$

and are reported in the following table:

	m_{self}	c_{self}
Chen et al. [1]	1.7118	0.046036
TrioCFD	1.7083341959859382	0.0515471257011517

Table VIII.1.3: Added mass and damping coefficients

Pressure and velocity fields are reported at final time in order to investigate such distributions. The mesh

velocity and the total displacement of the mesh are also plotted.

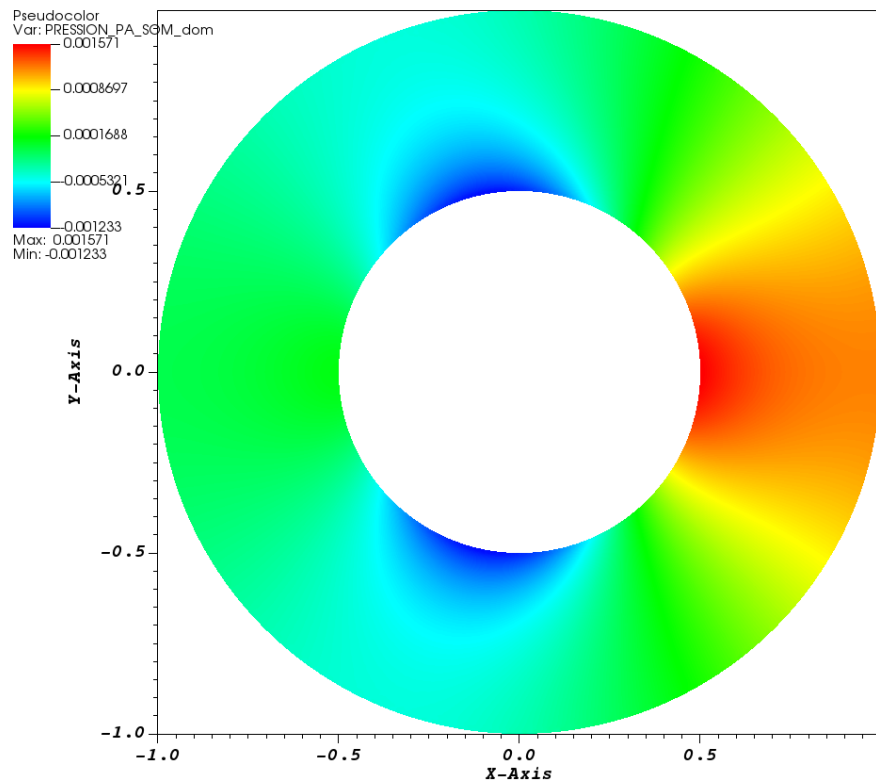


Figure VIII.1.4: TrioCFD PRESSION SOM

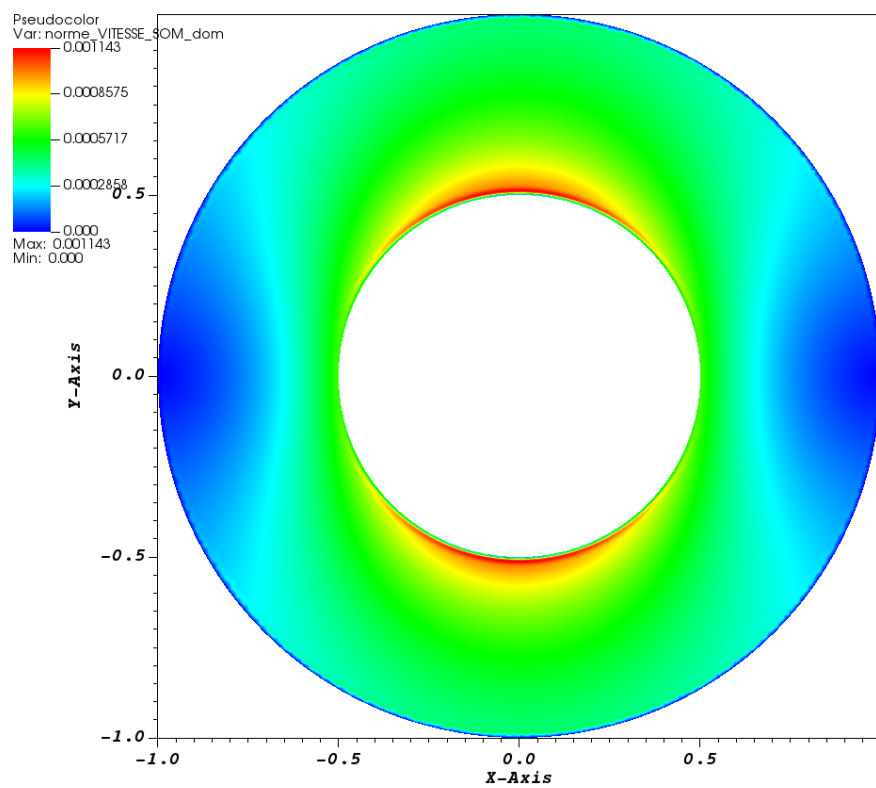


Figure VIII.1.5: TrioCFD VITESSE_magnitude SOM

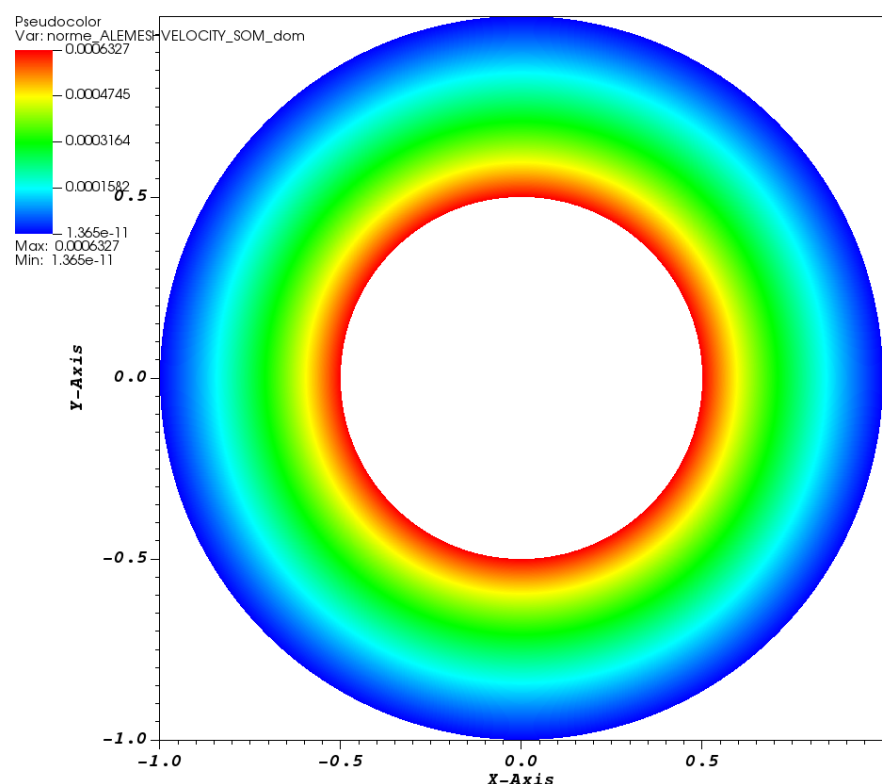


Figure VIII.1.6: TrioCFD Mesh velocity SOM

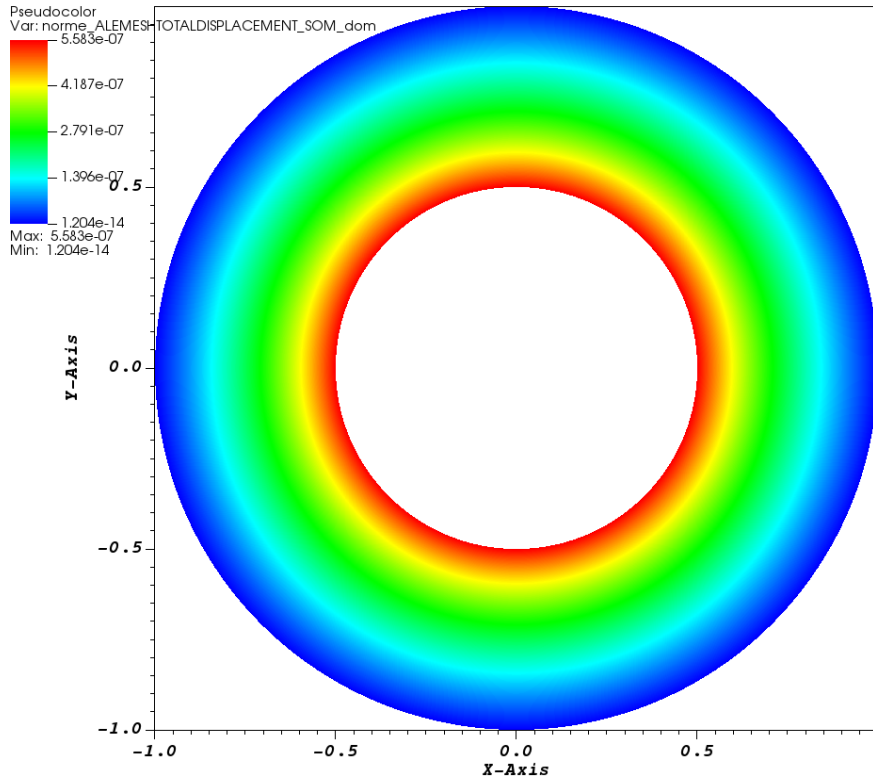


Figure VIII.1.7: TrioCFD Total displacement of the mesh SOM

1.5 Conclusion

The harmonic motion of a circular wall in a quiescent viscous fluid, enclosed by a concentric fixed wall, has been numerically simulated. A FEV method is applied to solve such a problem in conjunction with the ALE approach. The numerical results for the fluid force and the added coefficients successfully confirmed the analytical solution [1]. Remark: in order to reduce the numerical error a much more refined mesh must be used!

1.6 References

- 1. S. S. Chen, M. W. Wambsganss, and J. A. Jendrzejczyk. Added Mass and Damping of a Vibrating Rod in Confined Viscous Fluids, 1976.
- 2. CFD numerical simulation of a single-phase flow around a vibrating cylindrical tube, D. Panunzio, DES/ISAS/DM2S/SEMT/DYN/RS/2020-67015/A

1.7 Data Files

TwoCylinders

```
# Fluid annulus region confined between an inner wall moving with an harmonic motion and an outer
# Hydraulique 2D laminar with ALE #
# PARALLEL ONLY 4 #
dimension 2
Pb_hydraulique_ALE pb
Domaine_ALE dom
# BEGIN MESH #
```

```

# Read_med family_names_from_group_names dom MeshWithTwoCylinders MeshWithTwoCylinders.med #
# END MESH #
# BEGIN PARTITION
Partition dom
{
    Partition_tool metis { Nb_parts 2 }
    Larg_joint 2
    zones_name DOM
}
End
END PARTITION #
# BEGIN SCATTER #
Scatter DOM.Zones dom
# END SCATTER #
# For the Arbitrary Lagrangian-Eulerian framework: block to indicate the number of mobile
boundaries of the domain and specify the speed that must be imposed on them #
Imposer_vit_bords_ALE dom
{
    1 # number of mobile boundaries #
    CircleA Champ_front_ALE 2 0.01*0.06327167604329844*cos(0.06327167604329844*t) 0.0 # name and
}
# Solver used to solve the system giving the moving mesh velocity #
Solver_moving_mesh_ALE dom { Petsc Cholesky { } }
# I select a discretization #
VEFPreP1B ma_discretisation
# Time scheme, choice between: explicit or implicit #
Scheme_euler_implicit mon_schema
Read mon_schema
{
    # Time step #
    # Initial time [s] #
    tinit 0.
    # Min time step #
    dt_min 1.e-15
    # Output criteria #
    # .out files printing period #
    dt_impr 5.e-8
    # .sauv files printing period #
    dt_sauv 100.
    # facsec such as dt = facsec * min(dt(CFL),dt_max) ; for explicit scheme facsec <= 1. By defa
    facsec 1
    facsec_max 1
    solveur implicite_ALE
    {
        solveur gmres { diag seuil 1.e-12 nb_it_max 3 }
    }
    # Stop if one of the following criteria is checked: #
    # End time [s] #
    tmax 496.5
    # Max number of time steps #
    # nb_pas_dt_max 2 #
    # Convergence threshold (see .dt_ev file) #
    seuil_statio 1.e-15
}
# I define a medium #
Fluide_Incompressible milieu
Read milieu
{
    mu Champ_Uniforme 1 1.007e-3
    rho Champ_Uniforme 1 1000
}

```

```

# Gravity vector definition
Uniform_field my_gravity
Read my_gravity 2 0.0 0.0 #
# Association between the different objects #
Associate pb dom
Associate pb mon_schema
Associate pb milieu
Discretize pb ma_discretisation
Read pb
{
  Navier_Stokes_standard_ALE
  {
    # Pressure matrix solved with #
    solveur_pression petsc cholesky { }
    # Two operators are defined #
    convection { ALE { muscl } } # A convective scheme for ALE framework. Choice between: amo
    diffusion { }
    # Uniform initial condition for velocity #
    initial_conditions {
      vitesse Champ_Uniforme 2 0. 0.
    }
    # Boundary conditions #
    boundary_conditions {
      CircleA frontiere_ouverte_vitesse_imposee Champ_front_ALE 2 0.01*0.06327167604329844*cos
      CircleB paroi_fixe
    }
  }
  Post_processing
  {
    # Fields #
    format lata
    fields dt_post 100
    {
      pression_pa som
      vitesse som
      ALEMeshVelocity som
      ALEMeshTotalDisplacement som
    }
  }
}
# The problem is solved with #
Solve pb
# Not necessary keyword to finish #
End

```

Hydrodynamic interaction of two cylinders subjected to small oscillations

2.1 Purpose

The domain used for the numerical simulations is the one in Figure 1. As we can see from Figure 1., we have a 2-dimensional domain \mathcal{D} , with arbitrarily large length and width. In this domain, we have a homogeneous Newtonian incompressible fluid at rest, characterized by its volume mass density ρ and its kinematic viscosity ν . In fact, we have two cylinders, with radius R_j and center O_j , oscillating at an Ω angular frequency.

This validation test case has been created to compare TrioCFD ALE results with the theoretical solution of such a problem [1].

We investigate the force exerted by the fluid on the cylindrical tube subjected to a transverse excitation. We will seek, in particular, on the characteristics of the fluid force, represented by the added mass and damping coefficients.

A detailed analysis of the present test case is presented in [1].

Validation made by : M. A. Puscas.

Report generated 12/01/2021.

2.2 Problem Description

The domain used for the numerical simulations is the one in Figure 1.

Geometry

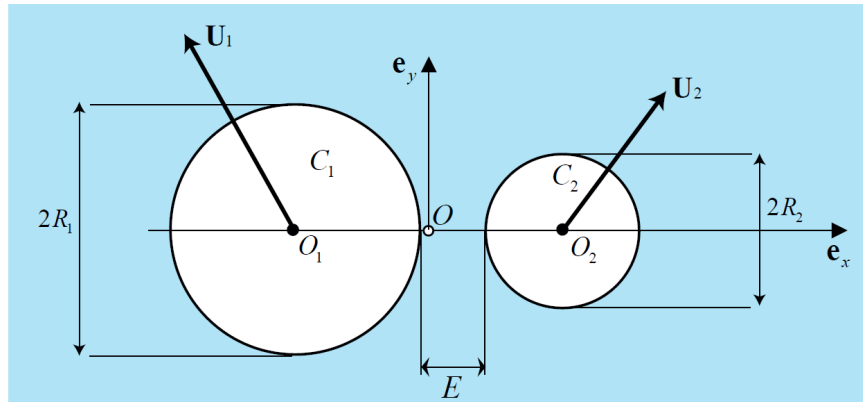


Figure 1. Schematic diagram of the system: two oscillating cylinders C_j with radii R_j , centers O_j , displacement vectors $\mathbf{U}_j(T)$, are immersed in a fluid of kinematic viscosity ν . The small oscillations of C_j generate an incompressible fluid flow. The midpoint of O_1 and O_2 is O and the separation distance is E .

Figure VIII.2.1: The domain

Initial Conditions and Boundary Conditions

The left cylinder (C_1) is fixed and the right one (C_2) moves with an harmonic motion alongside the x -axis: $\mathbf{U}_2(T) = u \sin(\omega T) \mathbf{e}_x$, where $u = 0.01$.

The left, right, upper and lower boundaries are fixed.

Initially, the fluid is at rest.

Fluid Properties

The tube bundle is immersed in a Newtonian and homogeneous fluid, with mass density ρ (1000 Kg/m^3) and kinematic viscosity ν ($1.007 * 10^{-6} \text{ m}^2/\text{s}$). The fluid flow generated by the oscillation of the right cylinder is assumed as incompressible and two-dimensional.

2.3 Case Setup

Grid

A refined mesh is used in the regions with large gradient fields whereas a loose mesh is used in the areas with low gradient fields.

Calculation has been partitioned on 10 processors, such that each processor worked with 20000-30000 elements.

Model Options

The fluid problem with moving boundaries is handled by the Arbitrary Lagrangian-Eulerian (ALE) method. In the ALE approach, the fluid flow is computed in a domain that is deformed in order to follow the movement of the fluid-solid interface. It provides a hybrid description not associated with the fluid particles and the laboratory coordinates. We associate the description with a moving imaginary mesh that follows the fluid domain.

2.4 Results

Validation Specific Informations

- Version TRUST : 1.8.2
- Problem: Pb_hydraulique_ALE
- Dimension: 2D
- Domain: Domaine_ALE
- Pressure solver: Solver_moving_mesh_ALE PETSC Cholesky
- Discretization: VEFPre1B
- Time scheme: Scheme_euler_implicit with solver implicite_ALE GMRES
- Medium: Fluide_Incompressible
- Hydraulic problem: Navier_Stokes_standard_ALE
- Convection scheme: ALE muscl
- Generated Test cases :
 - ./TwoOscillatingCylinders.data : /*jdd en annexe*/
- Performance Chart :

	host	system	Total CPU Time	CPU time/step	number of cell
./TwoOscillatingCylinders	is241762.intra.cea.fr	Linux	36266.2	8.15926	241618

Table VIII.2.1: Performance Chart

Plot Data

In this section the Least Squares (LS) and Collocation (COL) methods (theoretical approximation solutions) presented in [1] for the force per unit length exerted by the fluid over the cylinders and the added coefficients are compared with the TrioCFD results.

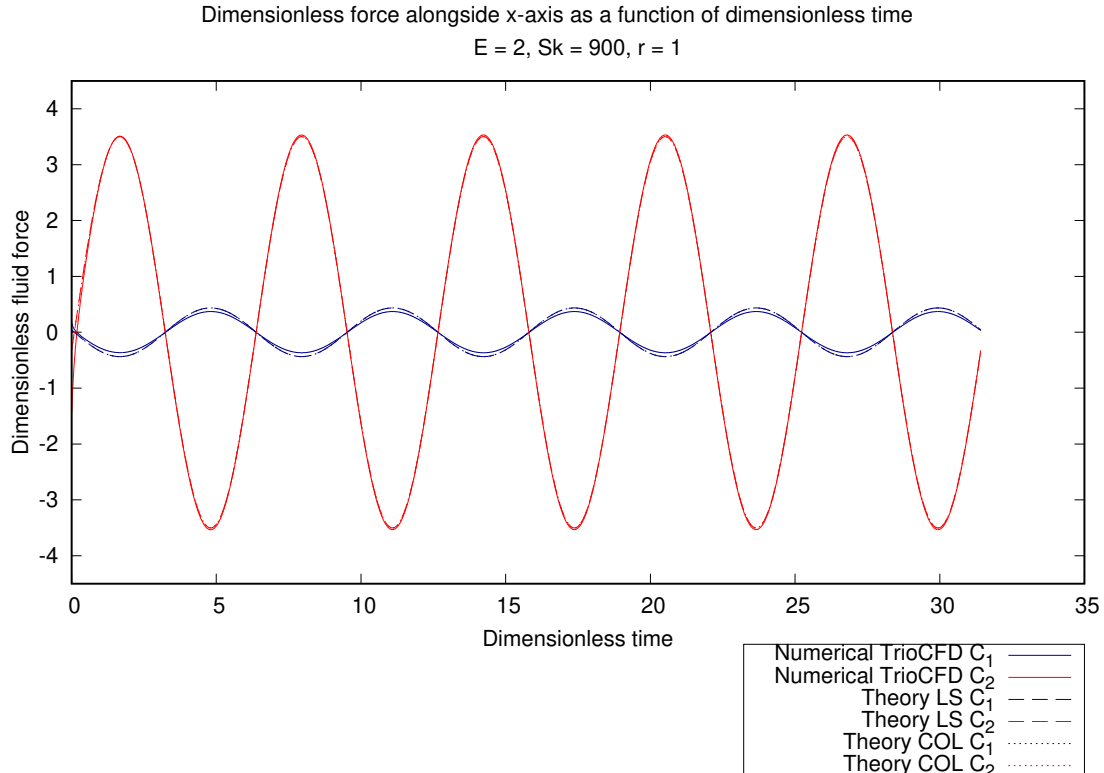


Figure VIII.2.2: Force per unit length of cylinder

For the theoretical calculation of the added coefficients, the reader is referred to [1]. Numerically, the added coefficients are computed with a Fourier product as:

$$\begin{aligned}
 m_{self} &= \frac{\langle \sin(\omega t), F_{C_2}(t) \rangle}{\rho u(R_2)^2 \omega^2} \quad \text{with} \quad \langle \sin(\omega t), F_{C_2}(t) \rangle = \frac{2}{5T} \int_0^{5T} \sin(\omega t) F_{C_2}(t) dt \\
 c_{self} &= \frac{\langle \cos(\omega t), F_{C_2}(t) \rangle}{\rho u(R_2)^2 \omega^2} \quad \text{with} \quad \langle \cos(\omega t), F_{C_2}(t) \rangle = \frac{2}{5T} \int_0^{5T} \cos(\omega t) F_{C_2}(t) dt \\
 m_{cross} &= \frac{\langle \sin(\omega t), F_{C_1}(t) \rangle}{\rho u(R_2)^2 \omega^2} \quad \text{with} \quad \langle \sin(\omega t), F_{C_1}(t) \rangle = \frac{2}{5T} \int_0^{5T} \sin(\omega t) F_{C_1}(t) dt \\
 c_{cross} &= \frac{\langle \cos(\omega t), F_{C_1}(t) \rangle}{\rho u(R_2)^2 \omega^2} \quad \text{with} \quad \langle \cos(\omega t), F_{C_1}(t) \rangle = \frac{2}{5T} \int_0^{5T} \cos(\omega t) F_{C_1}(t) dt
 \end{aligned} \tag{2.1}$$

, where F_{C_1} represents the fluid force acting on the left cylinder (the static one) and F_{C_2} represents the fluid force acting on the right cylinder (the moving one), and are reported in the following table:

	m_{self}	c_{self}	m_{cross}	c_{cross}
COL theory[1]	1.11	0.106	-0.138	-0.0136
LS theory[1]	1.11	0.105	-0.138	-0.0132
TrioCFD	1.117774855876004	0.10809948732840657	-0.11672369230757429	-0.011730376281497742

Table VIII.2.2: Added mass and damping coefficients

Pressure and velocity fields are reported at final time in order to investigate such distributions. The mesh velocity are also plotted.

DB: TwoOscillatingCylinders.lata
Time:34664.7

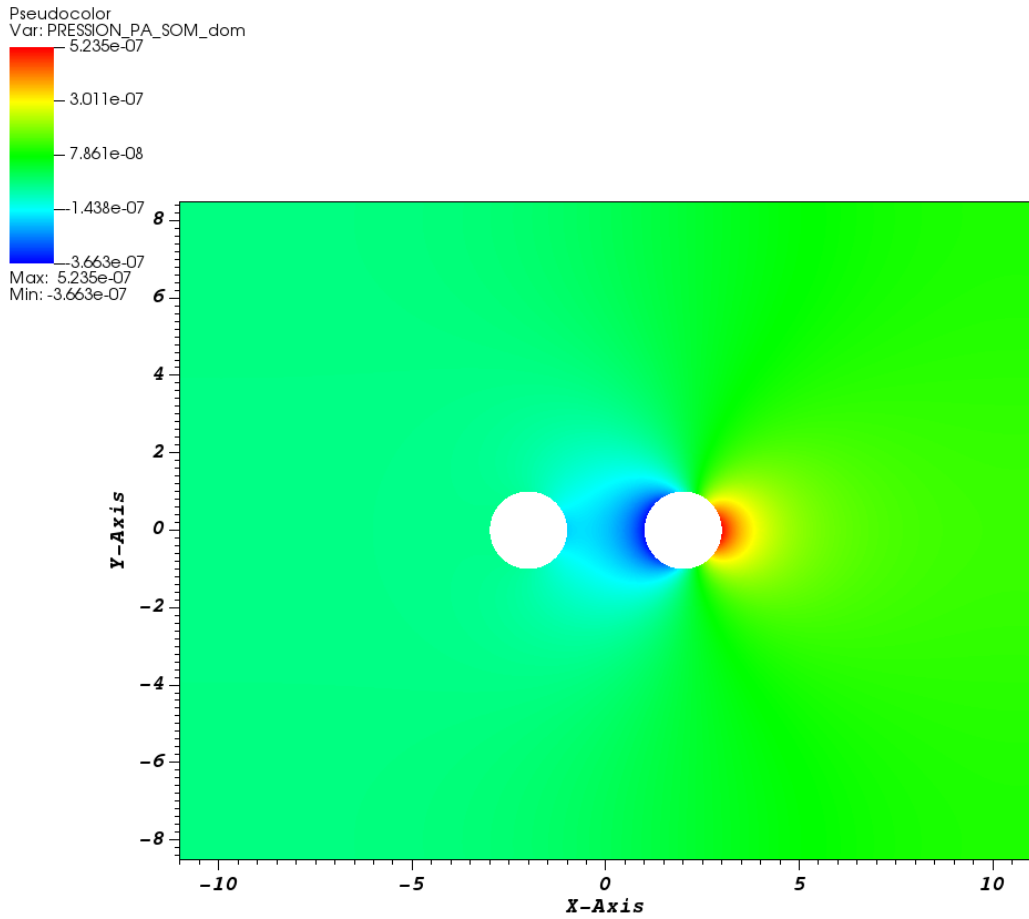


Figure VIII.2.3: TrioCFD PRESSION SOM

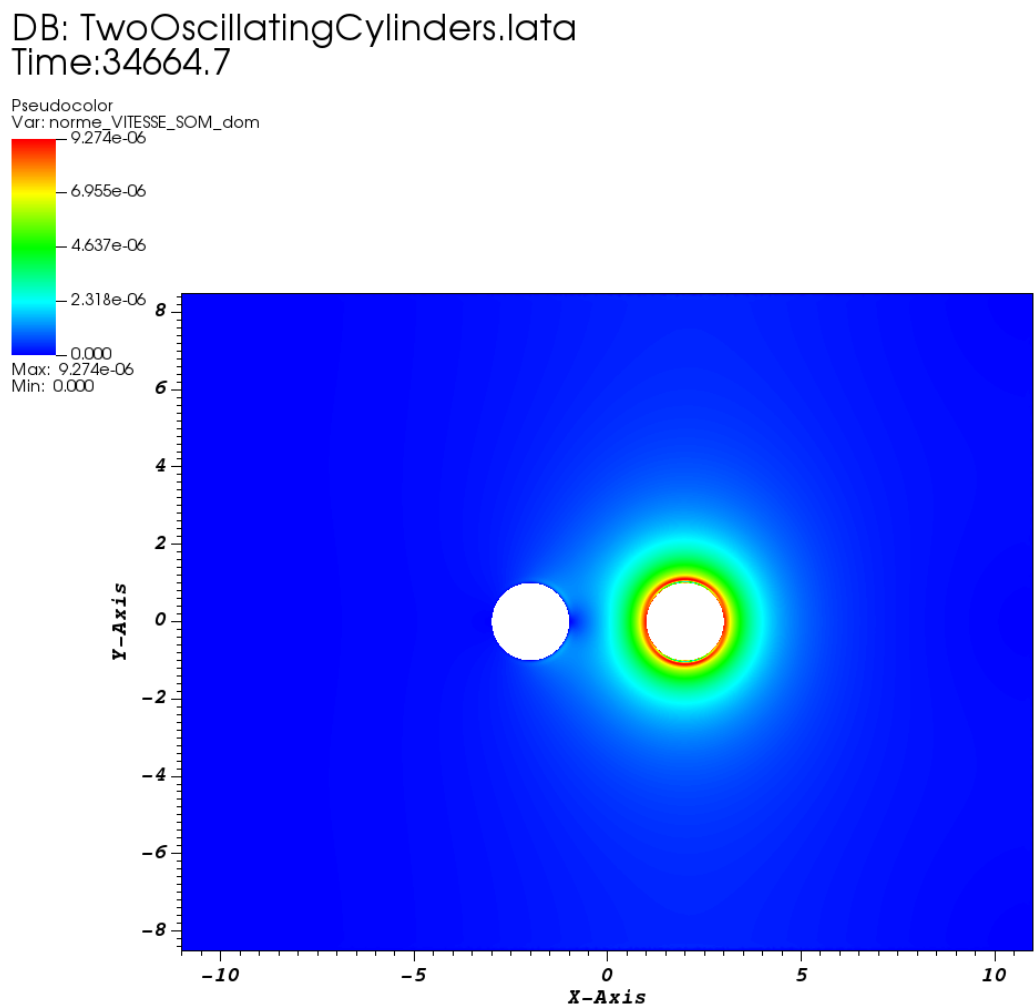


Figure VIII.2.4: TrioCFD VITESSE_magnitude SOM

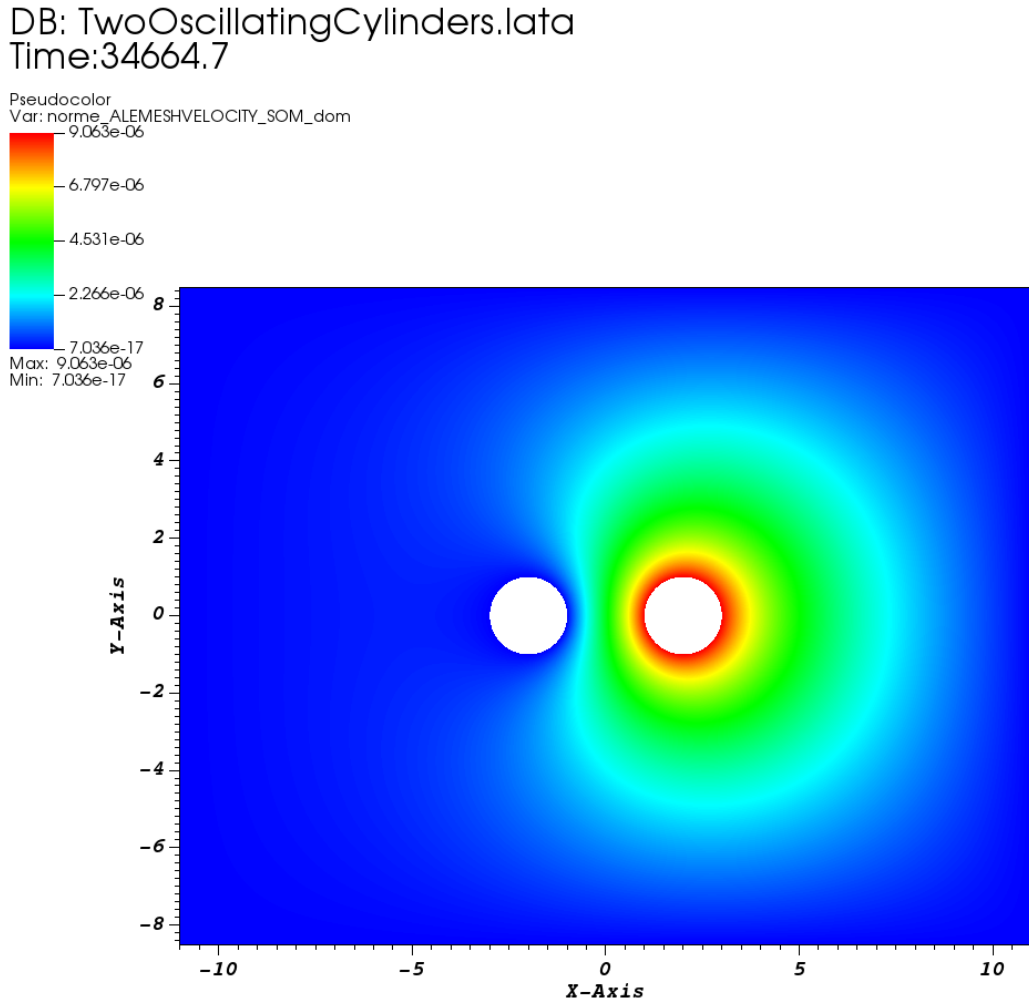


Figure VIII.2.5: TrioCFD Mesh velocity SOM

2.5 Conclusion

The harmonic motion of a circular wall in a quiescent viscous fluid, has been numerically simulated. A FEV method is applied to solve such a problem in conjunction with the ALE approach. The numerical results for the fluid force and the added coefficients are in good agreement with the theoretical COL and LS approximation solution [1].

Remark: in order to reduce the numerical error a much more refined mesh must be used!!!

2.6 References

- 1. New estimations of the added mass and damping of two cylinders vibrating in a viscous fluid, from theoretical and numerical approaches. R. Lagrange and Y. Fraigneau, Journal of Fluids and Structures, 2020.
- 2. CFD numerical simulation of a single-phase flow around a vibrating cylindrical tube, D. Panunzio, DES/ISAS/DM2S/SEMT/DYN/RS/2020-67015/A

2.7 Data Files

TwoOscillatingCylinders

```

# Hydrodynamic interaction of two cylinders subjected to small oscillations
# PARALLEL ONLY 10 #
dimension 2
Pb_hydraulique_ALE pb
Domaine_ALE dom
# BEGIN MESH #
# Read_med family_names_from_group_names dom TwoOscillatingCylinders TwoOscillatingCylinders.med
# END MESH #
# BEGIN PARTITION
Partition dom
{
    Partition_tool metis { Nb_parts 2 }
    Larg_joint 2
    zones_name DOM
}
End
END PARTITION #
# BEGIN SCATTER #
Scatter DOM.Zones dom
# END SCATTER #
imposer_vit_bords_ale dom
{
    1 # number of mobile boundaries #
    CylinderRight Champ_front_ALE 2 0.01*(9.063e-4)*cos((9.063e-4)*t) 0.0 # name and speed of the
    We have an oscillation position :  $g(t) = u \sin(\Omega t)$  —> derivative for velocity
#
}
# Solver used in order to solve the system giving the moving mesh velocity #
Solver_moving_mesh_ALE dom { Petsc Cholesky { } }
# I select a discretization #
VEFPreP1B ma_discretisation
# Time scheme, choice between: explicit or implicit #
Scheme_euler_implicit mon_schema
Read mon_schema
{
    # Time step #
        # Initial time [s] #
        tinit 0.
    # Min time step #
        dt_min 1.e-15
    # Output criteria #
        # .out files printing period #
        dt_impr 5.e-6
    # .sauv files printing period #
    # tcpumax 47.5 #
    # .sauv files printing period #
        periode_sauvegarde_securite_en_heures 23
    # facsec such as  $dt = facsec * \min(dt(CFL), dt_{max})$  ; for explicit scheme  $facsec \leq 1$ . By default
    facsec 1.
        facsec_max 1.
    solveur implicite_ALE
    {
        solveur gmres { diag seuil 1.e-12 nb_it_max 3 }
    }
    # Stop if one of the following criteria is checked: #
        # End time [s] ;  $T = 2\pi/R^2 \cdot \Omega = 6933$  (period in s) ; 5 periods #

```

```

tmax 34664
# Max number of time steps #
# nb_pas_dt_max 2 #
# Convergence threshold (see .dt_ev file) #
seuil_statio 1.e-15
}
# I define a medium #
Fluide_Incompressible milieu
Read milieu
{
  mu Champ_Uniforme 1 1.007e-3
  rho Champ_Uniforme 1 1000
}
# Gravity vector definition
Uniform_field my_gravity
Read my_gravity 2 0.0 0.0 #
# Association between the different objects #
Associate pb dom
Associate pb mon_schema
Associate pb milieu
Discretize pb ma_discretisation
Read pb
{
  Navier_Stokes_standard_ALE
  {
    # Pressure matrix solved with #
    solveur_pression petsc cholesky { }
    # Two operators are defined #
    convection { ALE { muscl } } # A convective scheme for ALE framework. Choice between: among
    diffusion { }
    # Uniform initial condition for velocity #
    initial_conditions {
      vitesse Champ_Uniforme 2 0. 0.
    }
    # Boundary conditions #
    boundary_conditions {
      CylinderRight frontiere_ouverte_vitesse_imposee Champ_front_ALE 2 0.01*(9.063e-4)*cos((9
      CylinderLeft paroi_fixe
      RectangularBox paroi_fixe
    }
  }
  Post_processing
  {
    # Fields #
    format lata
    fields dt_post 3000
    {
      pression_pa som
      vitesse som
      ALEMeshVelocity som
    }
  }
  # resume_last_time binaire TwoOscillatingCylinders_pb.sauv #
}
# The problem is solved with #
Solve pb
# Not necessary keyword to finish #
End

```

VIII.3

Vibrations of a cylinder in a square tube bundle immersed in a viscous fluid

3.1 Purpose

The importance of fluid-elastic forces in tube bundle vibrations can hardly be over-emphasized, in view of their damaging potential. In the last decades, advanced models for representing fluid-elastic coupling through added-coefficients have therefore been developed by the community of the domain.

In what follows, we aim to determine numerically the fluid added-coefficients (mass and damping), considering the case of a square tube bundle immersed in a viscous fluid at rest.

This validation test case has been created to compare TrioCFD ALE results with the experimental results obtained by the CEA/DYN laboratory for such a problem.

A mesh sensitivity analysis has been carried out, and it is here reported, to detect the best results from both a physical and numerical point of view.

Validation made by : M. A. Puscas and D. Panunzio.
Report generated 12/01/2021.

3.2 Problem Description

A 2D fluid in a set of circular cylinders, arranged in a square configuration (DIVA configuration), has been numerically simulated. Such a pattern is made up of three rows of three cylinders and a set of half cylinders for each square-side. The pitch between the cylinders is $P = 1.5D$, for both directions, where D is the diameter.

Geometry

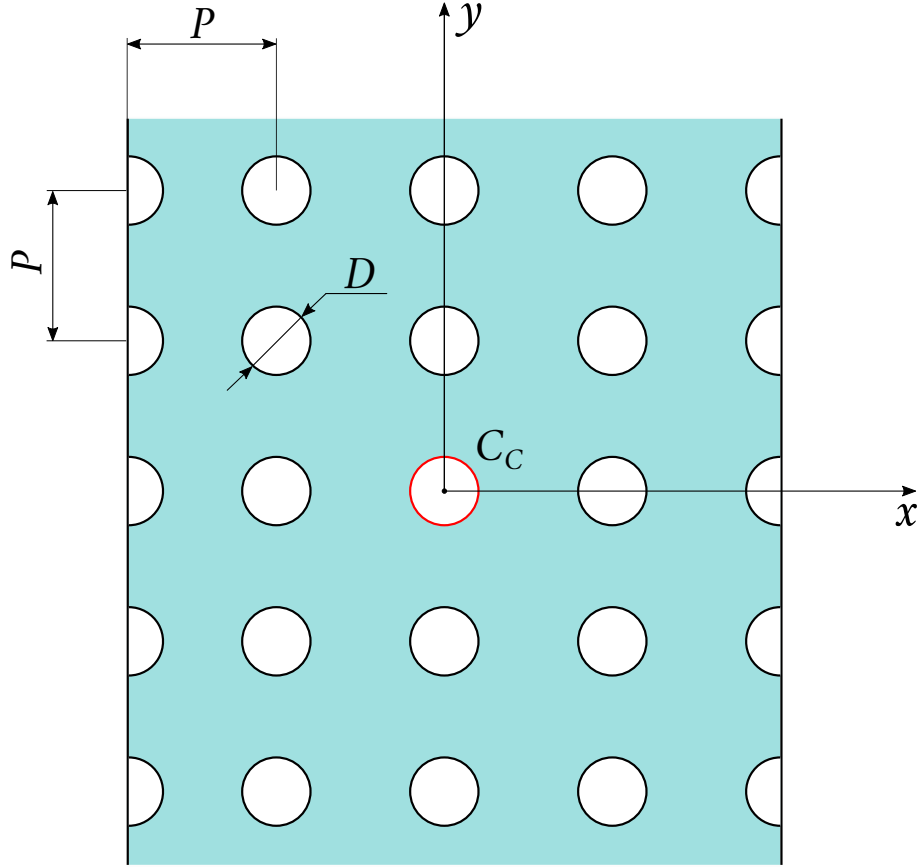


Figure VIII.3.1: DIVA geometry

Initial Conditions and Boundary Conditions

The central cylinder moves with an harmonic motion: $\mathbf{u} = U * \sin(\omega * t)\mathbf{e}_x$, where U : amplitude of displacement and ω : angular frequency of displacement.

The others cylinders (half and quarter cylinders included) are fixed. The left, right, upper and lower boundaries are fixed.

Initially, the fluid is at rest.

Fluid Properties

The tube bundle is immersed in a Newtonian and homogeneous fluid, with mass density ρ (1000 Kg/m^3) and kinematic viscosity ν ($1.007 * 10^{-6} \text{ m}^2/\text{s}$). The fluid flow generated by the oscillation of the central cylinder is assumed as incompressible and two-dimensional.

3.3 Case Setup

In this section are reported the adaptive meshes used during the simulations. Fictitious lines have been added in the design of the geometry of these meshes in order to divide the calculation domain into blocks and ensure a symmetrical discretization by the mesh module MG_CADSURF of SALOME.

Numerical simulations have been carried out on a set of adaptive meshes. The global size and two local sizes have been defined: a smaller one at the center and immediately adjacent cylinders (min_local_size) and a larger one (max_local_size) at the other boundaries (right and left walls, upper and lower borders, other cylinders).

By this way, a refined mesh is used in the regions with large gradient fields whereas a loose mesh is used in the areas with low gradient fields.

The main properties are summarized in the table below. Calculation has been partitioned on a number of processors such that each processor worked with 20000-30000 elements.

Grid

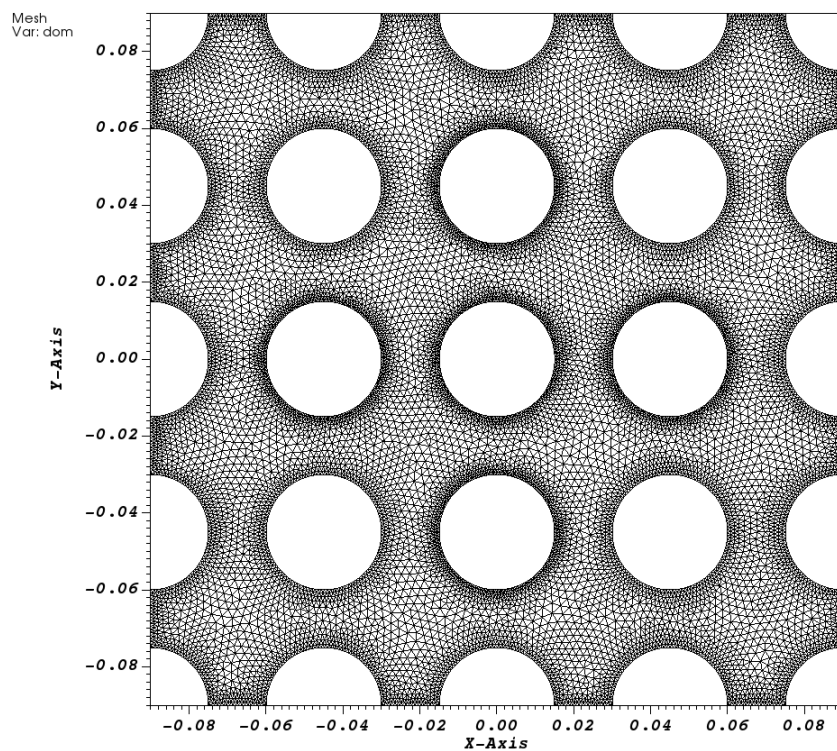


Figure VIII.3.2: Mesh_1

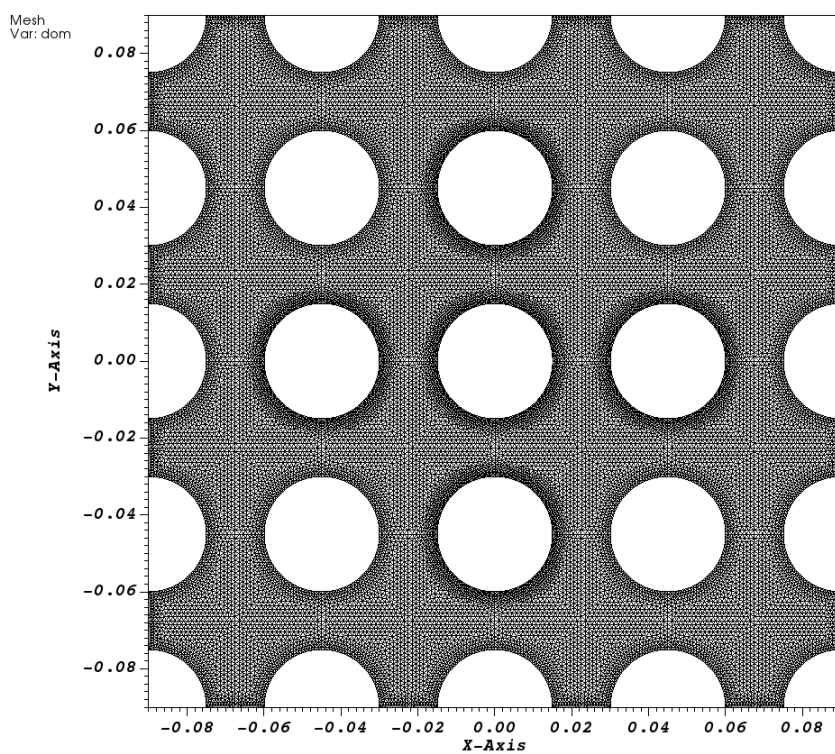


Figure VIII.3.3: Mesh_2

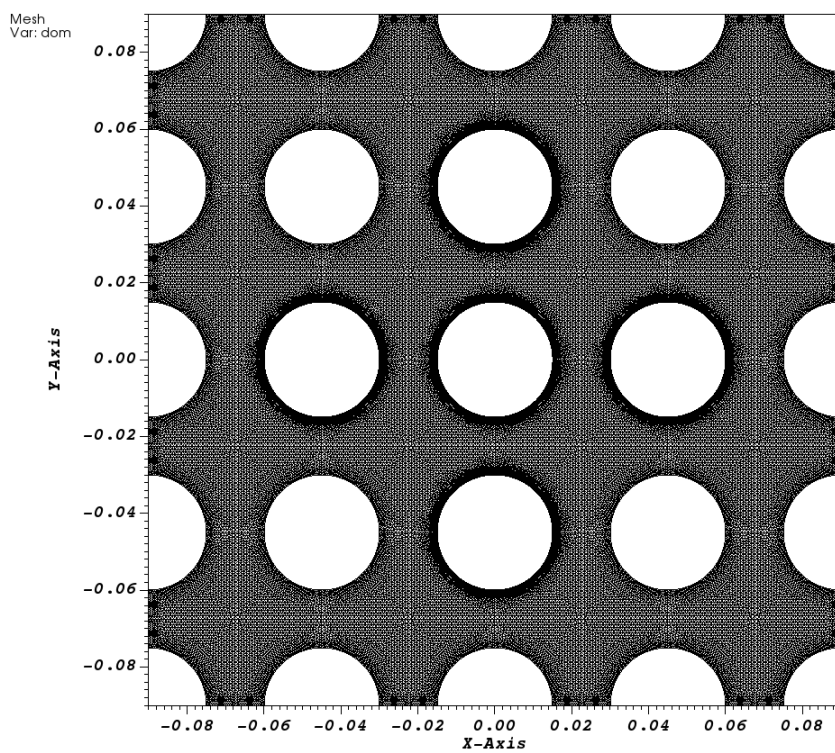


Figure VIII.3.4: Mesh_3

	Nb_elements	Nb_processors	global_size	max_local_size	min_local_size
Mesh_1	25806	1	0.0012	0.0008	0.0006
Mesh_2	51146	2	0.0011	0.0007	0.00055
Mesh_3	102080	4	0.0008	0.0005	0.0003

Table VIII.3.1: Meshes properties

Model Options

The fluid problem with moving boundaries is handled by the Arbitrary Lagrangian-Eulerian (ALE) method. In the ALE approach, the fluid flow is computed in a domain that is deformed in order to follow the movement of the fluid-solid interface. It provides a hybrid description not associated with the fluid particles and the laboratory coordinates. We associate the description with a moving imaginary mesh that follows the fluid domain.

3.4 Results

Validation Specific Informations

- Version TRUST : 1.8.2
- Problem: Pb_hydraulique_ALE
- Dimension: 2D
- Domain: Domaine_ALE
- Pressure solver: Solver_moving_mesh_ALE PETSC GCP
- Discretization: VEFPre1B
- Time scheme: Scheme_euler_implicit with solver implicite_ALE GMRES
- Medium: Fluide_Incompressible
- Hydraulic problem: Navier_Stokes_standard_ALE
- Convection scheme: ALE muscl
- Generated Test cases :
 - Mesh_1/DIVA.data : /*jdd en annexe*/
 - Mesh_2/DIVA.data :
 - Mesh_3/DIVA.data :
- Performance Chart :

	host	system	Total CPU Time	CPU time/step	number of cell
Mesh_1/DIVA	is241762.intra.cea.fr	Linux	1216.38	1.39068	25854
Mesh_2/DIVA	is241762.intra.cea.fr	Linux	2449.31	2.55786	51210
Mesh_3/DIVA	is241762.intra.cea.fr	Linux	8423.66	4.64793	102144
Total			12089.4		

Table VIII.3.2: Performance Chart

Plot Data

In this section the experimental results for the force per unit length exerted by the fluid over the center cylinder and the added coefficients are compared with the TrioCFD results. The numerical results are also given for the added coefficients for the North, South, East, West cylinders.

According to Chen [1], the analytical solution of the fluid force per unit length acting on the center cylinder is:

$$\mathbf{F}_x = \rho\pi \left(\frac{D}{2}\right)^2 U\omega^2 \left[m_{self} \sin(\omega t) - c_{self} \cos(\omega t) \right] \mathbf{e}_x \quad (3.1)$$

where $\rho = 1 \text{ kg/m}^3$, $D = 0.03 \text{ m}$, $U = 0.003 \text{ m}$ (amplitude of displacement), $\omega = 125.66 \text{ rad/s}$ (angular frequency of displacement) and m_{self} and c_{self} the added mass and damping coefficients, respectively.

The experimental solution is here depicted and compared with the numerical one, obtained by the sum of the pressure and viscous force acting on the center cylinder along x, for the following cases: TrioCFD with Mesh_1 (TrioCFD Mesh_1), TrioCFD with Mesh_2 (TrioCFD Mesh_2) and TrioCFD with Mesh_3 (TrioCFD Mesh_3). Simulations have been performed for $t = [0, 5T]$ where $T = 2\pi/\omega$.

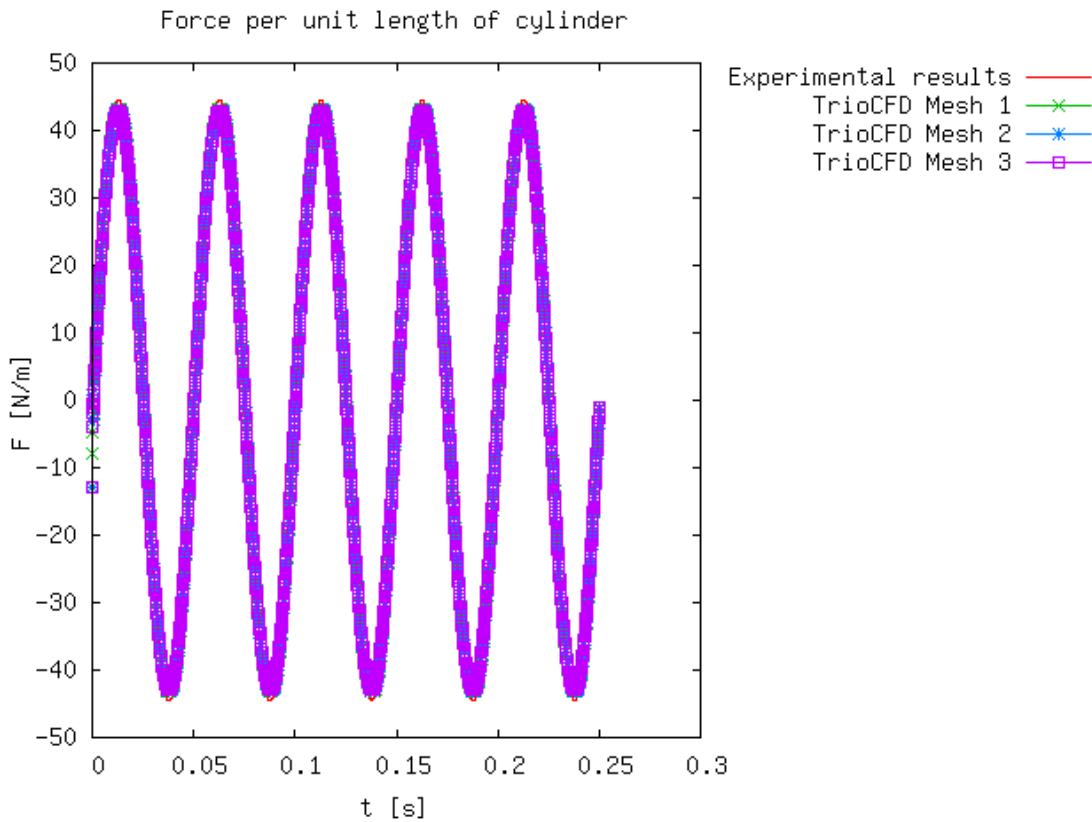


Figure VIII.3.5: Force per unit length of cylinder

The experimental calculation of the coefficients has been carried out on the test bench of the CEA/DYN laboratory. For the Center cylinder, numerically, the added coefficients are computed with a Fourier product as:

$$\begin{aligned} m_{i,self} &= \frac{\langle \sin(\omega t), F_i(t) \rangle}{\rho\pi(D/2)^2 U\omega^2} \quad \text{with} \quad \langle \sin(\omega t), F_i(t) \rangle = \frac{2}{5T} \int_0^{5T} \sin(\omega t) F_i(t) dt \\ c_{i,self} &= \frac{\langle \cos(\omega t), F_i(t) \rangle}{\rho\pi(D/2)^2 U\omega^2} \quad \text{with} \quad \langle \cos(\omega t), F_i(t) \rangle = \frac{2}{5T} \int_0^{5T} \cos(\omega t) F_i(t) dt \end{aligned} \quad (3.2)$$

and are reported in the following tables:

	$m_{x,self}$	$m_{y,self}$
Experimental solution	1.33	0
TrioCFD Mesh_1	1.3019721348357873	-7.605857973333032e-05
TrioCFD Mesh_2	1.2982005184007996	-1.4481185221385146e-05
TrioCFD Mesh_3	1.2863784550110966	3.3229574929748677e-06

Table VIII.3.3: Added mass coefficients for the Center cylinder

	$c_{x,self}$	$c_{y,self}$
Experimental solution	0.049	0
TrioCFD Mesh_1	0.06337958034901885	-0.0005286139963747906
TrioCFD Mesh_2	0.05818516392411184	5.5561084281979256e-05
TrioCFD Mesh_3	0.04019502856920335	9.949497999836866e-05

Table VIII.3.4: Added damping coefficients for the Center cylinder

For the Nord cylinder, numerically, the added coefficients are computed with a Fourier product as:

$$\begin{aligned} m_{i,cross}^{(N)} &= \frac{\langle \sin(\omega t), F_i^{(N)}(t) \rangle}{\rho\pi(D/2)^2 U \omega^2} \quad \text{with} \quad \langle \sin(\omega t), F_i^{(N)}(t) \rangle = \frac{2}{5T} \int_0^{5T} \sin(\omega t) F_i^{(N)}(t) dt \\ c_{i,cross}^{(N)} &= \frac{\langle \cos(\omega t), F_i^{(N)}(t) \rangle}{\rho\pi(D/2)^2 U \omega^2} \quad \text{with} \quad \langle \cos(\omega t), F_i^{(N)}(t) \rangle = \frac{2}{5T} \int_0^{5T} \cos(\omega t) F_i^{(N)}(t) dt \end{aligned} \quad (3.3)$$

and are reported in the following tables:

	$m_{x,cross}^{(N)}$	$m_{y,cross}^{(N)}$
TrioCFD Mesh_1	0.3716451051568068	-0.000624393117429535
TrioCFD Mesh_2	0.37017774843318185	-0.0006239603182541872
TrioCFD Mesh_3	0.36622957679188656	-0.00032139330224597126

Table VIII.3.5: Added mass coefficients for the Nord cylinder

	$c_{x,cross}^{(N)}$	$c_{y,cross}^{(N)}$
TrioCFD Mesh_1	0.019535844503870994	0.00012165505395679838
TrioCFD Mesh_2	0.018383779554499477	-2.0116860765459488e-05
TrioCFD Mesh_3	0.014070684928253053	1.9730052447409638e-05

Table VIII.3.6: Added damping coefficients for the Nord cylinder

For the Sud cylinder, numerically, the added coefficients are computed with a Fourier product as:

$$\begin{aligned} m_{i,cross}^{(S)} &= \frac{\langle \sin(\omega t), F_i^{(S)}(t) \rangle}{\rho\pi(D/2)^2 U \omega^2} \quad \text{with} \quad \langle \sin(\omega t), F_i^{(S)}(t) \rangle = \frac{2}{5T} \int_0^{5T} \sin(\omega t) F_i^{(S)}(t) dt \\ c_{i,cross}^{(S)} &= \frac{\langle \cos(\omega t), F_i^{(S)}(t) \rangle}{\rho\pi(D/2)^2 U \omega^2} \quad \text{with} \quad \langle \cos(\omega t), F_i^{(S)}(t) \rangle = \frac{2}{5T} \int_0^{5T} \cos(\omega t) F_i^{(S)}(t) dt \end{aligned} \quad (3.4)$$

and are reported in the following tables:

	$m_{x,cross}^{(S)}$	$m_{y,cross}^{(S)}$
TrioCFD Mesh_1	0.3716321159217623	0.0006268173866212407
TrioCFD Mesh_2	0.37017868337547066	0.0006312449715248159
TrioCFD Mesh_3	0.36622985354360077	0.00031931914828190106

Table VIII.3.7: Added mass coefficients for the Sud cylinder

	$c_{x,cross}^{(S)}$	$c_{y,cross}^{(S)}$
TrioCFD Mesh_1	0.019571861305805037	-4.2058900077802875e-05
TrioCFD Mesh_2	0.01838694264498712	-9.201904558928073e-07
TrioCFD Mesh_3	0.01407677264853862	-2.31158712989914e-05

Table VIII.3.8: Added damping coefficients for the Sud cylinder

For the Est cylinder, numerically, the added coefficients are computed with a Fourier product as:

$$\begin{aligned} m_{i,cross}^{(E)} &= \frac{\langle \sin(\omega t), F_i^{(E)}(t) \rangle}{\rho\pi(D/2)^2 U \omega^2} \quad \text{with} \quad \langle \sin(\omega t), F_i^{(E)}(t) \rangle = \frac{2}{5T} \int_0^{5T} \sin(\omega t) F_i^{(E)}(t) dt \\ c_{i,cross}^{(E)} &= \frac{\langle \cos(\omega t), F_i^{(E)}(t) \rangle}{\rho\pi(D/2)^2 U \omega^2} \quad \text{with} \quad \langle \cos(\omega t), F_i^{(E)}(t) \rangle = \frac{2}{5T} \int_0^{5T} \cos(\omega t) F_i^{(E)}(t) dt \end{aligned} \quad (3.5)$$

and are reported in the following tables:

	$m_{x,cross}^{(E)}$	$m_{y,cross}^{(E)}$
TrioCFD Mesh_1	-0.1695346218376064	-2.364244321848384e-05
TrioCFD Mesh_2	-0.16899767522974835	-5.567513694906019e-06
TrioCFD Mesh_3	-0.167456907865506	7.681848956910776e-07

Table VIII.3.9: Added mass coefficients for the Est cylinder

	$c_{x,cross}^{(E)}$	$c_{y,cross}^{(E)}$
TrioCFD Mesh_1	-0.005703513041916182	-7.580603222023263e-05
TrioCFD Mesh_2	-0.005162687708750583	1.3449725479030728e-05
TrioCFD Mesh_3	-0.003135362680928665	1.4709800856276483e-05

Table VIII.3.10: Added damping coefficients for the Est cylinder

For the West cylinder, numerically, the added coefficients are computed with a Fourier product as:

$$\begin{aligned} m_{i,cross}^{(W)} &= \frac{\langle \sin(\omega t), F_i^{(W)}(t) \rangle}{\rho\pi(D/2)^2 U \omega^2} \quad \text{with} \quad \langle \sin(\omega t), F_i^{(W)}(t) \rangle = \frac{2}{5T} \int_0^{5T} \sin(\omega t) F_i^{(W)}(t) dt \\ c_{i,cross}^{(W)} &= \frac{\langle \cos(\omega t), F_i^{(W)}(t) \rangle}{\rho\pi(D/2)^2 U \omega^2} \quad \text{with} \quad \langle \cos(\omega t), F_i^{(W)}(t) \rangle = \frac{2}{5T} \int_0^{5T} \cos(\omega t) F_i^{(W)}(t) dt \end{aligned} \quad (3.6)$$

and are reported in the following tables:

	$m_{x,cross}^{(W)}$	$m_{y,cross}^{(W)}$
TrioCFD Mesh_1	-0.17090980327872832	1.9446997890991688e-05
TrioCFD Mesh_2	-0.17029710552290866	-3.8546134761898e-06
TrioCFD Mesh_3	-0.16814290479870805	2.5000151420509838e-08

Table VIII.3.11: Added mass coefficients for the West cylinder

	$c_{x,cross}^{(W)}$	$c_{y,cross}^{(W)}$
TrioCFD Mesh_1	-0.005798446390031434	-9.845478567187751e-05
TrioCFD Mesh_2	-0.005383526084995071	1.7543187137375387e-05
TrioCFD Mesh_3	-0.0033006983562379297	2.5222616305933635e-05

Table VIII.3.12: Added damping coefficients for the West cylinder

Pressure and velocity fields are reported at final time in order to investigate such distributions for the following numerical cases: TrioCFD with Mesh_1 (TrioCFD Mesh_1), TrioCFD with Mesh_2 (TrioCFD Mesh_2) and TrioCFD with Mesh_3 (TrioCFD Mesh_3).

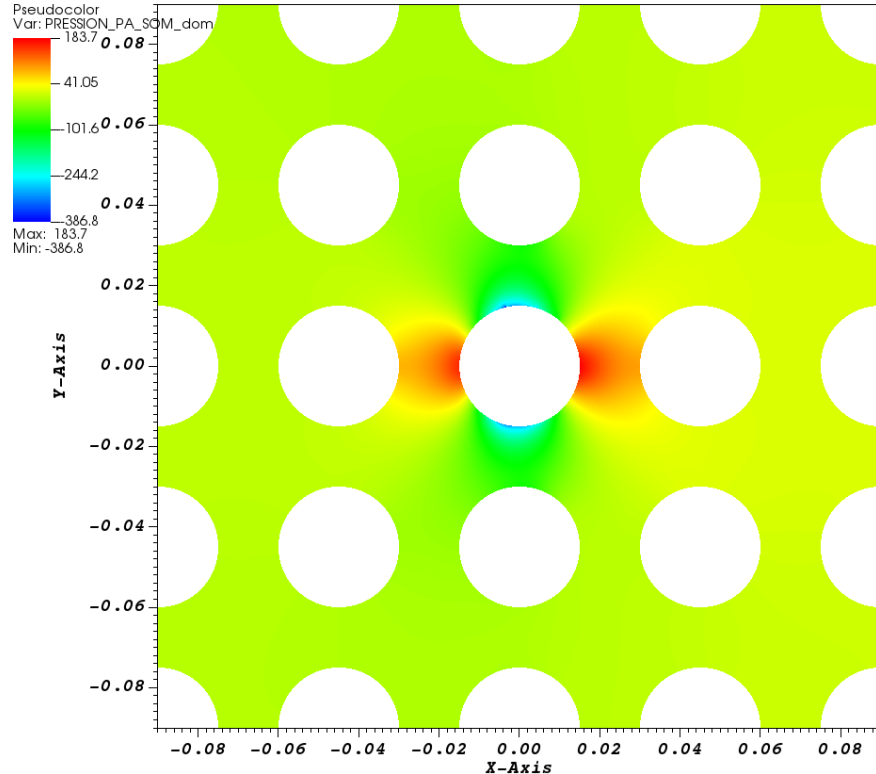


Figure VIII.3.6: TrioCFD Mesh_1 PRESSION SOM

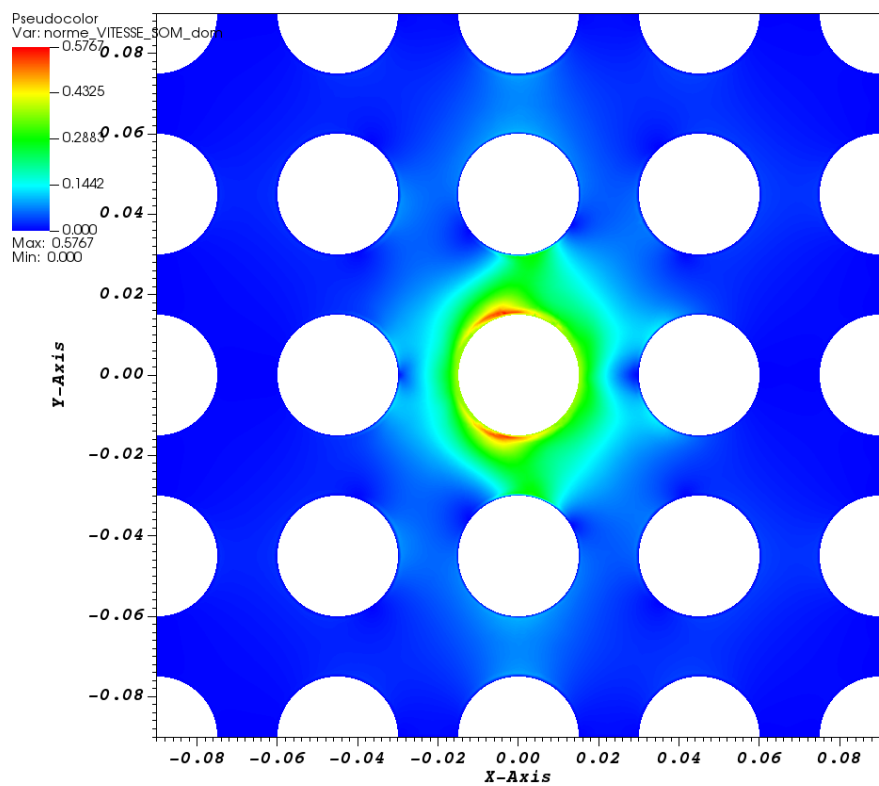


Figure VIII.3.7: TrioCFD Mesh_1 VITESSE_magnitude SOM

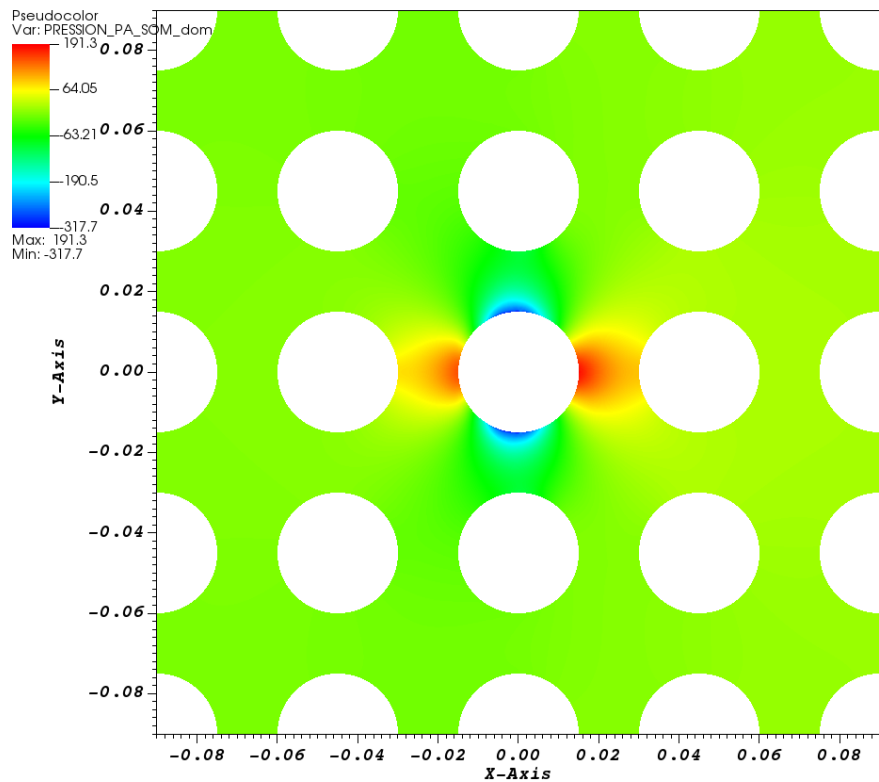


Figure VIII.3.8: TrioCFD Mesh_2 PRESSION SOM

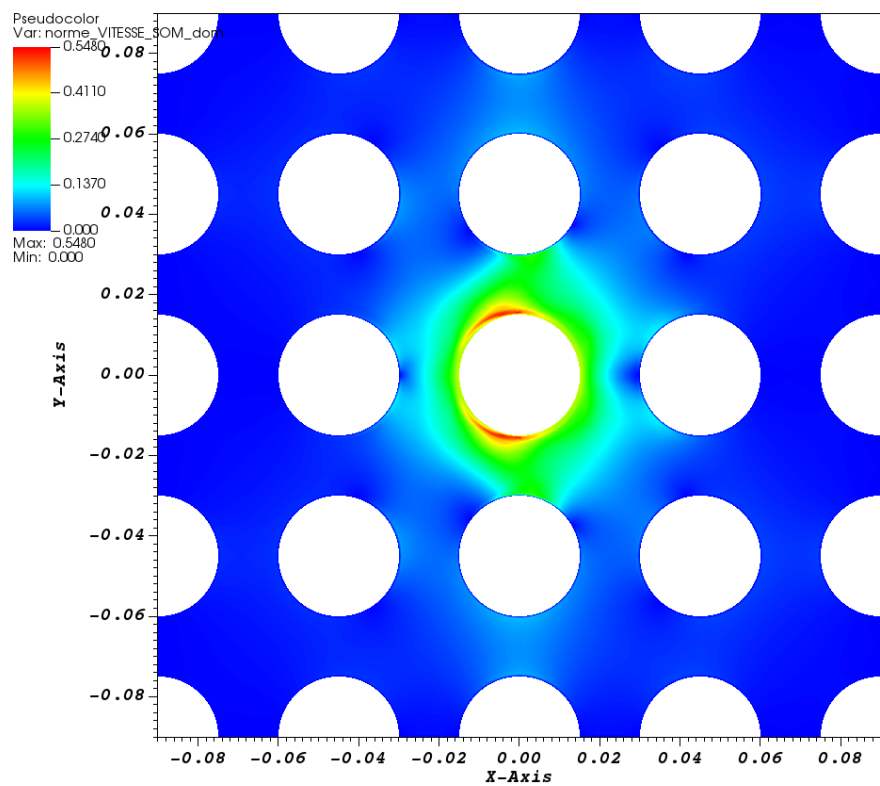


Figure VIII.3.9: TrioCFD Mesh_2 VITESSE_magnitude SOM

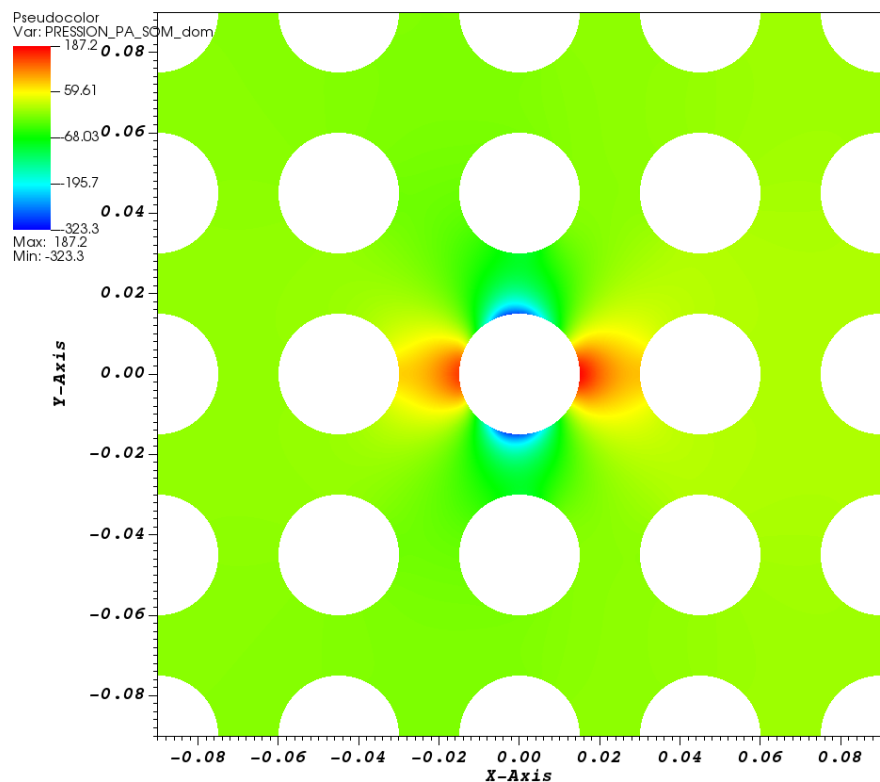


Figure VIII.3.10: TrioCFD Mesh_3 PRESSION SOM

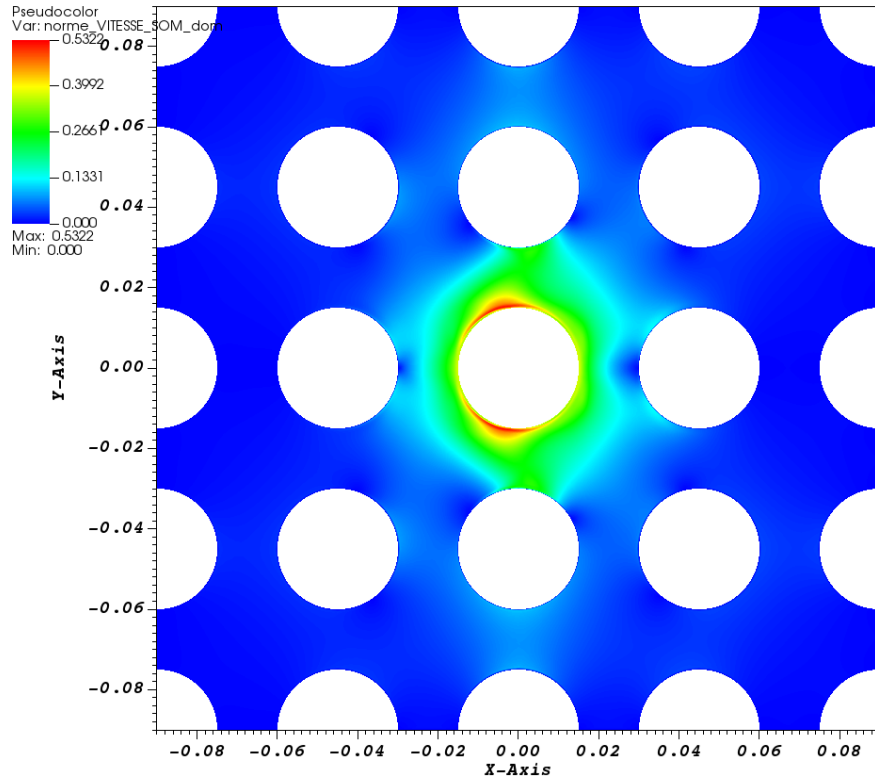


Figure VIII.3.11: TrioCFD Mesh_3 VITESSE_magnitude SOM

3.5 Conclusion

The harmonic motion of a cylinder in a quiescent viscous fluid, surrounded by a set of cylinders arranged in a square configuration, has been numerically simulated. A FEV method is applied to solve such a problem in conjunction with the ALE scheme. The numerical results for the fluid force and the added coefficients of the center cylinder are in good agreement with the experimental results. As theoretically expected, moreover, the coefficients along the y-axis are zero and the coefficients along x are symmetrical for the North-South and East-West cylinders respectively. This further shows the robustness of our numerical results.

3.6 References

- 1. Chen, S S. Flow-induced vibration of circular cylindrical structures, 1987.
- 2. CFD numerical simulation of a single-phase flow around a vibrating cylindrical tube, D. Panunzio, DES/ISAS/DM2S/SEMT/DYN/RS/2020-67015/A

3.7 Data Files

DIVA

```
# Hydraulique 2D laminar with ALE : DIVA configuration #
# Set of circular cylinders , arranged in a square configuration. The central cylinders moves w
#
# Moving domain #
# SEQUENTIAL CALCULATION #
dimension 2
Pb_hydraulique_ALE pb
```

```

Domaine_ALE dom
# BEGIN MESH #
Read_med family_names_from_group_names dom Mesh_1 MeshDIVA_1.med
# END MESH #
VerifierCoin dom { }
# BEGIN PARTITION
Partition dom
{
    Partition_tool metis { Nb_parts 2 }
    Larg_joint 2
    zones_name dom
}
End
END PARTITION #
# BEGIN SCATTER #
# Scatter DOM.Zones dom #
# END SCATTER #
# For the Arbitrary Lagrangian–Eulerian framework: block to indicate the number of mobile
boundaries of the domain and specify the speed that must be imposed on them #
Imposer_vit_bords_ALE dom
{
    1 # number of mobile boundaries #
    Cylindre_Centre Champ_front_ALE 2 0.003*125.66*cos(125.66*t) 0.0 # name and speed of the bords
}
# Solver used to solve the system giving the moving mesh velocity #
Solver_moving_mesh_ALE dom { PETSC GCP { precond ssor { omega 1.5 } seuil 1e-9 impr } }
# I select a discretization #
VEFPreP1B ma_discretisation
# Lire ma_discretisation { P0 P1 Changement_de_base_P1Bulle 1 Cl_pression_sommet_faible 1 } #
# Time scheme, choice between: explicit or implicit #
Scheme_euler_implicit mon_schema
Read mon_schema
{
    # Time step #
        # Initial time [s] #
        tinit 0.
    # Min time step #
        dt_min 1.e-15
    # Output criteria #
        # .out files printing period #
        dt_impr 5.e-6
    # tcpumax 47.5 #
    # .sauv files printing period #
        dt_sauv 100.
    # facsec such as dt = facsec * min(dt(CFL),dt_max) ; for explicit scheme facsec <= 1. By default
    facsec 1
        facsec_max 1
    solveur implicite_ALE
    {
        solveur gmres { diag seuil 1.e-12 nb_it_max 3 }
    }
    # Stop if one of the following criteria is checked: #
        # End time [s] #
        tmax 0.25
    # Max number of time steps #
        # nb_pas_dt_max 5 #
        # Convergence threshold (see .dt_ev file) #
        seuil_statio 1.e-15
    }
    # I define a medium #
Fluide_Incompressible milieu

```

```

Read milieu
{
  mu Champ_Uniforme 1 1.007e-3
  rho Champ_Uniforme 1 1000
}
# Gravity vector definition
Uniform_field my_gravity
Read my_gravity 2 0.0 0.0 #
# Association between the different objects #
Associate pb dom
Associate pb mon_schema
Associate pb milieu
Discretize pb ma_discretisation
Read pb
{
  Navier_Stokes_standard_ALE
  {
    # Pressure matrix solved with #
    solveur_pression PETSC GCP { precond ssor { omega 1.5 } seuil 1e-9 impr }
    # Two operators are defined #
    convection { ALE { muscl } } # A convective scheme for ALE framework. Choice between: among others,
    diffusion { }
    # Uniform initial condition for velocity #
    initial_conditions {
      vitesse Champ_Uniforme 2 0. 0.
    }
    # Boundary conditions #
    boundary_conditions {
      Cylindre_Centre frontiere_ouverte_vitesse_imposee Champ_front_ALE 2 0.003*125.66*cos(125.*theta)
      Cylindre_Nord paroi_fixe
      Cylindre_Sud paroi_fixe
      Cylindre_Est paroi_fixe
      Cylindre_Ouest paroi_fixe
      Paroi_Cylindre paroi_fixe
      Paroi_Gauche paroi_fixe
      Paroi_Droite paroi_fixe
      Periodique_Haut paroi_fixe
      Periodique_Bas paroi_fixe
    }
  }
  Post_processing
  {
    # Fields #
    format lata
    fields dt_post 0.025
    {
      pression_pa som
      vitesse som
        # vorticite som #
        ALEMeshVelocity som
        # ALEMeshTotalDisplacement som #
    }
  }
}
# The problem is solved with #
Solve pb
# Not necessary keyword to finish #
End

```

IX. Conclusion

THIS document is the first version of a **TrioCFD** validation report resulting of an analysis and a sorting work that have been done on its database. First, an important inventory job was carried out in order to sort the test cases for targeting quickly the use of **TrioCFD** in different CFD configurations. The inventory resulted in a single table with plenty information (LibreOffice format), where the test cases are classified into several subdomains of fluid flows. In this document, some of them have been selected and detailed because 1) they are well-known in the literature, 2) they present comparisons with other academic or commercial CFD codes, 3) they present comparisons with experimental data and 4) they cover an important and representative part of the physics of the code. In this report, the test cases are representative of five subdomains: “Laminar flow” (Part III), “Thermal laminar flow” (Part IV), “Turbulent flow” (Part V), “Thermal turbulent flow” (Part VI), “Front Tracking” (Part VII) and “Fluid/structure interactions with ALE” (Part VIII). The first four parts gather the test cases for single phase flows, coupled or not with turbulence models and thermal effects. Part VII is dedicated to two-phase flows with interface tracking and the last part (VIII) that has been added since the last version of this report focuses on fluid/structure interactions with Arbitrary Lagrangian-Eulerian Method (ALE). The corresponding datafiles were run with the 1.8.2 version of **TrioCFD** to check the achievement of computations. Meanwhile, an important work was carried out to update a new PRM template in order to standardize all validation sheets. For each one of them, let us remind that the PDF file is generated by running a bash script (command `Run_fiche-not_run`) which acts on a PRM file (previously, test cases must have been run). A PRM file is a set of specific instructions for interfacing the L^AT_EX commands with the **TrioCFD** results post-processed with **Gnuplot** or **Visit**. Its content can be freely chosen by authors which has the consequence that the number and titles of sections differ from one sheet to another one. The goal of the new PRM template is to harmonize their contents for a more homogeneous rendering of this report. The seven sections of the new PRM template detail the main stages of CFD modeling and describe the comparisons. All validation sheets in this report have been revised and enhanced by taking into account this new PRM template.

Perspective

Numerous other validation sheets already exist in the **TrioCFD** database and the job must be pursued. Hence, this document does not present an exhaustive list of what **TrioCFD** can do for CFD applications. It can be viewed as a simple “snapshot” that will be gradually improved and increased at each version release. The improvement will be simplified by the methodology and the tools which have been developed for PRM files. After checking and updating the validations sheets, they will be added in the future versions of this report. Among the available test cases, the sort will be pursued to separate those currently “in progress” and the others that lack quantitative comparisons. Multiple variations of the same test case appear in the database (e.g. “Poiseuille flow”). Some of them are simply a 3D extension of the same test case, or an extension with temperature equation or turbulence model. For instance, the laminar test case of “flow with a cylinder” (Chapter III.3) exists in turbulent version in two and three dimensions. Another example is given by the test case named “Backward facing step” which appears in four different versions: the first one is “two-dimensional”, the second one is “implicit”, the third one is “three-dimensional” and the last one is “heated in two dimensions”. More test cases of turbulent flow are also available, such as “Baglietto” and “Flow in curved pipe”. An effort will be done to extend the number of CFD subdomains such as “Quasi-compressible flow”, “Flow in porous media” and “fluid-structure interaction”. Finally several tests are dedicated to the “grid convergence” or “Miscellaneous test” of numerical options.